

**PEDIATRIC WHEELCHAIR AND HEADREST DESIGN GUIDELINES AND THE
EFFECT OF HEADRESTS ON RELATIVE INJURY RISK UNDER REAR IMPACT
CONDITIONS**

by

Susan Issen Fuhrman

Bachelor of Science Mechanical Engineering, Carnegie Mellon University, 1982

Submitted to the Graduate Faculty of
School of Health and Rehabilitation Sciences in partial fulfillment
of the requirements for the degree of
Doctor of Philosophy

University of Pittsburgh

2008

UNIVERSITY OF PITTSBURGH
SCHOOL OF HEALTH AND REHABILITATION SCIENCES

This dissertation was presented

by

Susan Issen Fuhrman

It was defended on

November 25, 2008

and approved by

Gina Bertocci, PhD, Departments of Mechanical Engineering, Bioengineering and Pediatrics,

University of Louisville

Shirley Fitzgerald, PhD, HSR&D REAP/RR&D REAP, James A. Haley Tampa VA, and

College of Nursing, University of Southern Florida

Patricia Karg, MSBME, Department of Rehabilitation Science and Technology

Richard Simpson, PhD, Department of Rehabilitation Science and Technology

Dissertation Advisor: David M. Brienza, PhD, Department of Rehabilitation Science and

Technology

Copyright © by Susan Issen Fuhrman

2008

**THE EFFECT OF PEDIATRIC WHEELCHAIR AND HEADREST PARAMETERS
ON RELATIVE INJURY RISK UNDER REAR IMPACT CONDITIONS AND
RESULTING DESIGN GUIDELINES FOR REAR IMPACT PROTECTION**

Susan Issen Fuhrman, Ph.D.
University of Pittsburgh 2008

The role that wheelchairs and wheelchair mounted headrests play in rear impact occupant protection for children who remain seated in wheelchairs while traveling in motor vehicles was investigated using sled testing and computer simulation. Study goals were to establish pediatric wheelchair and headrest design guidelines and to determine the effect of headrests on relative injury risk outcome measures under rear impact conditions. Two series of sled tests (16 mph, 11g) were conducted using a Hybrid III 6-year old anthropomorphic test device (ATD) seated in identically configured manual pediatric wheelchairs, with and without headrests. Wheelchairs remained intact and the ATD remained upright. Rear impact front wheelchair securement points were subjected to loads similar to previously described (Ha, DongRan, 2004) rear securement points in frontal impact, although Ha used the more severe 30mph, 20g frontal impact WC19 – *Wheelchairs Used as Seats in Motor Vehicles* (ANSI/RESNA, 2000) crash pulse. Sled test ATD data analysis indicated that wheelchair headrest use had a potentially protective effect based on pediatric head and neck injury risk outcomes. Sled test data established response corridors for MADYMO computer simulation model development, and defined statistical test target thresholds for model validation. Two simulation models were developed, with and without a headrest. The models validated well for tiedown loads, wheelchair acceleration, lap belt loads and chest acceleration. Outcomes related to head and neck response were not as strongly validated. Model ATD neck response characterization methods were developed. Finally,

parametric sensitivity analyses were used to develop wheelchair and headrest design guidelines for pediatric manual wheelchairs in rear impact for front securement point loads, rear wheel loads and seatback loads. Pediatric injury outcome measure sensitivity to wheelchair, headrest and crash pulse parameters was evaluated. Neck injury criteria (Nij) was sensitive to headrest placement; resulting recommendations specify placing the headrest as close as possible to the back of the head, and top of the headrest pad should be at least 5 cm above the head center of gravity. Effects of stiffer 6-year old ATD neck response on injury risk outcome measures were evaluated and found to reduce likelihood of severe neck injury.

TABLE OF CONTENTS

LIST OF TABLES	XII
LIST OF FIGURES	XV
LIST OF EQUATIONS.....	XX
LIST OF ACRONYMS	XXI
ACKNOWLEDGEMENTS	XXII
1.0 INTRODUCTION.....	24
2.0 BACKGROUND	27
2.1 SEATING COMPONENT SAFETY RESEARCH.....	29
2.1.1 Wheelchair related research	29
2.1.1.1 Wheelchair seatback loading and deflection.....	29
2.1.1.2 Wheelchair postural supports	31
2.1.2 Automotive related research.....	33
2.1.2.1 Automotive seatback research in rear impact	34
2.1.2.2 Automotive headrest research.....	37
2.1.2.3 Automotive occupant restraint research	38
2.2 HYBRID III 6-YEAR OLD ANTHROPOMORPHIC TEST DEVICE.....	39
2.2.1 Development of the Hybrid III 6-year old ATD.....	40
2.2.2 Hybrid III 6-year old ATD neck.....	42

2.3	ATD INJURY MEASURES.....	46
2.3.1	Neck injury criteria.....	47
2.3.2	Head injury criteria (HIC).....	49
2.3.3	Head acceleration.....	51
2.3.4	Chest acceleration.....	52
2.3.5	Excursion limits.....	52
2.4	RELEVANT AND RELATED STANDARDS.....	53
3.0	EXPLORATORY STUDIES	57
3.1	PRESCRIPTION PATTERNS OF SECONDARY POSTURAL SUPPORT DEVICES AND CONCERNS RELATED TO THEIR USE DURING VEHICLE TRANSPORTATION	57
3.1.1	Abstract.....	57
3.1.2	Introduction.....	58
3.1.3	Methods.....	59
3.1.4	Results	60
3.1.5	Discussion.....	62
3.2	HEAD VELOCITY	64
3.2.1	Introduction.....	64
3.2.2	Methods.....	64
3.2.3	Results	65
3.3	PENDULUM TESTING	68
3.3.1	Calculations	68
3.3.2	Pendulum testing methods	72

3.3.3	Pendulum testing results	73
4.0	CHARACTERIZATION OF PEDIATRIC WHEELCHAIR KINEMATICS AND WHEELCHAIR TIEDOWN AND OCCUPANT RESTRAINT SYSTEM LOADING DURING REAR IMPACT.....	76
4.1	INTRODUCTION	77
4.2	METHODS.....	79
4.3	RESULTS	82
4.4	DISCUSSION.....	89
4.5	CONCLUSIONS	93
5.0	EFFECT OF WHEELCHAIR HEADREST USE ON PEDIATRIC HEAD AND NECK INJURY RISK OUTCOMES DURING REAR IMPACT	96
5.1	INTRODUCTION	97
5.2	METHODS.....	99
5.3	RESULTS	104
5.3.1	Sled test results.....	105
5.3.2	Injury outcome measure results	108
5.4	DISCUSSION.....	114
5.5	CONCLUSIONS.....	119
6.0	DEVELOPMENT OF MADYMO SIMULATION MODELS	121
6.1	INTRODUCTION	122
6.2	METHODS.....	123
6.3	RESULTS	131
6.3.1	Statistical comparison between sled test data	131

6.3.1.1	Series HR sled test comparisons.....	132
6.3.1.2	Series NoHR sled test comparisons.....	144
6.3.2	Model HR validation.....	154
6.3.3	Model NoHR validation.....	164
6.4	DISCUSSION.....	174
7.0	CERVICAL SPINE STIFFNESS CHARACTERIZATION OF THE ENCRYPTED MADYMO HYBRID III 6-YEAR OLD ATD MODEL.....	186
7.1	INTRODUCTION	186
7.2	METHODS.....	188
7.3	RESULTS	194
7.4	DISCUSSION.....	198
8.0	PARAMETRIC SENSITIVITY ANALYSIS	207
8.1	INTRODUCTION	207
8.2	METHODS.....	209
8.2.1	Crash pulse parameter	213
8.2.2	Wheelchair parameters	214
8.2.3	Headrest parameters	219
8.2.4	ATD parameters.....	221
8.3	RESULTS	223
8.3.1	Results: wheelchair and headrest design guidelines	224
8.3.1.1	Wheelchair front securement point loads.....	224
8.3.1.2	Rear wheel loads	225
8.3.1.3	Wheelchair seatback joint deflection	226

8.3.1.4	Wheelchair seatback loads.....	227
8.3.1.5	Wheelchair headrest loads.....	228
8.3.2	Results: Pediatric injury outcome measures.....	230
8.3.2.1	Head acceleration.....	230
8.3.2.2	Chest acceleration.....	231
8.3.2.3	HIC – Head injury criteria.....	232
8.3.2.4	Nij – Neck injury criteria.....	233
8.3.3	Results: Effect of neck stiffness modification on injury outcome measures in read impact.....	234
8.3.3.1	Head and chest accelerations.....	235
8.3.3.2	Head injury criteria (HIC15).....	236
8.3.3.3	Neck injury criteria (Nij).....	237
8.4	DISCUSSION.....	238
8.4.1	Wheelchair and headrest design criteria.....	240
8.4.2	Injury risk outcomes.....	242
8.4.3	Effects of mATD neck restraint loads and moments on injury risk outcome measures.....	246
8.4.4	Study limitations.....	247
9.0	CONCLUSIONS.....	250
9.1	PROJECT REVIEW.....	250
9.2	RESULTS.....	251
9.3	LIMITATIONS.....	254
9.4	FUTURE WORK.....	256

APPENDIX A	258
BIBLIOGRAPHY	283

LIST OF TABLES

Table 1: Head injury criteria limits (Kleinberger, Michael et al., 1998; Eppinger et al., 1999)...	50
Table 2: Hybrid III child ATD out-of-position child protection values	51
Table 3: WC19 horizontal excursion limits (mm) (ANSI/RESNA, 2000).....	53
Table 4: Image scale data for WC0535 (Test 1).....	66
Table 5: Image scale data for WC0536 (Test 2).....	66
Table 6: Wheelchair test configurations	81
Table 7: Model HR components.....	126
Table 8: Pipkorn thresholds	130
Table 9: Right front tiedown load Series HR sled test data comparison.	133
Table 10: Left front tiedown load Series HR sled test data comparison.	134
Table 11: Wheelchair center of gravity acceleration Series HR sled test data comparison.	136
Table 12: Lap belt loads Series HR sled test data comparison.....	137
Table 13: Chest acceleration Series HR sled test data comparison.	138
Table 14: Head X-accelerations Series HR sled test data comparison.....	139
Table 15: Head Z-accelerations Series HR sled test data comparison.....	140
Table 16: Upper neck bending moment (My) Series HR sled test data comparison.....	141
Table 17: Upper neck force (Fx) Series HR sled test data comparison.....	142

Table 18: Upper neck force (Fz) Series HR sled test data comparison.	143
Table 19: Series HR target threshold summary.	144
Table 20: Right tiedown loads Series NoHR sled test data comparison.....	145
Table 21: Left tiedown loads Series NoHR sled test data comparison.....	145
Table 22: Wheelchair center of gravity acceleration Series NoHR sled test data comparison...	146
Table 23: Lap belt loads Series NoHR data comparison.	147
Table 24: Chest acceleration Series NoHR sled test data comparison.	148
Table 25: Head X-acceleration Series NoHR sled test data comparison.....	149
Table 26: Head Z-acceleration Series NoHR sled test data comparison..	150
Table 27: Upper neck bending moment (My) Series NoHR sled test data comparison.	151
Table 28: Upper neck force (Fx) Series NoHR sled test data comparison..	152
Table 29: Upper neck force (Fz) Series NoHR sled test data comparison..	153
Table 30: Series NoHR target threshold summary.	154
Table 31: Model HR front tiedown loads validation comparison.....	155
Table 32: Model HR wheelchair acceleration validation comparison.....	157
Table 33: Model HR lap belt load validation comparison.....	158
Table 34: Series HR chest acceleration validation comparison.....	159
Table 35: Model HR head acceleration validation comparison.....	161
Table 36: Model HR upper neck bending moment (My) validation comparison.....	162
Table 37: Model HR upper neck forces validation comparison.	164
Table 38: Model NoHR front tiedown loads validation comparison.....	166
Table 39: Model NoHR wheelchair center of gravity acceleration validation comparison	167
Table 40: Model NoHR lap belt loads validation comparison	168

Table 41: Model NoHR chest acceleration validation comparison.	170
Table 42: Model NoHR head acceleration validation comparison.	171
Table 43: Model NoHR upper neck bending moment (My) validation comparison.	172
Table 44: Model NoHR upper neck forces validation comparison.	174
Table 45: Comparison of target thresholds calculated from Series HR and Series NoHR sled testing.	177
Table 46: Model HR validation results summary for model validation against mean sled test results.	178
Table 47: Model NoHR validation results summary for model validation against mean sled test results.	178
Table 48: Side by side comparison of Model HR and Series HR.	181
Table 49: Side by side comparison of Model NoHR and Series NoHR.	182
Table 50: Summary of MADYMO neck elements.	191
Table 51: Neck testing velocity profile specifications.	194
Table 52: Comparison of injury risk criteria with protection reference values (PRV).	205
Table 53: Parametric sensitivity test matrix.	211
Table 54: Pediatric wheelchair and headrest design criteria in rear impact.	241
Table 55: Sensitivity of injury risk response measures to wheelchair, headrest and crash pulse parameters.	242
Table 56: Effects of increased neck restraint loads and moments on injury risk measures.	246

LIST OF FIGURES

Figure 1: Hybrid III ATD family	40
Figure 2: Percent of client who receive SPSDs by prescriber category	61
Figure 3: Level of wheelchair users' risk during transit for SPSDs	62
Figure 4: Location of head and scale targets	65
Figure 5: 6-year old ATD head velocities during rear impact with no headrests	66
Figure 6: Smoothed 6-year old ATD head velocity data	67
Figure 7: Photos of Pendulum Impact Tester with backrest and with headrest.....	69
Figure 8: Pendulum Impact Tester (PIT) schematic.....	70
Figure 9: Combined angle and mass of pendulum.....	71
Figure 10: Displacement and load cell data (16 point running average)	74
Figure 11: Fast Fourier Transform of data.....	74
Figure 12: Force displacement curve using a low pass filter.....	75
Figure 13: Photos of experimental set up.	81
Figure 14: Sled acceleration time-history for rear impact tests	83
Figure 15: Tests 2 (no headrest) and Test 5 (headrest) images during sled tests.....	84
Figure 16: Mean front caster vertical excursion for rear impacts.	85
Figure 17: Mean seatback to seat angle for rear impact tests	86

Figure 18: Mean seatback excursion upward along seatback canes for rear impact tests.	87
Figure 19: A comparison of mean peak wheelchair tiedown and occupant restraint loads for rear impact.....	88
Figure 20: A comparison of mean peak Series NoHR and HR WTORs loads in rear impact to frontal impact loads.....	91
Figure 21: Wheelchair set-up without a headrest	101
Figure 22: Wheelchair set-up with headrest	101
Figure 23: Detailed view of headrest identifying anterior-posterior headrest stem, headrest stem joint and vertical headrest stem.....	101
Figure 24: Rear impact sled test acceleration time history	105
Figure 25: ATD and wheelchair dynamic response with maximum ATD neck extension	108
Figure 26: Resultant linear head acceleration measured during rear impact sled tests.	108
Figure 27: HIC values for three time intervals: total test (unlimited), 36 ms, and 15 ms.	109
Figure 28: Nij peak values.	110
Figure 29: Neck Injury Criteria (Nij).....	111
Figure 30: Tolerance to concussion using combined rotational velocities and accelerations	112
Figure 31: MADYMO simulation models.....	125
Figure 32: Series HR front tiedown loads time-history	133
Figure 33: Series HR wheelchair center of gravity acceleration time-history	135
Figure 34: Series HR lap belt loads time-history	137
Figure 35: Series HR chest acceleration time-history.....	138
Figure 36: Series HR head acceleration time-history	139
Figure 37: Series HR upper neck bending moment (My) time-history	141

Figure 38: Series HR upper neck force time-history	142
Figure 39: Series NoHR front tiedown loading time-history.....	145
Figure 40: Series NoHR wheelchair center of gravity acceleration time-history	146
Figure 41: Series NoHR lap belt loads time-history.....	147
Figure 42: Series NoHR chest acceleration time-history.....	148
Figure 43: Series NoHR head acceleration time-history	149
Figure 44: Series NoHR upper neck bending moment (My) time-history	151
Figure 45: Series NoHR upper neck forces time-history.....	152
Figure 46: Series HR front tiedown load time-history with model response	155
Figure 47: Series HR wheelchair center of gravity acceleration time-history with model response	156
Figure 48: Series HR lap belt time-history with model response	158
Figure 49: Model HR chest acceleration time-history with model response.....	159
Figure 50: Series HR head acceleration time-histories with model response.....	160
Figure 51: Series HR upper neck bending moment (My) time-history with model response	162
Figure 52: Series HR upper neck force time-history with model response	163
Figure 53: Series NoHR front tiedown validation comparison	165
Figure 54: Series NoHR wheelchair center of gravity acceleration with model response	167
Figure 55: Series NoHR lap belt loads time-history with model response.....	168
Figure 56: Series NoHR chest acceleration time-history with model response.....	169
Figure 57: Series NoHR head acceleration time-history with model response	170
Figure 58: Series NoHR upper neck bending moment (My) time-history with model response	172
Figure 59: Series NoHR upper neck forces with model response	173

Figure 60: Model ATD head with labeled coordinate axis.....	180
Figure 61: MADYMO mATD neck displayed (left) with upper, mid and lower neck joints. Physical ATD neck schematic displayed (right) with D-plane location.....	189
Figure 62: Neck component test schematic for neck flexion test.....	193
Figure 63: MADYMO neck flexion and extension simulation models.....	195
Figure 64: Model pendulum velocity for neck flexion displayed with target velocity corridor.	196
Figure 65: Model pendulum velocity for neck extension displayed with target velocity corridor.	196
Figure 66: MADYMO Hybrid III 6-year old ATD Neck Flexion Response.	197
Figure 67: MADYMO Hybrid III 6-year old ATD Neck Extension Response.....	198
Figure 68: Comparison of experimental (pATD) and model (mATD) data for neck flexion testing.....	199
Figure 69: Comparison of experimental and model data for neck extension testing.....	200
Figure 70: Model ATD neck rotation during rear impact.....	202
Figure 71: Comparison of experimental (pATD) and model (mATD) neck flexion test data from 0 to 45 degrees of neck rotation.....	203
Figure 72: Comparison of neck extension test response from 0 to 60 degrees of neck rotation	204
Figure 73: Rear impact crash pulse.....	213
Figure 74: Seatback joint stiffness vs angular displacement load functions	215
Figure 75: Seatback joint stiffness unload functions.	216
Figure 76: Force-deflection for commercially available seatbacks with attachment hardware with model baseline and variation.	217
Figure 77: Headrest loading functions..	220

Figure 78: Headrest unloading functions.....	221
Figure 79: Characterization of MADYMO Hybrid III 6-year old ATD in flexion.	222
Figure 80: Characterization of MADYMO Hybrid III 6-year old ATD neck in extension with increasing resistive forces and moments in the mid-neck joint.	223
Figure 81: Wheelchair front securement point loads with response ranges.	225
Figure 82: Rear wheel loads with response ranges.	226
Figure 83: Wheelchair seatback joint deflection.	227
Figure 84: Wheelchair seatback loads with response ranges.....	228
Figure 85: Wheelchair headrest loads with response ranges.	229
Figure 86: Head accelerations.....	231
Figure 87: Chest accelerations.	232
Figure 88: HIC15 - Head injury criteria.	233
Figure 89: Nij - Neck injury criteria (tension-extension).	234
Figure 90: Response from additional mATD neck restraint loads on peak head and chest accelerations.....	236
Figure 91: Response from additional mATD neck restraint loads on HIC15 across two models.	237
Figure 92: Response from additional mATD neck restraint loads and moments on Nij (tension-extension) across two models.	238
Figure 93: Nij response displayed with headrest proximity leading surface position.	244
Figure 94: Nij displayed with headrest height.	245

LIST OF EQUATIONS

Equation 1: Neck injury criteria.....	48
Equation 2: Head injury criteria.....	50
Equation 3: Calculation of the center of mass of the pendulum.....	70
Equation 4: solving for acceleration.....	70
Equation 5: Moment of inertia around the pivot point.....	70
Equation 6: Potential energy.....	70
Equation 7: Rotational energy.....	71
Equation 8: Kinetic energy.....	71
Equation 9: Average signal.....	129
Equation 10: Mean value ratio.....	129
Equation 11: Correlation coefficient.....	129
Equation 12: Standard deviation.....	130
Equation 13: Moment about the occipital condyles.....	192

LIST OF ACRONYMS

The following table includes a list of acronyms for the reader's reference.

ATD	Anthropomorphic test device (crash test dummy)
FMVSS	Federal Motor Vehicle Safety Standards
H3 6yo ATD	Hybrid III 6-year old ATD
HIC	Head injury criteria
ISO	International Standards Organization
mATD	Model ATD
NASS	National Automotive Sampling System
Nij	Neck injury criteria
OEM	Original equipment manufacturer
pATD	Physical ATD
PSD	Postural support device
UMTRI	University of Michigan Transportation Research Institute
WC	Wheelchair
WC19	ANSI/RESNA WC19 – Wheelchairs Used as Seating in Motor Vehicle
WTORS	Wheelchair tiedown and occupant restraint system

ACKNOWLEDGEMENTS

Few students can complete a dissertation without a solid support team. I have been remarkably fortunate to have outstanding professional mentors and advisors. Tricia Karg has provided me with extensive support, direction, guidance, encouragement and friendship. Her keen insights, focus and attention to detail are unparalleled. Dave Brienza has an unmatched ability to cut to the core issues while squarely focusing his “eye on the ball.” Without Gina Bertocci’s direction, this dissertation simply would have never been conceived or completed. I owe a debt of gratitude to my entire committee for their support and encouragement. I am also grateful to the Department of Rehabilitation Science and Technology for taking a chance with this non-traditional student.

The SSSSN (Super South Side Support Network) provides an amazing culture of cooperation and camaraderie – from the faculty and staff to the students. The many standing inside jokes reflect the true friendship that we share. Perhaps we should be called the SSSF – Super South Side Family.

On a more personal note, no other graduate student has ever benefited from my extensive personal support and cheering team. Simply stated, my husband Michael Fuhrman is my true partner in all matters at all times. Our children, Chana, Ya’aqov, Rebecca, Elie and Leah have all made many sacrifices, given encouragement and helped in a million different ways - more than anyone could ever imagine. We are blessed with riches beyond measure.

This work was funded in part by the National Institute on Disability and Rehabilitation Research (NIDRR), Rehabilitation Engineering Research Center (RERC) on Wheelchair Transportation, Grant # H133E010302, in part by the University of Pittsburgh Clinical and Translational Science Award #5TL1RR024155, and in part by the National Science Foundation (NSF) Interdisciplinary Research Training in Assistive Technology (IGERT), Grant # DGE 0333420. The opinions expressed herein are those of the authors and are not necessarily reflections of the NIDRR or NSF.

1.0 INTRODUCTION

In 2000, over 1.5 million individuals used manual wheelchairs in the United States (Kaye et al., 2000); of these, 79,000 were children, representing 0.11% of the minor population. At this same prevalence rate, as of July 2005, the numbers rose to over 80,000 children under the age of 18 who use manual wheelchairs for their daily mobility needs (U.S. Census Bureau Public Information Office, 2006). Currently, mandatory federal safety standards and state-by-state legislation for car seats and seatbelts have served to help protect able-bodied individuals while traveling in motor vehicles. Yet, federal mandatory standards do not exist for wheelchairs for those individuals who travel in motor vehicles while remaining seated in their wheelchairs. To-date, efforts by researchers, manufacturers, clinicians and transporters have been primarily directed at establishing the voluntary frontal impact standards, *ANSI/RESNA WC-19: Wheelchairs Used as Seats in Motor Vehicles* (ANSI/RESNA, 2000) and *SAE J2249 Wheelchair Tiedowns and Occupant Restraints* (Society of Automotive Engineers, 1996).

While the greatest number of fatalities from motor vehicle accidents occur in frontal impact, rear impact accounts for the greatest number of occupant related injuries (Japan Traffic Safety Association, 1997; NHTSA, 1997). In response to this, automotive manufacturers have developed improved automotive headrests (Volvo, 2003; Saab, 2006). Our research (Fuhrman, S. I. et al., 2005) has indicated that wheelchair headrests

are prescribed for over 60% of all wheelchair users, and for 75-80% of all pediatric wheelchair users. However, wheelchair headrests are not required for transportation in a motor vehicle, and are designed to improve user function rather than for transportation safety in a motor vehicle. There has been no previous effort to investigate the role of headrests for the pediatric wheelchair-using population in rear impact.

The final result of this investigation is to provide valid and specific design guidelines for pediatric wheelchairs and headrests for rear impact protection. These efforts are intended to facilitate rear impact wheelchair standards development, to improve wheelchair safety design, and to assist in the development of wheelchair headrests that will provide effective occupant restraint during rear impact.

Initial efforts focused on directly measuring wheelchair and anthropomorphic test device (ATD) kinematics, wheelchair tiedown and occupant restraint system (WTORS) loading, and injury risk parameters. These measures were assessed and compared using data from multiple rear impact tests conducted with identical wheelchairs under identical test conditions for two cases: either equipped with a headrest, or not equipped with a headrest. Data from the rear impact tests established response corridors for validation of computer simulation models. Two separate computer models were then developed and validated: one with a headrest, and one without a headrest. The validated headrest-included computer model was then exercised to determine the effect of wheelchair and headrest design features on wheelchair kinematics and loading as well as on ATD injury risk parameters. Outcomes from this parametric sensitivity analysis are used to establish wheelchair and headrest design guidelines for rear impact. Comparisons between ATD outcomes yield information on relative injury risk addressing the effect of wheelchair

design features. A method for characterizing cervical spine stiffness of the encrypted MADYMO Hybrid III 6-year old ATD model was developed mirroring standard ATD neck component testing (National Highway Traffic Safety Administration, 2005). The sensitivity of the ATD injury parameters to ATD cervical spine stiffness was also evaluated.

2.0 BACKGROUND

According to Partners for Child Safety, children that are optimally restrained during travel in a motor vehicle are at significantly lower risk of abdominal injury than children who are not properly restrained (Nance et al., 2004), and 70% less likely suffer serious injury or die in vehicle accidents (Edwards and Sullivan, 1997). In 2001, over 44,000 children under three years of age were injured in motor vehicle accidents, while older children, ages 4-8 were injured in over 76,000 accidents (Iannelli). In 2002, over 227,000 children under age 15 were severely injured in automobile accidents (Yakupcin, 2005). It is estimated that in 2003 alone, over 14,000 individuals over the age of four were saved by wearing passenger restraints (National Highway Traffic Safety Administration, 2004). All states currently require child safety restraints for children through age four and some states such as Pennsylvania extend the regulations to age eight. In addition, many states require older children and adolescents to use adult safety belts while traveling in a motor vehicle (Insurance Institute for Highway Safety, 2006).

In 2002, the NHTSA reviewed rear impact protection (Department of Transportation, 2002) and found that in general, rollovers have the highest rate of fatal outcomes; frontal impacts result in the most fatal outcomes; and rear impacts result in the lowest rate of fatal outcomes. Soft tissue whiplash injuries occur most frequently and have the highest rate in rear impact. Using data from the NASS database from 1988-

1996, there is a 30% whiplash rate in rear impact regardless of the type of vehicle or the type of headrest. Ejected occupants were 14 times more likely to sustain cervical spine injuries than those who are properly restrained. Data from the Japan Traffic Safety Association (Japan Traffic Safety Association, 1997) indicate that the largest number of automotive fatalities result from frontal impacts; however, the largest number of injuries occurs in rear impact. Rear impact accounts for half the total number of injuries from all collisions. Fully 90% of rear impact injuries were neck injuries, accounting for 44% of all vehicular related injuries.

Not surprisingly, based on data from the NASS 1979-1986, the NHTSA, U.S. Department of Transportation found that smaller cars in rear impact show a higher rate of casualties in comparison with larger cars (1990). Rear impacts were categorized into three types: (type 1) simple rear impact, (type 2) impact from rear, then hits a car in front of it, and (type 3) other. Independent of the type of rear impact, this impact outcome difference appears to be much larger in rear impact than in other types of impacts.

The American Academy for Pediatrics recommends that all children under the height of 4'9" ride using child safety seats (Iannelli). Yet, children who use wheelchairs for their mobility needs frequently cannot or should not use child safety restraints for purposes of transportation in a motor vehicle. These children need their wheelchairs to provide them with the same level of safety during transportation in a motor vehicle as other children have while traveling in child safety seats that are positioned on the manufacturer installed vehicle seats and anchored to the vehicle frame.

Both federally approved child safety seats and manufacturer installed occupant vehicle seats also provide posterior head restraint. Yet, children riding in motor vehicles

while seated in their wheelchairs may not have headrests. More significantly, a wheelchair headrest is not an automotive posterior head restraint, nor is it designed for the purpose of passenger protection in a motor vehicle.

2.1 SEATING COMPONENT SAFETY RESEARCH

Seating component safety research for transportation in motor vehicles can be divided between research in the wheelchair transportation safety arena and research in the automotive safety realm. Occupant protection has focused on the integrity of the seat and seatback, and also on the postural supports such as headrests and head restraints.

2.1.1 Wheelchair related research

Seating component safety research for wheelchairs has examined wheelchair seatback loading and deflection, and secondary postural supports. Secondary postural supports include, but are not limited to, headrests, pelvic positioning belts and chest harnesses.

2.1.1.1 Wheelchair seatback loading and deflection

Quasi-static testing, sled testing and computer modeling have all been used to quantify wheelchair seatback loading and deflection. Quasi-static testing is relatively inexpensive and allows for direct measurement of load-deformation. Rear impact sled testing allows for the effects of the acceleration profile where the ATD loads the wheelchair.

Additionally, ATD related parameters can be measured. Computer simulation with a validated model allows the researcher to test many configurations quickly, and to isolate the effect of individual parameters.

Van Roosmalen et al developed a quasi-static test method to evaluate after market wheelchair seating system crashworthiness (van Roosmalen, L. et al., 2000b). The protocol mirrored the FMVSS 207 (Department of Transportation (DOT), 1993a) test method. The wheelchair seatback was loaded using an Instron. This loading accounted for the inertial effects on the seatback, but did not account for occupant seatback loading; this is consistent with low speed impact. Each of the wheelchair seating systems met the strength requirements of FMVSS 207. The paper additionally highlighted the conflicting design recommendations with a yielding seatback being more effective in reducing Abbreviated Injury Scale (AIS) 1 injuries such as whiplash, and stiffer seated reducing more severe AIS 2-6 injuries.

Manary and Schneider (Manary, M.A. and Schneider, 2004) conducted thirteen rear impact tests (16 mph, 10g) using the 187 lb. surrogate wheelchair base, an instrumented seat back, and the 50th percentile male Hybrid III ATD to investigate wheelchair seatback loading during rear impact. They adjusted the wheelchair seatback stiffness to produce maximum post-test seatback deflections of 15, 40, and 60 degrees. The study was conducted to determine the seatback forces in rear-impact crashes as a function of seat back stiffness, and to provide quantitative information for wheelchair manufacturers to improve wheelchair design and seatback strength during rear-impact loading.

Ha developed and validated a frontal impact model using a Mathematical Dynamic Modeling software (MADYMO) model (Ha, DongRan, 2004) and the 6-yr old Hybrid III anthropomorphic test device (ATD). She developed and validated a simulation model that included a manual pediatric wheelchair subjected to a 30 mph/ 20g frontal impact; her model did not contain a headrest. The model was used to conduct a parametric analysis. She investigated the effects of rear securement point vertical location with respect to the center of gravity, finding that securement points located above the center of gravity permitted a rearward rotation of the wheelchair during simulation. Seatback position relative to the rear wheel hub proved to be critical to rearward rotation. Seatback locations behind the wheel hub were associated with wheelchair rearward rotation. Many active wheelchair users choosing this type of configuration to allow them to “pop wheelies” to avoid vertical obstacles. A more upright seatback angle proved to be critical for preventing submarining during simulated impact testing. Using Head Injury Criteria (HIC) and Neck injury criteria (Nij) output, Ha determined that pediatric seated occupants may be subjected to neck and chest injury risk in case of severe frontal impact.

2.1.1.2 Wheelchair postural supports

A variety of methods have been used to evaluate postural support devices for their suitability for use during transportation. Investigations have used quasi-static testing, low speed dynamic testing and computer modeling. Karg tested postural supports using quasi-static testing (Karg, 1993). Later Forziati retested Karg’s headrests using a low speed dynamic test in rear impact with the 50th percentile Hybrid II ATD (Forziati, 1994). Paskoff used the results to develop a rear impact computer simulation (Paskoff, 1995).

Karg's thesis (Karg, 1993) reported the results of her investigation into the loading characteristics of Postural Support Devices (PSDs) to determine the safety of their use during transportation. Using quasi-static testing, she examined the deflection-load response by loading pelvic positioning belts, chest harnesses and headrests with an Instron®. Her overall results indicated that some PSDs were not sufficiently robust to sustain the anticipated loading of a crash event. Her headrest tests produced a variety of failure modes: headrest stems that bent, headrest stems that twisted, and mounting hardware that pulled out from the plywood base. She concluded that with some design modification, commercially available headrests could be effective in preventing rider neck injuries.

Forziati's thesis investigated chest harnesses and headrests in dynamic test conditions (Forziati, 1994). He used the Hybrid II 50th percentile male ATD and a low speed, 7 mph, rear impact crash pulse. His headrest test methodology provided repeatable results. He tested Karg's seven headrests and found that many of the headrests did not fail at this low speed. He also determined that the headrests did limit rearward head motion, with headrests at lower positions limiting the head motion more than headrests in a higher position. His conclusions paralleled Karg's; he asserted that with some design modifications, specifically a more robust vertical headrest stem design, headrests would be effective in more severe rear impact collisions.

Paskoff's thesis (Paskoff, 1995) examined wheelchair and headrest loading during rear impact. He justified his study citing data that indicated that while the percent of severe rear impacts is low (3.5%), rear impact contributes 24% of all automobile related injuries. He used two simulated crash pulses of 5 and 10 mph. Using DYNAMAN

simulation software, he investigated the effects on loading of backrest height (three levels), back stiffness (3 values), tiedown configuration (belt with pretension, without pretension, and rigid tiedown), and headrest stiffness (3 levels). The 50th-percentile male was used for this analysis, and a parametric sensitivity analysis was performed on the stiffness of the neck joints. His results indicated that the DYNAMAN model was not adversely sensitive to neck stiffness. The greatest limitation to his model was that it was not validated in rear impact. He used a model that had been previously validated in frontal impact, and then used force-deflection data from Karg's quasi-static testing thesis work to input into his rear impact model. He did not have an actual rear impact test pulse to use, so he scaled a previously measured 16 mph test pulse and used it in his model. His results indicated that higher seatbacks provided the best head protection at the lower speed, but at higher speed, the opposite effect was observed. Similarly, at lower speeds the rigid seatback provided the best protection, but at the higher speed, the less stiff seat back provided the best protection. He found that the presence of a headrest was the most important factor in prevention of neck injury during rear impact as evidenced by his non-validated computer simulation.

2.1.2 Automotive related research

Automotive research is extensive. The role of the seat, headrest and occupant restraints in rear impact has been well established (Viano, David C., 2002). The following sections describe current automotive research as it relates to rear impact.

2.1.2.1 Automotive seatback research in rear impact

Automotive researchers use field data, quasi-static testing, crash tests and modeling to analyze seatback performance. Several researchers (Saczalski et al., 1993; Thomson et al., 1993; Prasad et al., 1997) have noted conflicting design criteria for high and low speed impacts. Thomson et al (Thomson et al., 1993) reviewed seatback designs in frontal and rear impact conditions to determine the dynamic requirements of automobile seatbacks. For low impact, they found that significant occupant motion could be encountered in low speed impacts because of the elastic rebound of the seatback. At higher impact speeds, the seatback must cushion the occupant from the greater decelerations, maintain occupant's seat position, and prevent contact with interior objects. There is a conflict in these performance characteristics since seatback with stiffness adequate to resist high-speed collisions may provide excessive elastic response under less severe impacts.

Using field data, Saczalski et al (Saczalski et al., 1993) evaluated automotive seatback performance from 46 rear impact accidents, comparing advantages/disadvantages of seatback collapse. Results demonstrated that half of restrained front-seat occupants subjected to rear impact were partially or totally ejected when seatbacks collapsed. Most of those ejected experienced serious to fatal injuries, either from contact in the rear or outside of the vehicle. Stronger, less-yielding and non-collapsing seats are more likely to provide improved safety benefits over seat systems that collapse at relatively low energy levels. While energy absorption is important, the collapsing seats only provide a small fraction of the energy absorbing level needed to safely decelerate an occupant in a controlled fashion, even during the moderate impacts.

Thomson (Thomson et al., 1993) highlighted the need to reduce the relative motion between the head and torso citing the importance of the occupant's offset from the seatback. When occupants lean forward relative to the seatback, it increases the distance through which they move creating occupant offset. He concluded, dynamic loading of the seat will be reduced by adjusting the seatback to reduce this distance. James (James et al., 1991) concurred with Thomson (Thomson et al., 1993), stating that stiffer seatback may increase non-contact neck injury. The seat back deformation associated with seatback yield may reduce injury and societal harm.

Prasad et al (Prasad et al., 1997) investigated the relationship between passenger car seatback stiffness and occupant injury severity. Several commercially available seatbacks were tested using sled test and the Hybrid III 50th percentile male ATD. The rear impact test pulses had change in velocities (delta-Vs) of 5 – 15 mph. His results indicated that stiffer seat backs did not have consistent advantages over yielding seat backs over the entire range of delta-Vs tested. Higher seatback stiffness was associated with higher responses at the neck, thoracic spine, and lumbar spine. Even a seat with a head restraint located closer to the center of gravity of the occupant's head did not perform better than the baseline seat. The lower neck extension moment, measured by the lower neck load cell, was the parameter most sensitive to variation in seat design and crash severity.

Watanabe et al conducted low speed ($\Delta V = 5$ mph) rear impact sled testing to compare the effect of seat characteristics on the Hybrid III ATD and a ($n = 1$) human volunteer (Watanabe et al., 2000). They found that the structural differences between the Hybrid-III ATD and the human subject made it impossible to reproduce the whiplash

motion with the ATD in crash tests. Neck injury criteria (Nij) was decreased as seatback stiffness was reduced.

Molino conducted quasi-static testing of 25 production vehicle seat per FMVSS 207 to assess the rearward strength characteristics of a large number of current seat designs (Molino, 1998). He found two typical failure modes for automotive seat backs: plastic deformation of the members attached to the recliner, and failure of teeth in the recliner. Field data indicates that if a seatback breaks on impact, the need for head restraints is reduced because it may not become involved in altering occupant kinematics. Supporting the optimal design dichotomy between low severity and high severity rear crashes, the authors report that a recent NHTSA study using the National Automotive Sampling System (NASS) crashworthiness data system showed that when an automotive seat maintained its initial upright position after a rear impact, instead of ending up in a reclined position, the rate of whiplash injury increased. However, the data indicates that at up to an impact delta-V of 25 mph the injury cost was less when a seat maintained its upright position.

Gupta et al used MADYMO modeling and impact testing to investigate improving occupant protection through advanced seat design (Gupta et al., 1996). They sled tested using the delta-V 30 mph FMVSS 301 rear impact pulse (Department of Transportation (DOT), 1977) as well frontal delta-Vs of 12, 30, and 40 mph and determined that seatback bending stiffness strongly influenced occupant response in rear impact. A rigid seatback may contribute to occupant rebound. The authors hypothesized that some form of limited and controlled deformation of the front seats is a desirable compromise to reduce whiplash injury while at the same time preventing more serious

injury during severe rear impact collisions; occupant rebound and ramp up can be minimized by designing a seatback that deforms plastically in a controlled manner.

2.1.2.2 Automotive headrest research

Injury due to rear impact conditions has been of particular interest in the auto industry with research efforts directed at reducing neck injury. Seventy percent of car accident injuries involve whiplash injury (Volvo, 2003). Two mechanisms are potentially responsible for producing neck injury. Low speed injuries consist of tissue damage such as whiplash injury, which frequently resolves without intervention (Abbreviated Injury Scale – AIS 1). At higher speeds, more severe injuries predominate.

Lawrence and Siegmund (Lawrence and Siegmund, 2000) evaluated seatback and head restraint response in human subjects during low-speed rear-end automobile collisions. They tested four males, chosen for their anthropometric similarity to the 50th percentile male Hybrid III ATD, in low speed rear impact conditions (delta-V: 1-5 mph). They measured seatback loads, seatback deflection, and head restraint loads during vehicle-to-vehicle collisions with a single seat and seat position. Results indicated that head restraint and seatback response parameters varied linearly with speed change; none varied with seat belt use in rear impact. The authors concluded that during low-speed rear-end collisions, the seat back and head restraint are the primary interfaces between the vehicle and occupant. Automobile seats are the primary safety device for potentially preventing or mitigating whiplash-type injuries regardless of vehicle type. This result highlights the need for adequately robust seat backs and head restraints for wheelchairs during transportation in a motor vehicle.

In the automotive industry, both Saab (Saab, 2006) and Volvo (Johansson, 2006) have developed active headrest systems to reduce whiplash injury. The Saab Active Head Restraint (SAHR) activates during rear impact. As the rider presses back into the seat, the head restraint moves forward. Saab's SAHR has proven to reduce incidence of moderate and long term whiplash injury in Saab vehicle models with the system when compared to Saab vehicles without the SAHR (Viano, D. and Olsen, 2001). Volvo has shown that its Whiplash Injury Protection System (WHIPS) reduces short term injury by 33%; this data is supported by the Swedish Road Administration and the Insurance Institute for Highway Safety (Volvo, 2003). WHIPS operates by allowing the seatback and headrest to rotate together; the head and back remain in line, reducing neck forces and moments.

2.1.2.3 Automotive occupant restraint research

The clear benefit of occupant restraint use in automotive is reflected in national safety belt laws. Research has focused on evaluating field data, conducting crash testing and using modeling to quantify these benefits. Field data suggests that rear impact crashes contributed to less than 4% of the number of occupant fatalities from 1970-1985, yet played a key role in injury. (James et al., 1991) James et al found that lap belts are critical to occupant safety in rear impact and can effectively reduce injury by decreasing seatback ramp-up. Lap belts restrained hips and limited rearward and upward trajectory of the head and torso during rear impact. (James et al., 1991) Lap belts reduce the relative velocity of the occupant with respect to the vehicle interior, may reduce the forward rebound of the occupant, and contribute to a reduction in societal harm of 37-47%.

Wagner investigated 3-point occupant restraints in both humans and ATDs. He conducted crash tests ($\Delta V = 30$ mph) using the Hybrid II 50th percentile male and

standard Audi 80s (1979 model) (Wagner, 1979). Results demonstrated the effectiveness of the 3-point occupant restraint in preventing injury in human subjects. In some cases, ATD and human loading differed with the belt forces and the head acceleration values considerably lower with human occupants than with ATDs. Wagner attributed these differences to the human driver anticipating the impact and using his arms to brace himself against the steering wheel.

Saczalski et al (Saczalski et al., 1993) evaluated the potentially beneficial role of seat-mounted occupant restraints by conducted sled tests comparing the stiffer Mercedes Benz 500SL seatback with an integrated restraint and the BMW 850 seatback. Results indicated that the stiffer seat frame with seat-integrated belt system increased the occupant-protection effect in the event of a rear-end collision for those occupying the front seats, as well as those in the rear of the car. These results point to the potential improvement in occupant safety afforded by the 2002 adoption of the integrated lapbelt into WC19 – *wheelchairs used as seats in motor vehicles*. Thomson et al (Thomson et al., 1993) determined that rearward deflection of the seat base compromises the lap portion of the vehicle-mounted occupant restraint by creating more space for the occupant to move. This finding provides additional support for WC19 standard requiring wheelchair mounted lap belts.

2.2 HYBRID III 6-YEAR OLD ANTHROPOMORPHIC TEST DEVICE

The Hybrid III 6-year old ATD is part of the larger family of Hybrid III ATDs. The ATDs range in size from the 12-month old CRABI to the 95th percentile Hybrid III male.

The Hybrid III family of ATDs was first developed at GM in the mid-70's, and has been used in impact research since that time.



Figure 1: Hybrid III ATD family

2.2.1 Development of the Hybrid III 6-year old ATD

In 1976, the Children's hazard division, Bureau of Product Safety, Food and Drug Administration conducted study of the anthropometrics of children (Snyder et al., 1975). They measured 4027 infants and children from eight states, many daycare centers, preschools and elementary schools. Though cited limitations of their study included wriggling children and incomplete measurements, they determined the center of mass of the children in the supine and seated positions. To create the ATDs, Masterbody forms were crafted out of dental stone that conformed to the FDA measurements, the most comprehensive data available at the time (Young et al., 1976). In addition to the measurements made during the anthropometric study, many more measurements were needed to construct the ATD forms. Two additional children, a 3.5 and a 5.5 year old ($n = 2$) were extensively measured, and their data were then scaled to fit the study data. The model was cured, then cut into segments to determine masses and center of gravity (CG)

for each segment. The calculated values assume that all parts of the body are equally dense.

The mass and weight specifications of the currently used Hybrid III 6-year-old ATD are based on these average characteristic dimensions taken from anthropometry studies of 6-year old boys and girls (Society of Automotive Engineers: Dummy Testing Equipment Subcommittee, 2003). The current ATD physical dimensions are based on the anthropometric data previously collected during the 1970s from children in the United States (Irwin and Mertz, 1997), and the masses of the segments of the 6-yr-old ATD were obtained from the Masterbody Form.

The biomechanical basis for the Hybrid III 6-yr old ATD is outlined by Irwin and Mertz (Irwin and Mertz, 1997). This work, conducted in the 1990's, was still predicated on the FDA anthropometric study conduct by Snyder et al (Snyder et al., 1975) in the 1970's. Using this data, impact responses were scaled from the Hybrid III 50th percentile male, taking into account the differences in size, mass, and elastic modulus of pediatric bone. Head impact response requirements, and neck flexion and extension requirements as well as chest impact response requirements, knee impact response and knee drawer stiffness requirements were determined for all pediatric sizes. The resulting biofidelity requirements provided the basis for the development of CRABI 6, 12, and 18 month old and Hybrid III 3 and 6 year old child ATDs. It is noted that the elastic modulus of the bones was based on a limited study of the cranial bones of two newborns and one six year old (n=3).

The Hybrid III ATD was developed through joint efforts on the part of SAE and NHTSA. There was a major upgrade of the dummy in 1997 in response to the need to

evaluate the effects of airbags on children (First Technology Safety Systems, 2005). The Hybrid III was accepted for FMVSS 208 (NHTSA, 1993) in 1986, is considered the industry standard, and has extensive optional instrumentation available. In addition to the triaxial accelerometer pack for the head, thorax and pelvis, there are 6-axis load cells available for the upper and lower neck, lumbar spine and femur as well as a chest deflection transducer. The Hybrid III is proposed to replace the Hybrid II in FMVSS 213 (NHTSA, 1999).

2.2.2 Hybrid III 6-year old ATD neck

There has been a great deal of discussion concerning the Hybrid III 6-year old ATD and the mobility of the neck. The Hybrid III has several advantages over the Hybrid II ATD primarily in the area of instrumentation (First Technology Safety Systems, 2005). Specifically, the Hybrid II neck lacks instrumentation. The measurement devices available for the Hybrid II include head accelerometers for measuring HIC, three torso mounted uniaxial accelerometers, uniaxial accelerometers for the ball hip joints, and femur force gauges to measure knee impact forces. MADYMO does not have a Hybrid II 6-yr old ATD model, thus for modeling purposes it is preferable to sled test using the Hybrid III to establish the response corridors.

Many researchers have used the Hybrid III family of ATDs in the evaluation of rear impact crash events. It has been both examined and used extensively in the literature. Efforts have been made to highlight the strengths and limitations of the ATD as well as to use it as a human surrogate in crash tests.

In 2003, Sherwood, Shaw, et al. conducted a comparison of Hybrid III ATD tests, cadaver tests (age = 12 years old, n = 1) and MADYMO modeling in forward impact (Sherwood et al., 2003) as well as a review of field data. Three separate conditions were tested with the ATD: high booster seat, low booster seat, and 3-point belt only. The test pulse was the FMVSS 213 (NHTSA, 1999) forward acceleration pulse. In all cases significant ATD spine flexion was observed that resulted in the chin and face of the ATD coming in contact with the ATD's chest. The cadaver test conditions were similar to the ATD 3-point belt test. No booster seat was used, reflecting the cadaver age of 12 years. While the cadaver face also contacted the chest, this was caused by bending along the entire spine; ATD facial contact was due to flexion of the cervical spine alone – caused by the stiffness of the ATD's thoracic spine. The standard MADYMO 6-yr old ATD model was compared to a model that was modified by adding an additional one degree of freedom rotational joint in the mid-thorax. This modification allowed the model thoracic spine to behave more like the cadaver's spine – and more significantly reduced the upper neck N_{ij} and upper neck tensile load by half. The lower neck flexion moment was reduced by 2/3. Based on field data, the authors found that non-contact cervical spine injuries are extremely rare in children that are properly restrained in frontal impact crashes, yet sled tests with the Hybrid III 6-yr old ATD consistently exceed IARV in the neck. The authors concluded that the ATD response is not biofidelic; yet, the results from the MADYMO modeling show that the addition of thoracic spinal flexibility significantly decreases all forces and moments in the neck and improves the ATD's kinematics relative to the cadaver's.

In 1996, Öster and Trommler evaluated three different dummies: 6-yr old Hybrid III, Part 572 and TNO P6 (Oster and Trommler, 1996). The performance characteristics were compared using a series of sled tests. Two pulses were used – the Volvo 850 pulse and the ECE R.44 pulse – both are 30 mph pulses with different profiles. Results indicated that the Hybrid III sitting posture is better than the other two dummies; body measurements compare well. The head masses differ with the Part 572 having the lightest head and Hybrid III having the heaviest head. The differences in ATD kinematics can be attributed to the differences in the design of the spine and neck. The P6 has a soft spine and neck, which allows much greater motion. Hybrid III shows the lowest values for HIC. The P6 ATD had head-knee contact in every test except one; the Hybrid III demonstrated similar head-knee contact in only one test. Maximum accelerations for the part 572 and the Hybrid III were similar. The Hybrid III and part 572 proved to be repeatable test devices.

In 2003, Van Rooij, Sherwood, et al used the Hybrid III 6-yr old ATD and MADYMO modeling to examine the effect of pretensioning and force limiting of seatbelts on injury risk (Sherwood et al., 2003). This research team first validated the model with sled tests and then did a parametric study to determine the effects of seatbelt slack and force limiting seatbelts. They were far more successful at validating the lower neck load cells than they were for the upper neck load cell. They hypothesized that this was due to a difference in the orientation of the head at the time that the chin contacts the chest. In general, Nij, based on data from the upper load cell, provides reliable data until chin-chest contact. In addition, the lower neck load cell “bottoms out” at a Y-moment of 250Nm – the MADYMO model has no such limitations. In general, the researchers felt

that a close fit was obtained for all signals, except shoulder belt force and sternum deflection. They found that sternum deflection in the model was highly sensitive to shoulder belt chest location; small shoulder belt position changes significantly affected the sternum deflection. The model upper neck load cell response frequently differed from the experimental response. The researchers hypothesized that this was caused by the high model sensitivity to geometry and timing.

In 2004, Malott and Arbogast (Malott et al., 2004) used the Hybrid III 6-year old ATD to evaluate various occupant restraints (high back booster, low back booster, 3 point belt, integrated booster with belts, lap/shoulder belts with lap and shoulder guides and with shoulder guides only) and three crash configurations. They conducted sled tests in forward, side and oblique (30 degrees) impact configurations. For frontal impact, key findings include N_{ij} measures showing some differences among the restraint configuration, but in all configurations measured neck tension was high – just below or exceeding the IARV. For the oblique impact, while the peak head and chest numbers were lower for booster seats than for 3-pt belts, there was no clear pattern when looking at chest injury measures. The authors note, that similar to Van Rooij (van Rooij et al., 2003), chest displacement is highly dependant and sensitive to belt placement and the values should be viewed with caution. The authors' discussion points out that while the frontal tests produce high N_{ij} – especially for the high back booster seats, this is NOT reflected in real world data. Real world data from crashes involving booster seats demonstrate that injuries to this body region are extremely rare. Also, of note is the fact that the head did NOT contact the chest in any of these tests.

Most recently, Ha used the Hybrid III 6-year old ATD for her investigation into pediatric wheelchair frontal impact testing. She highlighted the advantages of using the Hybrid III as improved biofidelity and instrumentation capabilities (Hobson and Schneider, 2003). She achieved excellent validation of her MADYMO model with a ‘Global Score’ of 93%. (A score 75% is considered to be a good model.) Ha does highlight the lack of ATD validation with respect to actual biomechanical impact responses of humans or cadavers as a study limitation.

It seems most appropriate to use the Hybrid III 6-year old ATD for our study for a number of reasons. Department of Transportation regulations require the use of this ATD for safety testing for FMVSS 208 (NHTSA, 1993) and have proposed its use for FMVSS 213 (NHTSA, 1999). It is the industry standard. MADYMO modeling software supports it with a well validated model that is referred to extensively in the literature. In addition, the Hybrid III – 6 yr old ATD has a modified neck that reflects additional work done by GM with respect to airbag deployment tests.

2.3 ATD INJURY MEASURES

Several different measures have been used in an effort to predict the likelihood of human injury based on measurable criteria. Due to the impracticality and unethical nature of testing human subject response to injurious loading, a variety of surrogate measures has been used. Live human subject testing has been conducted at low non-injurious loads; higher loads have been tested with cadavers, sub-human primates, and non-primate

mammals. Additionally, both physical and mathematical models of the head or head and neck, have been used to establish measurable parameters to assess injury risk (Klinich et al., 1996; McLean and Anderson, 1997).

2.3.1 Neck injury criteria

Neck injury typically results from several specific mechanisms (King, 2000). The neck can be loaded axially in tension or compression, bending in flexion or compression, or laterally with bending. Each of these mechanisms combines to produce typical neck injuries. Compression-flexion injuries occur most often because of rollover or ejection from the vehicle; compression-extension injuries result from head contact with the windshield in frontal impact; tension-flexion injuries are very rare and have been produced in the testing lab with severe frontal impacts (120g) in sub-human primates; lateral bending injuries result from side-impact collisions; and tension-extension injuries result from rear impact. During the severe rear impact collision, it is thought that tension in the neck occurs as the neck is stretched out over the headrest or seatback. Neck injury tolerances have been historically difficult to determine because of structural non-linearity of the neck itself, intrinsic variability between biological subjects, and the effect of initial position and directional loading on outcomes. It is clear from field data that neck injury from rear impact is far more common than from frontal impact, and occurs with far less severe crashes in rear impact as compared to frontal impact.

The neck injury criteria (Nij) establishes critical limits for axial loading and bending moments. The Nij is defined as (Kleinberger, Michael et al., 1998):

Equation 1: Neck injury criteria

$$N_{ij} = \frac{F_z}{F_{int}} + \frac{M_y}{M_{int}}$$

Where, F_z = axial load

F_{int} = critical intercept load value used for normalization

M_y = bending moment

M_{int} = critical moment intercept value used for normalization

The critical values were developed during the 1980s by auto manufacturers using pigs and a 3-year old ATD. Identical crash tests were conducted on the pigs and on the ATDs. The identified pig injuries were matched with the instrumented outputs from the ATDs during identical testing. These force and bending moment critical values were then scaled for the remaining dummies in the Hybrid III ATD family. Tension/compression critical values for the Hybrid III small female and mid-sized male were determined independently using cadaver studies. The established critical values are not necessarily intended to represent the actual forces and moments that would severely injure an individual's neck; instead, the critical values are the forces and moments recorded by ATDs during impact that are thought to correspond to injury in humans. The difference takes into account limitations in the biofidelity of the ATD neck; the ATD recorded forces and moments correspond directly to injury in pigs during identical crash events.

The neck injury criteria (N_{ij}) is a linear combination of the normalized axial load and normalized bending moment. The N_{ij} is composed of two axes: i , axial load (tension (+)/compression(-)) and j , sagittal bending moment (flexion(+)/compression(-)) (Kleinberger, Michael et al., 1998). This divides neck injury into four injury mechanisms: N_{TE} tension-extension, N_{TF} tension-flexion, N_{CE} compression-extension, and N_{CF}

compression-flexion. There are two ways of evaluating neck injury. The first method is to compare the maximum axial loading and the maximum bending moments independently against the maximum allowable values using the FMVSS 208 alternative guidelines (National Highway Traffic Safety Administration, 1993). The second method is to compute the normalized neck injury criteria. A $N_{ij} = 1$ relates to a 15% probability of serious injury; $N_{ij} = 1.4$ relates to a 30% probability of serious neck injury.

2.3.2 Head injury criteria (HIC)

Research has shown that the likelihood of a brain injury resulting from an impact is related to both peak accelerations and time duration of those accelerations (McLean and Anderson, 1997). The head injury criteria (HIC) was developed by the NHTSA in 1972 to determine the likelihood of head injury and takes into account the effect of the acceleration time duration. (McHenry, 2004) The basic research on head acceleration due to impact and injury was first conducted by Gurdjian in 1955; he investigated the relationship between skull fractures and concussion and concluded that skull fracture severity was indicative of brain injury (Gurdjian et al., 1955). This information was later used to develop, first the Wayne State Tolerance Curve (WSTC) and later the Gadd Severity Index (GSI). The HIC is preferable to a simple measure of head acceleration as it takes into account the effect of the acceleration duration.

The HIC is calculated using the following equation:

Equation 2: Head injury criteria

$$\text{HIC} = \left[\frac{1}{(t_2 - t_1)} \int_{t_1}^{t_2} a(t) dt \right]_{\max}^{2.5} (t_2 - t_1)$$

a = linear head acceleration, (g)

t₂ - t₁ = time interval, (ms)

There have been two separate time intervals used: 36 ms (Kleinberger, Michael et al., 1998) and 15 ms (Eppinger et al., 1999). The time interval is selected using an algorithm to bracket the maximum linear head acceleration and maximize the HIC value. The HIC₃₆ with a time interval of 36 ms, is more sensitive to lower accelerations of longer duration. The HIC₁₅ with its shorter time interval, is less likely to yield a high value for less injury producing lower acceleration – longer duration impacts (McLean and Anderson, 1997). The HIC₃₆ is specified in FMVSS 213 – *Child Restraint Systems* (National Highway Traffic Safety Administration, 1999); both are specified in FMVSS 208 – *Occupant Crash Protection* (National Highway Traffic Safety Administration, 1993).

Table 1: Head injury criteria limits (Kleinberger, Michael et al., 1998; Eppinger et al., 1999)

	Mid-sized male	Small female	6 - year old	3 - year old	12month old
HIC ₃₆ Limit	1000	1000	1000	900	660
HIC ₁₅ Limit	700	700	700	570	390

Although, the ATD has issues related to biofidelity, the HIC values are a widely used measure to predict the probability of human injury. A HIC value of 1000 corresponds to a

23% probability of an AIS ≥ 3 injury, and a 16% chance of an AIS ≥ 4 injury (Cavanaugh, 2000).

2.3.3 Head acceleration

Peak linear head acceleration is used in calculating the HIC values. Rotational head acceleration has been linked to diffuse axonal injury (DAI) where the brain tissue is damaged through shearing. (Ommaya et al., 2002) Rotational accelerations may be more likely to cause head injury (Klinich et al., 1996; Kleinberger, Michael et al., 1998; Eppinger et al., 1999; Ommaya et al., 2002). Rotational acceleration is thought to be damaging because the resulting shear forces tear the bridging veins and/or axons within the brain. Most head accelerations are a combination of both linear and rotational acceleration. Research by Thibault et al (Thibault et al., 1987) suggests that in addition to the peak angular acceleration, the maximum change in angular velocity of the head is another useful parameter in assessing diffuse head injury.

The Hybrid III child ATD out-of-position child protection values are as follows:
(Klinich et al., 1996)

Table 2: Hybrid III child ATD out-of-position child protection values

	3 year old	6 year old
Peak head linear acceleration (g)	80	80
Delta-rotational head velocity (rad/sec)	34	33
Rotational head acceleration (rad/sec ²)	2200	2100

According to Ommaya (Ommaya et al., 2002) children with their small head masses, can sustain larger rotational head accelerations without injury than adults. His data indicate that adults are likely to sustain concussions at rotation accelerations of 4500 rad/sec², while newborns are likely to sustain concussions at 10,000 rad/sec².

2.3.4 Chest acceleration

Maximum chest acceleration is specified in both FMVSS 208 and FMVSS 213. They state in similar language that chest acceleration may not exceed 60g's except for intervals whose cumulative duration is ≤ 3 ms (National Highway Traffic Safety Administration, 1993; National Highway Traffic Safety Administration, 1999). These standards are for frontal impacts, where the ATD loads the occupant restraint and there is concern regarding both chest deflection and injuries resulting directly from the occupant restraints. In rear impact the ATD's torso is fully supported by the wheelchair seatback – providing that it does not fail.

2.3.5 Excursion limits

For individuals who use their wheelchairs while riding in a motor vehicle, WC19 addresses horizontal excursion limits for frontal impact in a 30 mph, 20g impact (ANSI/RESNA, 2000). The standard identifies maximum limits at the wheelchair P-point, ATD knee center, ATD front of the head, and ATD back of the head. Additionally, the WC19 minimum limit on the ratio of the knee excursion to the wheelchair excursion ($x_{\text{knee}}/x_{\text{wheelchair}} \geq 1.1$) ensures that the wheelchair does not load the occupant during

frontal impact. During rear impact, the ATD moves rearward, loading the wheelchair; thus, the knee excursion and the $x_{knee}/x_{wheelchair}$ ratio have limited applicability during rear impact test conditions.

The forward and rearward head excursion limits specified in WC19 apply directly to rear impact and may reflect injury risk to the wheelchair seated occupant. The head excursion limits for the 6-year old Hybrid III ATD are 450 mm forward and -350 mm rearward.

Table 3: WC19 horizontal excursion limits (mm) (ANSI/RESNA, 2000)

Measurement point	Excursion variable	ATD – Hybrid III		
		6-year old	Small female	Midsized and large male
Wheelchair point P	$X_{wheelchair}$	150	200	200
ATD knee center	X_{knee}	300	375	375
ATD front of head	X_{headF}	450	550	650
ATD back of head	X_{headR}	-350	-400	-450

2.4 RELEVANT AND RELATED STANDARDS

There are several standards related to wheelchair headrests during rear impact, though none address it directly in a dynamic crash test environment. WC19 – *Wheelchairs Used as Seats in Motor Vehicles* (ANSI/RESNA, 2000) is a frontal impact 30 mph / 20g crash test. It does not address headrests specifically, but requires that pieces over 3.5 ounces not become detached from the wheelchair during frontal impact. It would seem that this

basic criterion ensures that the headrest will, at the very least, not slide out of its mounting during an abrupt deceleration, possibly injuring occupants inside the motor vehicle. Yet, this requirement falls far short of ensuring headrest safety for the wheelchair user. There is no requirement that a WC19 wheelchair crash test include a headrest; although our research indicated that most pediatric wheelchairs are delivered either with a headrest or with a headrest mounting bracket. Even when the wheelchair is tested with an attached headrest, the 3.5 ounce requirement fails to address the need for headrest crashworthiness; necessary, since the headrest may effectively serve as a head restraint during evasive driving maneuvers or rear impact collision.

The ISO standard addresses the need for a robust wheelchair headrest during normal usage through both quasi-static testing and pendulum testing. ISO/FDIS 16840 - Part 3 (ISO, 2005b) provides the test methods to determine the ability of PSDs to withstand static, impact and repeated loading. Explicitly stated in the scope of the draft standard, is the note that it does not test the ability of the PSD to withstand vehicular crash conditions. For these tests, the PSD is mounted to a rigid test fixture and tested to failure. The specified pendulum impact test method is extremely severe; a 25 kg pendulum bob suspended from a 1.2 m pendulum drops from an increasing angle up to 90 degrees until the headrest exhibits structural failure. Based on the anticipated loading by the Hybrid III 6-year old ATD on the headrest during rear impact testing, this test exceeds the design requirements needed for rear impact loading under our test conditions.

The Japanese Industrial Standard (JIS) for head support PSDs calls for the same 25 kg / 1.2 m pendulum configuration as the ISO 16840-3 with test methodology specifying a 45 degree pendulum drop repeated 100 times (Hirose and Aikawa, 2005).

This is identical to the JIS wheelchair back rest impact test. The test method is, again, extremely rigorous and far exceeds the loading anticipated during a severe rear impact event.

Automotive standard FMVSS 202 (Department of Transportation (DOT), 2000) specifies head restraint requirements with the intent to reduce the frequency and severity of neck injury in rear-end and other collisions (Department of Transportation (DOT), 2004). It defines the physical requirements for automotive head restraints including size and position in the motor vehicle as well as requirements for quasi-static or dynamic testing. Dynamic testing specifies a rear impact deceleration of at least 8g's that results in an angular displacement of the head reference line of less than 45 degrees. The alternative quasi-static testing requirement is for the head restraint to be able to sustain an increasing rearward load of up to 200 lbs.

Automotive tests that may relate to wheelchair rear impact testing are the seatback tests and the fuel tank integrity test. FMVSS 207 – Seating Systems (Department of Transportation (DOT), 1993) specifies the requirements for forward facing automotive seats, attachment assemblies, and installation with the intention of reducing the incidence of failure during crashes. This standard requires a dynamic testing of the adjustment mechanisms at 20g rear impact in addition to quasi-static loading of the seatback in both forward and rearward directions, yet does not address head restraints directly.

The fuel tank integrity test, FMVSS 301 (Department of Transportation (DOT), 1977), incorporates a severe 30 mph rear impact test pulse to test for fuel tank integrity. The test is conducted with a Hybrid III 50th percentile male ATD, however there are no requirements for seatback integrity, head restraint integrity, or ATD containment.

FMVSS 213 – Child Restraint Systems (National Highway Traffic Safety Administration, 1999) is a 30 mph /20 g forward impact test pulse. The ECE R44.03 (Economic Commission for Europe, 2002b) is the European child restraints standard and features test pulse in front, side and rear impact. The ECE R44.03 rear impact test pulse is 18 mph /14 – 21g. Australia adopted standard AS 2942-1987 – Wheelchair Occupant Restraint Assemblies for Motor Vehicles, featuring a 10 mph, 8 – 15 g rear impact test pulse (Standards Association of Australia, 1987).

3.0 EXPLORATORY STUDIES

This dissertation was driven by our exploratory research which highlighted the frequency of headrest use for pediatric wheelchair users. Preliminary work also included developing a method for evaluating a wheelchair headrest design before using it in a full sled test.

3.1 PRESCRIPTION PATTERNS OF SECONDARY POSTURAL SUPPORT DEVICES AND CONCERNS RELATED TO THEIR USE DURING VEHICLE TRANSPORTATION

3.1.1 Abstract

A questionnaire was developed to better understand which postural support devices are most frequently prescribed for wheelchair users and to determine which postural support devices create the greatest concern for user safety during transit in motor vehicles. The questionnaire was posted on listserves used by seating and mobility clinicians. Seventeen clinicians responded to the questionnaire. Results indicate that prescription patterns are similar for both pediatric and adult clients. Pelvic positioning belts are prescribed most frequently followed by headrests, lateral supports and chest harnesses. The postural support device of most concern was the head restraint, followed by chest harnesses,

subASIS bars and headrests. Several clinicians indicated that specific secondary postural supports were required for transit in their districts.

3.1.2 Introduction

According to the Department of Transportation, over 500,000 individuals with disabilities who never leave their homes report difficulties with transportation (Everly et al., 1993). Accessible transportation has been identified by the National Organization on Disability as key to workplace and community integration; likewise, poor access to transportation acts as an integration barrier (National Organization on Disability, 2002). Once an individual who uses a wheelchair boards a vehicle, there can still be significant difficulties in safely transporting the wheelchair-seated occupant.

In general, wheelchairs are designed to enhance users' mobility, while automotive seats are designed to provide safety and comfort for occupants while anchored to the vehicle frame (Snell, 1999). Furthermore, wheelchair postural support devices that will enhance mobility may pose an injury risk during transportation. Primary postural support devices are defined as the seat and the seatback; secondary postural support devices (SPSD) are all other postural supports including: headrests, chest harnesses, neck supports, head straps, pelvic positioning belts, lateral supports, etc.

Current standards primarily address the issues of SPSDs in three ways (Society of Automotive Engineers, 1996; ISO, 1999c; ISO, 1999d; ANSI/RESNA, 2000; ISO, 2005a). One is through recommendations that wheelchair and WTORS manufacturers are required to include in their user instructions and warnings, and through required product labeling. The second is through a design requirement that all sharp edges be covered with

energy-absorbing material to minimize the potential for puncture injuries and lacerations in a crash. Finally, wheelchair standards require that no rigid components with a mass greater than 100 g become detached from the wheelchair during the frontal impact test.

In contrast, automotive manufacturers take a different approach and look at seat components such as headrests as safety devices to prevent whiplash associated disorders(Welcher and Szabo, 2001). While wheelchair users' seating needs may vary, it is necessary to evaluate which SPSDs are commonly used and which ones create safety concerns. Evaluation of the performance of the most frequently used SPSDs will provide information that can be used to enhance the safety of the wheelchair-seated rider.

The purpose of this research was to determine: usage rates for specific SPSDs, adult usage as compared to pediatric usage, differences in prescribing practices of clinicians that have pediatric versus adult clients, SPSDs that are of most concern to clinicians, and specific requirements of school districts for use of SPSDs.

3.1.3 Methods

A questionnaire was developed to gather information on SPSD practice. Data of interest were clinician descriptions of clients including percent of adult and pediatric clients and the distribution of diagnoses in their caseloads. The questionnaire queried clinicians on the approximate percentage of their clients that use specific secondary postural support devices. For each device, clinicians used a Likert scale to indicate the degree of their concern for injury from the device in a crash, and to describe the nature of their concerns. Last, the questionnaire asked clinicians to identify which SPSD are required for students or adults who are transported in their district or program.

The questionnaire was evaluated for understandability and clarity by two clinicians in the Center for Assistive Technology (University of Pittsburgh Medical Center Health System) and then posted on the following listserves: SIG 09 (RESNA), RESNA listserve, and Tech SIS (AOTA). Responses were entered into an Excel spreadsheet and ranked.

3.1.4 Results

Seventeen clinicians responded including seven occupational therapists, five physical therapists, and three rehabilitation engineers. Most of the respondents (15) have a mixed clinical practice with both pediatric and adults clients. Results are presented for three categories: all clinicians, those that have >80% adult clients, and those that have $\geq 20\%$ pediatric caseload. A 20% pediatric caseload corresponds to approximately one day per week. The clinicians reported having been in practice on average for 14.9 ± 9.2 years, with a range of 3 – 30 years, and a median of 15 years experience. One clinician sees only adult clients and did not respond to those questions pertaining to pediatric clients; likewise another clinician sees only pediatric clients and did not respond to those questions pertaining to adults.

The data for adult clients indicated that clinicians that see fewer pediatric clients prescribe secondary postural supports less frequently than those that see more pediatric clients. Yet, when the adult-client data was ranked, there were only small differences between respondents that saw more pediatric clients and those that saw fewer. All respondents ranked pelvic positioning belts, headrests, lateral supports and chest harnesses in the top four most frequently prescribed SPSPDs. All categories ranked head

restraints (head straps and neck supports) and subASIS bars as least frequently prescribed.

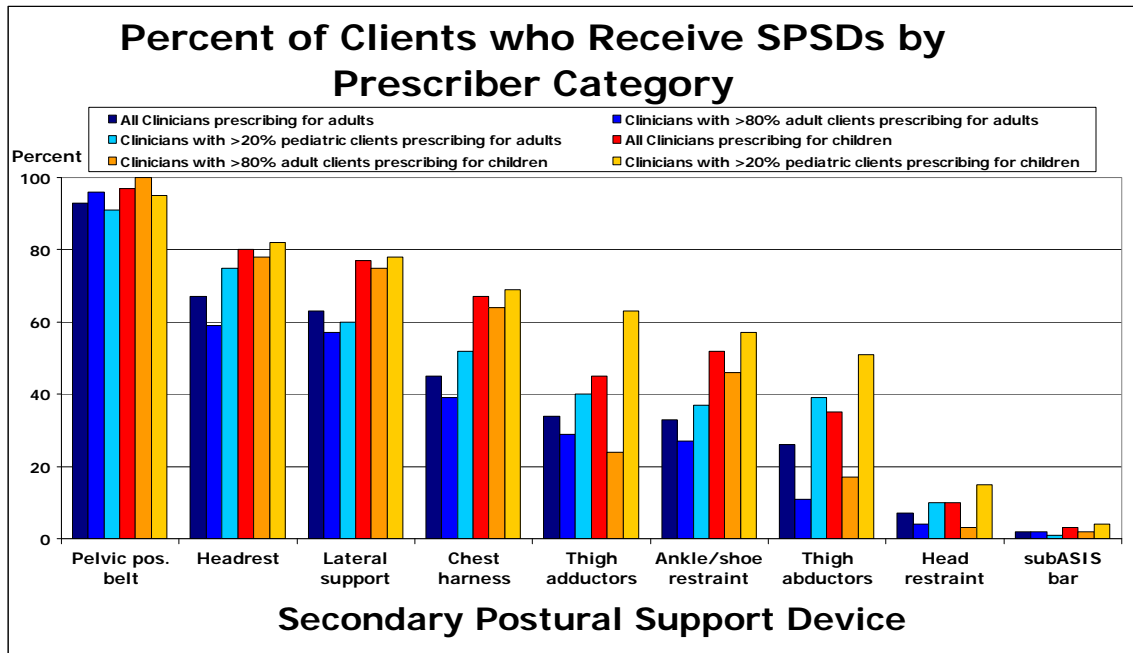


Figure 2: Percent of client who receive SPSDs by prescriber category

The prescription patterns for pediatric clients were similar to those for adult clients, for all three categories. Those clinicians that see at least 20% pediatric caseload prescribe SPSDs for their pediatric clients more frequently than those clinicians that see fewer pediatric clients. Yet, the four most frequently prescribed SPSDs are the same for all categories and the same as for adult clients. Of note, the ranks are the same, but the frequency of prescription for pediatric clients is higher than for adult clients, sometimes 1.5 times as high.

All practitioners reported concern for use of head restraints during a crash. Most also ranked chest harnesses and subASIS bars high for concern in a crash. This concern was related to improper usage and to entrapment when emergency evacuation is needed. Of least concern were lateral supports and thigh adductors. These responses were similar

for both pediatric and adult clients as well as for clinicians that treat adults and for those that treat more children.

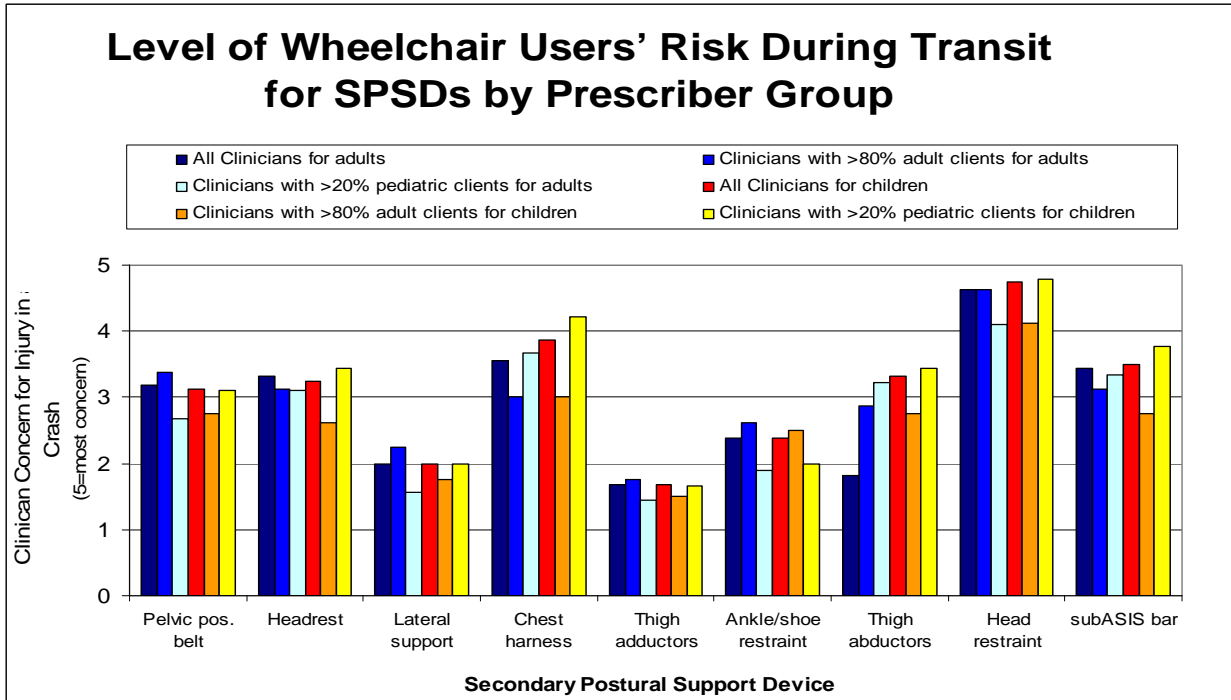


Figure 3: Level of wheelchair users' risk during transit for SPSDs

Six clinicians (35%) reported their program or district require specific SPSDs for transport. The most frequent requirements are for pelvic positioning belts, headrests and chest supports. According to the respondents, many school districts will not transport a child in a wheelchair unless the child has all of these devices – regardless of the child’s functional needs.

3.1.5 Discussion

This survey was designed to aid this research team in determining which SPSDs warrant further investigation. The two issues are frequency of prescription and concern for crash

safety. While pelvic positioning belts are usually prescribed, clinicians are not concerned about their safety – except when they may be confused with occupant restraints that meet federal safety standards. Conversely, while head straps and subASIS bars are infrequently prescribed, there is a great deal of concern about their safety during transit.

The greatest concern expressed in the survey echoed a survey done in two states over ten years ago (Everly et al., 1993). At that time, respondents were asked in their survey to make recommendations for improvement of the methods of safe transportation; their most often cited recommendation was to provide head/neck support. It is extremely important for children riding on school buses to have their faces in a visible position. Children that use wheelchairs for mobility may also have respiratory or seizure problems and it is imperative that their faces be visible for signs of distress.

This was a small study (n=17) and survey respondents were self-selected. As such, they may be more aware of wheelchair transportation safety devices and practices than the typical seating specialist; this subset of clinicians may differ in prescribing patterns than the general population. Future work could focus on several areas. A larger study could be conducted to sample a greater number of clinicians. Specific questions could be added to clarify which SPSDs are commonly used together and in what combinations. In addition, clinicians could be asked which geographic area or school district they represent so that geographic representation could be assured.

3.2 HEAD VELOCITY

3.2.1 Introduction

We initially tested two identical pediatric manual wheelchairs without headrests. In addition to the subsequent full analyses of all wheelchair, wheelchair tiedown and occupant restraint systems, and ATD responses from sled testing, this preliminary study initially focused on the pediatric head response under rear impact conditions. The purpose of this preliminary analysis was to characterize the kinematics of the head for subsequent headrest evaluation.

3.2.2 Methods

Kinematics of the Hybrid III 6-year old ATD were evaluated using two identical Quickie brand Zippie transit-option pediatric manual wheelchairs (17.9 kg) with a rear impact crash pulse of 25.8 km/h, 10g. The crash pulse was proposed for use in developing a draft voluntary industry standard evaluating wheelchair performance in rear impact. Wheelchairs were equipped with a planar seat and seat back. A four-point surrogate wheelchair tiedown and three-point occupant restraint system (WTORS) was used for these tests (ANSI/RESNA, 2000). While the tests were instrumented to measure loads and accelerations of the ATD, WTORS loads and wheelchair kinematics, this preliminary study focuses solely on the head motion. High contrast targets were placed the ATD head and on a 12 inch scale that was bolted to the crash sled a shown in Figure 4.

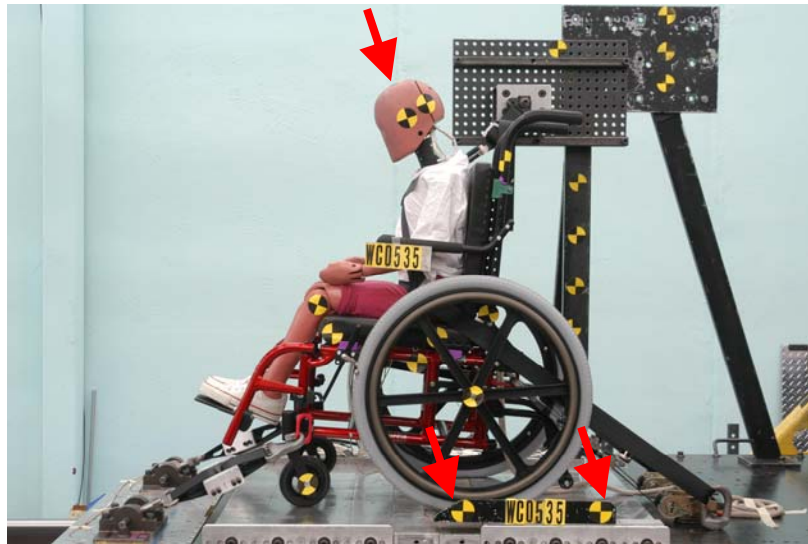


Figure 4: Location of head and scale targets

High speed video cameras (1000 frames/sec) were used to record the test. A strobe flash was used to synchronize the video data with instrumentation output. Both tests had the identical experimental set up with the exception of the seat back location. In Test 1 (WC0535) the bottom edge of the seat back was located 25 mm above the seat cushion; in Test 2 (WC0536) the bottom edge of the seat back was in contact with the seat cushion. A program was written in Matlab to acquire the coordinates of nine target locations (Fuhrman, S. I. et al., 2005).

The scale was determined by sampling the location of the scale targets for 50 frames (50 ms). The difference in the pixel location was computed, then scaled using the known distance between the targets of 12 inches.

3.2.3 Results

Separate scaling factors were calculated for each crash test. Scaling results are as follows:

Table 4: Image scale data for WC0535 (Test 1)

wc0535	Distance (pixels)	inches/pixel	cm/pixel	m/pixel
mean:	187.8042	0.063897	0.162297	0.001623
min:	186.8298	0.063578	0.161488	0.001615
max:	188.7447	0.06423	0.163143	0.001631
range:	1.914894	0.000652	0.001655	1.66E-05
SD:	0.349608	0.000119	0.000302	3.02E-06

Table 5: Image scale data for WC0536 (Test 2)

wc0536	Distance (pixels)	Inches/pixel	cm/pixel	m/pixel
mean:	187.3617	0.064047	0.162681	0.001627
min:	186.7234	0.063794	0.162036	0.00162
max:	188.1064	0.064266	0.163236	0.001632
range:	1.382979	0.000472	0.0012	1.2E-05
SD:	0.375392	0.000128	0.000326	3.26E-06

Head velocities were calculated using 2.0 ms intervals for the x and y components separately, then combined using vector addition.

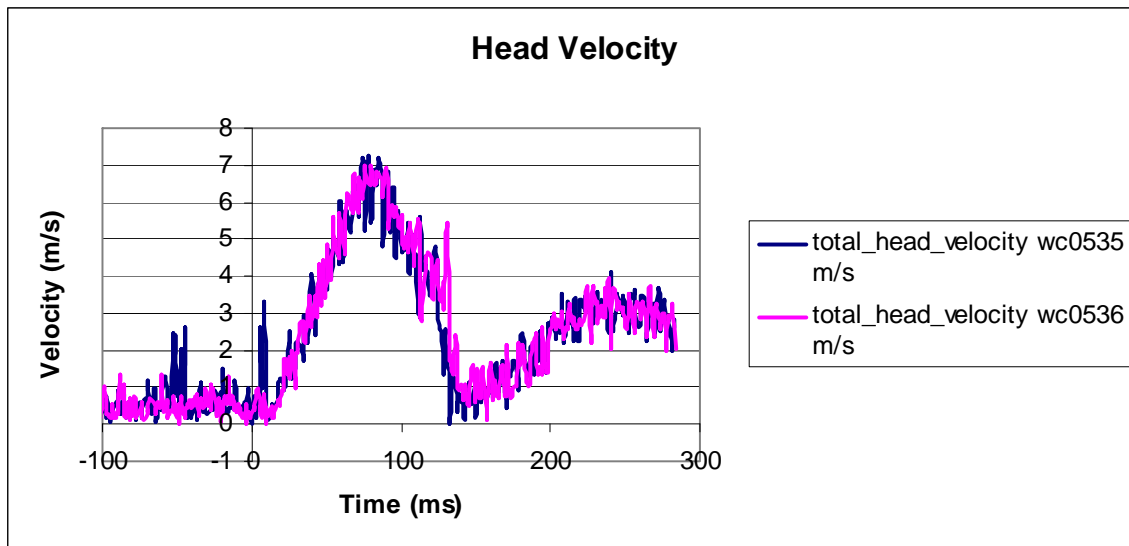


Figure 5: 6-year old ATD head velocities during rear impact with no headrests

Data from Figure 5 appear quite noisy. This is a result from determining the pixel location of each target. A simple smoothing was to the curves by using a 5-point running average (Figure 6).

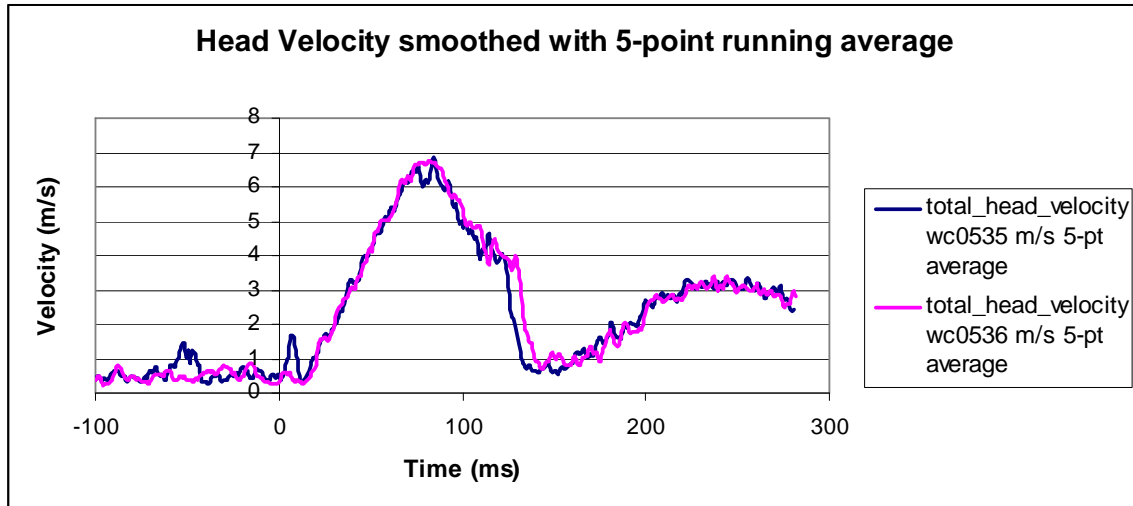


Figure 6: Smoothed 6-year old ATD head velocity data

Time zero corresponds to strobe flash during the test run. It was used to synchronize the two trials. The head hit the seat back at ~130 ms. The difference between the two curves at that time is the difference between the two trials for when the head hit the seat back. As would be expected, the head hit the seat back sooner (wc0535) when the seatback was in the raised position. The curves are otherwise similar. Maximum head velocity was 7 m/s.

3.3 PENDULUM TESTING

Preliminary pendulum testing of the wheelchair headrest was conducted for two purposes: to determine that the headrest would be of adequately robust design to sustain the loading by the ATD during rear impact crash tests, and to establish the force-displacement relationship during dynamic testing for use in the modeling. Data from the first two sled tests without a headrest were used to determine maximum head velocities. The results were then used to calculate the equivalent pendulum geometry. The headrests were pendulum tested, and results indicated that the headrest was suitable for rear impact sled tests. Force-displacement curves were established.

3.3.1 Calculations

Dynamic pendulum testing of the proposed pediatric headrest was conducted before conducting sled tests of the Zippie Pediatric Wheelchair with the headrest attached. A calculation of the appropriate test configuration is as follows. All pendulum testing was conducted using the pendulum impact tester (PIT). All calculations are based on data from the two previously conducted sled tests with a 16 mph, 10g crash test sled pulse. Targets were placed on the Hybrid III 6-year old ATD: two on the head and one on the knee. High-speed video (1000 frames/sec) recorded the crash test. Target coordinate data were acquired for the test crash. Head velocities were calculated from this data. Maximum head velocity was determined to be 7 meters/second. The mass of the ATD head is 3.47 ± 0.05 kg (7.66 ± 0.10 lbs). (Society of Automotive Engineers: Dummy Testing

Equipment Subcommittee, 2003) Maximum momentum of the ATD head was calculated using: momentum = mass x velocity.

The following is a calculation to determine the pendulum displacement needed to create a momentum equivalent to the momentum of the ATD head during rear impact testing. This information was used to pendulum test the headrest in anticipation of the rear impact sled tests and to also determine the dynamic force-displacement response of the headrest and seatback configuration to input into the MADYMO modeling.

The pendulum test jig includes a pendulum bob weighing 16 lbs, and a 48 inch steel pendulum arm weighing 30 lbs. All quantities were converted to metric units for purposes of the calculation.

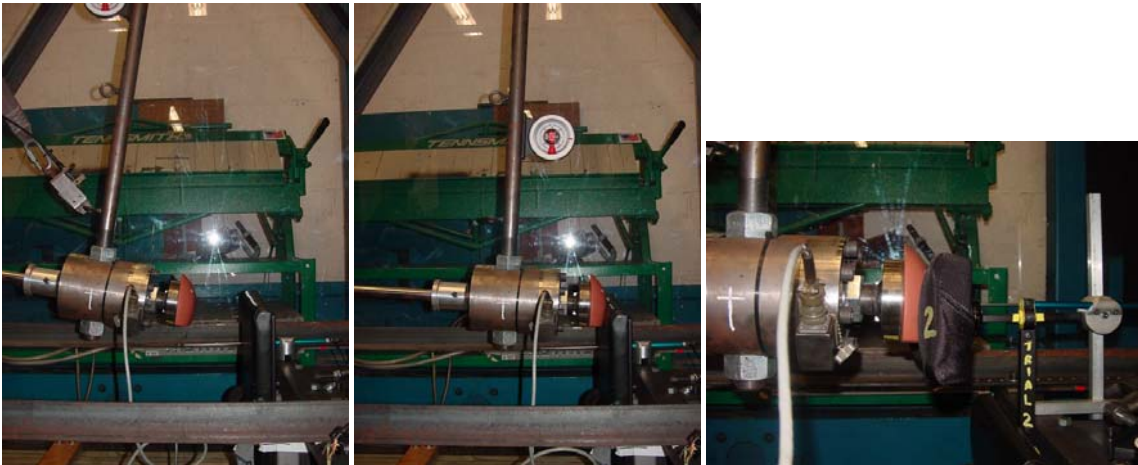


Figure 7: Photos of Pendulum Impact Tester with backrest and with headrest

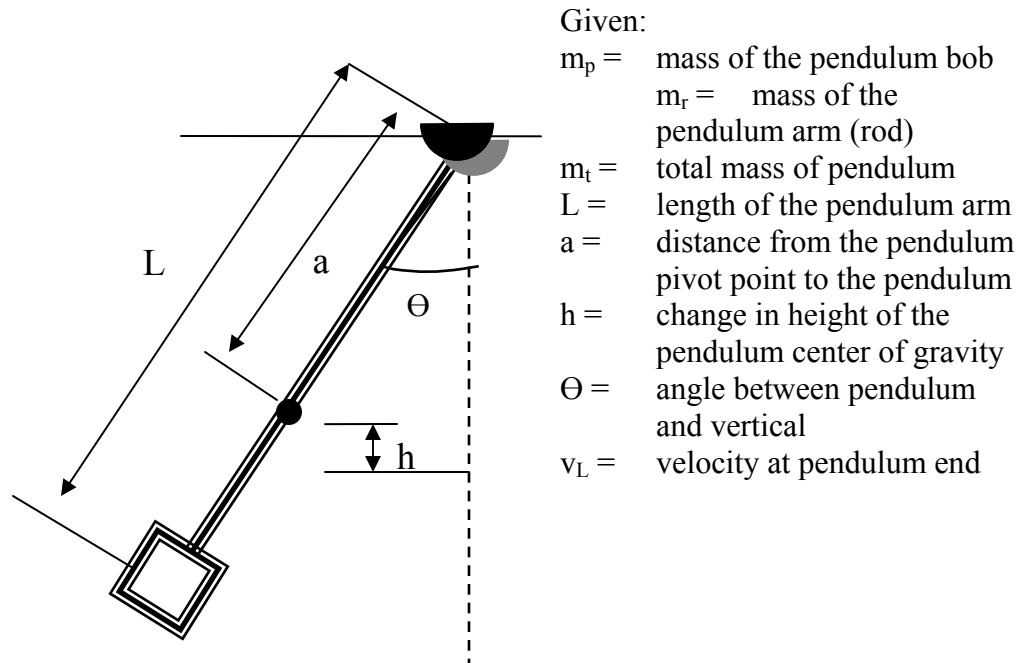


Figure 8: Pendulum Impact Rester (PIT) schematic

Equation 3: Calculation of the center of mass of the pendulum

$$\sum \Gamma = -m_p(L-a) + m_r(a - L/2) = 0$$

Equation 4: solving for acceleration

$$a = L[m_p + (m_r/2)] / (m_p + m_r)$$

Equation 5: Moment of inertia around the pivot point

$$I = (1/3)m_rL^2 + m_pL^2$$

Assuming conservation of energy:

Potential Energy = Rotational Energy + Kinetic Energy

Equation 6: Potential energy

Potential Energy = m_tgh

$$= (m_p + m_r)g[1-\cos(\Theta)]a$$

Equation 7: Rotational energy

$$\begin{aligned}\text{Rotational Energy} &= (1/2)I\omega^2 \\ &= (1/2)I(v_L/L)^2\end{aligned}$$

Equation 8: Kinetic energy

$$\begin{aligned}\text{Kinetic Energy} &= (1/2)m_t v_a^2 \\ &= (1/2)m_t (av_L/L)^2\end{aligned}$$

By solving the equations for Θ as a function of the mass of the pendulum bob, we get:

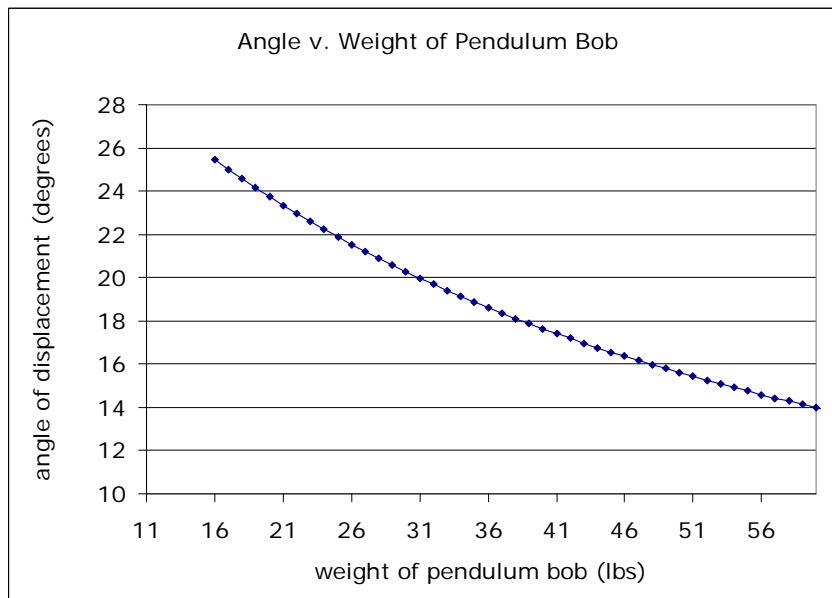


Figure 9: Combined angle and mass of pendulum

3.3.2 Pendulum testing methods

Pendulum testing was conducted in phases; the first to determine pendulum test repeatability and the second to determine the load-deflection characteristics of the headrest assembly. An additional goal of the headrest testing was to confirm that the headrest selected for eventual sled testing would be adequately robust and would not fail during testing. Rather than mount the headrest stem into a rigid jig, it was determined that pendulum testing would be more likely to yield results similar to sled testing if the headrest could be mounted with the same configuration as it is on a wheelchair. For all the headrest tests, the headrest stem was mounted to the back of the wheelchair seat back with the standard manufacturer supplied mounting hardware.

The first phase of the testing was focused at determining the quality of the instrumentation and data acquisition system. It was determined that these tests could be conducted directly on the seatback. This afforded the opportunity to test the equipment without potentially damaging the headrest. The impact surface of the pendulum bob was fitted with the skullcap pieces from the Hybrid III 6-year old ATD in an effort to replicate the impact profile that the headrest will see during sled testing. The padded seatback was secured to the test jig and positioned such that the PIT contacted the top portion of the seatback. Virtual Work Bench was used for data acquisition with the sampling rate set at 0.001 second. For the repeatability test, using a magnetic protractor, the pendulum was displaced 10 degrees from the vertical, the data recorder was started and the pendulum was released. This test was repeated (n=10). Data were imported into excel to review the output.

The test set up for the headrest testing use the PIT, also equipped with the skullcap pieces. The seatback was fixed to the test jig fixture using two C-clamps. The position of the seatback was adjusted so that the pendulum struck the midline of the headrest, directly in front of the a/p headrest stem. The top of the headrest was located 23 inches from the bottom edge of the wheelchair seatback. The a/p headrest stem was pinned at the headrest stem joint to prevent slippage in the a/p direction. An oil paint parker was used to mark both the seatback and the test jig to confirm that there was no vertical slippage during the test. A load cell and displacement probe were used to collect data, which was fed into Virtual Work Bench software. The PIT pendulum pre-test displacement angle was measured using a magnetic protractor fixed to the pendulum arm.

3.3.3 Pendulum testing results

Repeatability:

Ten identical pendulum drops we conducted using a wheelchair seat back. The load cell data was extremely noisy with a large noise component at 60 Hz. The data presented below was averaged over 16-data points – creating a simple low pass filter. Although the data was noisy, it was repeatable with peak loads of 80 ± 3.8 kg – within the accuracy of the load cell.

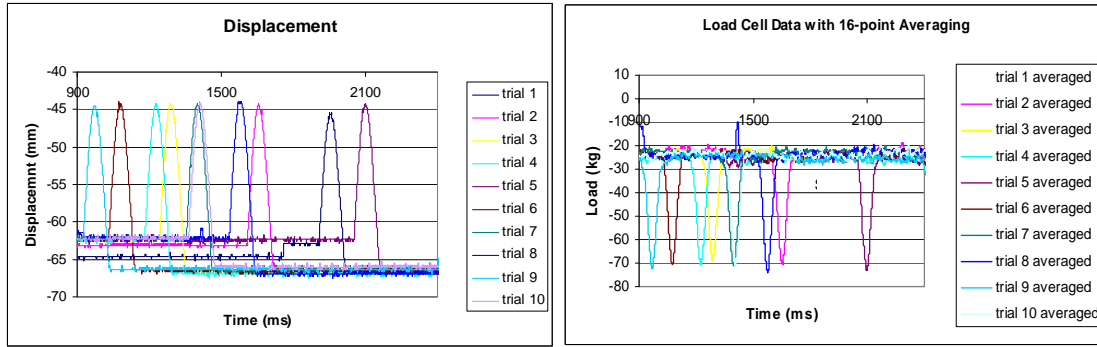


Figure 10: Displacement and load cell data (16 point running average)

For the actual headrest testing, a variety of filters was tested including notch filtering and low pass Butterworth filter. A fast Fourier transform (FFT) was done on the load cell data, and it indicated that the impact event occurred at a frequency of less than 15 Hz. Based on this, the minimum sampling rate should be 0.02 seconds. A trial was done at the rate, but it was not adequate to capture the peak loads. A sampling rate of 0.001 seconds was used. Note in the figure below that there is a large noise component at 60Hz.

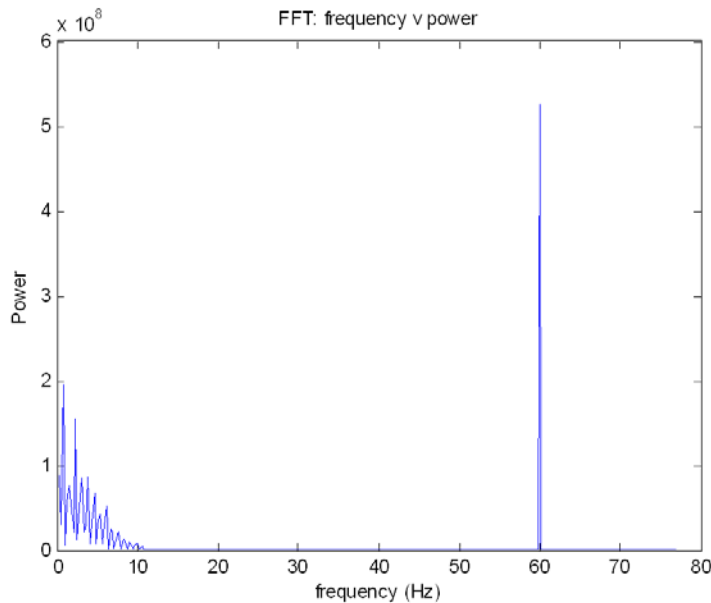


Figure 11: Fast Fourier Transform of data

A Butterworth filter was used to remove all frequencies over 30 Hz and to obtain the following force-displacement curve.

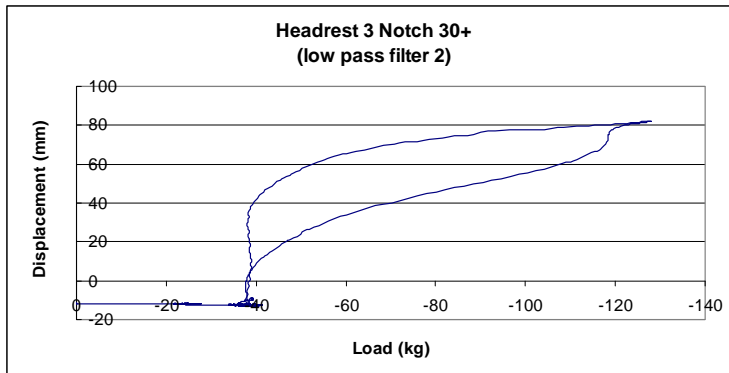


Figure 12: Force displacement curve using a low pass filter

Test results from testing the seatback demonstrate that the PIT produces repeatable, though noisy results. Using filtering to greatly reduce the signal noise from the load cell data yields a headrest force-displacement curve that will be used in the computer modeling. The difference between the loading and unloading curves reflects a small amount (2 degrees) of plastic deformation in the headrest stem that occurred during each test.

4.0 CHARACTERIZATION OF PEDIATRIC WHEELCHAIR KINEMATICS AND WHEELCHAIR TIEDOWN AND OCCUPANT RESTRAINT SYSTEM LOADING DURING REAR IMPACT

This study characterizes pediatric wheelchair kinematic responses and wheelchair tiedown and occupant restraint system (WTORS) loading during rear impact. It also examines the kinematic and loading effects of wheelchair headrest inclusion in rear impact. In two separate rear impact test scenarios, identical WC19-compliant manual pediatric wheelchairs were tested using a seated Hybrid III 6-year old anthropomorphic test device (ATD) to evaluate wheelchair kinematics and WTORS loading. Three wheelchairs included no headrests, and three were equipped with slightly-modified wheelchair-mounted headrests. Surrogate WTORS properly secured the wheelchairs; 3-point occupant restraints properly restrained the ATD. All tests used a 26 km/h, 11 g rear impact test pulse. Headrest presence affected wheelchair kinematics and WTORS loading; headrest-equipped wheelchairs had greater mean seatback deflections, mean peak front and rear tiedown loads and decreased mean lap belt loads. Rear impact tiedown loads differed from previously measured loads in frontal impact, with comparable tiedown load levels reversed in frontal and rear impacts. The front tiedowns carried larger loads in rear impact despite lower impact severity. These outcomes have implications for wheelchair and tiedown design, highlighting the need for all four

tiedowns to have an equally robust design, and have implications in the development of rear impact wheelchair transportation safety standards.

4.1 INTRODUCTION

The number of individuals who use wheelchairs in the United States is increasing. LaPlante (LaPlante and Center, 2003) reports that the number of individuals using wheelchairs quadrupled between the years 1969 and 1995, for every age group from under age six to over age 65. In 2002, over 1.6 million individuals used manual wheelchairs in the United States (Kaye et al., 2002); of these, 88,000 were children. As of July 2005, over 80,000 children used manual wheelchairs for their daily mobility needs (U.S. Census Bureau Public Information Office, 2006).

Wheelchair transportation safety focuses on enabling those who remain seated in their wheelchairs during transportation to travel more safely. Current mandatory federal motor vehicle safety standards serve to protect adults and children who travel in vehicle seating installed by original equipment manufacturers (Department of Transportation (DOT), 1982b; Department of Transportation (DOT), 1993; National Highway Traffic Safety Administration, 1993) or in child restraint systems (National Highway Traffic Safety Administration, 1999). Federal motor vehicle safety standards do not extend to wheelchairs, even when used as seating in motor vehicles. The Food and Drug Administration (FDA) classifies wheelchairs as physical medical devices and are covered only as they pertain to medical use (U.S. Food and Drug Administration, 2007).

Domestic and international voluntary safety standards have been developed for wheelchairs used as seating in motor vehicles (ANSI/RESNA, 2000; ISO, 2008) for frontal impact conditions. The frontal impact priority reflects the potential severity of frontal impacts. Fatalities from motor vehicle accidents occur most often from frontal impacts, with rear impacts accounting for the largest number of occupant related injuries(Japan Traffic Safety Association, 1997). Interest in rear impact for wheelchair-seated motor vehicle occupants has mirrored increased efforts in the automotive industry to improve occupant protection through the use of improved head restraint systems(Viano, D. and Olsen, 2001; Farmer et al., 2003), as well as federal motor vehicle safety standards related to head restraint in rear impact(Department of Transportation (DOT), 2000).

Our research indicates that 80% of children who use wheelchairs are also prescribed wheelchair-mounted headrests(Fuhrman, S. I. et al., 2005). Initial studies have demonstrated that wheelchair-mounted headrests have the potential to reduce the severity of head and neck injury in rear impact(Fuhrman, S. I. et al.). Yet, there are no studies that investigate the effects of headrest use on wheelchair kinematics or WTORS loading. Testing of adult and pediatric ANSI/RESNA WC19-compliant wheelchairs with no headrests in rear impact showed that front tiedown loading is significantly higher in rear impact than in frontal impact and that adult wheelchairs structurally failed under rear impact loading(Fuhrman, S. I. et al., 2006; Manary, M. A. et al., 2007; Salipur et al., 2007). This investigational baseline study is an initial effort to characterize wheelchair kinematics and WTORS loading for manual pediatric wheelchairs and to evaluate the effects of headrest use on these outcomes during rear impact. Results from this

investigation will provide information needed for the development of design guidelines for pediatric wheelchairs for rear impact protection. Ultimately, our efforts are intended to assist rear impact wheelchair standards development, wheelchair safety design improvements, and wheelchair headrest development, in providing effective occupant restraint during rear impact.

4.2 METHODS

Two series of three identical Quickie brand¹ Zippie WC19-compliant pediatric manual wheelchairs (17.9 kg) were tested using a seated Hybrid III 6-year old ATD and subjected to a 26 km/h, 11g rear impact crash pulse. Series NoHR (Tests 1-3) was tested without any type of headrest; Series HR (Tests 4-6) was tested using a slightly-modified Sunrise Medical single-pad headrest. The headrest was modified by inserting a 3.2 mm (1/8") diameter pin into the headrest stem joint to prevent rearward slippage of the horizontal headrest stem with respect to the vertical headrest stem. The rear impact test pulse used for sled testing was chosen based on its correspondence in severity to that used in the ANSI/RESNA WC19 frontal impact wheelchair standard (ANSI/RESNA, 2000). Similar to the frontal impact crash pulse (48 km/h, 20g), the rear impact crash pulse (26 km/h, 10 g) represents an impact more severe than 95% of National Automotive Sampling System (NASS) rear impact field data (Flannagan and Manary,

¹ Quickie is a brand of Sunrise Medical <http://www.sunrisemedical.com/index.jsp>

2005). At the time of testing, our crash pulse conformed with the then proposed International Organization for Standardization (ISO) test pulse for use in development of a draft voluntary industry standard for wheelchair performance evaluation in rear impact (Flannagan and Manary, 2005).

All tests included matched components and identical experimental configurations with the exception of seatback position (Table 6) during two separate test series. In Test 1 (NoHR Series) the seatback was positioned with the top of the seatback level with the ATD shoulder; the bottom edge of the seatback location was 2.5 cm above the seat cushion. In all subsequent tests (Tests 2-6) the bottom of the seatback was positioned in contact with the seat cushion. All wheelchairs were identically equipped with planar seating and upright seatbacks (90-degree position). Standard Quickie® snap back hardware with quick release pins attached the seating and seatbacks to the tubular wheelchair frame². The pins locked the U-shaped brackets around the tubular frame components. The seat and seatback were initially positioned with a 5 degree posterior tilt as measured from the horizontal and vertical planes, respectively. Four-point strap-type surrogate tiedowns secured the wheelchairs; three-point surrogate occupant restraints restrained the ATD(ANSI/RESNA, 2000). The seated ATD was positioned with posterior torso, thighs and feet in full contact with wheelchair components (Figure 13).

² This attachment hardware is standard equipment on Quickie WC19-compliant wheelchairs. Quickie ® part no.: 920591

Table 6: Wheelchair test configurations

Test	Seatback position	Headrest	Series
1	Bottom edge of seatback is positioned 2.5 cm above top edge of seat cushion	No headrest	NoHR
2	Bottom edge of seatback contacts top edge of seat cushion		
3	Bottom edge of seatback contacts top edge of seat cushion		
4	Bottom edge of seatback contacts top edge of seat cushion	Headrest included	HR
5	Bottom edge of seatback contacts top edge of seat cushion		
6	Bottom edge of seatback contacts top edge of seat cushion		

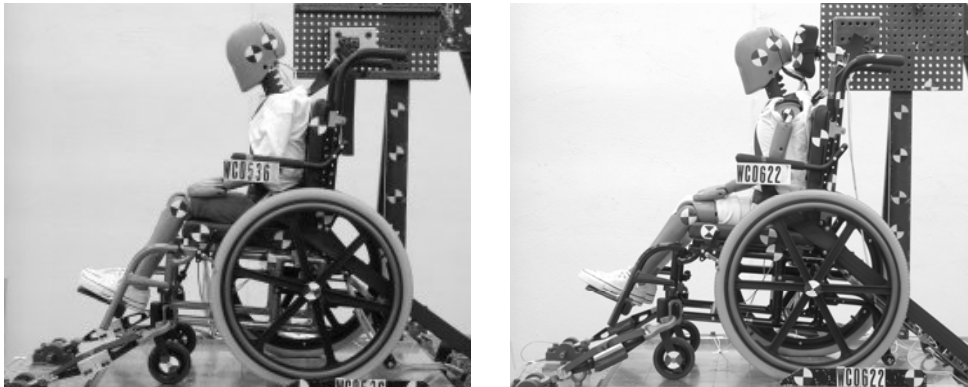


Figure 13: Photos of experimental set up. Test 2 pre-test photo (left) with no headrest (NoHR), Test 5 pre-test photo (right) with slightly-modified headrest (HR).

Occupant restraint and rear wheelchair tiedown loads were measured using belt load cells³; front wheelchair tiedown loads were measured using rod-end load cells⁴. High contrast targets were placed on the wheelchair at: center of gravity, rear axle, caster hub, seat pan (2), and seatback. High-speed video cameras⁵ (1000 frames/sec) were used

³ Denton webbing load cells, model no.: 3255

⁴ Manufactured by University of Michigan Transportation Research Institute, capacity: 20,000 lb.

⁵ Redlake, model no.: HG-100K

to record the test. Kinematic data were used to describe wheelchair response to the rear impact crash pulse. A Matlab⁶ program was written to acquire the coordinates of target locations(Fuhrman, Michael G., 2005). Graphs were generated from the video image data for the seatback to seat angle, seat rotation, caster excursion, and seatback excursion along the wheelchair seatback canes. A strobe flash synchronized video data with instrumentation output. Instrumentation data were recorded every 0.1 ms and filtered per SAE J211 (Society of Automotive Engineers, 1995).

4.3 RESULTS

In all tests, the sled reached the targeted acceleration and change in velocity, with sled acceleration plateau average levels between -9.6 and -10.0 g, sled acceleration peaks between -11.0 and -11.3 g (Figure 14), and sled velocity changes between 25.0 and 25.6 km/h. Figure 14 displays sled test acceleration time-history and sled acceleration pulse reproducibility.

⁶ Matlab® is a product of Mathworks, <http://www.mathworks.com>

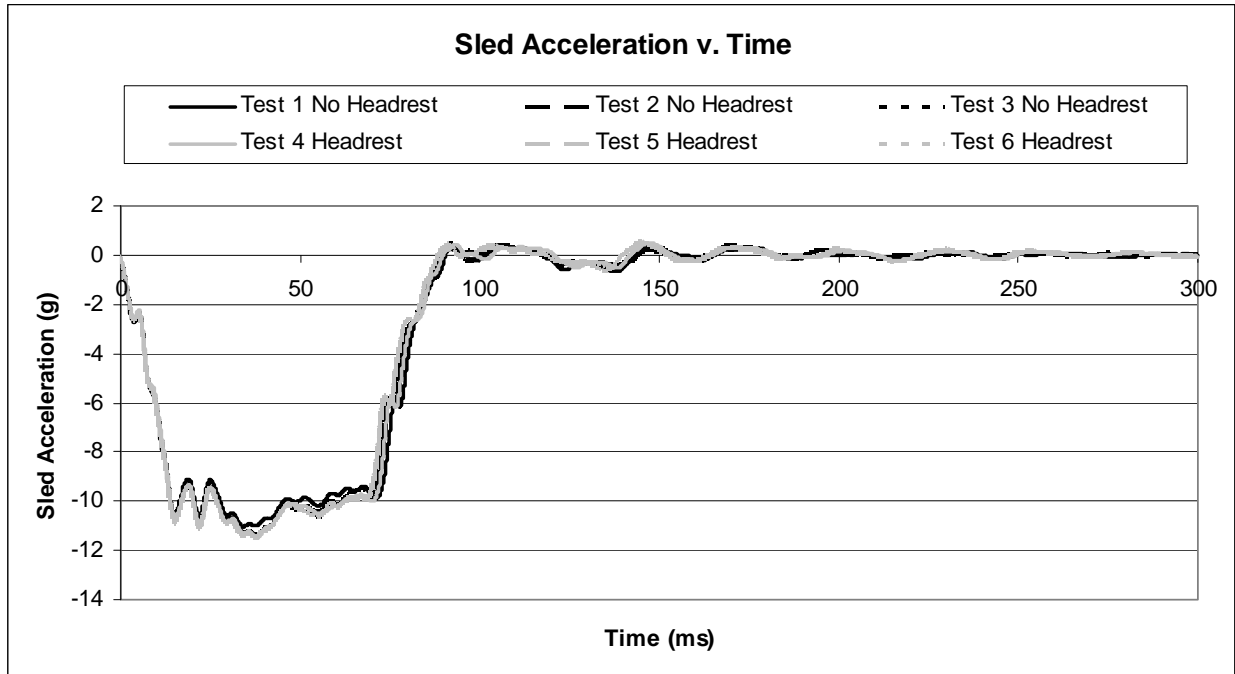


Figure 14: Sled acceleration time-history for rear impact tests indicating high test pulse reproducibility and average peak sled accelerations of -9.6 to -10.0 g.

The commercially available Zippie wheelchairs remained structurally intact and the ATD maintained an upright posture during all rear impact tests. During sled impact testing, the wheelchairs rotated rearward with the front casters rising off the sled platform at the time of maximum sled horizontal excursion. Wheelchair rearward rotation continued until caster vertical excursion reached its peak and remained elevated for the remainder of the test (Figure 15).

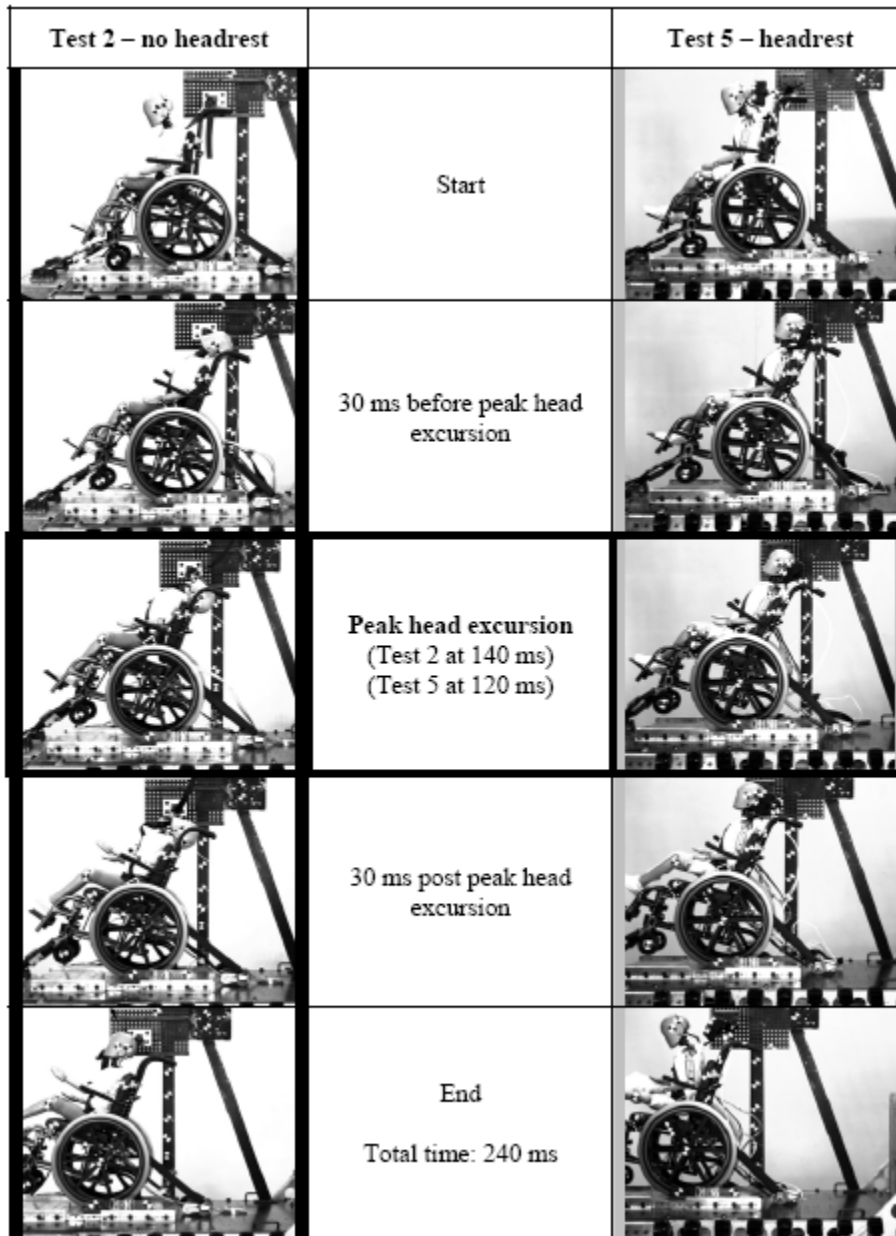


Figure 15: Tests 2 (no headrest) and Test 5 (headrest) images during sled tests. Note front caster vertical excursion. The wheelchairs remained intact and the ATD remained upright throughout the test.

Caster vertical excursion was measured from initial caster hub target position. Mean caster vertical excursion time histories indicate that Series HR peaked higher and earlier than Series NoHr. Series HR had peak vertical caster excursions between 9.1-11.5

cm, peaking between 126 ms and 132 ms. Maximum vertical excursions were 8.8 to 9.9 cm for Series NoHR without headrests and occurred later between 130 and 147 ms. As shown in Figure 16 following the maximum excursion, the wheelchair casters remained elevated off of the sled platform.

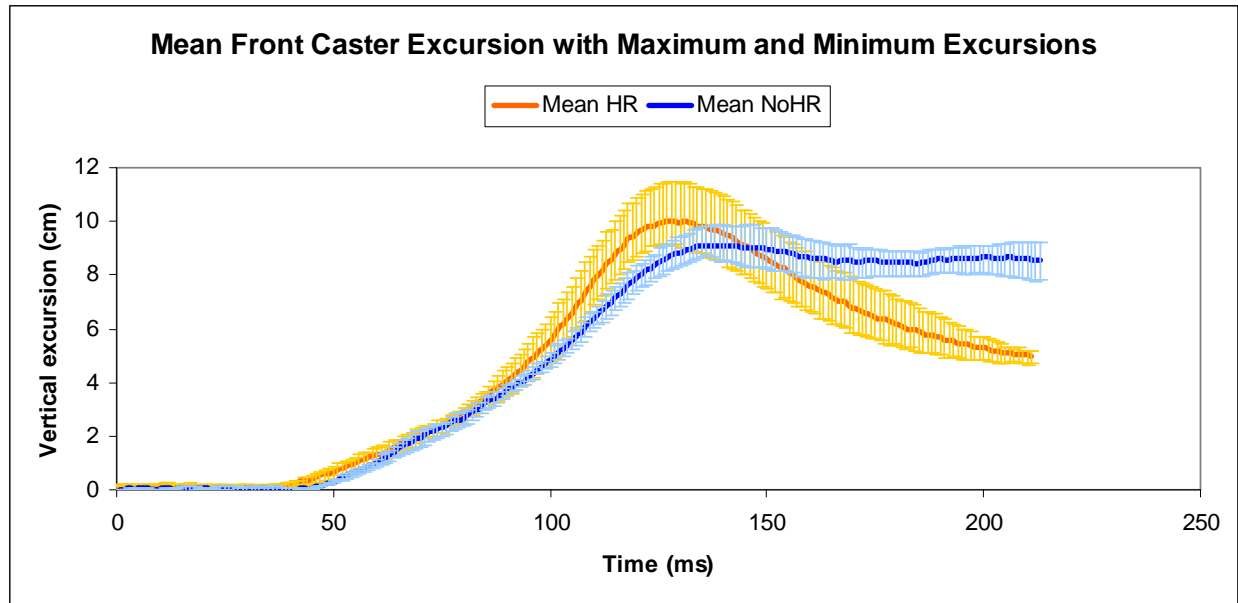


Figure 16: Mean front caster vertical excursion for rear impacts. Maximum-minimum ranges are displayed for Series HR and Series NoHR.

Standard equipment on the test wheelchairs included a metal bracket that attached the seatback canes to the horizontal members of the wheelchair frame, and fixed the seatback to seat pan frame per user specifications. During testing both elastic deflection and plastic deformation of the seatback canes occurred as the seatback was pushed rearward, and then only partially returned to its original position. The canes were permanently deformed at the location where they attached to the bracket. Initial seatback to seat pan angle for all tests was 90 degrees with a 5 degree posterior tilt. During testing

the seatback canes flexed rearward and sustained plastic deformation as evidenced by the seat-seatback angle's failure to return to its original position (Figure 17). Series HR mean seatback to seat pan angle exceeded Series NoHR at all times during the test. Maximum mean seatback to seat pan angle in Series NoHR was 100 degrees at 94 ms (peak angle, 98.8-100.2 degrees; time, 92-94 ms). Maximum mean seatback to seat angle in Series HR occurred later (107 ms) and was slightly larger, 102 degrees (peak angles, 100-104 degrees; time 98-107 ms). On average the canes were permanently deformed rearward between 4 and 6 degrees.

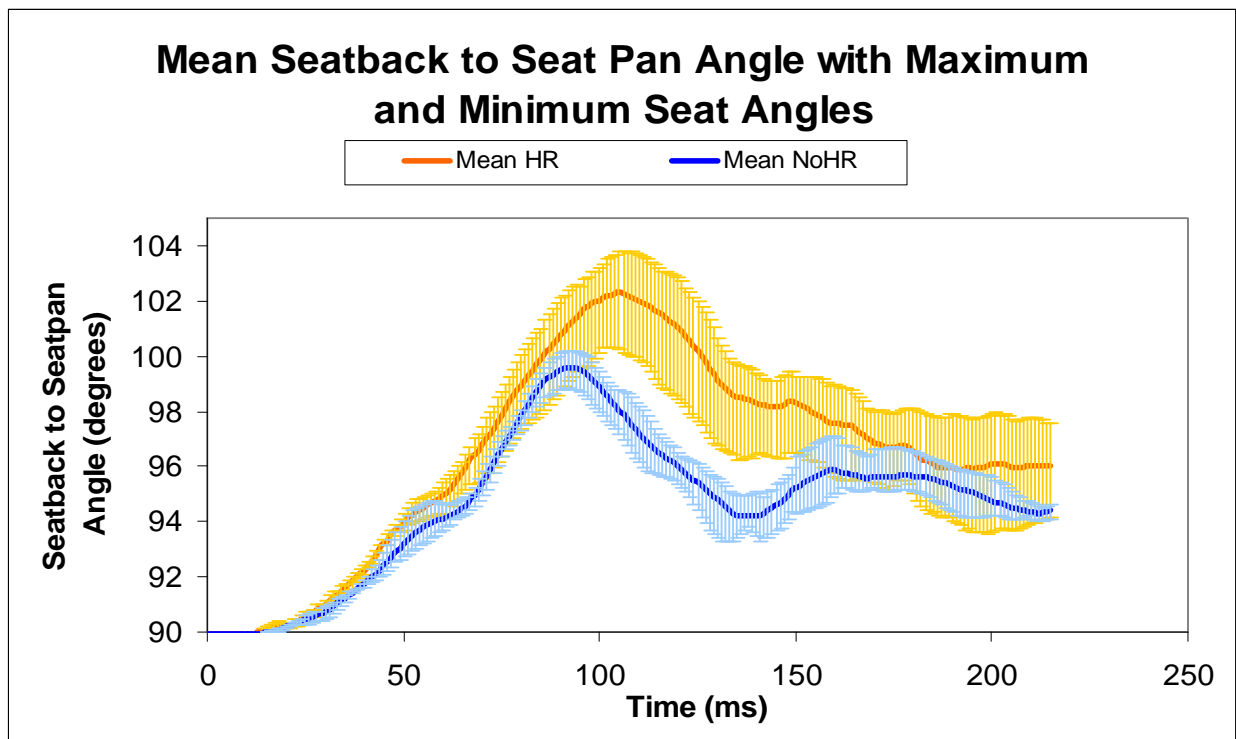


Figure 17: Mean seatback to seat angle for rear impact tests. Initial seatback to seat angle was 90 degrees for all tests. Maximum-minimum ranges are displayed for Series HR and Series NoHR. Maximum seatback angle was 98.8 to 103.8 degrees across all tests.

Seatback attachment hardware did not fail and remained mounted to the canes. Although attached to the canes, hardware permitted the seatback to slide upward along the canes. Mean peak excursions were similar for both tests with Series HR peaking earlier (1.47 cm at 99ms) compared to Series NoHR (1.49 cm at 125 ms). Maximum seatback upward excursion along seatback canes (Figure 18) was 0.6 to 2.7 cm at time 117 to 126 ms for Series NoHR. Series HR had excursions of 1.3 to 1.7 cm that occurred earlier at time 93 to 99 ms. Series NoHR displays greater variability than Series HR.

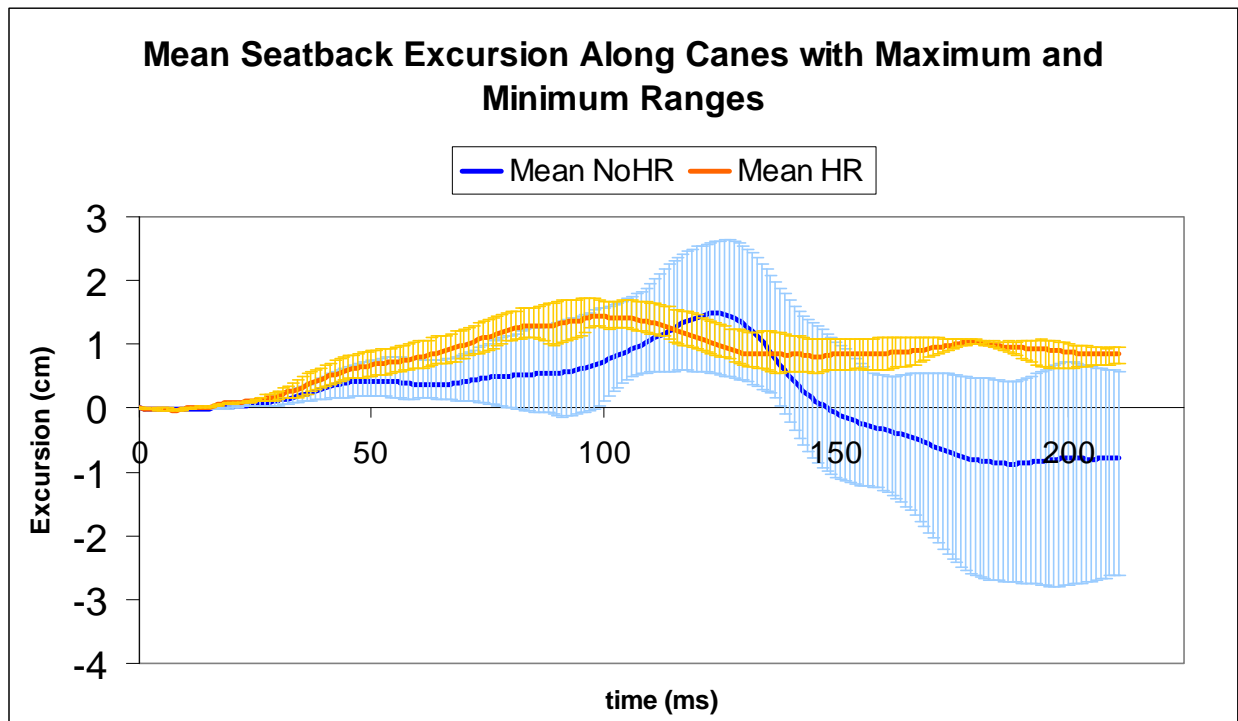


Figure 18: Mean seatback excursion upward along seatback canes for rear impact tests. Maximum-minimum ranges are displayed for Series HR and Series NoHR.

Figure 19 displays mean peak wheelchair tiedown and occupant restraint loads for series NoHR and Series HR. The graph indicates that the front tiedowns carry larger peak loads during rear impact than the rear tiedowns across both test series. Series HR mean

peak front and rear tiedown loads exceeded Series NoHR mean peak tiedown loads. Maximum-minimum front tiedown load ranges reflect a larger range for Series NoHR tiedowns than for Series HR. Test 3 (Series NoHR) had high peak front tiedown loads (5423N and 5390N), that may have resulted from high pre-test tiedown tightening. Pre-test tiedown loads were not measured.

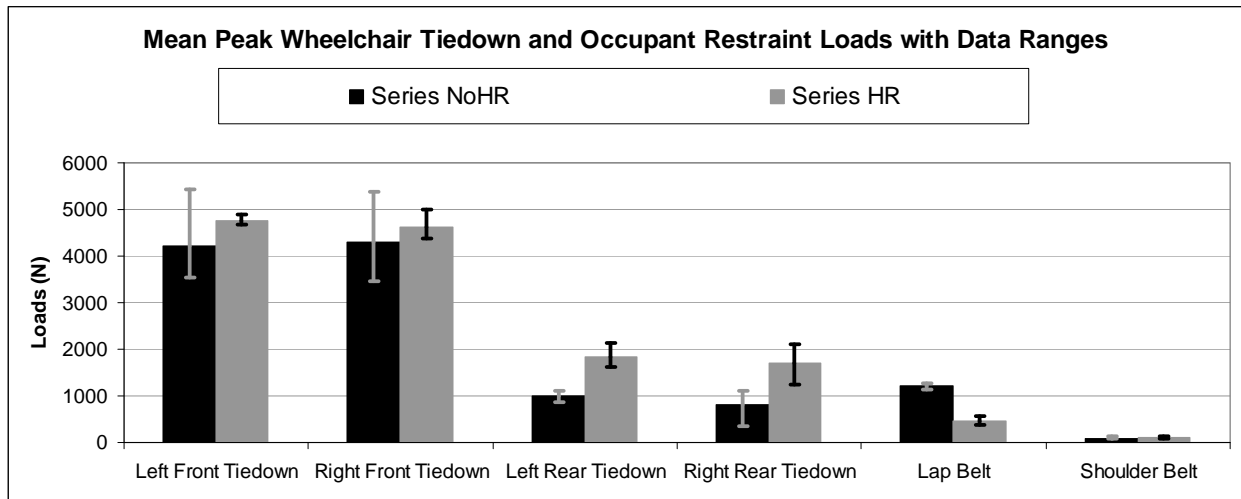


Figure 19: A comparison of mean peak wheelchair tiedown and occupant restraint loads for rear impact. Maximum-minimum ranges are displayed for Series HR and Series NoHR. Mean peak tiedown loads are greater for Series HR than for Series NoHR.

Figure 19 indicates low peak shoulder belt loads measured during rear impact (Series NoHR, 79 -131 N; Series HR, 68-126 N). During rear impact shoulder belts carry almost no load, remaining slack during most of the test. Lap belt loads were also low during rear impact (Series NoHR, 1125-1267 N; Series HR, 384-560 N) and primarily limit the ATD sliding up the seatback during impact. Both components of the occupant restraint limited ATD excursion during rebound.

4.4 DISCUSSION

The pediatric wheelchair tested in this study is representative of a pediatric manual wheelchair with a WC19 transit option. Previously, this wheelchair model had been successfully sled impact tested per ANSI/RESNA WC19 in frontal impact (Rehabilitation Engineering Research Center on Wheelchair Transportation Safety, 2007). There is no published wheelchair standard for rear impact, and the wheelchair was not designed specifically to withstand rear impact loading. It is a noteworthy and encouraging finding that the pediatric wheelchairs remained structurally intact and the Hybrid III 6-year old ATD remained in an upright posture during our rear impact testing. This contrasts sharply with Manary's sled test results (Manary, M. A. et al., 2007) conducted with adult manual WC19-compliant wheelchairs and the Hybrid III 50th percentile male, where all wheelchairs experienced structural failures including failure of the seatback attachment hardware, seatback cane failure and front securement point failure. Our positive results indicate that commercial WC19-compliant pediatric manual wheelchairs have the potential to be crashworthy under rear impact conditions.

During rear impact, our test wheelchairs rotated rearward with the seatback rotating rearward and downward and the casters rising above the test sled. This rotational motion can be attributed to the location of the tiedown securement points on the wheelchair. The front tiedown securement point locations low on the frame, and below the wheelchair CG, may have contributed to the wheelchair rotation observed during our testing. WC19-compliant wheelchair securement point locations have been successfully tested in frontal impact per ANSI/RESNA WC19 and are thus not adjustable by the consumer. Results from rear impact studies can provide additional design guidance to

wheelchair manufacturers. Previous research conducted on frontal impacts indicates that wheelchair rotation during impact is sensitive to tiedown securement point height with respect to wheelchair center of gravity (Bertocci, G. E. et al., 1996a). This research further indicates that primary load-bearing tiedown securement points located close to the wheelchair center of gravity reduces wheelchair rotation in frontal impact; a similar finding would be expected in rear impact, and warrants further investigation.

WTORS loading patterns differ notably in rear impact from frontal impact. Figure 20 compares our mean peak WTORS loads against Ha's previously measured loads (Ha, DongRan, 2004) for the same model wheelchair and ATD tested in frontal impact using the ANSI/RESNA WC19 (48 kph, 20 g) crash pulse (ANSI/RESNA, 2000). Mean peak wheelchair tiedown and occupant restraint loads for frontal impact are shown as Series FI. Front tiedown mean peak loads measured in our rear impact sled tests exceeded Ha's corresponding rear tiedown mean peak loads previously measured in frontal impact sled tests. Series FI testing was conducted with vehicle anchored occupant restraints. During the frontal impact the ATD loaded the occupant restraints and the wheelchair loaded the tiedowns. In rear impact the ATD loads the wheelchair, and the front tiedowns experience the combined loads of the ATD and the wheelchair. Thus, although the rear impact crash pulse (16 mph, 10g) was less severe than the frontal impact crash pulse (30 mph, 20g) the loading on the primary load-bearing tiedowns is greater in rear impact.

In rear impact, the rear tiedowns are primarily loaded during the rebound phase of the impact. Greater peak rear tiedown loads were measured during Series HR testing (3472-5423 N) than during Series NoHR (345-1117 N) testing, reflecting greater rebound

in headrest-included tests than in tests conducted without headrests. Front tiedown loads, which carry rebound loading in frontal impact, were not measured during Ha's study.

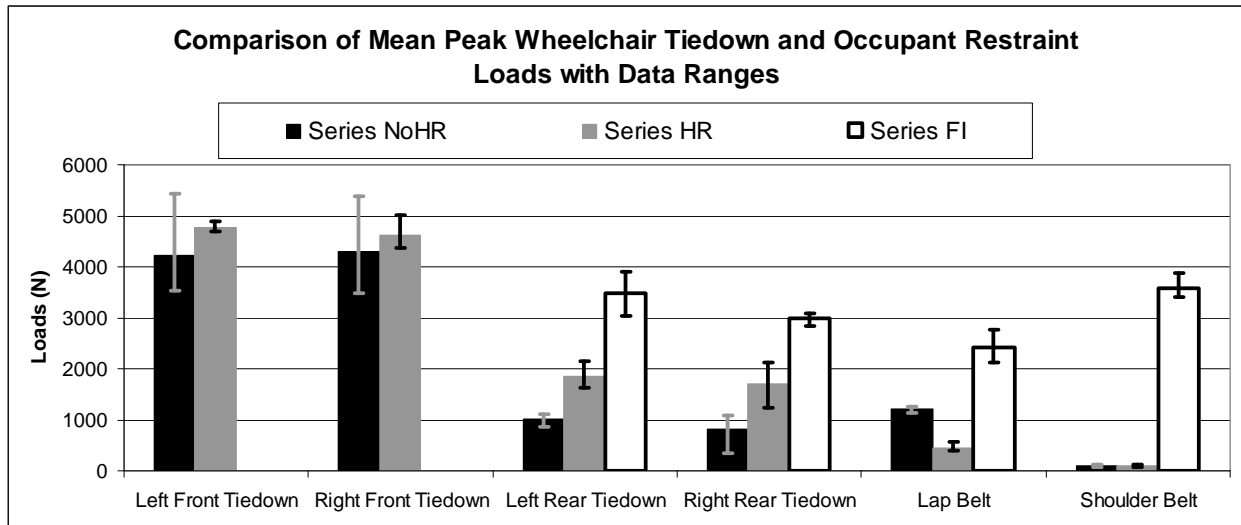


Figure 20: A comparison of mean peak Series NoHR and HR WTORS loads in rear impact to frontal impact loads from test Series FI(Ha, DongRan, 2004). Maximum-minimum ranges are displayed for Series HR and Series NoHR.

Since during frontal impact occupant restraint primarily occurs as the ATD loads the belts and in rear impact occupant restraint occurs primarily as the ATD loads the wheelchair, occupant restraints carry greater loads during frontal impact compared to rear impact. Figure 20 contrasts the relatively large peak shoulder belt loads (3411-3884 N) measured during frontal impact with smaller peak shoulder belt loads (Series NoHR, 79 - 131 N; Series HR, 68-126 N) measured during rear impact. During rear impact shoulder belts carry almost no load, remaining slack during most of the test. Likewise, lap belt loads were much lower during rear impact (Series NoHR, 1125-1267 N; Series HR, 384-560 N) than during frontal impact (2134-2766 N).

In rear impact, peak lap belt loading occurs during rebound. Our tests results indicate that despite evidence of greater rebound during Series HR as evidenced by rear tiedown loading, headrest included tests resulted in less loading of the lap belt than Series NoHR. The ATD kinematic response to rear impact is complex. During all rear impact tests the ATD head and neck extends rearward, but as seen in Figure 15, much more so in tests conducted without headrests. In Series NoHR the greater head and neck rotational response would tend to cause the ATD pelvis and lower torso to rotate upward and forward loading the lap belt as opposed to the Series HR where the head and neck rotation is limited by the headrest. In addition, in Series HR, the greater seatback rearward deflection and head to headrest interaction absorb energy and may reduce the loading on the lap belts when compared to Series NoHR.

Series HR experienced greater rearward wheelchair rotations, greater vertical caster excursions, and greater seatback deflections followed by greater rebound than Series NoHR tests. The additional rotational moment caused by the ATD head impacting the wheelchair headrest contributed to greater seatback deflection and rearward rotation of the wheelchair as described by seatback cane flexion and by caster upward vertical excursion. As shown in Figure 17, Series HR seatback canes flexed more, and then rebounded back close to the post-test position of the non-headrest equipped seatback canes. In Figure 16, Series HR initially had greater front caster upward excursions than Series NoHR, then Series HR rebounded to a lower position than Series NoHR, reflecting greater rebound for the headrest-included tests.

The seatback attachment hardware successfully retained the seatback during rear impact testing, however it did permit the seatback to slide upward along the wheelchair

canes. In all tests the ATD shear loading of the seatback forced the seatback to slide upward along the canes. In Series HR, friction from head contact with the headrest served to reduce the maximum upward seatback excursion. In Series NoHR the posterior aspect of the ATD head subsequently contacted the top of the seatback, driving the seatback downward after the peak excursion. Test 1 (Series NoHR) experienced the greatest seatback total excursions along the canes due to the initial positioning of the seatback during that test. The bottom edge of the Test 1 seatback component was initially positioned 2.5 cm above the seat cushion. During this test, the ATD torso forced the seatback upward along the canes, then the ATD head forced the seatback downward past the initial position until the bottom edge of the seatback was pressed against the seat cushion – approximately 2.5 cm below its starting position.

Some study limitations included potential inaccuracies when identifying target locations as the targets became obscured from view during the wheelchair rearward rotation. An additional study limitation is that the tiedowns were not tightened to a specified tension pre-test, which may have contributed to variability in the peak measured tiedown loads.

4.5 CONCLUSIONS

Wheelchair loading and response in rear impact differs markedly from that in frontal impact. In frontal impact, the ATD accelerates forward during impact. When vehicle-mounted occupant restraints are used, the ATD's forward acceleration loads only the occupant restraints; the wheelchair is then loaded by the ATD only during rebound.

Conversely, in rear impact the ATD accelerates rearward, loading the wheelchair seatback during the initial impact; the occupant restraints are then loaded principally during rebound. In rear impact, the wheelchair provides the primary occupant restraint creating much higher loads on both the wheelchair and front tiedowns. Comparisons between Series NoHR and Series HR indicated that headrest presence increased WTORS loading and seatback deflections. These factors must be considered when developing wheelchair transportation standard testing protocols for rear impact, as well as in the design of wheelchairs intended to serve as a motor vehicle seat.

Choice of this wheelchair model afforded the opportunity to make direct comparisons to Ha's frontal impact study (Ha, DongRan, 2004). Our 26 km/h 11 g rear impact test pulse is less severe than the frontal impact pulse used in WC19 sled testing or in Ha's research. Due to the differences in the loading patterns, results indicate that peak front tiedown loads in our tests are comparable to those measured on rear tiedowns by Ha, despite the fact that the rear impact test pulse was less severe.

Ha's study used vehicle-mounted occupant restraints, and during her testing the rear tiedowns were loaded only by the wheelchair. Had she used wheelchair-mounted occupant restraints, the rear tiedowns would experience a far higher combined load similar to but greater than the type of combined loading seen in rear impact testing. This is a key design consideration for securement points and WTORS.

This exploratory study of tiedown loads during rear impact demonstrates that tiedown load levels are comparable, but reversed in frontal and rear impacts, with front tiedowns carrying larger loads in rear impact even at lower impact severity. Of key importance is that front tiedowns frequently have a less robust design and, therefore, may

not provide adequate protection during rear impact. In addition, the large front tiedown loads found in rear impact reinforce the need to use all four tiedown straps every time that a wheelchair rider uses the wheelchair as a vehicle seat during transportation.

While the tests were instrumented to measure ATD loads and accelerations, this study focused solely on WTORS loads and wheelchair kinematics. Use of one commonly-prescribed pediatric manual wheelchair model provides a clear indication of the additional effects of headrest use in rear impact on wheelchair kinematics as well as a direct comparison to WTORS loads in frontal impact. However, these same results are similarly limited by the study of a single wheelchair model in a single configuration. Additional research is indicated to evaluate the effects of wheelchair and securement point geometry including center of gravity location, rear wheel position and securement point location, as well as the effects of wheelchair weight and ATD weight on wheelchair kinematics and WTORS loading. Additional research is also needed to determine loading on individual wheelchair components to facilitate improved wheelchair design for rear impact.

5.0 EFFECT OF WHEELCHAIR HEADREST USE ON PEDIATRIC HEAD AND NECK INJURY RISK OUTCOMES DURING REAR IMPACT

Comparative risks or benefits to wheelchair-seated pediatric occupants in motor vehicles associated with wheelchair headrest use during rear impact were evaluated using pediatric head and neck injury outcome measures. A Hybrid III 6-year old anthropomorphic test device (ATD), seated in identical WC19-compliant pediatric manual wheelchairs, was used to measure head and neck response during a 25 km/h (16 mph), 11g rear impact. ATD responses were evaluated across two test scenarios: three sled tests conducted without headrests, and three with slightly modified commercial headrests. Head and neck injury outcomes measures included: linear head acceleration, head injury criteria (HIC) values, neck injury criteria (Nij) values, and combined rotational head velocity and acceleration. Neck and head injury outcome measures improved by 34-70% in sled tests conducted with headrests compared to tests without headrests. Headrest use reduced Nij values and the likelihood of concussion from values above established injury thresholds to values below injury thresholds. Injury measure outcome reductions suggest lower head and neck injury risks for wheelchair-seated children using wheelchair-mounted headrests as compared to non-headrest users in rear impact. Use of relative comparisons across two test scenarios served to minimize effects

of ATD biofidelity limitations.

5.1 INTRODUCTION

In 2000, over 1.5 million individuals used manual wheelchairs in the United States (Kaye et al., 2000); of these, 79,000 were children, representing one out of every thousand children. As of July 2005, over 80,000 children used manual wheelchairs for their daily mobility needs (U.S. Census Bureau Public Information Office, 2006). Mandatory federal safety standards and state-by-state legislation for car seats and occupant restraint systems have served to help protect individuals using manufacturer-installed vehicle seats while traveling in motor vehicles (Rivara et al., 1999; Houston et al., 2001). Yet, federally mandated wheelchair safety standards do not exist for adults and children who travel in motor vehicles while remaining seated in their wheelchairs.

Many wheelchair users are unable to or prefer not to transfer to motor vehicle seats or child car seats and instead remain seated in their wheelchairs during transportation in a motor vehicle. Our goal is to make transportation in motor vehicles as safe for those who travel while seated in their wheelchairs as it is for those who travel in original equipment manufacturer (OEM)-installed vehicle seats (2005). Historically, most wheelchair transportation safety research has focused on frontal impact events. Most fatalities from motor vehicle accidents occur in frontal impact; however, rear impacts account for the largest number of occupant related injuries (Japan Traffic Safety Association, 1997; NHTSA, 1997). In response to this concern, vehicle manufacturers have successfully focused research efforts on effective head restraint development,

resulting in reduced incidence of neck injury to OEM-seated passengers in rear impacts (Viano, D. and Olsen, 2001; Farmer et al., 2003). Our research (Fuhrman, S. I. et al., 2005) indicates that wheelchair headrests are prescribed for over 60% of all wheelchair users, and for 80% of all pediatric wheelchair users. Despite high wheelchair-mounted headrest usage rates on wheelchairs and automotive industry interest in automotive headrest improvements, there have been no previous efforts to investigate the potentially beneficial effects of wheelchair headrest use for pediatric wheelchair-users in rear impact.

Historically, efforts by researchers, manufacturers, clinicians and transporters have been primarily directed at establishing voluntary frontal impact standards: *ANSI/RESNA WC19 - Wheelchairs Used as Seats in Motor Vehicles* (ANSI/RESNA, 2000) and *SAE - J2249 Wheelchair Tiedown and Occupant Restraint Systems for Use in Motor Vehicles* (Society of Automotive Engineers, 1996). ANSI/RESNA WC19 specifies design and performance requirements for wheelchairs used as seating in motor vehicles. SAE J2249 establishes requirements for wheelchair tiedown and occupant restraint systems (Schneider et al., 1999). Wheelchair transportation rear impact standards development is part of the current work plan by national and international standards committees.

The purpose of this investigational baseline study was to quantify and establish the potential benefit or harm of headrest use for wheelchair-seated pediatric occupants traveling in motor vehicles during rear impact. This study is an initial effort to describe pediatric injury risk in rear impact by using a pediatric anthropomorphic test device (ATD) to measure kinematics and injury risk parameters in rear impact. Since wheelchair-mounted headrests are not necessarily designed to provide occupant

protection during motor vehicle travel and are frequently prescribed, this study provides new data on pediatric ATD head and neck response as it relates to identifying associated risks or benefits of wheelchair headrest use in rear impact. It is anticipated that results from this investigation will contribute to the fundamental knowledge needed for pediatric wheelchair and headrest design guidelines development for rear impact protection. Ultimately, our efforts are intended to assist rear impact wheelchair standards development, wheelchair safety design improvements, and crashworthy wheelchair headrest development, thereby providing effective occupant protection during rear impact.

5.2 METHODS

The potential effect of headrest use on pediatric head and neck responses in rear impact collisions was assessed using a 6-year old Hybrid III ATD seated in a manual pediatric wheelchair. Two scenarios were compared and evaluated: wheelchairs not equipped with headrests (“no headrest”) and wheelchairs equipped with headrests (“headrest”). Six identical Sunrise Medical Quickie® Zippie® pediatric manual wheelchairs (17.9 kg) that comply with ANSI/RESNA WC19 (ANSI/RESNA, 2000) were used during testing: Tests 1-3 conducted without headrests, and Tests 4-6 conducted with identical slightly modified Sunrise Medical single-pad headrests. Data were collected for all tests and were used to determine established injury criteria values. Results were compared between scenarios and against established injury protection reference values and published injury thresholds.

All sled tests were conducted at the University of Michigan Transportation Research Institute (UMTRI)⁷ using a pneumatic, rebound-type accelerator designed to simulate typical crash velocities and accelerations. The targeted rear impact crash pulse consisted of a change in velocity of 16 mph (26 km/h) and 10-12g's sustained for 60 ms. At the time of testing, the crash pulse conformed with the currently proposed International Organization for Standardization (ISO) test pulse for use in development of a draft voluntary industry standard for wheelchair performance evaluation during rear impact (personal written communication with ISO TC173/SC1/WG6 committee members: ISO proposed rear impact standards and crash pulse severities on Nov 14, 2005). All wheelchairs were tested with wheelchair seatbacks positioned at a 90-degree seat-to-back angle with five degrees of posterior tilt. The ATD was appropriately positioned in the wheelchair. The ATD head was initially positioned no more than 1 cm forward of the headrest. Wheelchairs were properly secured according to ANSI/RESNA WC19 – Annex A using four-point strap-type surrogate wheelchair tiedowns; the ATD was restrained with a properly positioned three-point occupant restraint system (ANSI/RESNA, 2000). All wheelchairs were equipped with matched components and identically configured (Figures 21 and 22) with the exception of the slightly modified headrest. In Tests 4-6, where a headrest was used, the headrest was modified by inserting a 0.32 cm (1/8 inch) diameter pin into the headrest stem joint to prevent headrest anterior-posterior slippage during rear impact (Figures 22 and 23).

⁷University of Michigan Transportation Research Institute, 2901 Baxter Road, Ann Arbor, MI 48109-2150.

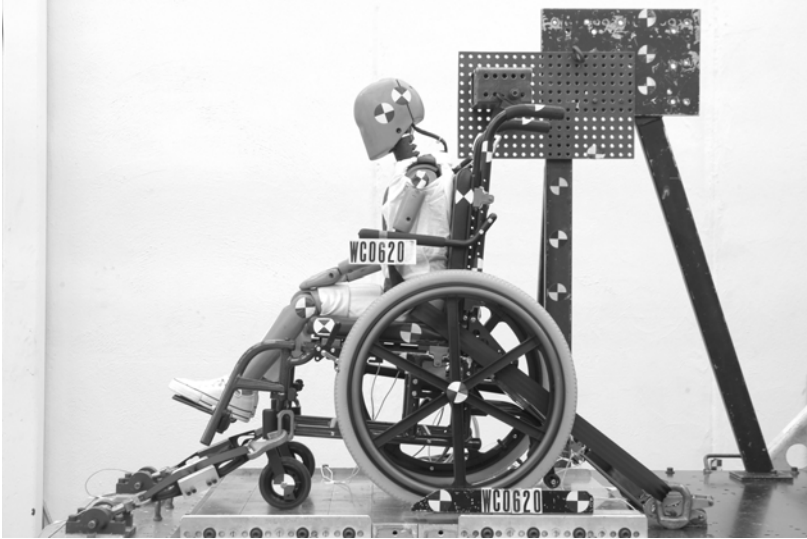


Figure 21: Wheelchair set-up without a headrest (Tests 1, 2 and 3). The wheelchair is secured with a four-point, strap-type tiedown system; the ATD is restrained with a 3-point occupant restraint.

Figure 22: Wheelchair set-up with headrest (Test 4, 5 and 6). A pin was inserted into the headrest stem joint to prevent anterior-posterior slippage. A high-contrast target (indicated by white arrow) marks the pin location.

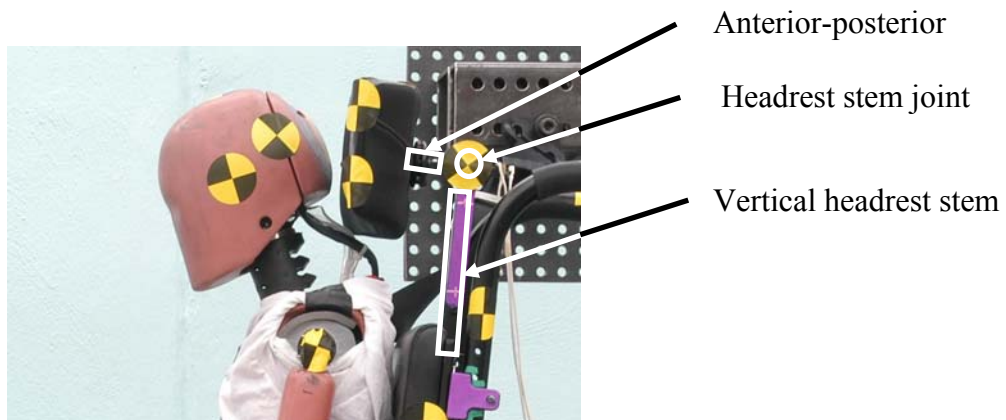


Figure 23: Detailed view of headrest identifying anterior-posterior headrest stem, headrest stem joint and vertical headrest stem.

The Hybrid III 6-year old ATD represented the pediatric occupant in all tests. ATD instrumentation captured head accelerations, neck axial forces and neck bending moments during rear impact testing. A tri-axial accelerometer⁸ was positioned at the head center of gravity (CG) and measured linear head accelerations; an upper neck load cell⁹ was positioned at the C1-C2 cervical spine level and measured neck loads and moments. High-contrast markers were placed on the head (two), shoulder and knee to indicate position throughout the test. Tests were recorded using two high-speed video cameras (1000 frames/sec) positioned to capture the side and top views. Transducer data were recorded every 0.1 ms and filtered according to SAE J211 (Society of Automotive Engineers, 1995).

Several different injury outcome measures were used to predict likelihood of head and neck injury based on measured data from the sled tests. Based on physical experimental and mathematical models of the head and/or neck, measurable parameters have been established to predict injury risk (Klinich et al., 1996; McLean and Anderson, 1997). Maximum linear head acceleration, head injury criteria (HIC) values, neck injury criteria (Nij) values, and combined rotational head velocity and acceleration were compared across test scenarios and used to determine comparative injury risk (Nahum and Melvin, 1993).

Kinematic data from the tests described the ATD dynamic response to rear impact. A Matlab® (Mathworks¹⁰) program was used to acquire and track high-contrast

⁸ Endevco, Model no. 7264C-2KTZ

⁹ First Technology Safety Systems, Model no. IF-205

¹⁰ <http://www.mathworks.com/products/matlab>

marker location coordinates. Kinematic data from video images were used to calculate rotational head velocity and rotational head acceleration in the sagittal plane for comparison to various injury thresholds. Both subdural hematoma (SDH) and diffuse axonal injury (DAI) proposed thresholds are related to rotational velocity and rotational acceleration (Lowenhielm, 1978; Margulies and Thibault, 1992; Ommaya et al., 2002).

The automotive industry has historically quantified injury using the Abbreviated Injury Scale (AIS) (Chawda et al., 2004). The AIS ranks injuries from 1 to 6 with AIS = 1 being minor and AIS = 6 being unsurvivable (Association for the Advancement of Automotive Medicine, 2005). A range of injury types are associated with each AIS level and are dependent on the injury type and body region (Van Rensburg, 2004; Association for the Advancement of Automotive Medicine, 2005).

Linear head acceleration, neck loads and neck moments, were used to calculate head injury criteria (HIC) values and neck injury criteria (Nij) values, respectively. HIC values were calculated using Equation 1 (McHenry, 2004). HIC_{15} , HIC_{36} , and HIC_{un} ¹¹ were calculated using corresponding time intervals measured in milliseconds.

HIC is dependent on both magnitude of head acceleration and duration of exposure. Peak head accelerations are associated with greater injury risk when sustained for longer time intervals. The various time intervals described by HIC_{15} , HIC_{36} , and HIC_{un} capture different aspects of head acceleration. The short 15 ms time interval is effective at capturing the intensity of the peak acceleration. The longer 36 ms and unlimited time intervals are more effective at capturing the effect of lower peak accelerations of longer time duration.

¹¹ “un” denotes unlimited time interval

The neck injury criteria (Nij) reflects combined loading mechanisms: neck axial loading (i) and neck bending moments (j) (King, 2000). Neck axial loads occur as tension or compression; neck bending moments occur as the neck flexes or extends. Axial loading and bending moments combine to produce observed neck injuries, with rear impacts responsible for most tension-extension injuries, which range from less severe whiplash injuries to more severe cervical spinal cord injuries (King, 2000). Nij (Equation 2) establishes critical limits for neck axial loading and bending moments (Kleinberger, Michael et al., 1998). Nij components were measured using the upper neck load cell, located at the ATD C1-C2 cervical spine level. The axial loads and bending moments were normalized using established critical values (Kleinberger, Michael et al., 1998).

5.3 RESULTS

Recorded sled impact acceleration pulses across tests indicate a high level of test repeatability. The structural integrity of wheelchairs was maintained across all tests. Sled test videos allowed for qualitative comparisons between tests conducted with and without headrests. Injury outcome measures indicate reductions in the likelihood of serious head and/or neck injury for Tests 4-6 conducted with headrests compared to Tests 1-3 conducted without headrests.

5.3.1 Sled test results

In all tests, peak sled impact acceleration levels were between 11.0g and 11.6g, and change in sled velocity (delta-V) was between 15.5 and 15.9 mph (25.0 and 25.6 km/h), meeting the targeted crash pulse. Figure 24 shows sled test acceleration profiles and demonstrates sled acceleration pulse repeatability.

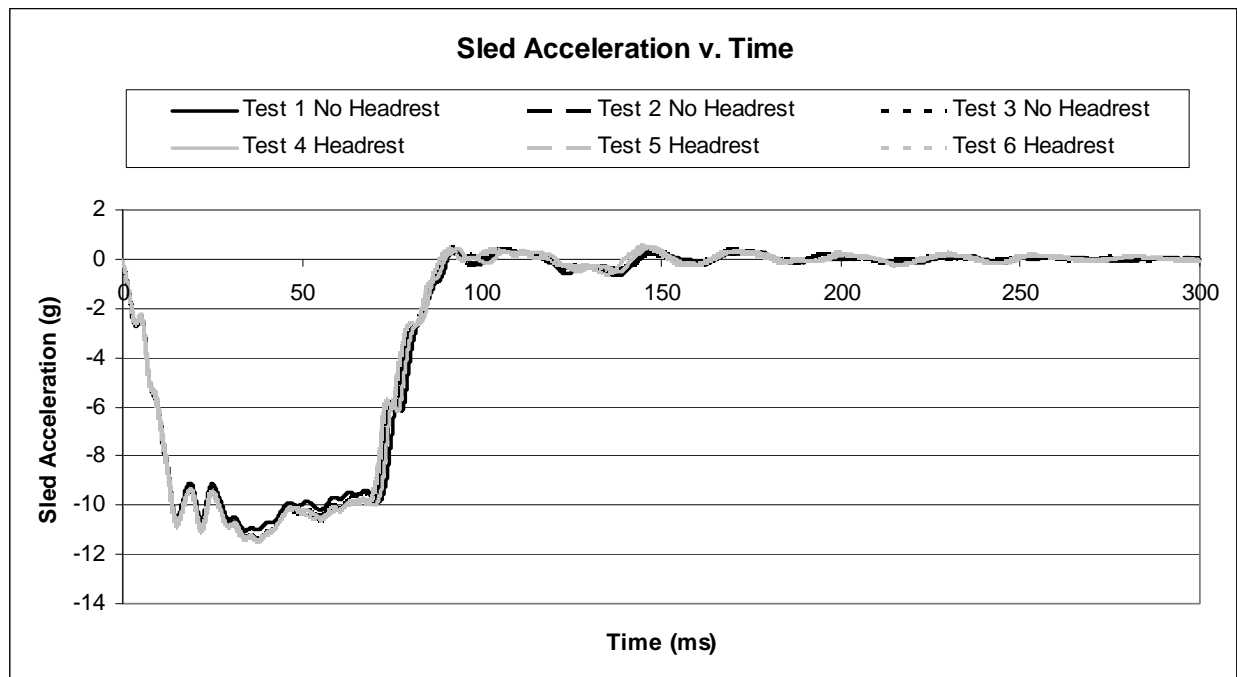


Figure 24: Rear impact sled test acceleration time history demonstrating an acceleration of approximately 11 g's and acceleration pulse repeatability.

The Zippie® wheelchairs remained structurally intact, and the ATD maintained an upright posture throughout all rear impact tests. Headrests and headrest attachment hardware also remained intact; vertical headrest stems deformed less than 5 degrees in all tests conducted with headrests. Vertical headrest stem bending occurred at the point where the mounting bracket secured the vertical headrest stem to the wheelchair seatback.

Initial visual inspection of sled test video images (Figure 25) suggests neck extension reductions with headrest use. Figure 25 compares typical video images captured as the ATD head reached maximum rearward excursion during Test 2 (no headrest) and Test 5 (headrest). During Test 2, conducted without a headrest, the posterior aspect of the ATD head contacts the top of the seatback. During Test 5 (headrest), video images illustrate the headrest limiting rearward head excursion and neck extension while the headrest remains intact.

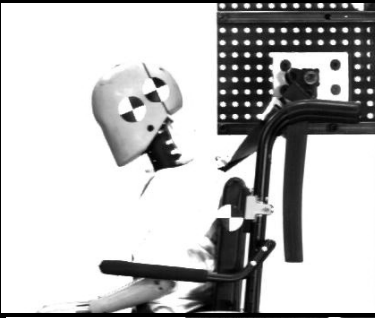
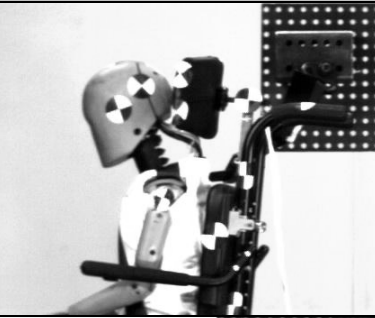
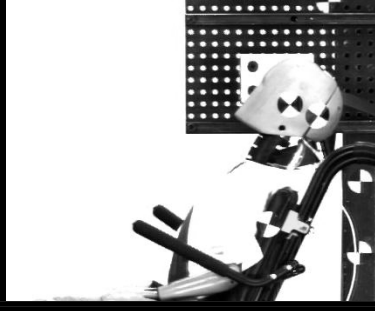
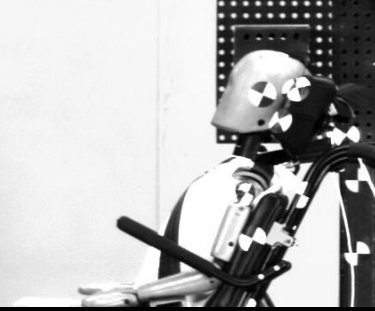
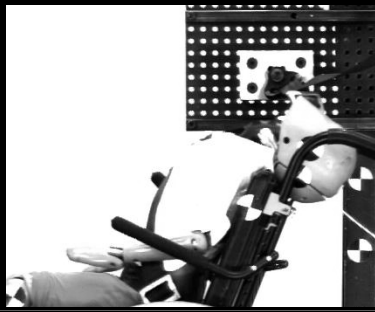
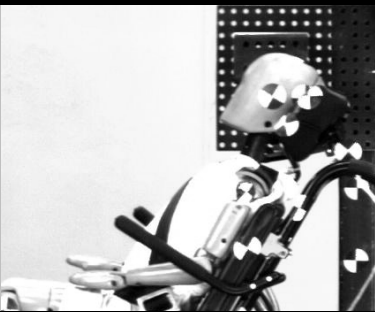
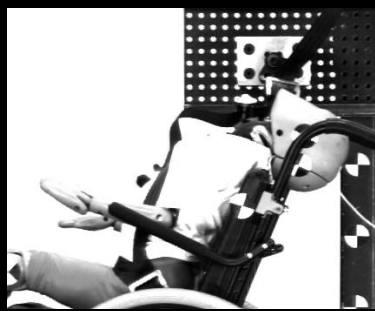
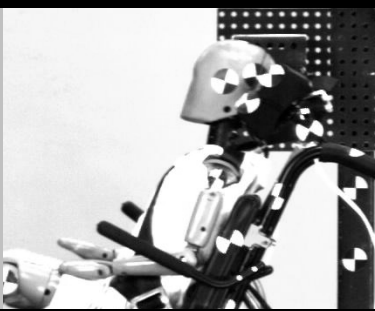

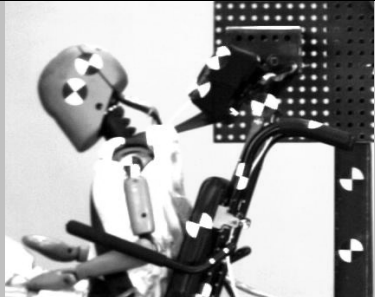
Test 2 – no headrest		Test 5 – headrest
	Start	
	30 ms before peak head excursion	
	Peak head excursion (Test 2 at 140 ms) (Test 5 at 120 ms)	
	30 ms post peak head excursion	
	End Total time: 240 ms	

Figure 25: ATD and wheelchair dynamic response with maximum ATD neck extension. Test 2 (no headrest) displays ATD rearward head rotation and contact with the top of the seatback. The headrest limits rearward head excursion in Test 5 (headrest).

5.3.2 Injury outcome measure results

Resultant linear head acceleration results (Figure 26) show higher peak head accelerations and longer durations of these accelerations during Tests 1-3 (without headrests) compared against Tests 4-6 (with headrests). Tests 1-3 show secondary acceleration peaks occurring during head-seatback contact. When compared to a proposed linear head acceleration protection reference value (PRV) of 80g (Klinich et al., 1996), a low probability of associated head injury is predicted for all test scenarios.

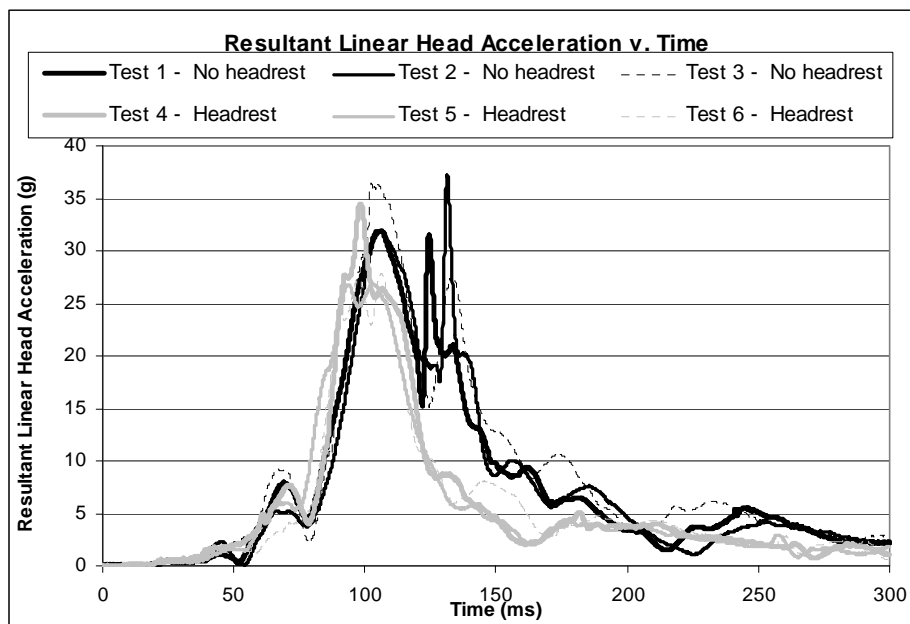


Figure 26: Resultant linear head acceleration measured during rear impact sled tests. Tests 1-3 (no headrests) have higher acceleration peaks of longer duration than Tests 4-6 (headrests). Head to seatback contact cause secondary peaks in Tests 1-3.

HIC value results calculated for 15 ms duration, 36 ms duration, and the complete test are indicated in Figure 27. HIC PRVs for the 6-year old ATD are: $HIC_{un}=1000$, $HIC_{36}=1000$, $HIC_{15}=700$ (Irwin and Mertz, 1997). These levels are associated with a 23% chance of AIS head injury level ≥ 3 (Klinich et al., 1996); AIS scores of 3 may include head injuries such as skull injuries occurring at the base of the skull, or compound, commuted or depressed skull fractures (Association for the Advancement of Automotive Medicine, 2005). Tests 4-6 conducted with headrests yielded average HIC values that were 34% lower than Tests 1-3 conducted without headrests, although all HIC values were below PRVs.

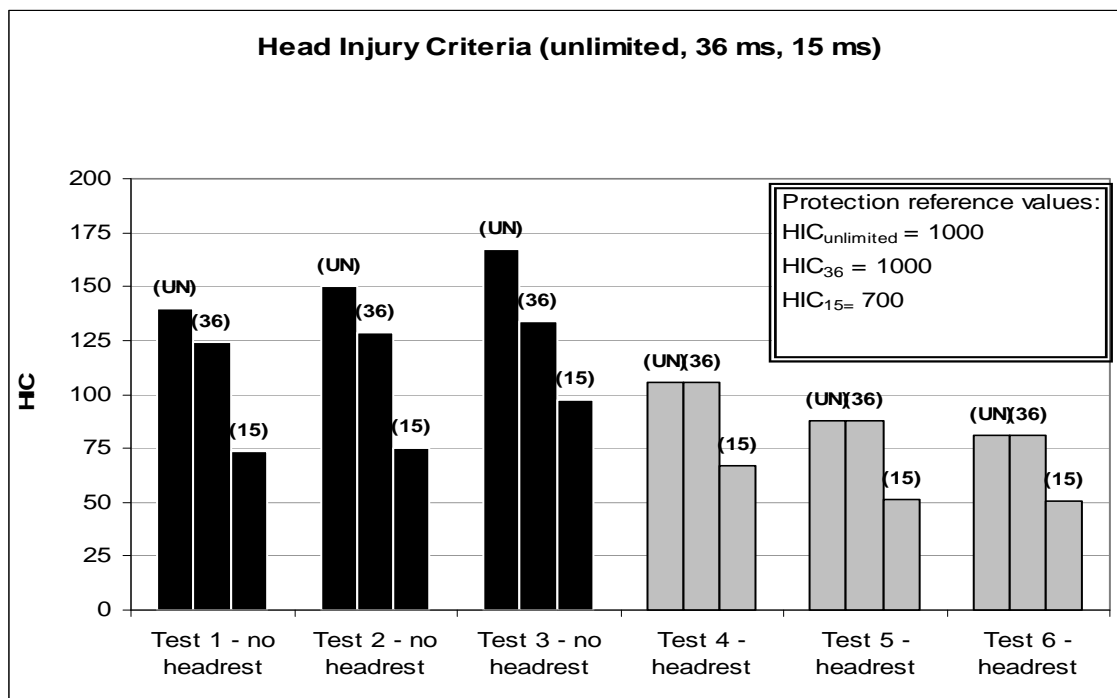


Figure 27: HIC values for three time intervals: total test (unlimited), 36 ms, and 15 ms. All values are below established PRVs. Tests 4-6 (headrests) produced mean HIC values 34% lower than mean values for Tests 1-3 (no headrests).

Figure 28 and Figure 29 highlight improved neck response with headrest use. $N_{ij} \geq 1$ is the PRV and is associated with a 22% probability of an AIS ≥ 3 injury (National

Highway Traffic Safety Administration, 1993; Eppinger et al., 1999). In general, the most injurious mechanism observed during rear impact is measured during the tension-extension portion of Nij (Klinich et al., 1996). Our Nij results indicate that ATD neck response in rear impact without a headrest exceeds the PRV of Nij=1. This occurs when the ATD neck reaches maximum extension and the neck is loaded axially in tension.

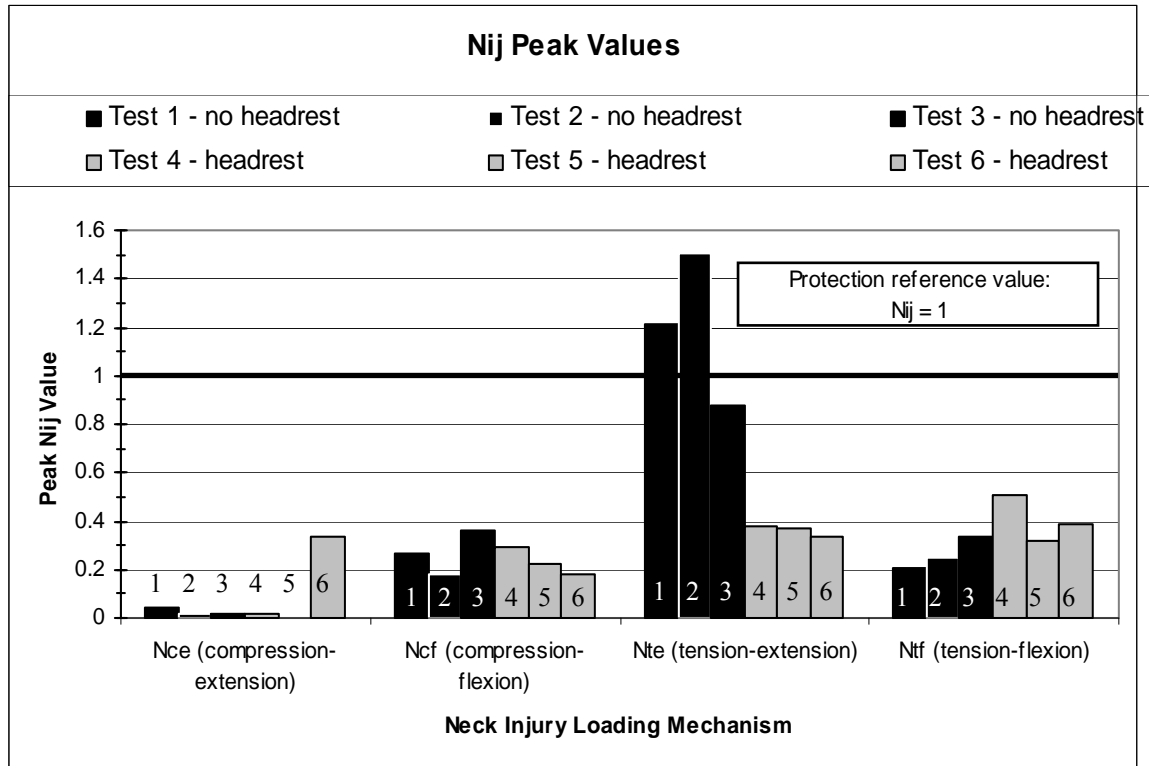


Figure 28: Nij peak values. Tests 4-6 (headrests) have mean Nij values 70% lower than Tests 1-3 (no headrests). Tests 1 and 2, both lacking headrests, exceed the PRV during tension-extension.

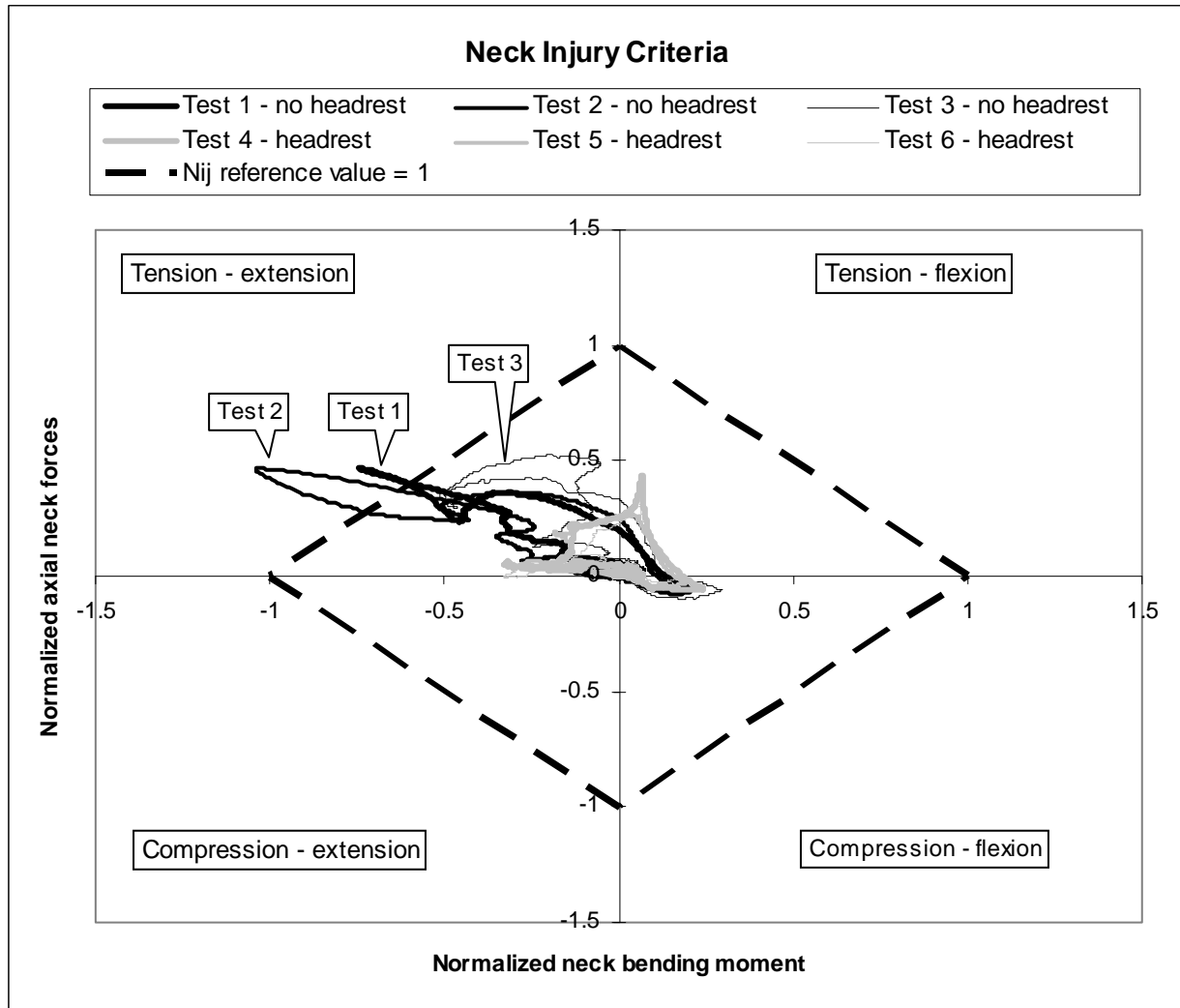


Figure 29: Neck Injury Criteria (Nij). Nij outcomes are divided into four quadrants, plotting axial neck loading (tension-compression) against neck bending moments (flexion-extension). Values outside the Nij=1 reference value exceed established PRVs. Tests 1 and 2 (no headrests) exceed Nij=1.

Nij peak magnitudes are shown in Figure 28. Tension-extension loading is the primary loading mechanism resulting from our tests. In tests conducted without headrests, the mean Nij peak for tension-extension is over four times larger than Nij peaks from the other loading mechanisms. Tests 4-6 (headrest) had a 70% average reduction in peak $N_{\text{tension-extension}}$ (N_{te}) compared with Tests 1-3 without headrests.

Figure 29 plots combined neck axial loading and bending moments over the entire test duration allowing comparison between tests and against the neck injury criteria ($N_{ij} = 1$), designated by the dashed diamond-shaped line. Figure 29 illustrates the extent and duration of the N_{ij} response that exceeds the PRV. Results from Tests 4-6 (with headrest) are all well within the PRV of $N_{ij} = 1$, appearing as grey curves close to the origin. Results from Tests 1 and 2 (black curves), which do not include headrests, lie outside the PRV (dashed line) and indicate that the PRV is exceeded during the tension-extension portion of the impact response.

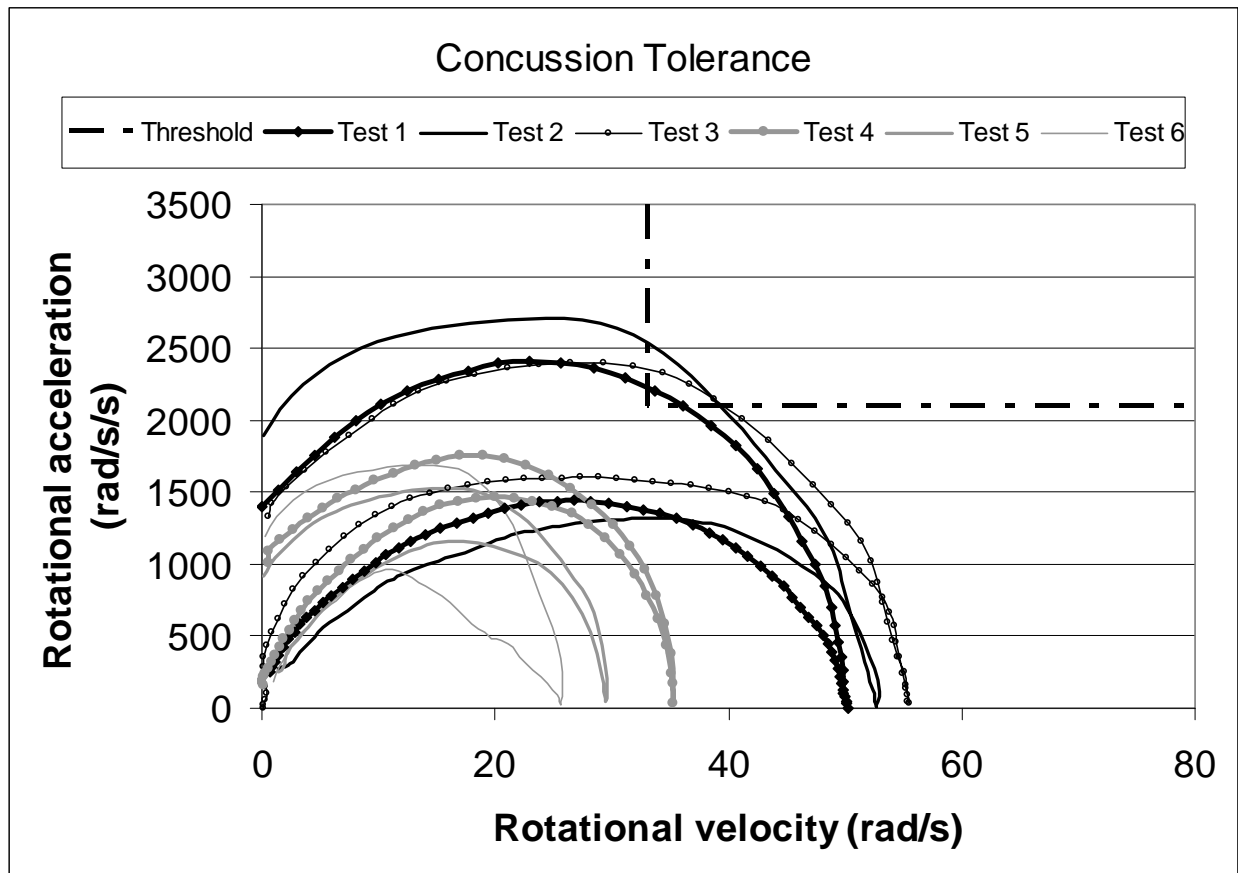


Figure 30: Tolerance to concussion using combined rotational velocities and accelerations. Tests 1-3 (no headrests), exceeded the proposed thresholds (Ommaya et al., 2002). Tests 4-6 (headrests) values are all below the threshold.

Combined rotational head velocity and rotational head acceleration (Figure 30) indicate that headrests reduced rotational effects on the head. Injurious rotational head accelerations can occur with or without an acceleration inducing head impact. A proposed combined rotational acceleration and velocity threshold with head impact, for a 6-year old, is 2100 rad/s^2 in combination with an rotational velocity limit of 33 rad/s (Ommaya et al., 2002). This rotational head response threshold establishes a 50 percent probability of cerebral concussion (Klinich et al., 1996; Ommaya et al., 2002), and is used for comparison purposes in our study. In our testing, the ATD head impacted the headrest in Tests 4-6, and impacted the wheelchair seatback in Tests 1-3 (Figure 5), hence the Ommaya 2100 rad/s^2 , 33 rad/s threshold is appropriate for our comparative purposes. PRVs for non-impact induced rotational head accelerations are much higher. Sturtz (Sturtz, 1980) suggests a scaled peak rotational head acceleration PRV for the 6-year old of 7390 rad/s^2 for indirectly caused rotational head accelerations with a duration limit of 10 msec based on Ommaya's results (Ommaya and Hirsch, 1971). Figure 30 displays the 2100 rad/s^2 , 33 rad/s threshold for accelerations with impact, (indicated by the dashed line) along with rotational velocities and accelerations measured for each test. Tests 4-6 (headrests) are indicated in grey and fall below the threshold, while Tests 1-3 (no headrests) are indicated in black and extend above the threshold. Thus, Tests 1-3 conducted without headrests indicate a risk of concussion under these conditions.

Even without impact, rotational head accelerations have been shown to cause subdural hematoma (SDH) (Pounder, 1997). SDH is caused by rupture of the bridging veins between the cerebral cortex and the superior sagittal sinus, with SDHs more likely to result from rotational head accelerations caused by impact to the occiputs (Kleiven,

2003; Depreitere et al., 2006). Lowenhielm (Lowenhielm, 1978) established an SDH threshold of rotational head acceleration 4500 rad/s^2 coupled with a maximum change in rotational head velocity of 50 rad/s for a ten year old. In our testing, Tests 1-3 (no headrests) produced peak head accelerations of $2412\text{-}2709 \text{ rad/s}^2$. Tests 4-6 (with headrests) had lower peak rotational accelerations of $1529\text{-}1755 \text{ rad/s}^2$. In our testing, the 50 rad/s maximum change in rotational head velocity was met or exceeded only by Tests 1-3 conducted without headrests. However, since all peak accelerations are below the threshold, this would suggest that in our rear impact sled tests, pediatric occupants would be unlikely to sustain SDH.

Experimental test data was compared against a proposed DAI threshold (Margulies and Thibault, 1992). All test results were below the DAI threshold, with Tests 4-6 (headrests) further below the threshold than Tests 1-3 (no headrests). Results indicate that it is unlikely that the rotational head response induced by our rear impact crash scenarios would be likely to cause DAI.

5.4 DISCUSSION

Each injury outcome measured showed peak value reductions for tests with a headrest as compared to tests without a headrest; Linear head accelerations, HIC values, Nij values, rotational head velocity, and rotational head acceleration all demonstrated reductions in excess of 34%, and in some cases as high as 70%. This is an important study finding since 80% of pediatric wheelchairs are prescribed with headrests and some school systems require wheelchair users to have a headrest for transportation purposes

(Fuhrman, S. I. et al., 2005). Our findings suggest that children who remain seated in wheelchairs while traveling in motor vehicles and who do not use headrests may be exposed to increased risk of head and neck injuries. Safety benefits may be gained by developing commercial wheelchair-mounted headrests that provide rear impact protection in addition to postural support for individuals who travel in motor vehicles while seated in their wheelchairs.

Automobile manufacturers have successfully focused design efforts on creating automotive head restraints that afford increased passenger safety in rear impact (Viano, D. and Olsen, 2001; Farmer et al., 2003) with 33% reductions in neck injury such as whiplash injuries or acute neck strains. The importance of neck injury protection during travel in a motor vehicle is also reflected in the Federal Motor Vehicle Safety Standard FMVSS 202 – *Head Restraints for Passenger Vehicles* (Department of Transportation (DOT), 2000), which is intended to reduce the likelihood of neck injury in rear impact. Our test video images graphically depict the role that head rotation and neck extension played in our test results (Figure 25) and the potentially protective effects of wheelchair-mounted headrest use for limiting the rearward head motion. These results were particularly encouraging as wheelchair-mounted headrests are not primarily designed for transportation safety. Our key Nij findings of 70% reductions in peak Nte to values below PRV, are associated with a reduced likelihood of neck injuries ranging from ligamentous sprains and strains to far more serious neck injuries. Furthermore, it is anticipated that headrests that can provide occupant protection during rear impact would also provide enhanced neck protection within the dynamic vehicular environment during normal driving events.

Assuming wheelchair integrity, an adequately restrained occupant and a properly secured wheelchair, our low HIC values for both scenarios indicate that primary injury mechanisms in rear impact are not due to contact-type head injuries such as skull fractures. In general, linear head accelerations tend to be severe when the head forcibly contacts hard surfaces such as vehicle interiors. In our tests, head contact occurred only with well-padded seatbacks or headrests, resulting in low linear head accelerations and low HIC values. Our test set up did not show a significant reduction in the likelihood of skull fractures with the addition of a headrest since all HIC values were well below PRVs. However, reduction of real-world head excursion by use of a headrest will reduce the likelihood of head contact with the vehicle interior. Headrest use did reduce HIC values by approximately 34% since the linear accelerations produced by the ATD tested in headrest-equipped wheelchairs were lower and of shorter duration than those produced by the ATD in wheelchairs without headrests.

Ommaya et al. (Ommaya et al., 2002) summarized their previous work indicating that the brain is more sensitive to rotational head motion in combination with linear acceleration than to linear acceleration alone. Peak rotational acceleration can occur with or without a causative head impact. Damage from rotational acceleration can cause damage to bridging veins resulting in subdural hematoma (SDH) or trauma to axons resulting in concussion or diffuse axonal injury (DAI). DAI are brain injuries that result from shear forces causing trauma to the axons within the brain with resulting injuries ranging from mild concussion to persistent vegetative state (Margulies and Thibault, 1992; Klinich et al., 1996). DAI occurs primarily due to rotational accelerations that may or may not include head impact. Margulies' proposed DAI criterion relates peak

rotational head acceleration against peak change in rotational head velocity. In our tests, the wheelchair-mounted headrest appears to have further reduced the likelihood of injuries from SDH and DAI injuries (including concussion) as indicated by the reductions in the combined head rotational velocity and acceleration to levels below Ommaya's, Lowenhielm's and Margulies' proposed thresholds (Lowenhielm, 1978; Margulies and Thibault, 1992; Ommaya et al., 2002).

Biofidelity is a potential limitation in all testing using human surrogates. This study used the Hybrid III 6-year old ATD whose biomechanical response was based on the Hybrid III 50th percentile male, and scaled using pediatric anthropometric and mass data and the elastic modulus of pediatric bone (Irwin and Mertz, 1997). This ATD was upgraded in 1997 to reflect more recent evaluations of airbag deployment effects on children (First Technology Safety Systems, 2005). The ATD represents the current state of the science for human biofidelity of a 6 year old child, yet is potentially representative of only the narrow portion of the able-bodied population described by the 50th percentile 6-year old. In an effort to address ATD biofidelity limitations, responses were examined and compared across scenarios. Children with disabilities may have additional biomechanical response differences from the Hybrid III 6-year old ATD. However, it is expected that biomechanical responses of children with hypo- or hypertonia would demonstrate similar trends across headrest scenarios, with the wheelchair-mounted postural headrest offering increased occupant protection.

The Hybrid III 6-year old ATD neck has come under scrutiny for its biomechanical response characteristics; discussion has focused on possible disproportionately high neck mobility (Sherwood et al., 2003). Nonetheless, a number of

researchers have used pediatric Hybrid III ATDs to evaluate impact crash events (Oster and Trommler, 1996; Sherwood et al., 2003; Ha, DongRan, 2004; Malott et al., 2004). Possible ATD biofidelity limitations include a stiff thoracic spine (Sherwood et al., 2003) that causes a disproportional amount of the spinal bending to occur in the cervical spine rather than being distributed along both the cervical and thoracic regions. This may have affected our results by magnifying the head and neck responses. However, our primary focus was on comparison of headrest versus non-headrest scenarios, which yielded comparative outcome data and percentage reductions in injury risk outcome measures for the headrest scenario.

Other potential limitations in ATD biofidelity include that while results in frontal impact tests produced high N_{ij} , injuries associated with these high values are not reflected in field data (Malott et al., 2004). Yet, comparisons between the 6-year old Hybrid III, Part 572 and TNO P6 ATDs demonstrated superior Hybrid III biofidelity (Oster and Trommler, 1996). Accordingly, the Hybrid III 6-year old ATD has been used to examine the effect of pre-tensioning and force limiting of seatbelts on injury risk and relied on for computer model validation (Sherwood et al., 2003; Ha, DongRan, 2004). It has been used to evaluate various child occupant restraints (Malott et al., 2004) where N_{ij} values have been compared to establish protection reference values, and has extensive instrumentation capabilities with 46 available data channels (First Technology Safety Systems, 2005). The Hybrid III was adopted for FMVSS 208 testing in 1986 (National Highway Traffic Safety Administration, 1993), is considered the industry standard, and has extensive optional instrumentation available. The Hybrid III child ATDs are proposed to replace the Hybrid II ATD in FMVSS 213 (National Highway Traffic Safety

Administration, 1999). Given this evidence, using the Hybrid III 6-year old ATD was the most appropriate ATD choice for our study.

Many of the injury PRVs and thresholds used in this study were initially developed for the 50th percentile male ATD and scaled for smaller ATDs. Scaling parameters include size, mass and modulus of elasticity of bone. Many scaling parameters have been based on limited testing (Young et al., 1976; Klinich et al., 1996; Irwin and Mertz, 1997; Society of Automotive Engineers: Dummy Testing Equipment Subcommittee, 2003). Furthermore, DAI and SDH injury thresholds were derived from primate testing (Ommaya and Hirsch, 1971; Sturtz, 1980; Ommaya, 1985; Margulies and Thibault, 1992). However, it has been accepted in the scientific literature that PRVs can be effectively used to compare various scenarios such as we have done in this study.

In our tests, the ATD was seated in an upright position with the headrest in optimal proximity to the head. These factors may influence injury risk outcome measures. Future research will investigate the effect of seatback angle and suboptimal headrest placement on the injury risk outcome measures using computer simulations.

5.5 CONCLUSIONS

Study findings indicate that slightly-modified commercially available wheelchair headrests can maintain structural integrity in rear impact. When compared to headrest non-use, headrest use has the potential to provide increased head and neck occupant protection during rear impact for children seated in wheelchairs in motor vehicles. Every injury outcome measure value assessed was reduced with wheelchair headrest use as

compared to non-use. These results support current recommendations that a properly positioned wheelchair-mounted headrest can help protect the head and neck of a wheelchair-seated occupant in a rear impact (RERC on Wheelchair Transportation Safety, 2007; University of Michigan, 2007). Future research efforts will focus on development of wheelchair headrest design guidelines that specify characteristics suitable for rear-impact crashworthiness.

6.0 DEVELOPMENT OF MADYMO SIMULATION MODELS

Two computer simulation models of pediatric manual wheelchair in rear impact were developed using MADYMO simulation software; one model included a simple single pad headrest, the second included no headrest. Initially, two series of three sled tests each were conducted using a seated Hybrid III 6-year old anthropomorphic test device (ATD) to load identical manual pediatric wheelchairs. Series HR (headrest included), equipped with a simple single-pad headrest, and Series NoHR (no headrest) were both tested with a 16 mph/11g/60 ms impact. Sled, wheelchair, and ATD kinematics were measured and used to establish time-history response corridors for simulation model comparison and validation purposes. Parameters examined for model validation include wheelchair tiedown loads, wheelchair center of gravity acceleration, lap belt loading, chest acceleration and head acceleration. Model outputs were visually compared to sled test response corridors, and statistically compared to sled test mean responses for mean ratios, correlations, and standard residuals. Results indicate that the models are validated and can be used to explore the effects of wheelchair and headrest design on injury risk during rear impact and for the development of design guidelines for rear impact.

6.1 INTRODUCTION

Federal Motor Vehicle Safety Standards (FMVSS) serve to protect occupants traveling in motor vehicles. Standards specify design and performance requirements that manufacturers must meet for a variety of vehicle safety features (Department of Transportation (DOT), 1977; Department of Transportation (DOT), 1982a; Department of Transportation (DOT), 1993; National Highway Traffic Safety Administration, 1993; Department of Transportation (DOT), 2000; Department of Transportation (DOT), 2002). FMVSS also specifies standards for after market child restraint devices designed to provide occupant protection for infants, toddlers and children (National Highway Traffic Safety Administration, 1999). Although both children and adults with physical disabilities may continue to use their wheelchairs as seating while traveling in motor vehicles, FMVSS does not specify wheelchair crashworthiness safety standards to protect them in the motor vehicle environment. ANSI/RESNA (ANSI/RESNA, 2000) and ISO (ISO, 1999b; ISO, 1999a; ISO, 2005a) have developed voluntary frontal impact standards for wheelchairs used as seating in motor vehicles. No current mandatory or voluntary standard exists for wheelchairs used as seating in motor vehicles in rear impact.

The majority of fatal automotive accidents occur in frontal impact, yet the majority of all injuries result from rear impact (Transportation National Highway Traffic Safety Administration, 1990). FMVSS 202 – *Head Restraints for Passenger Vehicles* (Department of Transportation (DOT), 2000) mandates head restraint standards for passenger vehicles, specifying minimum height and component strength requirements. Again, there are no comparable protections for the wheelchair-seated occupants in rear impact. Wheelchair standards development research depends heavily on costly sled

testing and on computer simulation modeling to reproduce the vehicle crash dynamics. Once a computer simulation model is validated it can be used to assess outcomes that may be difficult to measure with physical sled testing, as well as to evaluate the effects of multiple wheelchair configurations to aid in crashworthy wheelchair design.

Previous computer simulation models have examined frontal impacts for both children and adults. A seated Hybrid III 6-year old ATD was used with a pediatric manual wheelchair (Ha, D. et al., 2007), and a seated Hybrid III 50th percentile male ATD has been used with adult wheelchairs (Bertocci, G. E. et al., 1996b; Bertocci, G. E. et al., 1999; Bertocci, GE and Szobota, 2000; Bertocci, G. et al., 2000; Leary and Bertocci, 2001; Souza and Bertocci, 2001; Van Roosmalen, L. et al., 2001). Salipur (Salipur et al., 2007) used sled testing in rear impact to examine wheelchair tiedown and occupant restraint system (WTORS) loading for adults using manual wheelchair; we have also using sled testing in rear impact to examine WTORS loading (Fuhrman, S. I. et al., 2006) and also to compare the effect of wheelchair mounted headrests on pediatric head and neck injury (Fuhrman, S. I. et al., 2008). The computer simulation models described herein are the first simulation of the pediatric wheelchair in rear impact.

6.2 METHODS

These MADYMO simulation models were designed to accurately mimic the response of a Zippie (Sunrise Medical) manual pediatric wheelchair, loaded with a seated Hybrid III 6-year old ATD during a 16 mph, 11g rear impact, sustained for 60 ms. In both the models and in the sled tests, the wheelchair was properly secured according to

ANSI/RESNA WC19 – Annex A using a four-point strap-type surrogate wheelchair tiedown; the ATD is restrained with a properly positioned three-point occupant restraint system (ANSI/RESNA, 2000). MADYMO is a simulation software package that allows the user to create dynamic rigid multi-body computer simulation models. MADYMO is used extensively within the automotive industry and the simulation package includes pre-constructed and validated multi-body models of all frequently used Hybrid III ATDs. MADYMO users create their own models with user specified geometries and properties, and can then import the ATD models directly into their own simulation models. Development of well-validated models allow for subsequent exercise of the models, contributing to design guidelines for wheelchairs used as seating in motor vehicles in rear impact.

The MADYMO models were built using inputs from sled testing: crash pulse, tiedown geometry, wheelchair geometry, and ATD position, as well as material properties and contact responses. The MADYMO simulation models used input data from two series of three sled tests each, which were conducted using identical wheelchairs and configurations. Series NoHR sled tests were conducted with no headrest and formed the basis for Model NoHR; Series HR sled tests were conducted with a wheelchair-mounted single-pad headrest and formed the basis for Model HR. During physical sled testing, transducers collected data for sled acceleration, WTORS loads, wheelchair center of gravity acceleration, as well as head and chest accelerations and neck axial loading and neck bending moments. Visual targets identified the rear wheel hub, front caster hub, wheelchair seat cushion (2), wheelchair seatback, ATD head (2),

and ATD knee. Model data are filtered per SAE J211 (Society of Automotive Engineers, 1995).

Model HR and Model NoHR were then developed (Figure 31). The more complex headrest included model (Model HR) was developed first and validated against sled test Series HR data. The model with no headrest (Model NoHR) was created second by removing the headrest from Model HR and validating those results against sled test Series NoHR data. Each MADYMO model is composed of several systems that individually represent the reference space (track), test sled, wheelchair, Hybrid III 6-year old ATD, tiedowns, finite element lap and shoulder belts. Systems are composed of separate bodies, with surfaces, and user-defined properties and contacts between surfaces. Bodies are joined with revolute, translational, bracket and combination joints, with specified joint properties. The systems are then accelerated by the sled test pulse and gravity.

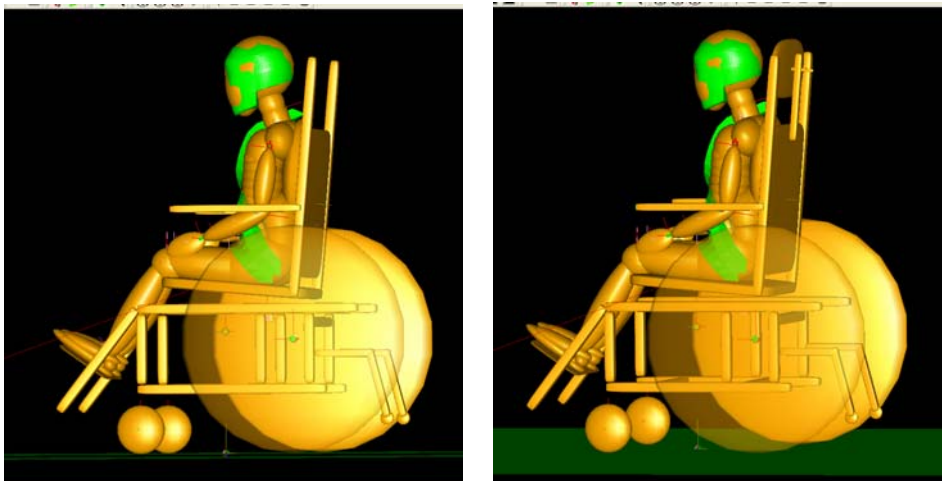


Figure 31: MADYMO simulation models. Model NoHR (left), Model HR (right).

Table 7 lists and describes the Model HR systems. The Model HR track system defines the reference space. Model HR sled is a plane; a translational joint connects it to the track allowing the sled to travel along the track. The sled system also has four

tiedown anchor points and three occupant restraint anchor points for wheelchair tiedown and occupant system (WTORS) anchorage.

Table 7: Model HR components

System	Bodies	Surfaces	Joints
Track	reference space	track surface	
Sled	Sled body	sled surface	translational joint between sled and track
		tiedown anchor points (4)	defined locations
		occupant restraint anchor points (3)	defined locations
Wheelchair	Frame CG body	all frame tubing	free joint between frame CG and sled
	rear wheels bodies (2)	Left wheel, right wheel	revolute joint between frame and rear wheel (2)
	front caster bodies (2)	left caster, right caster	revolute joint between frame and front casters (2)
	seatback	seatback, headrest, seatback canes	revolute joint between frame and seatback
	seat pan	seat pan	bracket joint between frame and seat pan
	wheelchair accelerometer	accelerometer surface	bracket joint between frame and accelerometer
		tiedown securement points (4)	defined locations
ATD (TNO, 2005)	ATD bodies (28)	ATD surface elements (51)	ATD joints (28)
Lap belt	Finite element belt	50 elements	defined securement point locations (sled)
Shoulder belt	Finite element belt	65 elements	defined securement point locations (sled)
Tiedown belts	Simple belts	n/a, line element belts	attachment points on wheelchair and sled

The wheelchair system is composed of eight individual bodies. The wheelchair frame is a single rigid body, each wheel is a separate body, the seat pan and seatback are separate bodies, and the wheelchair accelerometer is a separate body. Four tiedown securement points are defined on the wheelchair frame. Each body has associated

surfaces as indicated in Table 7. Of note, the headrest surfaces are defined with respect to the seatback body. Joints establish relationships between the bodies. All wheels attach to the frame with revolute joints. The seatback also uses a revolute joint to attach to the wheelchair frame, allowing it to deflect during rear impact. The accelerometer body is attached to the frame with a bracket joint mirroring its position on the physical wheelchair during sled testing.

The Hybrid III 6-year ATD system used in Model HR is provided as part of the MADYMO software package (TNO, 2005). It is a complex system with 28 individual bodies, 51 associated surfaces and 28 joints defining the relationships between the bodies. The Hybrid III 6-year old ATD system has also had limited validation against a single frontal impact sled test.

The lap and shoulder belt systems are created using the MADYMO “belt-fitter” software tool. Once the occupant restraint anchor points are defined, the user directs the software to create a 2-D finite element mesh for each occupant restraint belt. The lapbelt has 50 elements; the shoulder belt has 65 elements.

Tiedown belts are modeled as line elements securing the model wheelchair to the test sled. Tiedown anchor points are defined on the model sled, securement points on the wheelchair. The location of these points was determined by the position of the anchor points on the physical test sled, and the securement point on the physical wheelchair.

Model NoHR has identical elements as Model HR with the exception of the headrest related surfaces. After Model HR was built and validated, Model NoHR was constructed by eliminating the headrest pad, vertical and horizontal headrest stems, and

all head to headrest contact data. Head to seatback contact definitions were added to Model NoHR to define the contacts between the ATD head and the seatback.

Experimental response outcome corridors were established independently for each experimental test series, Series HR and Series NoHR, for tiedowns loads, wheelchair accelerations, lap belt loads, chest accelerations, upper neck forces, upper neck moments and head accelerations. For each series and each outcome, sled test data were time matching across tests, then compared to determine the maximum and minimum time-history plots. Model data were then plotted together with the experimental response corridors allowing visual comparisons between the experimental and model data. These comparisons were also useful during model development, as undesirable model responses could be evaluated against experimental kinematics and loading.

Strength of model results and their predictive capabilities are fully dependent on model validity. Statistical evaluation of model responses compared to experimental response corridors quantifies model strength. Model data were evaluated against mean experimental data. Pipkorn and Eriksson (Pipkorn and Eriksson, 2003) suggest several tests and result thresholds for evaluating the validity of mathematical models. Parameters were evaluated using four tests: (1) mean ratio comparison, (2) correlation, (3) standard deviation of the residual, and (4) a comparison of the time and magnitude of peak occurrence (box maximum). Mean value ratio (Equation 10) is the ratio of the overall means of the two data sets, with target values of 80-120%.

Equation 9: Average signal

$$\bar{s} = \frac{\sum f_i}{n}$$

\bar{s} = average signal

f_i = signal to be compared

n = number of samples

Equation 10: Mean value ratio

$$\text{Mean value ratio} = \frac{\bar{s}_1}{\bar{s}_2}$$

\bar{s}_1 = average signal for data set 1

\bar{s}_2 = average signal for data set 2

Our target threshold for correlation (r) between the mean sled test and model time-history is $r \geq 0.80$ (Equation 11).

Equation 11: Correlation coefficient

$$r = \frac{\sum_{i=1}^n (f_i - \bar{f})(g_i - \bar{g})}{\sqrt{\sum_{i=1}^n (f_i - \bar{f})^2 \sum_{i=1}^n (g_i - \bar{g})^2}}$$

f_i = measured signal, \bar{f} = average signal

g_i = predicted signal, \bar{g} = average signal

Maximum standard deviation (Equation 12) of the residual target is not to exceed 20% of the peak value.

Equation 12: Standard deviation

$$\sigma_e = \sqrt{\frac{n \sum f_i^2 - (\sum f_i)^2}{n(n-1)}}$$

f_i = residual

n = number of data points

Box maximum is a comparison of the peak value for each time-history; the target window at the maximum value in the time-history is to be within $\pm 20\%$ of the peak value and ± 5 ms (Table 8).

Table 8: Pipkorn thresholds

Pipkorn thresholds		
Statistical test	Target threshold	Description
Mean Value Ratio	0.8-1.20	Ratio of average values
Correlation	≥ 0.80	Compares the shape of the signals
Standard deviation of the residual	≤ 0.20	Standard deviation of the residual, should be within 20% of the peak value of the test
Box maximum	+/- 5ms, +/-20%	Compares the time of peak occurrence and peak magnitude between data series

Pipkorn (Pipkorn and Eriksson, 2003) qualifies these thresholds with the assertion that “thresholds based on the predictions of the model do not need to have a closer fit to the results from one experiment than the fit between the results from two mechanical tests.” Target thresholds for statistical measures were modified to reflect the variability observed between the sled tests within each test series.

6.3 RESULTS

Results are divided into three sections. The first section presents the results from the statistical comparison of sled test data to establish revised target thresholds when variability between experimental data exceeded Pipkorn thresholds. Thresholds are used for full model validation. The second and third sections separately present results from Model HR and Model NoHR validation.

Sled test time-history responses were first compared for front left and right tiedown loads, wheelchair acceleration, lap belt loads, chest acceleration, head acceleration in the X (fore-aft) and Z (vertical) directions, upper neck loads in the X (fore-aft) and Z (axial) directions and upper neck moments. Data for each test series are compared only within the test series; for example, Series HR sled test data from Tests 4-6 are compared only against each other and later against Model HR outcomes. Comparisons are used to: (1) establish a mean time-history response, (2) create minimum-maximum response corridors, (3) quantify comparisons between sled tests, and (4) quantify the fit between model results of the experimental sled tests. Model results are compared to the mean sled test time-history response and to the individual sled test time-history responses, replicating the comparisons made between the sled tests.

6.3.1 Statistical comparison between sled test data

Per Pipkorn's recommendation (Pipkorn and Eriksson, 2003), statistical comparisons were made between sled tests within each test series to verify target thresholds for statistical evaluation. Pipkorn's target thresholds were used unless inter-sled sled test

comparisons exceeded Pipkorn's thresholds. In those cases, the target thresholds for model validation were revised to reflect experimental variability. Series HR included three sled tests: Test 4, Test 5 and Test 6. Comparisons were made between each possible pair of sled tests: Test 4 to 5, Test 4 to 6, and Test 5 to 6. Series NoHR included three tests: Test 1, Test 2 and Test 3. However, as previously described (Table 6), Test 1 seatback position differed from Test 2 and 3. Test 1 was the first sled test of a pediatric wheelchair in rear impact. Based on information from therapists, the decision was made to conduct the first test with the top of the seatback positioned level with the ATD shoulder. Large seatback excursions along the seatback canes were noted during the sled test. In subsequent sled tests (Tests 2-6) all wheelchairs were configured with the seatback bottom edge positioned in direct contact with the seat cushion. For purposes of validating Model NoHR, only Test 2 and Test 3 were used since they alone were configured identically to the model. Test 1 was not used to establish target validation thresholds, model response corridors, nor model validation.

6.3.1.1 Series HR sled test comparisons

Comparison within the Series HR sled test series are shown in Figure 32 through Figure 38. Sled test data indicate that the right front tiedown and the chest acceleration are the most repeatable outcome measure. Across all outcome measures, the box maximum test comparison most often fails to meet the Pipkorn target window ($\pm 20\%$, $\pm 5\text{ms}$). When observed variability exceeds Pipkorn's thresholds, revised target thresholds are established for each outcome measure. Target thresholds are used for subsequent model validation.

Front tiedown loading (Figure 32) is examined below, with right (Table 9) and left (Table 10) tiedowns considered separately. The experimental results are compared against each other and against the mean for the right front tiedown. They correlate exceptionally well ($r = 0.99$), with peak maximums occurring within Pipkorn's peak maximum window of $\pm 20\%$ peak matched within ± 5 ms. The standard deviation of the residual and the mean value ratios all compare well for the experimental data.

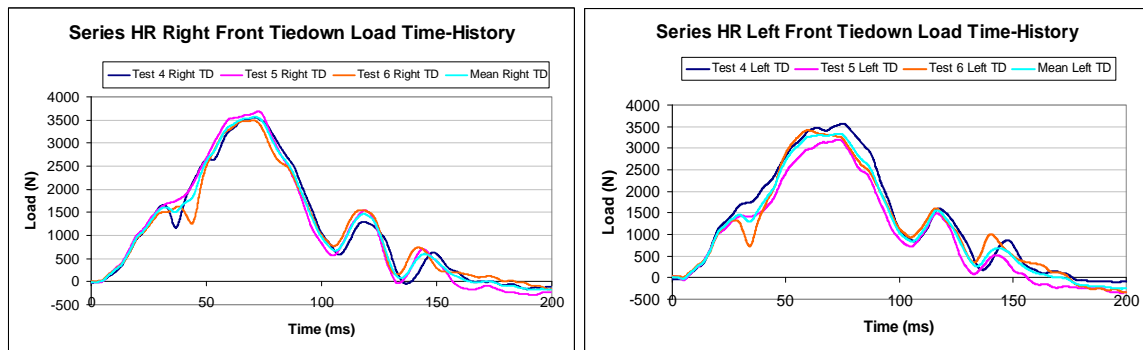


Figure 32: Series HR front tiedown loads time-history

Table 9: Right front tiedown load Series HR sled test data comparison. All values meet Pipkorn thresholds.

Right Tiedown				
test comparison	Mean value Ratio (0.8-1.20)	Correlation ≥ 0.80	Standard residual ≤ 0.20	Box max $\pm 20\%$, ± 5ms
Test 4 to mean	0.99	0.99	0.00	$\pm 20\%$, ± 5 ms
Test 5 to mean	0.98	0.99	0.00	$\pm 20\%$, ± 5 ms
Test 6 to mean	0.95	0.99	0.00	$\pm 20\%$, ± 5 ms
4 to 5	0.99	0.99	0.00	$\pm 20\%$, ± 5 ms
4 to 6	0.96	0.99	0.00	$\pm 20\%$, ± 5 ms
5 to 4	1.02	0.99	0.00	$\pm 20\%$, ± 5 ms
5 to 6	0.97	0.99	0.00	$\pm 20\%$, ± 5 ms
6 to 4	1.06	0.99	0.00	$\pm 20\%$, ± 5 ms
6 to 5	1.03	0.99	0.00	$\pm 20\%$, ± 5 ms
Target Thresholds	Mean value Ratio (0.8-1.20)	Correlation ≥ 0.80	Standard residual ≤ 0.20	Box max $\pm 20\%$, ± 5ms

Left front tiedown loading experimental results compare favorably for the mean value ratio (with two exceptions), correlation and standard deviation of the residual. The box max does not consistently capture the peak maximum window. The target threshold range for the mean value ratio is expanded to 0.78-1.27, reflecting the experimental data variability. The target box maximum window is similarly expanded to +/-20%, +/-16ms to reflect the experimental results.

Table 10: Left front tiedown load Series HR sled test data comparison. Black values indicate results that meet Pipkorn thresholds. Values with asterisk indicate results that exceed Pipkorn thresholds.

Left Tiedown				
test comparison	Mean value ratio (0.8-1.20)	Correlation ≥ 0.80	Standard residual ≤ 0.20	Box max +/- 20%, +/- 5ms
Test 4 to mean	1.10	0.99	0.00	+/-20%, +/-5ms
Test 5 to mean	0.89	0.98	0.00	+/-20%, +/-5ms
Test 6 to mean	1.01	0.99	0.00	+/-20%, +/-15ms*
4 to 5	0.78	0.99	0.00	+/-20%, +/-5ms
4 to 6	0.92	0.98	0.00	+/-20%, +/-16ms*
5 to 4	1.27	0.99	0.00	+/-20%, +/-5ms
5 to 6	1.17	0.98	0.00	+/-20%, +/-14ms*
6 to 4	1.09	0.98	0.00	+/-20%, +/-16ms*
6 to 5	0.86	0.98	0.00	+/-20%, +/-14ms*
Target Thresholds	Mean value ratio (0.78-1.27)	Correlation ≥ 0.80	Standard residual ≤ 0.20	Box max +/- 20%, +/- 16ms

Sled test results (Figure 33) from the wheelchair center of gravity (CG) acceleration time-history compare well for the mean values, correlation and standard residual (Table 11). However, the box maximums compare less well. The wheelchair acceleration has two sets of peaks; each is considered separately. This reduces the sensitivity of this measure to relative heights of a multi-peak curve. The first peak has a box max target window of +/-24%, +/-9ms, and the second peak's box maximum target window is slightly larger (+/-27%, +/-11ms).

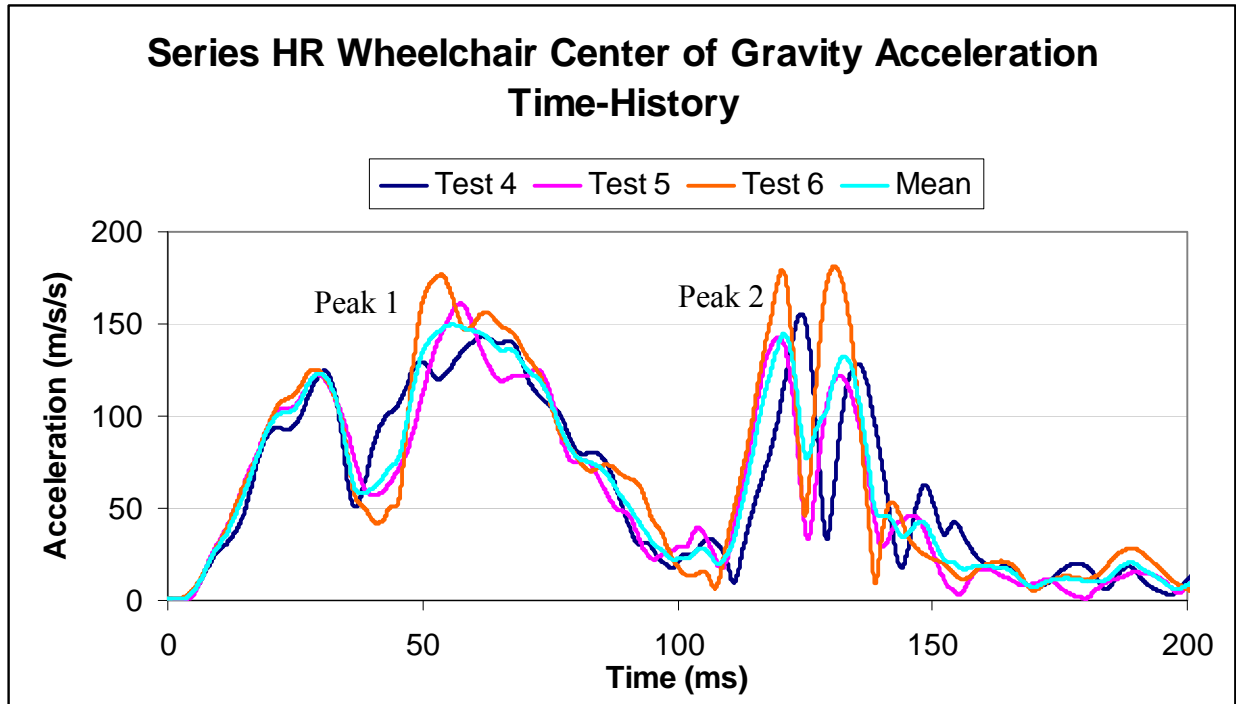


Figure 33: Series HR wheelchair center of gravity acceleration time-history

Table 11: Wheelchair center of gravity acceleration Series HR sled test data comparison. Black values indicate results that meet Pipkorn thresholds. Asteriks indicate results that exceed Pipkorn thresholds.

Wheelchair center of gravity acceleration					
test comparison	Mean value ratio (0.8-1.20)	Correlation ≥ 0.80	Standard residual ≤ 0.20	First peak Box max +/- 20%, +/- 5ms	Second peak Box max +/- 20%, +/- 5ms
Test 4 to mean	1.01	0.95	0.00	+/-20%, +/-7ms*	+/-20%, +/-5ms
Test 5 to mean	0.95	0.99	0.00	+/-20%, +/-5ms	+/-20%, +/-5ms
Test 6 to mean	1.04	0.98	0.00	+/-20%, +/-5ms	+/-26%*, +/-10ms*
4 to 5	0.94	0.90	0.00	+/-20%, +/-5ms	+/-20%, +/-5ms
4 to 6	1.02	0.87	0.00	+/-24%*, +/-9ms*	+/-20%, +/-7ms*
5 to 4	1.06	0.90	0.00	+/-20%, +/-5ms	+/-20%, +/-5ms
5 to 6	1.09	0.97	0.00	+/-20%, +/-5ms	+/-27%*, +/-11ms*
6 to 4	0.98	0.87	0.00	+/-20%, +/-9ms*	+/-20%, +/-7ms*
6 to 5	0.92	0.97	0.00	+/-20%, +/-5ms	+/-22%*, +/-11ms*
Target Thresholds	Mean value ratio (0.8-1.20)	Correlation ≥ 0.80	Standard residual ≤ 0.20	First peak Box max +/- 24%, +/- 9ms	Second peak Box max +/-27%, +/- 11ms

Lap belt load experimental data (Figure 34) correlates well (Table 12), but the magnitude of the data is not closely reproducible yielding a range of mean value ratios of 0.64-1.54. Likewise the target box maximum is expanded to reflect the maximum peak variability.

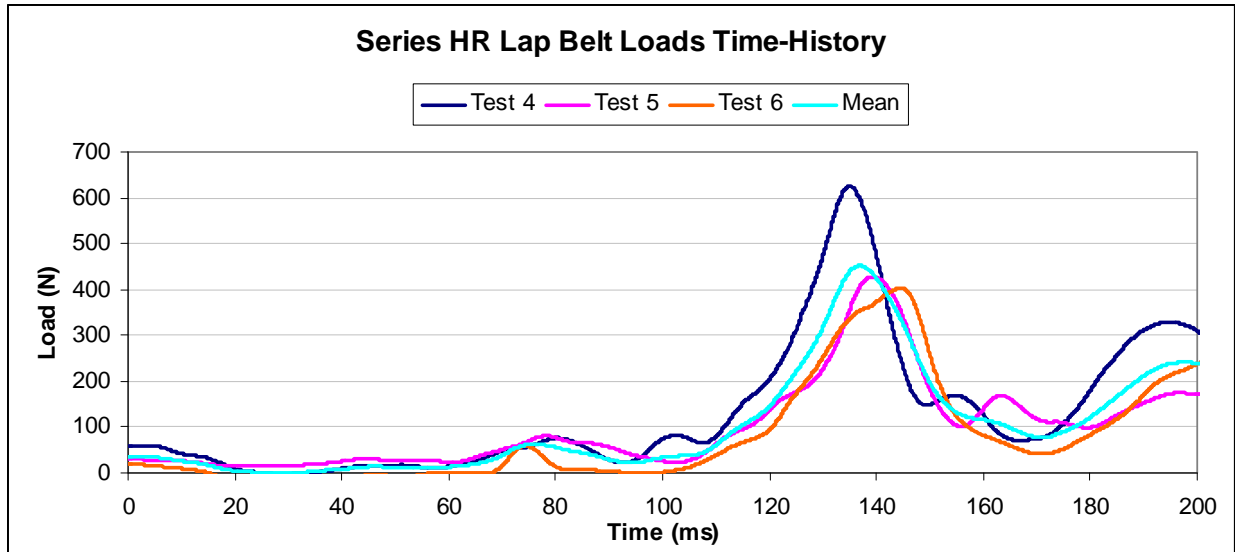


Figure 34: Series HR lap belt loads time-history

Table 12: Lap belt loads Series HR sled test data comparison. Black values indicate results that meet Pipkorn thresholds. Asterisks indicate results that exceed Pipkorn thresholds.

Lap belt				
test comparison	Mean value ratio (0.8-1.20)	Correlation ≥ 0.80	Standard residual ≤ 0.20	Box max +/- 20%, +/- 5ms
Test 4 to mean	1.31*	0.96	0.00	+/-40%*, +/-5ms
Test 5 to mean	0.85	0.96	0.00	+/-20%, +/-5ms
Test 6 to mean	0.89	0.96	0.00	+/-20%, +/-8ms*
4 to 5	0.64*	0.87	0.00	+/- 34%*, +/-5ms
to 6	0.68*	0.87	0.00	+/-34%*, +/-10ms*
5 to 4	1.54*	0.87	0.00	+/-51%*, +/-5ms
5 to 6	1.05	0.95	0.00	+/-20%, +/- 6ms*
6 to 4	1.47*	0.85	0.00	+/-52%*, +/-10ms*
6 to 5	0.95	0.91	0.00	+/-20%, +/-6ms*
Target Thresholds	Mean value ratio (0.64-1.54)	Correlation ≥ 0.80	Standard residual ≤ 0.20	Box max +/-51%, +/-10ms

Chest accelerations experimental data (Figure 35) compares well with mean value ratios, correlations, standard residuals and peak maximums all meeting the criteria (Table 13).

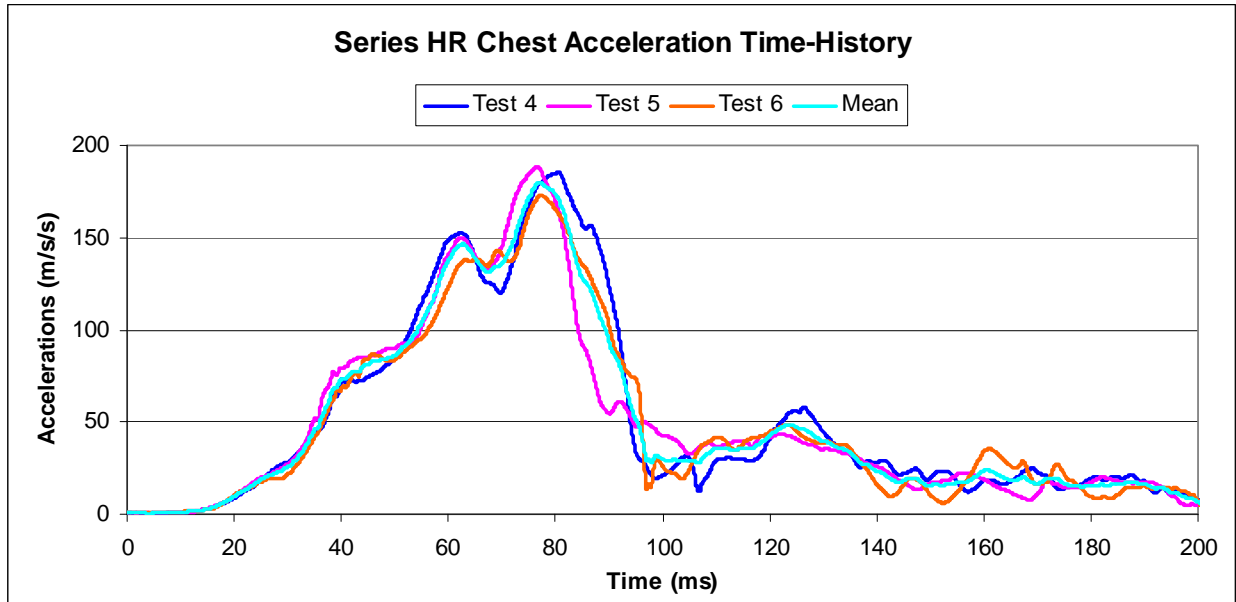


Figure 35: Series HR chest acceleration time-history

Table 13: Chest acceleration Series HR sled test data comparison. All values meet Pipkorn thresholds.

Chest acceleration				
Test Comparison	Mean value ratio (0.8-1.20)	Correlation ≥ 0.80	Standard residual ≤ 0.20	Box max $\pm 20\%$, $\pm 5ms$
mean to 4	1.02	0.99	0.00	$\pm 20\%$, $\pm 5ms$
mean to 5	0.99	0.98	0.00	$\pm 20\%$, $\pm 5ms$
mean to 6	0.99	0.99	0.00	$\pm 20\%$, $\pm 5ms$
4 to 5	0.97	0.95	0.00	$\pm 20\%$, $\pm 5ms$
4 to 6	0.97	0.98	0.00	$\pm 20\%$, $\pm 5ms$
5 to 4	1.03	0.95	0.00	$\pm 20\%$, $\pm 5ms$
5 to 6	0.99	0.97	0.00	$\pm 20\%$, $\pm 5ms$
6 to 4	1.03	0.98	0.00	$\pm 20\%$, $\pm 5ms$
6 to 5	1.00	0.97	0.00	$\pm 20\%$, $\pm 5ms$
Target Thresholds	Mean value ratio (0.8-1.20)	Correlation ≥ 0.80	Standard residual ≤ 0.20	Box max $\pm 20\%$, $\pm 5ms$

Head accelerations are considered separately by component (Figure 36). For the head motion, X-acceleration is the forward-rearward direction. The Z-acceleration occurs in the up-down direction. For all head accelerations, the mean value ratio, correlations

and standard deviation of the residual all meet the target thresholds (Table 14 and Table 15). For both the X-acceleration and Z-accelerations, the target box maximum is expanded to reflect the experimental data variability.

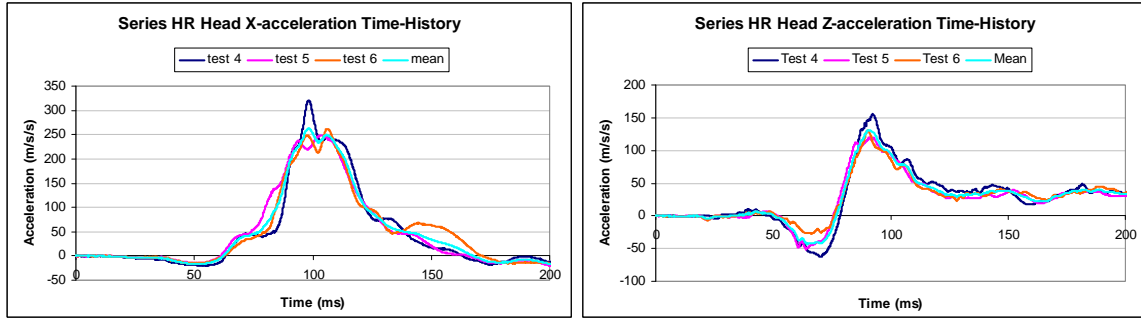


Figure 36: Series HR head acceleration time-history

Table 14: Head X-accelerations Series HR sled test data comparison. Black values indicate results that meet Pipkorn thresholds. Asterisks indicate results that exceed Pipkorn thresholds.

Head X acceleration				
Test Comparison	Mean value ratio (0.8-1.20)	Correlation ≥ 0.80	Standard residual ≤ 0.20	Box max +/- 20%, +/- 5ms
mean to 4	0.97	0.99	0.00	+/-22%*, +/-5ms
mean to 5	0.99	0.98	0.00	+/-20%. +/-6ms*
mean to 6	1.03	0.99	0.00	+/-20%, +/-9ms*
4 to 5	1.03	0.97	0.00	+/-23%*, +/-6ms*
4 to 6	1.07	0.97	0.00	+/-20%, +/-9ms*
5 to 4	0.97	0.97	0.00	+/-29%*, +/-6ms*
5 to 6	1.03	0.98	0.00	+/-20%, +/-5ms
6 to 4	0.93	0.97	0.00	+/-23%*, +/-9ms*
6 to 5	0.97	0.98	0.00	+/-20%, +/-5ms
Target Thresholds	Mean value ratio (0.8-1.20)	Correlation ≥ 0.80	Standard residual ≤ 0.20	Box max +/- 29%, +/- 9ms

Table 15: Head Z-accelerations Series HR sled test data comparison. Black values indicate results that meet Pipkorn thresholds. Asterisks indicate results that exceed Pipkorn thresholds.

Head Z acceleration				
Test Comparison	Mean value ratio (0.8-1.20)	Correlation ≥ 0.80	Standard residual ≤ 0.20	Box max +/- 20%, +/- 5ms
mean to 4	0.99	0.99	0.00	+/-20%, +/-5ms
mean to 5	0.94	0.99	0.00	+/-20%, +/-5ms
mean to 6	1.07	0.99	0.00	+/-20%, +/-5ms
4 to 5	0.94	0.96	0.00	+/-23%*, +/-5ms
4 to 6	1.07	0.97	0.00	+/-20%, +/-5ms
5 to 4	1.06	0.96	0.00	+/-29%*, +/-6ms*
5 to 6	1.14	0.97	0.00	+/-20%, +/-5ms
6 to 4	0.93	0.97	0.00	+/-30%*, +/-5ms
6 to 5	0.97	0.98	0.00	+/-20%, +/-5ms
Target Thresholds	Mean value ratio (0.8-1.20)	Correlation ≥ 0.80	Standard residual ≤ 0.20	Box max +/- 30%, +/- 6ms

Neck bending moment experimental data (Figure 37) correlates well, but the mean value ratio comparison is weak. The box maximum threshold is also not met consistently. The mean value ratio is very sensitive when the means are low numbers, particularly when the means are composed of both positive and negative numbers. In our case all the mean values are close to zero (-1 to 1), while the range of experimental values is -12.23 to 22.39. Small mean values magnify the differences and misleadingly suggest a poor fit where none may exist. The target box maximum is expanded to reflect the variability of the data.

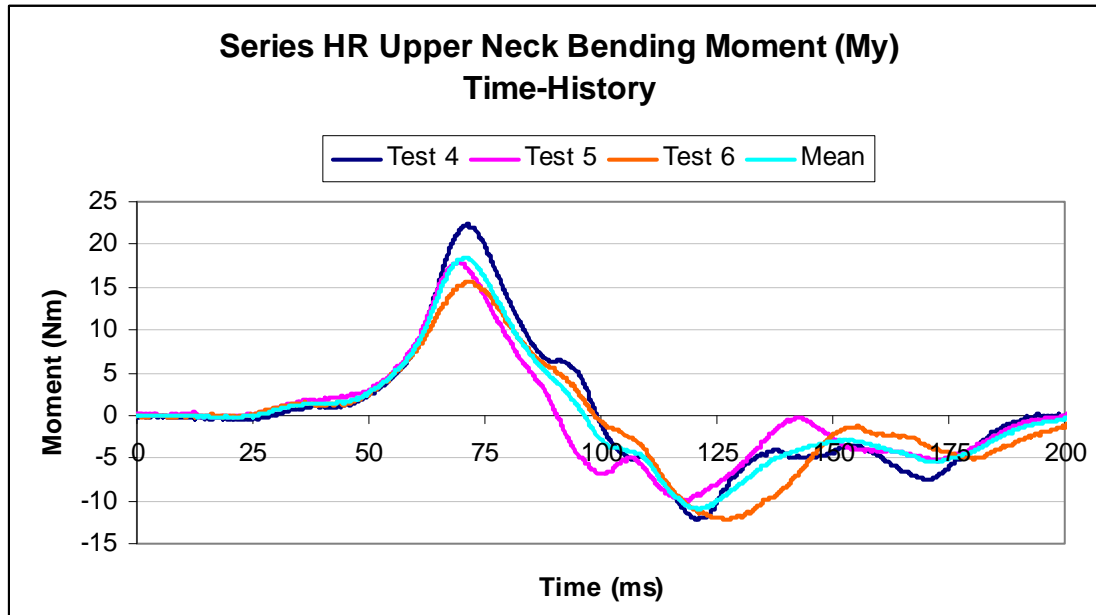


Figure 37: Series HR upper neck bending moment (My) time-history

Table 16: Upper neck bending moment (My) Series HR sled test data comparison. Black values indicate results that meet Pipkorn thresholds. Asterisks indicate results that exceed Pipkorn thresholds.

Upper neck My				
test comparison	Mean value ratio (0.8-1.20)	Correlation ≥ 0.80	Standard residual ≤ 0.20	Box max +/- 20%, +/- 5ms
Test 4 to mean	1.49*	0.99	0.00	+/-22%*, +/- 5ms
Test 5 to mean	0.89	0.96	0.00	+/-20%, +/-5ms
Test 6 to mean	0.62*	0.97	0.00	+/-20%, +/-5ms
4 to 5	0.60*	0.93	0.01	+/-20%, +/-5ms
4 to 6	0.42*	0.95	0.01	+/-31%*, +/-5ms
5 to 4	1.67*	0.93	0.00	+/-25%*, +/-5ms
5 to 6	0.69*	0.89	0.01	+/-20%, +/-5ms
6 to 4	2.40*	0.95	0.00	+/-45%*, +/-5ms
6 to 5	1.45*	0.89	0.01	+/-20%, +/-5ms
Target Thresholds	Mean value ratio (0.42-2.40)	Correlation ≥ 0.80	Standard residual ≤ 0.20	Box max +/- 45%, +/- 5ms

Upper neck force experimental data is compared by component (Figure 38). Series HR upper neck force (Fx) time-history results display the translational upper neck

force (Table 17); Fz (Table 18) is the neck axial loading. Both upper neck forces correlate well, but the Fx mean value ratio comparison fails to consistently meet the Pipkorn criteria. The Fx box maximum typically but not always meets the criteria window, and the target window is expanded to reflect this. Fz peak maximums occur at the same time but vary widely in magnitude. This is reflected both in narrow target window and in the large amount of variability in peak magnitudes. As mentioned before, the mean value ratio is very sensitive when the means are low numbers, particularly when the means are composed of both positive and negative numbers as is true again in this case.

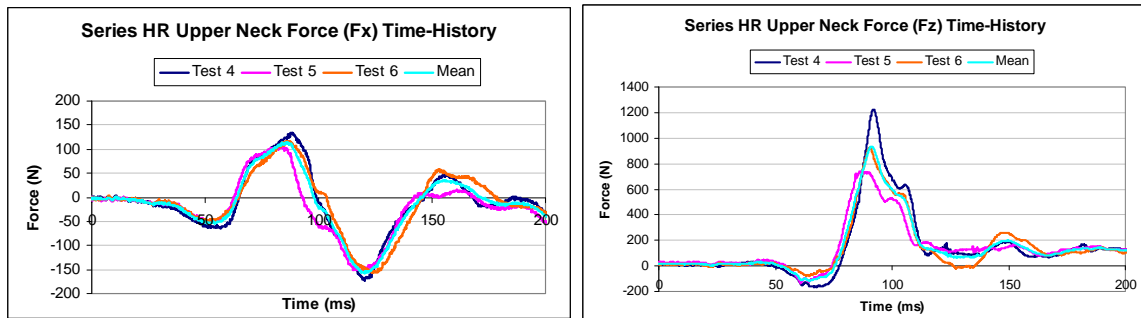


Figure 38: Series HR upper neck force time-history

Table 17: Upper neck force (Fx) Series HR sled test data comparison. Black values indicate results that meet Pipkorn thresholds. Asterisks indicate results that exceed Pipkorn thresholds.

Upper neck Fx				
test comparison	Mean value ratio (0.8-1.20)	Correlation ≥ 0.80	Standard residual ≤ 0.20	Box max $\pm 20\%$, $\pm 5ms$
Mean to Test 4	0.86	0.98	0.00	$\pm 20\%$, $\pm 5ms$
Mean to Test 5	1.41*	0.96	0.00	$\pm 20\%$, $\pm 5ms$
Mean to Test 6	0.72*	0.98	0.00	$\pm 20\%$, $\pm 5ms$
4 to 5	1.24*	0.92	0.00	$\pm 20\%$, $\pm 5ms$
4 to 6	0.91	0.96	0.00	$\pm 20\%$, $\pm 5ms$
5 to 4	0.80	0.92	0.00	$\pm 24\%*$, $\pm 5ms*$
5 to 6	0.72*	0.90	0.00	$\pm 20\%$, $\pm 5ms$
6 to 4	1.10	0.96	0.00	$\pm 20\%$, $\pm 5ms$
6 to 5	1.37*	0.90	0.00	$\pm 20\%$, $\pm 5ms$
Target Thresholds	Mean value ratio (0.72-1.41)	Correlation ≥ 0.80	Standard residual ≤ 0.20	Box max $\pm 24\%$, $\pm 5ms$

Table 18: Upper neck force (Fz) Series HR sled test data comparison. Black values indicate results that meet Pipkorn thresholds. Asterisks indicate results that exceed Pipkorn thresholds.

Upper neck Fz				
test comparison	Mean value ratio (0.8-1.20)	Correlation ≥ 0.80	Standard residual ≤ 0.20	Box max +/- 20%, +/- 5ms
Mean to Test 4	1.00	0.98	0.00	+/-31%*, +/-5ms
Mean to Test 5	1.03	0.96	0.00	+/-21%*, +/-5ms
Mean to Test 6	0.97	0.99	0.00	+/-20%, +/-5ms
4 to 5	1.02	0.92	0.00	+/-40%*, +/-5ms
4 to 6	0.96	0.97	0.00	+/-25%*, +/-5ms
5 to 4	0.97	0.91	0.00	+/-66%*, +/-5ms
5 to 6	0.94	0.94	0.00	+/-25%*, +/-5ms
6 to 4	1.04	0.97	0.00	+/-33%*, +/-5ms
6 to 5	1.07	0.94	0.00	+/-20%, +/-5ms
Target Thresholds	Mean value ratio (0.80-1.20)	Correlation ≥ 0.80	Standard residual ≤ 0.20	Box max +/- 66%, +/- 5ms

Table 19 summarizes Series HR sled test comparisons. Pipkorn thresholds were adequate to capture variability in correlation and standard deviation of the residual. Mean value target thresholds were expanded to reflect sled test variability for the left tiedown loads, lapbelt loads, upper neck bending moment (My) and upper neck force (Fx). In nearly every case, the target box maximums were expanded based on sled test comparison results. Results from this comparison will be used to validate Model HR.

Table 19: Series HR target threshold summary. Asterisks indicate modified thresholds reflecting experimental variability between individual Series HR sled tests.

Series HR Target Threshold Summary					
	Mean value	Correlation	SD of Resid	Box max 1	Box max 2
Right TD	0.8-1.2	≥ 0.80	≤ 0.20	20%, 5ms	
Left TD	0.78-1.27*	≥ 0.80	≤ 0.20	20%, 16ms*	
WC accel	0.8-1.2	≥ 0.80	≤ 0.20	24%*, 9ms*	27%*, 11ms*
Lapbelt	0.64-1.54*	≥ 0.80	≤ 0.20	51%*, 10ms*	
Chest accel	0.8-1.2	≥ 0.80	≤ 0.20	20%, 5ms	
Head x-accel	0.8-1.2	≥ 0.80	≤ 0.20	20%*, 9ms*	
Head z-accel	0.8-1.2	≥ 0.80	≤ 0.20	30%*, 6ms*	
Neck My	0.42-2.40*	≥ 0.80	≤ 0.20	45%*, 5ms	
Neck Fx	0.72-1.41*	≥ 0.80	≤ 0.20	24%*, 5ms	
Neck Fz	0.8-1.2	≥ 0.80	≤ 0.20	66%*, 5ms	

6.3.1.2 Series NoHR sled test comparisons

The following tables present data from Series NoHR comparisons. Test 2 and Test 3 are first tested against the mean and then against each other. The right front tiedown sled test results are very reproducible as is the wheelchair center of gravity acceleration. Similar to Series HR, the left front tiedown loading response has more variability than the right front tiedown. Several of the parameters have multiple peaks. Each peak was evaluated separately for the box maximum.

Series NoHR tiedown loads (Figure 39) were very reproducible for the right front tiedown loads (Table 20), with all measures meeting the Pipkorn thresholds (Pipkorn and Eriksson, 2003). The left front tiedown loads (Table 21) exceed the mean value ratio test; target thresholds for model validation reflect this larger variability between left front tiedown sled test data.

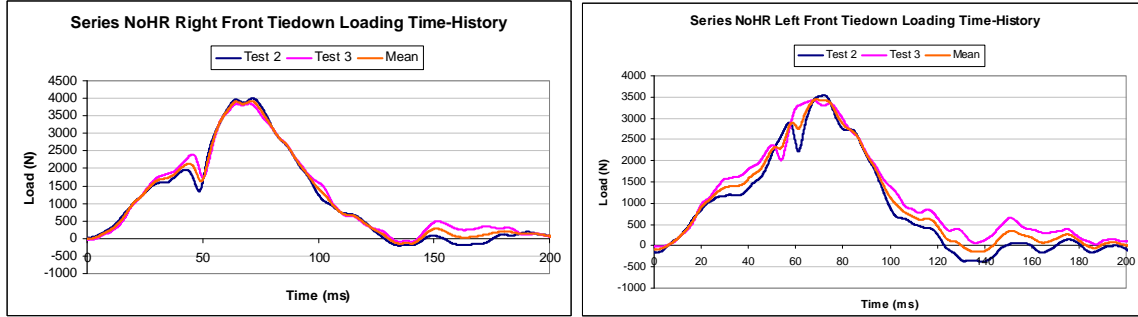


Figure 39: Series NoHR front tiedown loading time-history

Table 20: Right tiedown loads Series NoHR sled test data comparison. All results meet Pipkorn thresholds.

Right Tiedown				
test comparison	Mean value Ratio (0.8-1.20)	Correlation ≥ 0.80	Standard residual ≤ 0.20	Box max $\pm 20\%$, $\pm 5ms$
mean to 2	0.95	0.99	0.00	$\pm 20\%$, $\pm 5ms$
mean to 3	1.06	0.99	0.00	$\pm 20\%$, $\pm 5ms$
2 to 3	1.11	0.99	0.00	$\pm 20\%$, $\pm 5ms$
3 to 2	0.90	0.99	0.00	$\pm 20\%$, $\pm 5ms$
Target Thresholds	Mean value ratio (0.80-1.20)	Correlation ≥ 0.80	Standard residual ≤ 0.20	Box max $\pm 20\%$, $\pm 5ms$

Table 21: Left tiedown loads Series NoHR sled test data comparison. Black values indicate results that meet Pipkorn thresholds. Asterisks indicate results that exceed Pipkorn thresholds.

Left Tiedown				
test comparison	Mean value Ratio (0.8-1.20)	Correlation ≥ 0.80	Standard residual ≤ 0.20	Box max $\pm 20\%$, $\pm 5ms$
mean to 2	0.75*	0.99	0.00	$\pm 20\%$, $\pm 5ms$
mean to 3	1.25*	0.99	0.00	$\pm 20\%$, $\pm 5ms$
2 to 3	1.66*	0.98	0.00	$\pm 20\%$, $\pm 5ms$
3 to 2	0.60*	0.98	0.00	$\pm 20\%$, $\pm 5ms$
Target Thresholds	Mean value ratio (0.60-1.66)	Correlation ≥ 0.80	Standard residual ≤ 0.20	Box max $\pm 20\%$, $\pm 5ms$

Series NoHR wheelchair center of gravity acceleration (Figure 40) reflects good data reproducibility (Table 22). The response curves have two main peaks. Each peak

was considered separately to determine the box maximum. The box max criteria is very sensitive to the relative heights of subsequent peaks in the same curve. In case, both the first and second peaks meet the Pipkorn box maximum criteria.

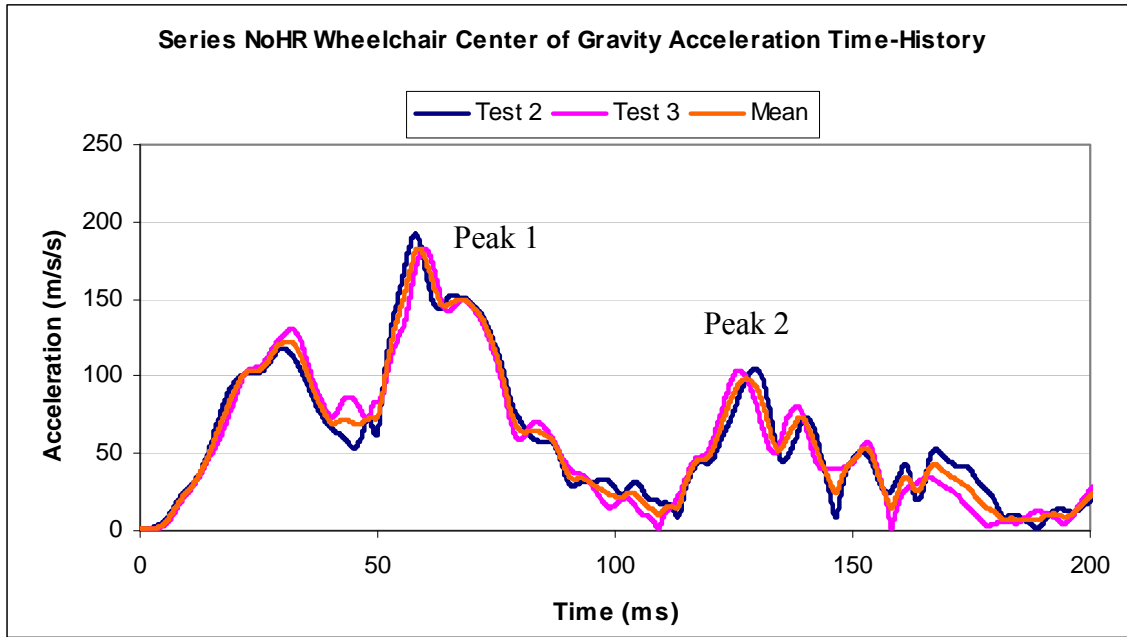


Figure 40: Series NoHR wheelchair center of gravity acceleration time-history

Table 22: Wheelchair center of gravity acceleration Series NoHR sled test data comparison. All results meet Pipkorn thresholds.

Wheelchair CG acceleration					
Test comparison	Mean value Ratio (0.8-1.20)	Correlation ≥ 0.80	Standard residual ≤ 0.20	First peak: Box max +/- 20%, +/- 5ms	Second peak: Box max +/- 20%, +/- 5ms
mean to 2	1.02	0.99	0.00	+/-20%, +/-5ms	+/-20%, +/-5ms
mean to 3	0.98	0.99	0.00	+/-20%, +/-5ms	+/-20%, +/-5ms
2 to 3	0.96	0.97	0.00	+/-20%, +/-5ms	+/-20%, +/-5ms
3 to 2	1.04	0.97	0.00	+/-20%, +/-5ms	+/-20%, +/-5ms
Target Thresholds	Mean value ratio 0.80-1.20	Correlation ≥ 0.80	Standard residual ≤ 0.20	Box max +/- 20%, +/- 5ms	Box max +/- 20%, +/- 5ms

Series NoHR lap belt loads (Figure 41) compare well although the two tests peak 10 ms apart (Table 23). The mean value ratio is slightly greater than the Pipkorn criteria and the expanded threshold reflects the variability between the tests. The data correlate well ($r = 0.83$). The box maximum target window does not capture both peaks; the target window is expanded to reflect these differences.

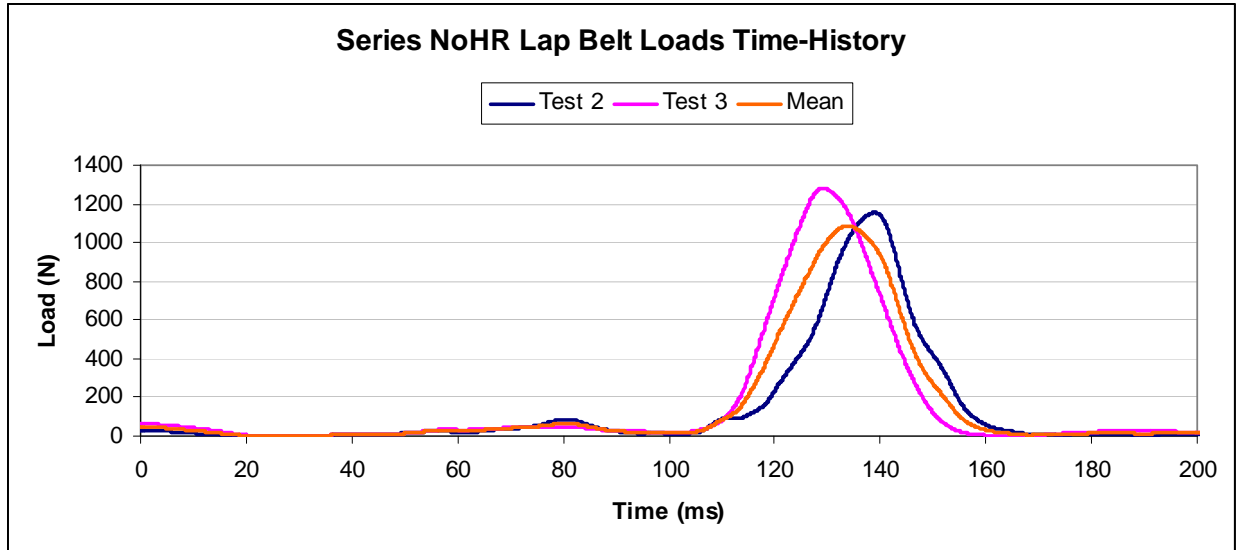


Figure 41: Series NoHR lap belt loads time-history

Table 23: Lap belt loads Series NoHR data comparison. Black values indicate results that meet Pipkorn thresholds. Asterisks indicate results that exceed Pipkorn thresholds.

Lap belts				
	Mean value Ratio (0.8-1.20)	Correlation ≥ 0.80	Standard residual ≤ 0.20	Box max +/- 20%, +/- 5ms
test comparison				
mean to 2	0.89	0.94	0.00	+/-20%, +/-6ms*
mean to 3	1.10	0.96	0.00	+/-20%, +/-5ms
2 to 3	1.24*	0.83	0.00	+/-20%, +/-10ms*
3 to 2	0.81	0.83	0.00	+/-20%, +/-10ms*
Target Thresholds	Mean value ratio 0.80-1.24	Correlation ≥ 0.80	Standard residual ≤ 0.20	Box max +/- 20%, +/- 10ms

Series NoHR chest accelerations (Figure 42) correlate very well, $r \geq 0.92$ (Table 24). The mean value ratio and standard deviation of the residual also meet the Pipkorn thresholds. This curve also had two main peaks. The first peaks match well and fall within the $\pm 20\%$, $\pm 5\text{ms}$ target window. The second set of peaks all occur at the same time ($\pm 5\text{ms}$), but the magnitude of the peak varies between tests.

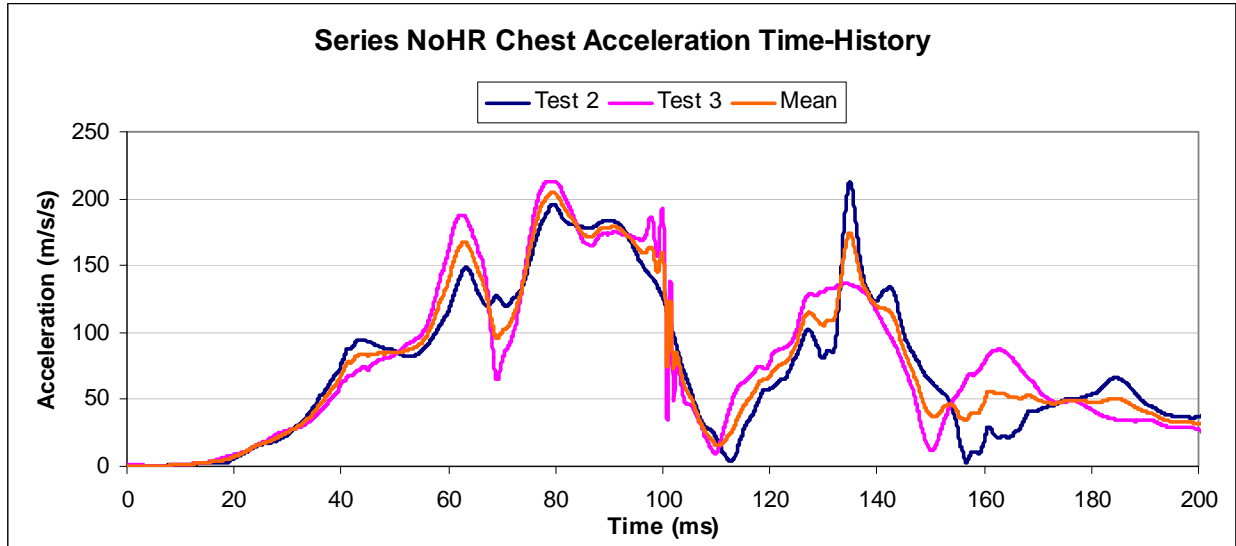


Figure 42: Series NoHR chest acceleration time-history

Table 24: Chest acceleration Series NoHR sled test data comparison. Black values indicate results that meet Pipkorn thresholds. Asterisks indicate results that exceed Pipkorn thresholds.

Chest acceleration					
Test comparison	Mean value ratio (0.8-1.20)	Correlation ≥ 0.80	Standard residual ≤ 0.20	First peak: Box max $\pm 20\%$, $\pm 5\text{ms}$	Second peak: Box max $\pm 20\%$, $\pm 5\text{ms}$
mean to 2	0.99	0.98	0.00	$\pm 20\%$, $\pm 5\text{ms}$	$\pm 22\%^*$, $\pm 5\text{ms}$
mean to 3	1.00	0.98	0.00	$\pm 20\%$, $\pm 5\text{ms}$	$\pm 22\%^*$, $\pm 5\text{ms}$
2 to 3	1.00	0.92	0.00	$\pm 20\%$, $\pm 5\text{ms}$	$\pm 36\%^*$, $\pm 5\text{ms}$
3 to 2	1.00	0.92	0.00	$\pm 20\%$, $\pm 5\text{ms}$	$\pm 56\%^*$, $\pm 5\text{ms}$
Target Thresholds	Mean value ratio 0.80-1.20	Correlation ≥ 0.80	Standard residual ≤ 0.20	Box max $\pm 20\%$, $\pm 5\text{ms}$	Box max $\pm 56\%$, $\pm 5\text{ms}$

Series NoHR head acceleration profiles are compared for each component separately; head X-acceleration (Figure 43) in the fore-aft direction, and head Z-acceleration (Table 26) in the vertical direction. Head acceleration in the x-direction correlates well, however the mean value ratio and box maximum demonstrated greater variability than the Pipkorn thresholds would predict. The thresholds for model validation of the head x-acceleration reflect this greater variability between tests. Head z-accelerations compare well and meet all test criteria.

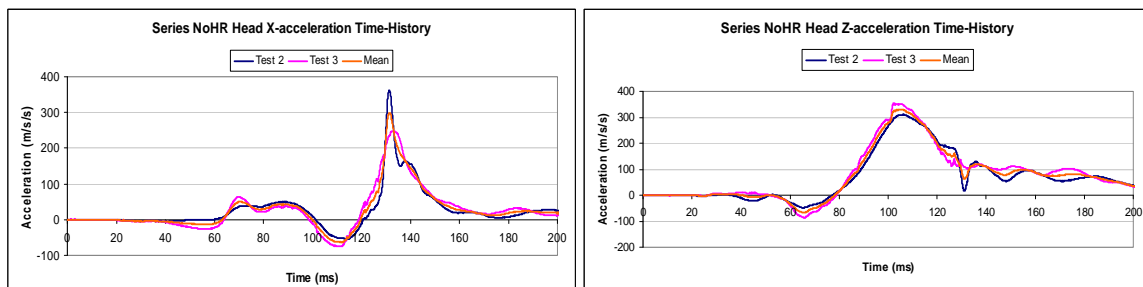


Figure 43: Series NoHR head acceleration time-history

Table 25: Head X-acceleration Series NoHR sled test data comparison. Black values indicate results that meet Pipkorn thresholds. Asterisks indicate results that exceed Pipkorn thresholds.

Head X acceleration				
test comparison	Mean value Ratio (0.8-1.20)	Correlation ≥ 0.80	Standard residual ≤ 0.20	Box max $\pm 20\%$, $\pm 5ms$
mean to 2	1.11	0.98	0.00	$\pm 22\%*$, $\pm 5ms$
mean to 3	0.88	0.98	0.00	$\pm 20\%$, $\pm 5ms$
2 to 3	0.79*	0.92	0.00	$\pm 32%*$, $\pm 5ms$
3 to 2	1.26*	0.92	0.00	$\pm 46%*$, $\pm 5ms$
Target Thresholds	Mean value ratio 0.79-1.26	Correlation ≥ 0.80	Standard residual ≤ 0.20	Box max $\pm 46\%$, $\pm 5ms$

Table 26: Head Z-acceleration Series NoHR sled test data comparison. All results meet Pipkorn thresholds.

Head Z acceleration				
test comparison	Mean value Ratio (0.8-1.20)	Correlation ≥ 0.80	Standard residual ≤ 0.20	Box max +/- 20%, +/- 5ms
mean to 2	0.92	0.99	0.00	+/-20%, +/-5ms
mean to 3	1.07	0.99	0.00	+/-20%, +/-5ms
2 to 3	1.15	0.97	0.00	+/-20%, +/-5ms
3 to 2	0.86	0.97	0.00	+/-20%, +/-5ms
Target Thresholds	Mean value ratio 0.80-1.20	Correlation ≥ 0.80	Standard residual ≤ 0.20	Box max +/- 20%, +/- 5ms

Series NoHR upper neck bending moment, M_y , (Figure 44) does not replicate well between tests (Table 27). The mean value ratio has a very wide range. As discussed before, this reflects the ratios of values that are close to zero. When ratios are made up of small numbers, the ratios can get quite large - particularly with denominators are close to zero. The correlation is a bit low ($r = 0.77$). The maximum peaks occur at the same time (+/- 5ms), however the peak magnitudes differ (+/-105%). The magnitude of the reported difference is dependent on the primary curve, for example, 25% of 80 is the same as 20% of 100. So, this percentage can appear to over-represent the differences between the curves.

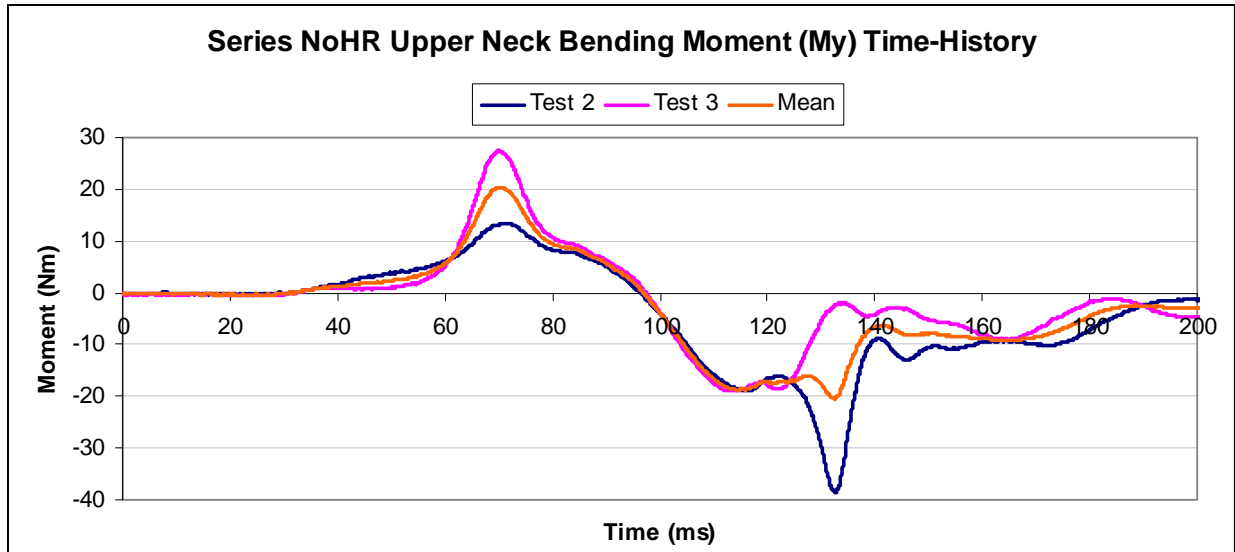


Figure 44: Series NoHR upper neck bending moment (My) time-history

Table 27: Upper neck bending moment (My) Series NoHR sled test data comparison. Black values indicate results that meet Pipkorn thresholds. Asterisks indicate results that exceed Pipkorn thresholds.

Upper neck My				
test comparison	Mean value Ratio (0.8-1.20)	Correlation ≥ 0.80	Standard residual ≤ 0.20	Box max $\pm 20\%$, $\pm 5ms$
mean to 2	1.73*	0.95	0.00	$\pm 35\%*$, $\pm 5ms$
mean to 3	0.26*	0.94	0.00	$\pm 36\%*$, $\pm 5ms$
2 to 3	0.15*	0.77*	0.00	$\pm 105\%*$, $\pm 5ms$
3 to 2	6.55*	0.77*	0.00	$\pm 53\%*$, $\pm 5ms$
Target Thresholds	Mean value ratio 0.15-6.67	Correlation ≥ 0.77	Standard residual ≤ 0.20	Box max $\pm 105\%$, $\pm 5ms$

Series NoHR upper neck forces (Figure 45) are examined by component; Fx (Table 28) is the force acting in the fore-aft direction, Fz (Table 29) is the axial force in the upper neck. The Fx curve has two main peaks, each is considered separately. The negative mean ratio test results for Fx reflect the fact that the two tests have means of opposite signs (positive/negative). The Fx correlation is low, the first peaks meet the

target window. The second set of peaks occur close to the same time (+/-6ms), but differ in magnitude.

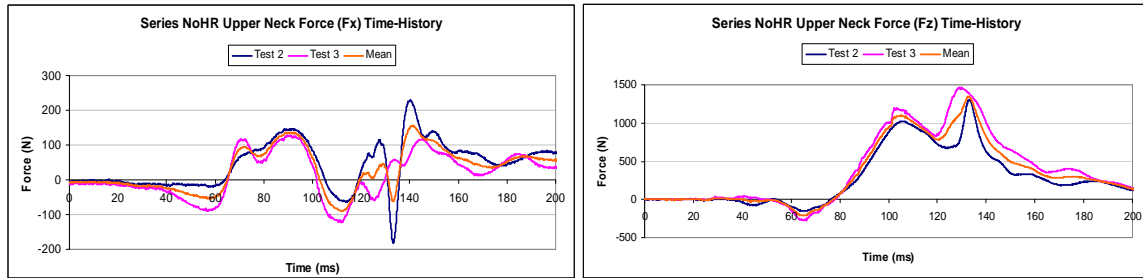


Figure 45: Series NoHR upper neck forces time-history

Table 28: Upper neck force (Fx) Series NoHR sled test data comparison. Black values indicate results that meet Pipkorn thresholds. Asterisks indicate results that exceed Pipkorn thresholds.

Upper neckForce (Fx)					
Test comparison	Mean value Ratio (0.8-1.20)	Correlation ≥ 0.80	Standard residual ≤ 0.20	First peak: Box max +/- 20%, +/- 5ms	Second peak: Box max +/- 20%, +/- 5ms
mean to 2	2.54*	0.94	0.00	+/-20%, +/-5ms	+/-49%*, +/-5ms
mean to 3	-0.54*	0.94	0.00	+/-20%, +/-5ms	+/-26%*, +/-5ms
2 to 3	-0.21*	0.77*	0.00	+/-20%, +/-5ms	+/-51%*, +/-6ms*
3 to 2	-4.71*	0.77*	0.00	+/-20%, +/-5ms	+/-95%*, +/-6ms*
Target Thresholds	Mean value ratio (-4.71) - 2.54	Correlation ≥ 0.77	Standard residual ≤ 0.20	Box max +/- 20%, +/- 5ms	Box max +/- 95%, +/- 6ms

Fz demonstrates greater repeatability. The mean ratio target is expanded to reflect the variability of the data, however the other measures all meet the original target values.

There is only one main peak in Fz.

Table 29: Upper neck force (Fz) Series NoHR sled test data comparison. Black values indicate results that meet Pipkorn thresholds. Asterisks indicate results that exceed Pipkorn thresholds.

Upper neck Fz				
test comparison	Mean value Ratio (0.8-1.20)	Correlation ≥ 0.80	Standard residual ≤ 0.20	Box max +/- 20%, +/- 5ms
mean to 2	0.82	0.99	0.00	+/-20%, +/-5ms
mean to 3	1.17	0.99	0.00	+/-20%, +/-5ms
2 to 3	1.44*	0.97	0.00	+/-20%, +/-5ms
3 to 2	0.70*	0.97	0.00	+/-20%, +/-5ms
Target Thresholds	Mean value ratio 0.70 – 1.44	Correlation ≥ 0.80	Standard residual ≤ 0.20	Box max +/- 20%, +/- 5ms

For most comparisons, the correlations and standard deviation of the residual appear to reflect the consistency between tests. The mean value ratio is very sensitive when there are both positive and negative values. The box maximum frequently captured both test during a small time interval, but the magnitude frequently exceeded the target threshold of +/-20%.

Table 30 summarizes Series NoHR sled test comparisons. Pipkorn thresholds were adequate to capture variability in standard deviation of the residual. Correlations between sled tests was weaker for the upper neck bending moment (my) and the upper neck force (Fx). Mean value target thresholds were expanded to reflect sled test variability for the left tiedown loads, head x-acceleration, upper neck bending moment (My) and upper neck forces (Fx, Fz). Target box maximums were expanded based on sled test comparison results for lapbelt loads, chest acceleration, head x-acceleration, upper neck bending moment (My) and upper neck force (Fx). Results from this comparison will used to validate Model NoHR.

Table 30: Series NoHR target threshold summary. Asterisks indicate modified thresholds reflecting experimental variability between individual Series HR sled tests.

Series NoHR Target Threshold Summary					
	Mean value	Correlation	SD of Resid	Box max 1	Box max 2
Right TD	0.8 – 1.2	≥ 0.80	≤ 0.20	20%, 5ms	
Left TD	0.60* – 1.66*	≥ 0.80	≤ 0.20	20%, 5ms	
WC accel	0.80 – 1.20	≥ 0.80	≤ 0.20	20%, 5ms	20%, 5ms
Lapbelt	0.80 – 1.24	≥ 0.80	≤ 0.20	20%, 10ms*	
Chest accel	0.80 – 1.20	≥ 0.80	≤ 0.20	20%, 5ms	56%*, 5ms
Head x-accel	0.79* – 1.26*	≥ 0.80	≤ 0.20	46%*, 5ms	
Head z-accel	0.80 – 1.20	≥ 0.80	≤ 0.20	20%, 5ms	
Neck My	0.15 – 6.67*	$\geq 0.77^*$	≤ 0.20	105%*, 5ms	
Neck Fx	(-4.71)* – 2.54*	$\geq 0.77^*$	≤ 0.20	20%, 5ms	95%*, 6ms*
Neck Fz	0.70* – 1.44*	≥ 0.80	≤ 0.20	20%, 5ms	

6.3.2 Model HR validation

Results from Model HR validation are presented both graphically and numerically for each parameter: front tiedown loads (right and left), wheelchair center of gravity acceleration, lap belt loads, chest acceleration, head acceleration (x and z directions), neck loads (transverse and axial), and neck bending moment. All graphs (Figure 46 - Figure 52) are presented with the experimental response corridor displayed in grey and Model HR response superimposed on the corridor in red. Experimental response corridors are bounded on the upper edge by the maximum value from the time-matched sled test data, and on the lower edge by the minimum values.

Right and left front tiedowns are considered independently. Right tiedown load response corridor is narrower than the left tiedown load corridor reflecting the closer experimental reproducibility from the sled tests. Although right and left front tiedown

load experimental response corridors differ, all comparisons between sled tests meet Pipkorn target thresholds. Model HR right and left tiedown load response comparisons to each sled test and mean sled test data indicate that right and left Model HR tiedown loads meet the target criteria and are well validated.

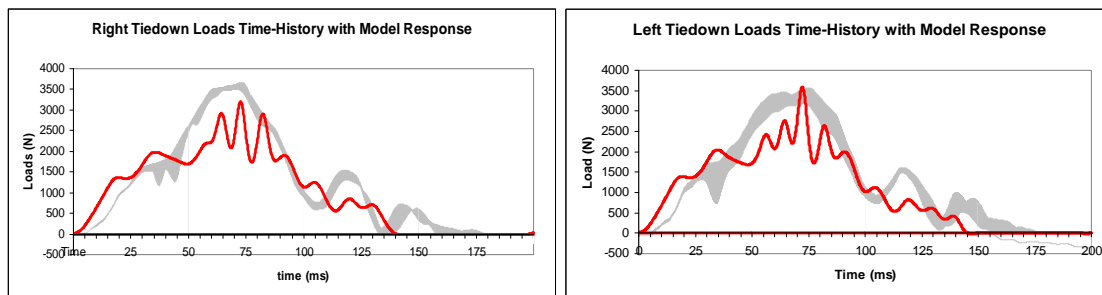


Figure 46: Series HR front tiedown load time-history with model response

Table 31: Model HR front tiedown loads validation comparison. Asterisks indicate values that exceed target validation thresholds.

Front Tiedown Loads				
Right Tiedown				
Target Thresholds	Mean value Ratio (0.8-1.20)	Correlation ≥ 0.80	Standard residual ≤ 0.20	Box max +/- 20%, +/- 5ms
Model HR to Test 4	1.18	0.92	0.00	+/-20%, +/-5ms
Model HR to Test 5	1.17	0.92	0.00	+/-20%, +/-5ms
Model HR to Test 6	1.13	0.90	0.00	+/-20%, +/-5ms
Model HR to mean	1.20	0.92	0.00	+/-20%, +/-5ms
Left Tiedown				
Target Thresholds	Mean value Ratio (0.8-1.23)	Correlation ≥ 0.80	Standard residual ≤ 0.20	Box max +/- 20%, +/- 5ms
Model HR to Test 4	1.28*	0.92	0.00	+/-20%, +/-5ms
Model HR to Test 5	1.01	0.93	0.00	+/-20%, +/-5ms
Model HR to Test 6	1.18	0.88	0.00	+/-20%, +/-5ms
Model HR to mean	1.16	0.92	0.00	+/-20%, +/-5ms

Series HR wheelchair acceleration response corridor reflects dual peaks (Figure 47). The first peak occurs between 50 – 60 ms, and the second occurs between 120-135 ms. Target box maximum validation thresholds were expanded to account for experimental variability (Table 32). Model HR wheelchair acceleration captures both peak target windows, meets correlation criteria, mean value ratio test, and the standard deviation of the residual is less than 20% of the peak. Model HR wheelchair acceleration is well validated.

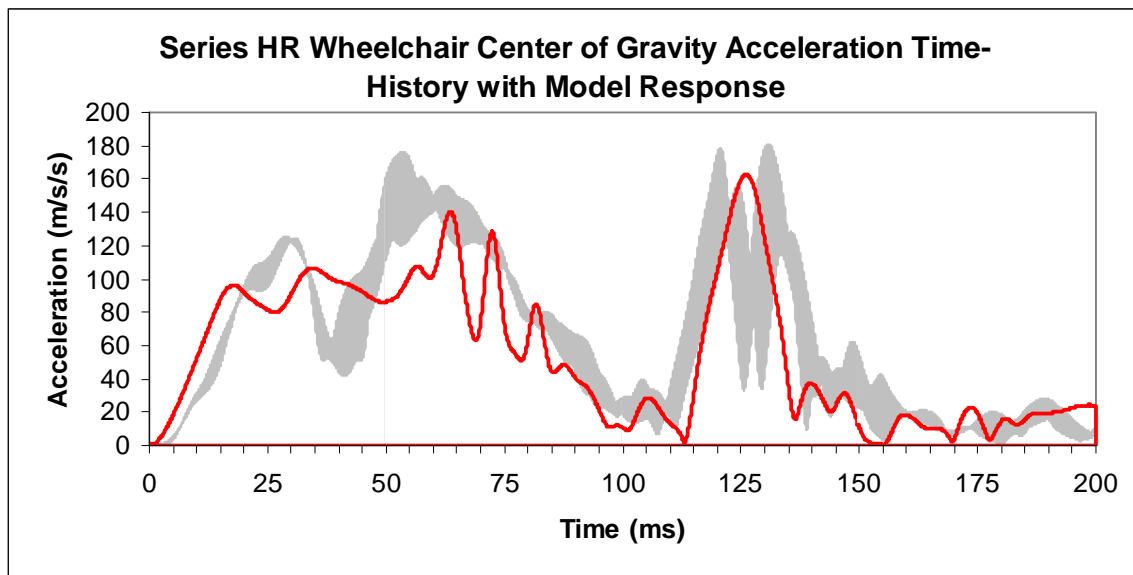


Figure 47: Series HR wheelchair center of gravity acceleration time-history with model response

Table 32: Model HR wheelchair acceleration validation comparison. Asterisks indicate values that exceed target validation thresholds.

Wheelchair center of gravity acceleration					
Target Thresholds	Mean value ratio (0.8-1.20)	Correlation ≥ 0.80	Standard residual ≤ 0.20	First peak Box max +/- 24%, +/- 9ms	Second peak Box max +/- 27%, +/- 11ms
Model HR to Test 4	1.14	0.83	0.00	+/-20%, +/-5ms	+/-20%, +/-5ms
Model HR to Test 5	1.10	0.81	0.00	+/-20%, +/-7ms	+/-20%, +/-7ms
Model HR to Test 6	1.22*	0.80	0.00	+/-27%*, +/-11ms*	+/-20%, +/-5ms
Model HR to mean	1.15	0.84	0.00	+/-20%, +/-8ms	+/-20%, +/-6ms

Series HR experimental lap belt loads repeatably peaked at nearly the same time, however the magnitude of this peak varied by up to 50% when compared between sled tests (Figure 48). This also affected the target threshold mean value ratio. Both target validation criteria were modified to mirror experimental variability. Using the modified thresholds, Model HR lap belt loads meet the target responses for each validation criteria (Table 33). Model HR lap belt loads are well validated.

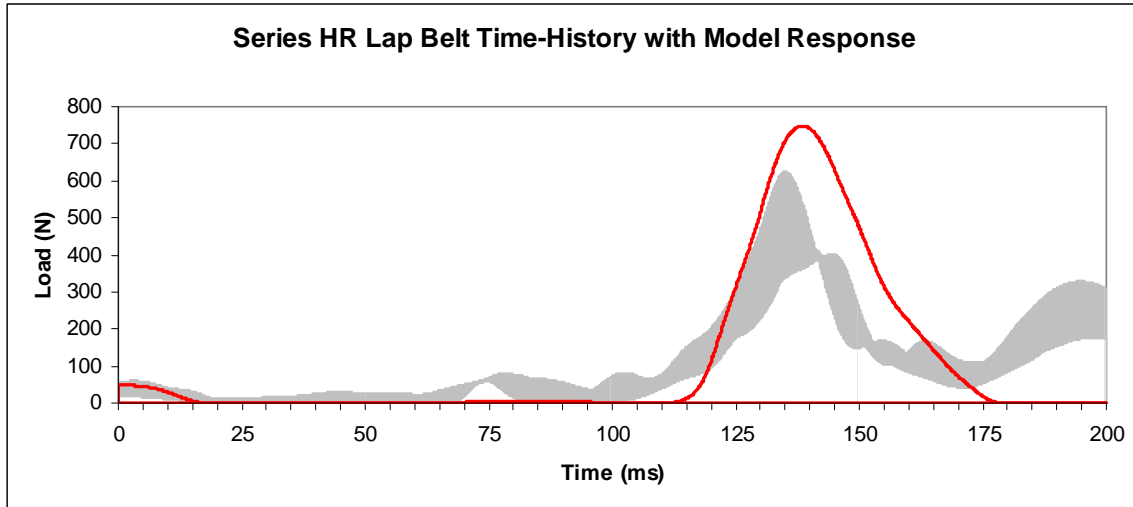


Figure 48: Series HR lap belt time-history with model response

Table 33: Model HR lap belt load validation comparison. Asterisks indicate values that exceed target validation thresholds.

Lap belt				
Target Thresholds	Mean value ratio (0.64-1.54)	Correlation ≥ 0.80	Standard residual ≤ 0.20	Box max +/-51%, +/-10ms
Model HR to Test 4	1.22	0.74*	0.00	+/-20%, +/-5ms
Model HR to Test 5	0.79	0.88	0.00	+/-45%, +/-5ms
Model HR to Test 6	0.82	0.87	0.00	+/-45%, +/-7ms
Model HR to mean	0.93	0.85	0.00	+/-40%, +/-5ms

Series HR experimental chest accelerations varied little between consecutive sled tests (Figure 49); target validation thresholds were not modified from Pipkorn suggested values. Model HR chest acceleration closely follows Series HR chest acceleration response corridor. Correlations between the model and sled test data all meet or exceed $r = 0.90$ (Table 34). Mean value ratios, standard deviation of the residual, and box maximums meet or exceed the target validation criteria. Model HR chest accelerations are well validated.

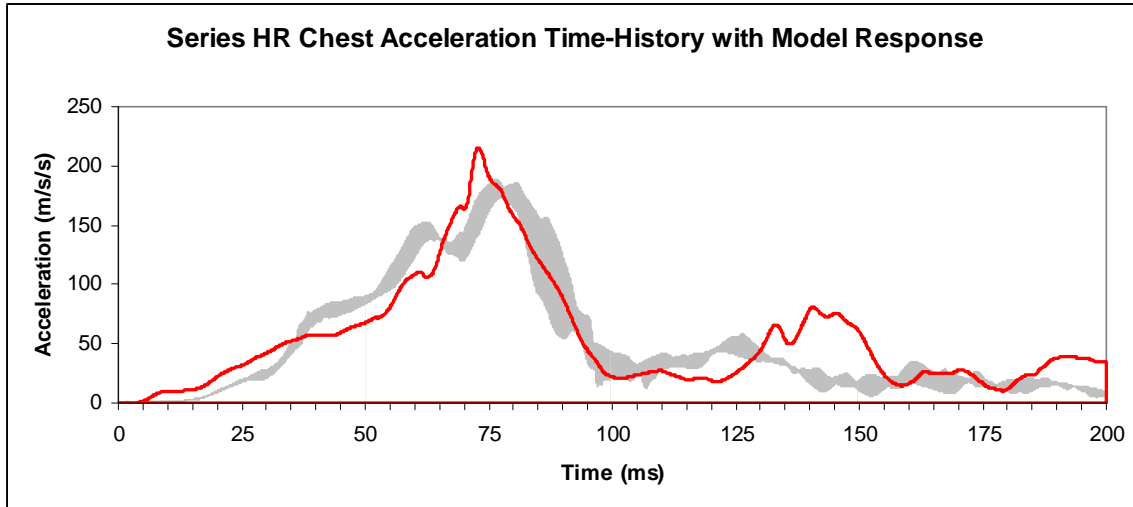


Figure 49: Model HR chest acceleration time-history with model response

Table 34: Series HR chest acceleration validation comparison, Asterisks indicate values that exceed target validation thresholds.

Chest acceleration				
Target Thresholds	Mean value ratio (0.8-1.20)	Correlation ≥ 0.80	Standard residual ≤ 0.20	Box max $\pm 20\%$, $\pm 5ms$
Model HR to Test 4	0.95	0.90	0.00	$\pm 20\%$, $\pm 8ms^*$
Model HR to Test 5	0.92	0.91	0.00	$\pm 20\%$, $\pm 5ms$
Model HR to Test 6	0.91	0.90	0.00	$\pm 20\%$, $\pm 5ms$
Model HR to mean	0.93	0.91	0.00	$\pm 20\%$, $\pm 5ms$

Head accelerations are considered separately as it is primarily the head x-acceleration that contributes to wheelchair headrest loads. Head x-acceleration is head acceleration in the anterior-posterior direction. Head z-acceleration measures vertical head accelerations. Figure 50 displays Series HR head x- and z-acceleration response corridors with Model HR head acceleration data superimposed in red. Model HR head x-accelerations follow the trend of the response corridor, with lower peak values. Model HR head z-acceleration data follow the response corridor well during the initial portion of the impact event (0-145 ms), then decrease during rebound (145-180 ms).

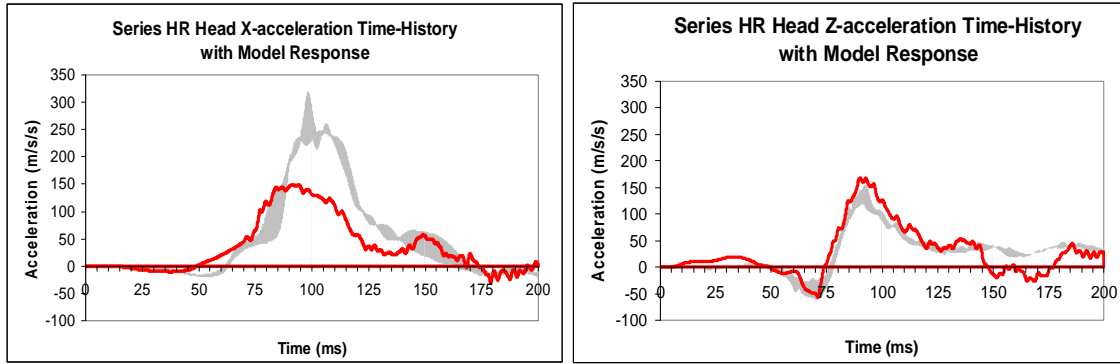


Figure 50: Series HR head acceleration time-histories with model response

Series HR experimental head acceleration comparisons indicated that Pipkorn’s target box maximum was inadequate to capture the variability of peak responses. Target box maximum thresholds were modified for head x-acceleration (+/-29%, +/-9ms) and for head z-acceleration (+/-30%, +/-6ms), reflecting sled test results (Table 35). Model HR head x-acceleration validation comparisons mirror the graphical representation. Model x-acceleration data follow experimental trends and model response data meet correlation criteria. The box maximum target window is not met for head x-acceleration, which would be anticipated based on reviewing Figure 50 (left) head x-acceleration graph. Model HR head z-acceleration meets all statistical test target criteria. Model HR head x-acceleration is partially validated; Model HR z-acceleration is well validated.

Table 35: Model HR head acceleration validation comparison, Asterisks indicate values that exceed target validation thresholds.

Head acceleration

Head X acceleration

	Mean value ratio (0.8-1.20)	Correlation ≥ 0.80	Standard residual ≤ 0.20	Box max +/- 29%, +/- 9ms
Target Thresholds				
Model HR to Test 4	1.13	0.83	0.00	+/-120%*, +/-5ms
Model HR to Test 5	1.17	0.91	0.00	+/-67%*, +/-11ms*
Model HR to Test 6	1.21*	0.88	0.00	+/-76%*, +/-13ms*
Model HR to mean	1.16	0.88	0.00	+/-78%*, +/-11ms*

Head Z acceleration

	Mean value ratio (0.8-1.20)	Correlation ≥ 0.80	Standard residual ≤ 0.20	Box max +/- 30%, +/- 6ms
Target Thresholds				
Model HR to Test 4	1.02	0.87	0.00	+/-20%, +/-5ms
Model HR to Test 5	0.96	0.87	0.00	+/-30%, +/-5ms
Model HR to Test 6	1.07	0.85	0.00	+/-23%, +/-5ms
Model HR to mean	1.02	0.88	0.00	+/-23%, +/-5ms

Series HR experimental upper neck bending moment (My) response correlated well, however the mean value ratio and box maximum windows were not captured by the Pipkorn criteria. Figure 51 displays the experimental response corridor with Model HR upper neck bending moment. Note that all experimental peak values are all within +/-25 Nm. With values this low, the mean values are also low, and their ratio is very sensitive to small differences.

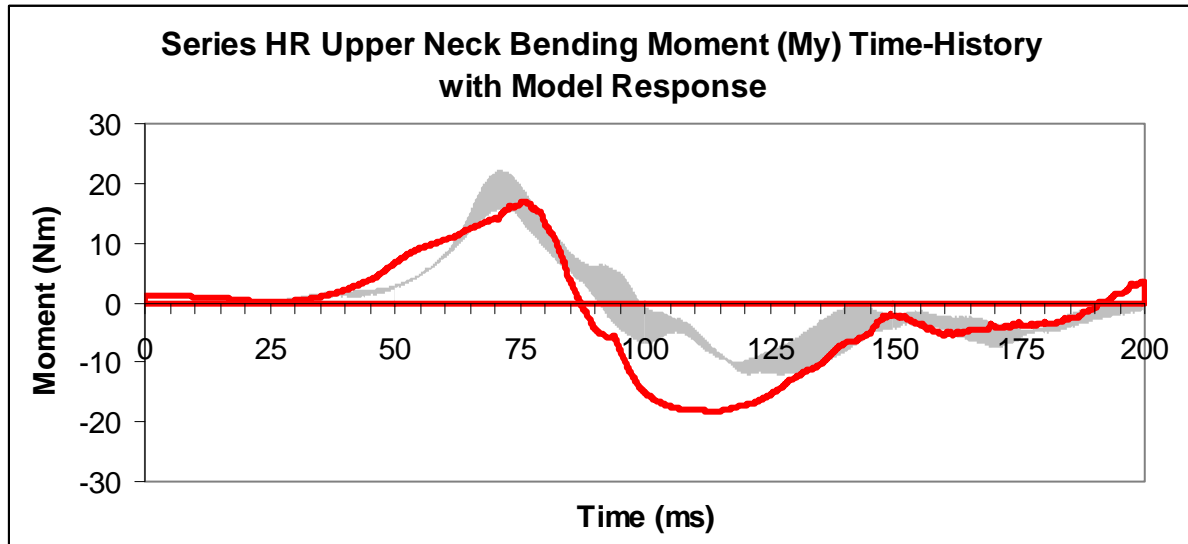


Figure 51: Series HR upper neck bending moment (My) time-history with model response

Model HR upper neck bending moment validation criteria are adjusted to reflect variability of the experimental data. Model HR data correlate well with Series HR experimental data, have standard deviation of the residuals of less than 20% of the peak value, and produce peaks that fall well within the variability of the experimental data. The mean value ratio does not meet the modified target criteria. The Model HR upper neck bending moment is partially validated.

Table 36: Model HR upper neck bending moment (My) validation comparison. Asterisks indicate values that exceed target validation thresholds.

Upper neck My	Mean value ratio (0.42-2.40)	Correlation ≥ 0.80	Standard residual ≤ 0.20	Box max +/- 45%, +/- 5ms
Model HR to Test 4	-0.05*	0.81	0.01	+/-32%, +/-5ms
Model HR to Test 5	0.14*	0.91	0.01	+/-20%, +/-7ms
Model HR to Test 6	0.26*	0.83	0.02	+/-20%, +/-5ms
Model HR to mean	0.11*	0.87	0.01	+/-20%, +/-6ms

Figure 52 displays Series HR upper neck forces. Fx is the transverse neck force; Fz is the axial force. Model HR Fx data follow the trends of Series HR experimental data with model peaks occurring preceding experimental peaks by 5 ms. The Fx model response is also greater than experimental data. Model HR upper neck Fz response follows the trends seen in Series HR Fz response corridor, with lower model response than experimental response.

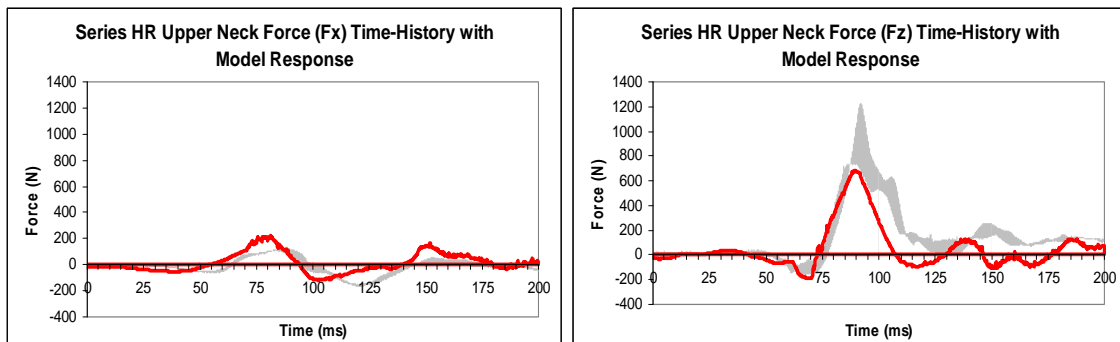


Figure 52: Series HR upper neck force time-history with model response

Model HR upper neck Fx fails to meet the mean value, correlation or box maximum criteria (Table 37). The correlation is low and reflects the sensitivity of correlation to time shifts between the curves. The peak model response occurs early, but is captured in time by the 5 ms window; the peak model response is 50% greater than the experimental data. Mean value ratios reflect a model mean that is positive and experimental means that are negative. Model HR upper neck Fz correlates well, meets the standard deviation of the residual criteria, and is captured by the box maximum window. Mean value ratios exceed the target thresholds. Model HR upper neck Fx and Fz are partially validated, with Fx less well validated than Fz.

Table 37: Model HR upper neck forces validation comparison. Asterisks indicate values that exceed target validation thresholds.

Upper neck force				
Upper neck Fx				
Target Thresholds	Mean value ratio (0.72-1.41)	Correlation ≥ 0.80	Standard residual ≤ 0.20	Box max +/- 24%, +/- 5ms
Model HR to Test 4	-1.35*	0.70*	0.00	+/-42%*, +/-8ms*
Model HR to Test 5	-1.15*	0.67*	0.00	+/-51%*, +/-5ms
Model HR to Test 6	-1.90*	0.74*	0.00	+/-50%*, +/-5ms
Model HR to mean	-0.98*	0.65*	0.00	+/-50%*, +/-5ms
Upper neck Fz				
Target Thresholds	Mean value ratio (0.80-1.20)	Correlation ≥ 0.80	Standard residual ≤ 0.20	Box max +/- 66%, +/- 5ms
Model HR to Test 4	3.28*	0.80	0.00	+/-80%*, +/-5ms
Model HR to Test 5	3.30*	0.88	0.00	+/-20%, +/-5ms
Model HR to Test 6	3.17*	0.81	0.00	+/-35%, +/-5ms
Model HR to mean	3.24*	0.84	0.00	+/-37%, +/-5ms

6.3.3 Model NoHR validation

Model NoHR was built using Model HR as the foundation. The model headrest was then removed from the Model HR to create Model NoHR. During review of the sled test videos, the posterior surface of the ATD head contacted the top edge of the seatback during impact. Model ATD head to seatback contacts were created and modified within Model NoHR. The following figures and tables compare Model NoHR responses to Series NoHR experimental data, both graphically and numerically. All figures display the response corridor established by two sled tests, Test 2 and Test 3, conducted with identical wheelchair configurations.

Model NoHR front tiedown loads were considered separately for the left and right front tiedowns (Figure 53). Series NoHR right front tiedown load response corridor is visibly narrower than the left front response corridor; based on statistical comparisons, target thresholds were expanded for the left front tiedowns. Model NoHR front tiedowns response were super-imposed on the experimental response corridors in red. The model right tiedown appears low, while the left front tiedown more accurately reproduces the experimental test data.

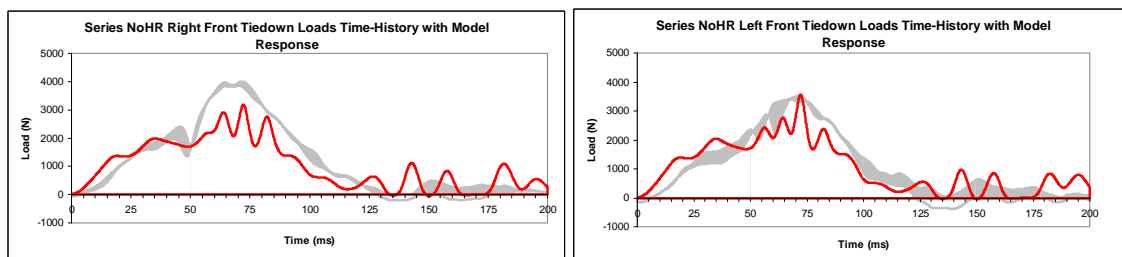


Figure 53: Series NoHR front tiedown validation comparison

Numerical comparisons of Model NoHR front tiedown loads confirm observations from the graphs (Table 38). Model NoHR right tiedown load response meets each statistical test criteria with the exception that experimental peaks are slightly greater than 20% higher than Model NoHR values. Model NoHR left front tiedown load compares favorably with Series NoHR experimental data with correlations greater than or equal to 0.91, mean value ratios with target range, standard deviation of the residuals less than 20% of peak values, and box maximum target windows capturing the peak values. Model NoHR right tiedowns are partially validated, and left tiedowns are well validated.

Table 38: Model NoHR front tiedown loads validation comparison. Asterisks indicate values that exceed target validation thresholds.

Front Tiedowns				
Right Tiedown				
Target Thresholds	Mean value ratio (0.80-1.20)	Correlation ≥ 0.80	Standard residual ≤ 0.20	Box max +/- 20%, +/- 5ms
Model to Test 2	0.99	0.92	0.00	+/- 26%, +/-5ms
Model to Test 3	0.99	0.92	0.00	+/- 21%, +/- 5ms
Model to mean	1.20	0.92	0.00	+/- 24%, +/- 5ms
Left Tiedown				
Target Thresholds	Mean value ratio (0.60-1.66)	Correlation ≥ 0.80	Standard residual ≤ 0.20	Box max +/- 20%, +/- 5ms
Model to Test 2	0.72	0.92	0.00	+/-20%, +/-5ms
Model to Test 3	1.07	0.91	0.00	+/-20%, +/-5ms
Model to mean	0.89	0.92	0.00	+/-20%, +/-5ms

Series NoHR wheelchair acceleration response corridor is very narrow; experimental data comparisons meet Pipkorn thresholds. Model NoHR wheelchair accelerations follow the trend of the experimental data. There are two main peaks (Figure 54), and each is evaluated separately in the numerical comparison (Table 39).

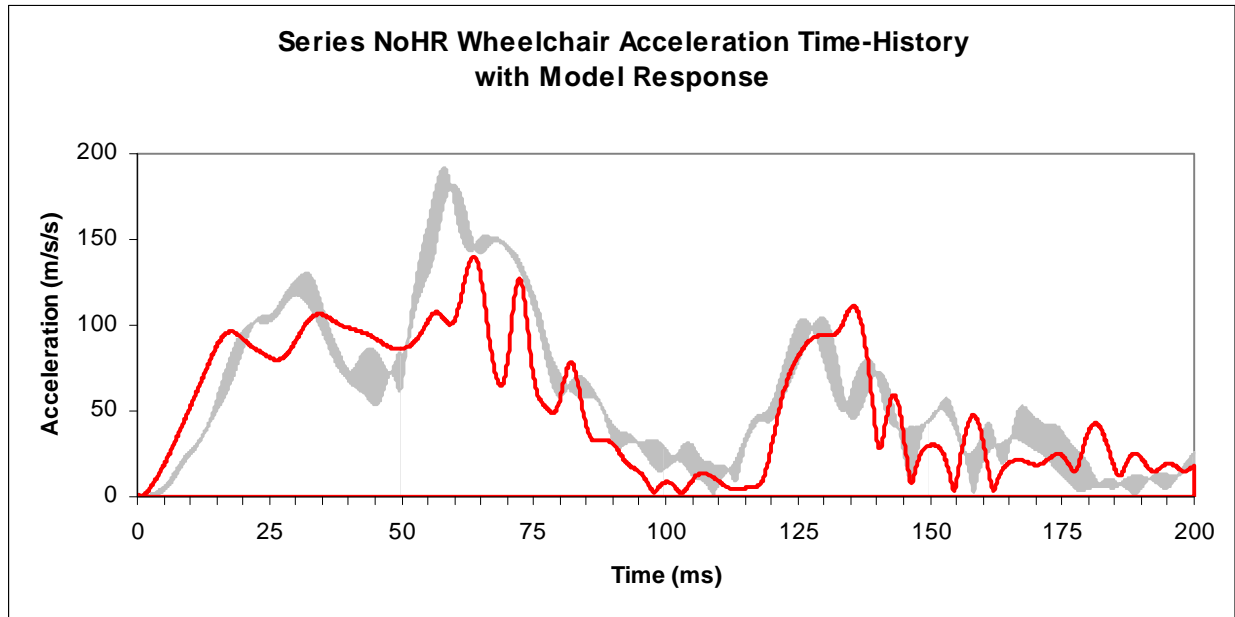


Figure 54: Series NoHR wheelchair center of gravity acceleration with model response

Numerical comparisons of Model NoHR wheelchair acceleration to Series NoHR experimental data (Table 39) indicate that mean value ratio, correlations and standard residuals all meet the Pipkorn validation criteria. Peak 1 box maximum occurs within the window, however peak experimental responses exceed 20% of the model response. Similarly, peak 2 responses are within the target threshold for size, but occur 2-5 ms later. Model NoHR wheelchair acceleration is partially validated.

Table 39: Model NoHR wheelchair center of gravity acceleration validation comparison. Asterisks indicate values that exceed target validation thresholds.

Wheelchair CG acceleration					
Target Thresholds	Mean value ratio 0.80-1.20	Correlation ≥ 0.80	Standard residual ≤ 0.20	Peak 1: box max +/- 20%, +/- 5ms	Peak 2: box max +/- 20%, +/- 5ms
Model to Test 2	1.16	0.85	0.00	+/-37%*, +/-6ms*	+/-20%, +/-7ms*
Model to Test 3	1.12	0.88	0.00	+/-31%*, +/-5ms	+/-20%, +/-10ms*
Model to mean	1.14	0.87	0.00	+/-31%*, +/-5ms	+/-20%, +/-8ms*

Series NoHR lap belt loads experimental data display a double peak caused by Test 2 and Test 3 peaking separately and 10 ms apart (Figure 55). This creates a larger target validation threshold for model to experimental data comparisons. Model NoHR lap belt load response appears to closely follow the experimental response corridor.

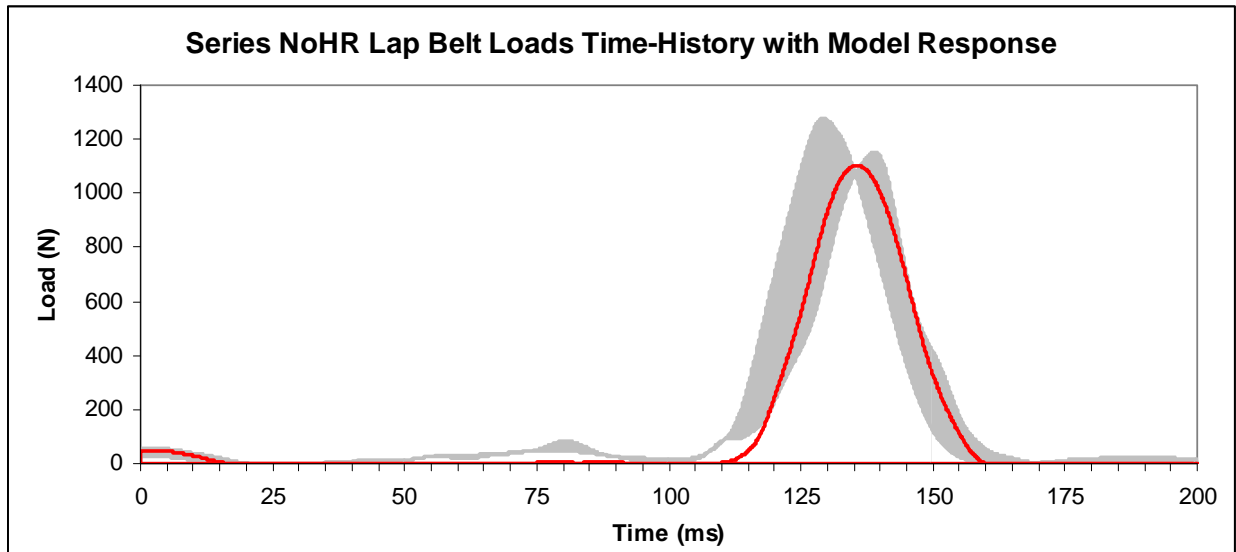


Figure 55: Series NoHR lap belt loads time-history with model response

Numerical comparisons of Model NoHR lap belt response (Table 40) support observations from the graphical comparison. The model data meet the revised validation criteria, and Model NoHR lap belts are well validated.

Table 40: Model NoHR lap belt loads validation comparison. Asterisks indicate values that exceed target validation thresholds.

Lap belts	Mean value ratio	Correlation	Standard residual	Box max
Target Thresholds	0.80-1.24	≥ 0.80	≤ 0.20	+/-20%, +/-10ms
Model to Test 2	1.09	0.98	0.00	+/-20%, +/-5ms
Model to Test 3	1.27*	0.89	0.00	+/-20%, +/-7ms
Model to mean	1.18	0.98	0.00	+/-20%, +/-5ms

Series NoHR chest acceleration data varied between each sled test, with several peaks (Figure 56). Target validation thresholds reflect variability between the two sled tests. The first two peaks in the model response are evaluated against the sled test data using the box maximum criteria; peak 1 occurs at 70 ms, peak 2 occurs at 135 ms. Model response appears to fall within or below the experimental corridors.

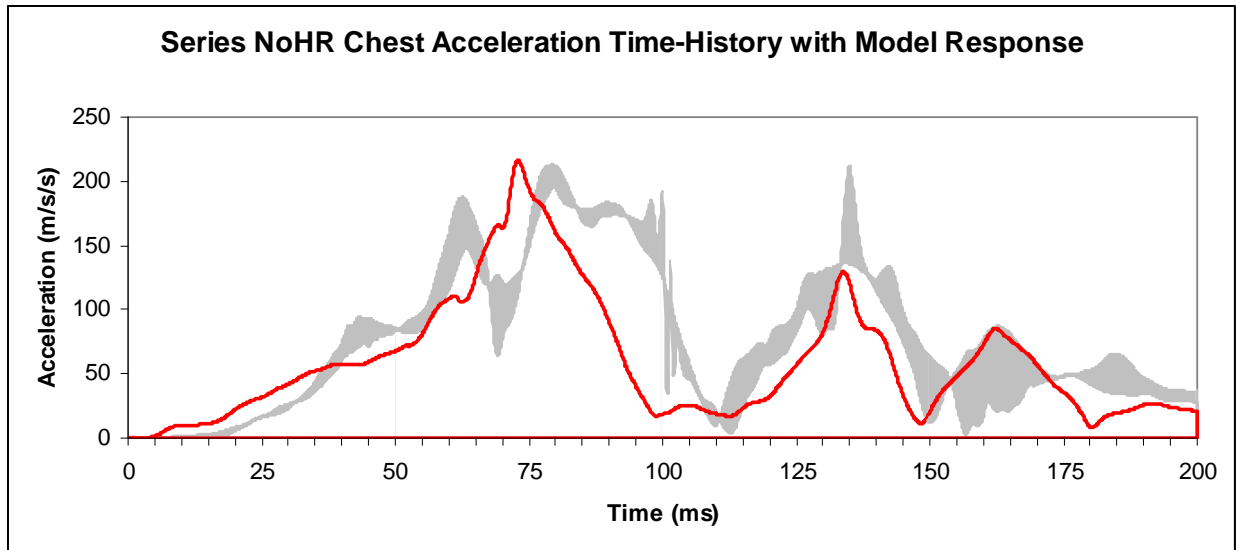


Figure 56: Series NoHR chest acceleration time-history with model response

Numerical comparisons support observational impressions (Table 41). Mean value ratios indicate that the average experimental value exceeds the model value by 30%. The data correlate well, and the standard deviation of the residuals are low. The first peak has the same magnitude as the experimental data, but occurs 7 ms earlier. Peak 2 box maximum target window captures the experimental data. Model NoHR chest accelerations are partially validated.

Table 41: Model NoHR chest acceleration validation comparison. Asterisks indicate values that exceed target validation thresholds.

Chest acceleration					
Target Thresholds	Mean value ratio 0.80-1.20	Correlation ≥ 0.80	Standard residual ≤ 0.20	Peak 1: box max +/- 20%, +/- 5ms	Peak 2: box max +/- 56%, +/- 5ms
Model to Test 2	1.31*	0.77*	0.00	+/-20%, +/-7ms*	+/-65%*, +/-5ms
Model to Test 3	1.30*	0.80	0.00	+/-20%, +/-7ms*	+/-20%, +/-5ms
Model to mean	1.31*	0.81	0.00	+/-20%, +/-7ms*	+/-35%, +/-5ms

Similar for Model HR, Model NoHR head accelerations (Figure 57) are considered separately by direction, with x-acceleration in the fore-aft direction and z-acceleration in the vertical direction. Model NoHR head x-accelerations peak with the response corridor. The z-accelerations follow the experimental response corridor trend, but appear low.

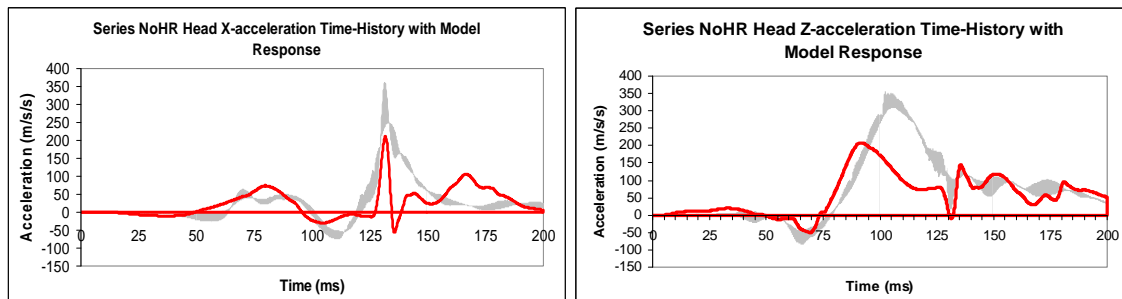


Figure 57: Series NoHR head acceleration time-history with model response

Model NoHR head x-accelerations do not correlate well. However, the peak maximum is captured by the box maximum. The mean value ratio meets the criteria as does the standard deviation of the residual. Model NoHR head x-acceleration is partially validated. Model NoHR head z-acceleration correlates better than the x-accelerations and

nearly meets the correlation criteria. The mean value ratio and standard deviation of the residual both meet the validation thresholds. Model NoHR head z-acceleration does not increase adequately, peaks early and low. Model NoHR head z-acceleration is partially validated.

Table 42: Model NoHR head acceleration validation comparison. Asterisks indicate values that exceed target validation thresholds.

Head Acceleration				
Head X acceleration				
	Mean value ratio	Correlation	Standard residual	Box max
Target Thresholds	0.79-1.26	≥ 0.80	≤ 0.20	+/- 46%, +/- 5ms
Model to Test 2	1.29*	0.57*	0.00	+/-72%*, +/-5ms
Model to Test 3	1.11	0.51*	0.00	+/-20%, +/-5ms
Model to mean	1.20	0.55*	0.00	+/-42%, +/-5ms
Head Z acceleration				
	Mean value ratio	Correlation	Standard residual	Box max
Target Thresholds	0.80-1.20	≥ 0.80	≤ 0.20	+/- 20%, +/- 5ms
Model to Test 2	1.09	0.77*	0.00	+/-50%*, +/-14ms*
Model to Test 3	1.29*	0.74*	0.00	+/-71%*, +/-11ms*
Model to mean	1.19	0.78*	0.00	+/-59%*, +/-15ms*

Series NoHR upper neck bending moment sled test responses had a great deal of variability, which is reflected in the target validation thresholds. Model NoHR upper neck bending moment response appears to follow the experimental trends closely (Figure 58). Note that all peak bending upper neck bending moments are between +/-40 Nm; this can contribute to high mean value ratios.

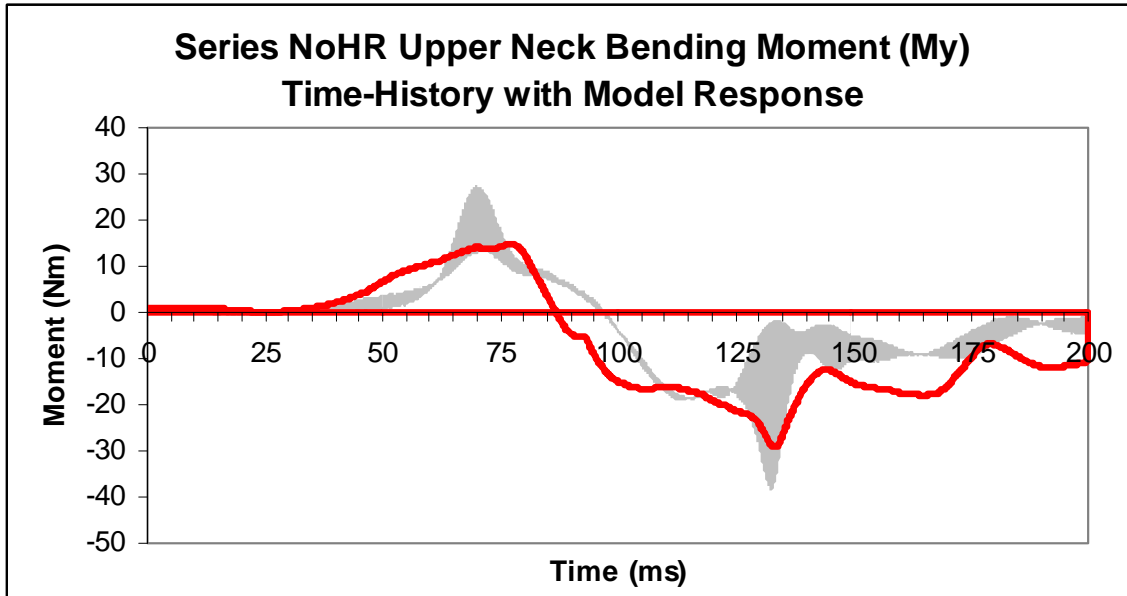


Figure 58: Series NoHR upper neck bending moment (My) time-history with model response

Table 43 compares the model to the experimental test data using modified target thresholds. The model to mean correlations are greater than comparisons between the model and individual sled test data, or the correlation between the two sled tests ($r = 0.77$). All Model NoHR upper neck bending moment data compare well to the sled test data, with only box maximum occurring 1-3 ms late. Model NoHR upper neck bending moments validate well.

Table 43: Model NoHR upper neck bending moment (My) validation comparison. Asterisks indicate values that exceed target validation thresholds.

Upper neck My	Mean value ratio	Correlation	Standard residual	Box max
Target Thresholds	0.15-6.67	≥ 0.77	≤ 0.20	+/- 105%, +/- 5ms
Model to Test 2	0.69	0.89	0.00	+/-20%, +/-6ms*
Model to Test 3	0.30	0.78	0.01	+/-88%, +/-8ms*
Model to mean	0.46	0.90	0.01	+/-40%, +/-7ms*

Model NoHR upper neck forces are considered individually by component (Figure 59). Fx acts in the transverse direction; Fz acts axially along the neck. Graphical comparisons suggest that Model NoHR Fx follow the experimental data trends closely. Fz model data also appear to follow experimental trends but have a more muted response. Expanded target validation thresholds reflect experimental response corridors.

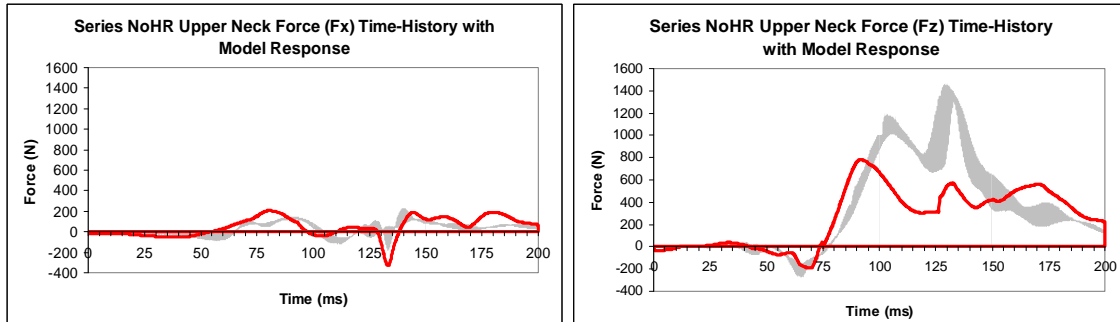


Figure 59: Series NoHR upper neck forces with model response

Upper neck Fx responses have two peaks, the first at 80 ms and the second at 140 ms. Fx correlations are low between sled tests ($r = 0.77$) and Model NoHR correlations with experimental data do not meet this revised target threshold. Mean value ratios are within the target range as are the standard deviations of the residuals. The first peaks do not capture the experimental peaks with the box maximum window, but the second peaks are well within the target window. Model NoHR upper neck Fx is validated for mean value ratio, standard residual and Peak 2 box maximum. Model NoHR upper neck Fz has stronger correlations although they do not meet the target threshold. Mean value ratios and standard deviation of the residual meet the modified target thresholds. Model NoHR peak maximum occurs at the same time as the experimental data, but is far lower. Model NoHR upper neck Fz is validated for mean value ratio and standard residual, partially validated for box maximum, and not validated for correlation.

Table 44: Model NoHR upper neck forces validation comparison. Asterisks indicate values that exceed target validation thresholds.

Upper Neck Forces					
Upper neck Fx					
Target Thresholds	Mean value ratio -4.71-2.54	Correlation ≥ 0.77	Standard residual ≤ 0.20	Peak 1: box max +/- 20%, +/- 5ms	Peak 2: box max +/- 95%, +/- 6ms
Model to Test 2	1.13	0.68*	0.00	+/-30%*, +/-12ms*	+/-22%, +/-5ms
Model to Test 3	0.20	0.57*	0.00	+/-35%*, +/-11ms*	+/-38%, +/-5ms
Model to mean	0.67	0.68*	0.00	+/-39%*, +/-11ms*	+/-20%, +/-5ms
Upper neck Fz					
Target Thresholds	Mean value ratio 0.70 – 1.44	Correlation ≥ 0.80	Standard residual ≤ 0.20	Box max +/- 20%, +/- 5ms	
Model to Test 2	1.21	0.76*	0.00	+/-138%*, +/-5ms	
Model to Test 3	0.99	0.74*	0.00	+/-130%*, +/-5ms	
Model to mean	1.44	0.77*	0.00	+/-158%*, +/-5ms	

6.4 DISCUSSION

Sled test comparisons indicate that variability between consecutive sled tests within the same test series often exceeded the Pipkorn-recommended thresholds. Pipkorn-recommended thresholds were not met for 31% of the measures compared for sled test Series HR, and for 28% of the measures for Series NoHR (Table 45).

Proposed mean value ratio thresholds of 0.80-1.20 produce an unusual situation illustrated by the Series NoHR lap belt loading, where the ratio Test 2/Test 3 = 0.80

(meets threshold) but the ratio of Test 3/Test 2 = 1.24 (exceeds threshold). To avoid this incongruity, I recommend that the baseline threshold be amended to 0.80-1.24. Also care must be taken when interpreting the mean value ratio. The mean value ratio is extremely sensitive for means close to zero, and meaningless when the mean of one data set is positive and the second data set is negative. This will most often occur when mean values are close to zero.

Sled test Series HR box maximum did not meet the Pipkorn thresholds 81% of the time. This would lead one to conclude that either the target window is too small, or that the test set up is not tightly controlled. Both statements may be true. There were three tests in Series HR, which provided more opportunities for differences between sled tests than for Series NoHR with just two tests. More importantly, ATD positioning for the sled test is not well controlled. During test set-up the ATD is positioned upright and symmetrically in the wheelchair. However, ATD joint positions and angles are not measured when positioning the ATD. ATD joint responses were not recalibrated before or between sled tests. It is difficult to determine if each joint is positioned in exactly the same position with each test, or if the non-recalibrated ATD produces identical joint responses for each tests.

During sled testing, the test sled is initially accelerated, then it travels on the test track at nearly constant velocity before being subjected to the deceleration pulse at time = 0 ms. All data are recorded from time = -25 ms, occurring 25 milliseconds before crash pulse activation. Initial sled acceleration causes the ATD to accelerate forward against the 3-point occupant restraints; then during the constant velocity period, the ATD returns to nearly the original position. This return motion is poorly controlled as it is

rebound from the initial acceleration, when the 3-point occupant restraints produced asymmetric loading of the ATD. This in turn causes asymmetric loading of the front tiedowns. The shoulder belt portion of the occupant restraint fits over the ATD right shoulder, and thus exerts greater limits on the forward motion of the ATD right shoulder than on the left. This asymmetry of the initial loading during the pre-recorded acceleration period of the sled test results in greater variability between the left front tiedown loads than to the right tiedown loads.

The model does not capture the initial unrecorded acceleration from 0 to 9 mph. (Note delta-V is 16 mph: 9 mph sled speed at impact, 7 mph sled return speed at rebound.) Instead it starts the simulation with a velocity of 9 mph applied to each system in the model (track, wheelchair, ATD). Then the actual crash pulse recorded during testing is applied solely to the test sled. The tiedown, wheelchair and ATD responses all result from sled deceleration.

Table 45: Comparison of target thresholds calculated from Series HR and Series NoHR sled testing.

Asterisks indicate validation thresholds that were modified to reflect sled test variability.

	Series HR					Series NoHR				
	Mean value	Correlation	SD of Resid	Box max 1	Box max 2	Mean value	Correlation	SD of Resid	Box max 1	Box max 2
Right TD	0.8-1.2	≥0.80	≤0.20	20%, 5ms		0.8-1.2	≥0.80	≤0.20	20%, 5ms	
Left TD	0.78-1.27*	≥0.80	≤0.20	20%, 16ms*		0.60-1.66*	≥0.80	≤0.20	20%, 5ms	
WC accel	0.8-1.2	≥0.80	≤0.20	24%*, 9ms*	27%*, 11ms*	0.80-1.20	≥0.80	≤0.20	20%, 5ms	20%, 5ms
Lapbelt	0.64-1.54*	≥0.80	≤0.20	51%*, 10ms*		0.80-1.24	≥0.80	≤0.20	20%, 10ms*	
Chest accel	0.8-1.2	≥0.80	≤0.20	20%, 5ms		0.80-1.20	≥0.80	≤0.20	20%, 5ms	56%*, 5ms
Head x-accel	0.8-1.2	≥0.80	≤0.20	20%, 9ms*		0.79-1.26*	≥0.80	≤0.20	46%*, 5ms	
Head z-accel	0.8-1.2	≥0.80	≤0.20	30%*, 6ms*		0.80-1.20	≥0.80	≤0.20	20%, 5ms	
Neck My	0.42-2.40*	≥0.80	≤0.20	45%*, 5ms		0.15-6.67*	≥0.77*	≤0.20	+105%*, 5ms	
Neck Fx	0.72-1.41*	≥0.80	≤0.20	24%*, 5ms		-4.71 - 2.54*	≥0.77*	≤0.20	20%, 5ms	95%*, 6ms*
Neck Fz	0.8-1.2	≥0.80	≤0.20	66%, 5ms		0.70 - 1.44*	≥0.80	≤0.20	20%, 5ms	

Overall, the Model HR is fully validated for tiedown loads, wheelchair accelerations, lap belts loads and chest accelerations, with all tests for these outcomes meeting target thresholds (Table 46). Model NoHR is also well validated for tiedown loads, wheelchair accelerations, lap belt loads and chest acceleration, with 86.3% of these tests meeting the target thresholds (Table 47). It is when we review the results of the neck forces and bending moments in combination with the head accelerations that a closer examination must be made.

Table 46: Model HR validation results summary for model validation against mean sled test results.

Black values indicate results meet target thresholds. Asterisks indicate results exceed target threshold.

Model HR	Mean value ratio	Correlation	Standard residual	Box max	Statistical tests met
Right front tiedown load	1.2	0.92	0.00	+/-20%, +/-5ms	4 / 4
Left front tiedown load	1.16	0.92	0.00	+/-20%, +/-5ms	4 / 4
Wheelchair CG accel	1.15	0.84	0.00	+/-20%, +/-8ms +/-20%, +/-6ms	5 / 5
Lap belt Load	0.93	0.85	0.00	+/-40%, +/-5ms	4 / 4
Chest acceleration	0.93	0.91	0.00	+/-20%, +/-5ms	4 / 4
Head x-acceleration	1.16	0.88	0.00	+/-78%*, +/-11ms*	3 / 4
Head z-acceleration	1.02	0.88	0.00	+/-23%, +/-5ms	4 / 4
Upper neck bending moment (My)	0.11*	0.87	0.01	+/-20%, +/-6ms	3 / 4
Upper neck Fx	-0.98*	0.65*	0.00	+/-50%*, +/-5ms	1.5 / 4
Upper neck Fz	3.24*	0.84	0.00	+/-37%, +/-5ms	3 / 4
Percent validated	70%	90%	100%	86%	

Table 47: Model NoHR validation results summary for model validation against mean sled test results. Black values indicate results meet target thresholds. Asterisks indicate results exceed target thresholds.

Model NoHR	Mean value ratio	Correlation	Standard residual	Box max	Statistical tests met
Right front tiedown load	1.2	0.92	0	+/- 24%*, +/- 5ms	3.5 / 4
Left front tiedown load	0.89	0.92	0	+/-20%, +/-5ms	4 / 4
Wheelchair CG accel	1.14	0.87	0	+/-31%*, +/-5ms +/-20%, +/-8ms*	4 / 5
Lap belt Load	1.18	0.98	0	+/-20%, +/-5ms	4 / 4
Chest acceleration	1.31*	0.81	0	+/-20%, +/-7ms* +/-35%, +/-5ms	3.5 / 5
Head x-acceleration	1.2	0.55*	0	+/-42%, +/-5ms	3 / 4
Head z-acceleration	1.19	0.78*	0	+/-59%*, +/-15ms*	2 / 4
Upper neck bending moment (My)	0.46	0.90	0.01	+/-40%, +/-7ms*	3.5 / 4
Upper neck Fx	0.67	0.68*	0	+/-39%, +/-11ms* +/-20%, +/-5ms	3 / 5
Upper neck Fz	1.44	0.77*	0	+/-158%, +/-5ms	2.5 / 5
Percent validated	90%	60%	100%	62%	

The target thresholds based on sled test responses are adjusted for 31% of the Series HR measures and for 28% of the Series NoHR measures, reflecting the variability between sled tests within the same test series. This may be a reflection of the neck response characteristics and sensitivity to ATD placement. The wheelchair is anchored to the sled with tiedowns, then the sled deceleration forces are translated upward through the entire system. First the sled decelerates, followed by the wheelchair, ATD torso, and then the head is last. All perturbations in the system are magnified in the head response.

The neck response for the 6-year old ATD has not been validated in rear impact, however its response should be predictable and repeatable. The Hybrid III 6-year old ATD differs from the other ATDs in the Hybrid III family as its neck was upgraded in 1997 to enable the 6-year old ATD to be used to evaluate airbag aggressiveness (First Technology Safety Systems, 2005).

Compounding issues surrounding the Hybrid III 6-year old ATD neck, the MADYMO Hybrid III 6-year old ATD has been validated against a single sled test (TNO, 2005) only in frontal impact. During review of the kinematic files in rear impact, it is clear that the MADYMO model neck produces greater extension in rear impact and does not reflect the visually stiffer ATD neck on the videos (Table 48 and Table 49).

Both Model HR and Model NoHR have neck bending moment responses that correlate well with sled test data. This correlation hides a subtle difference between the sled test data and the model response. In both cases, at ~85 ms, the model neck bending moment response goes into extension earlier than in the sled test responses. Effects of the

negative bending moment can be observed in the side by side video comparisons (Table 48 and Table 49).

In both sets of side by side comparisons, it appears that the MADYMO model neck is far less stiff than the test ATD neck. In Model HR, the excessive neck extension reduces the neck forces and also reduces the head accelerations along the x-axis (Figure 60), impacting validation. Likewise in Model NoHR, the neck extension reduces the neck forces and head accelerations. In Model NoHR the larger neck extension affects the head accelerations in both the x- and z-directions, because of rotated head position.

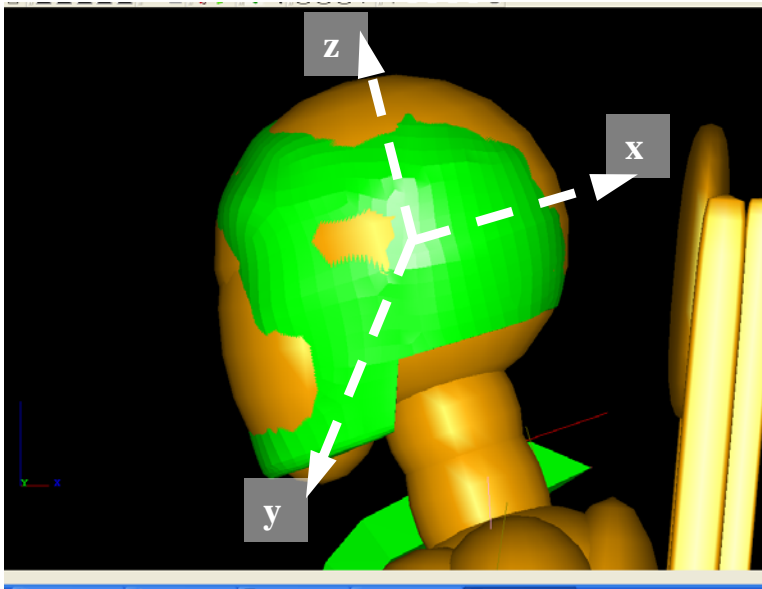


Figure 60: Model ATD head with labeled coordinate axis. X-axis is fore-aft direction. Y-axis is lateral direction. Z-axis is vertical direction.

Table 48: Side by side comparison of Model HR and Series HR

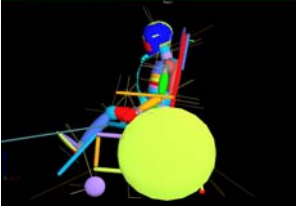
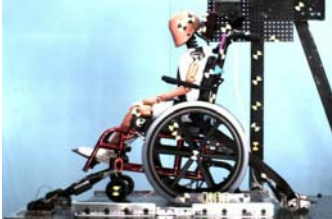
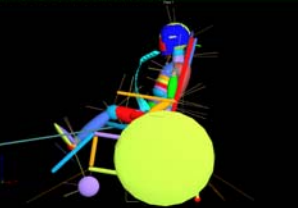

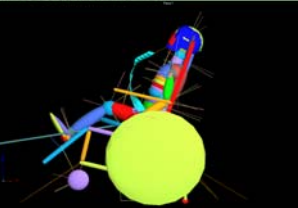

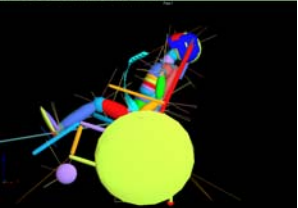
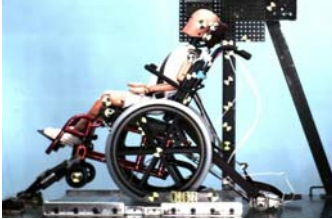
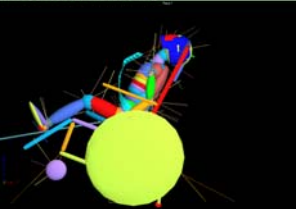

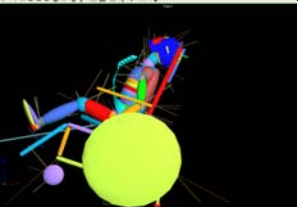

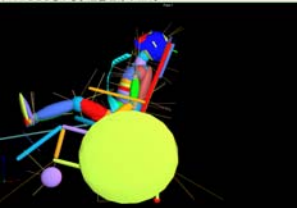
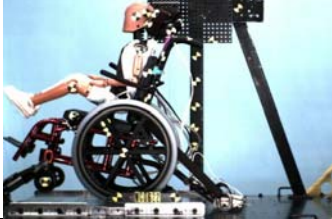



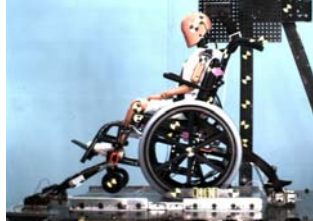
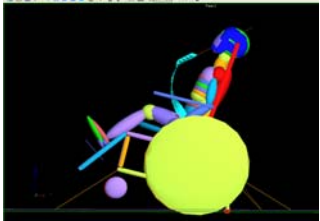

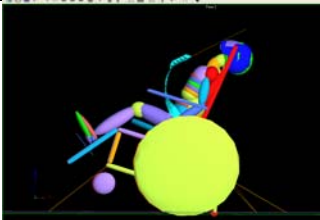


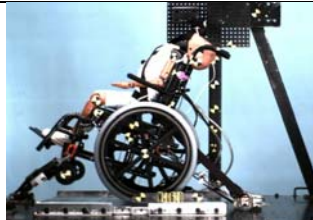
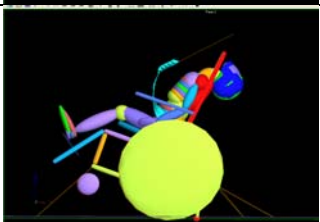

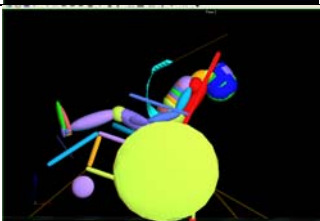

Model HR	Time	Series HR
	51 ms Model and sled test appear to compare well.	
	71 ms	
	91 ms	
	111 ms Model neck extends, exceeding the bending of the ATD neck.	
	131 ms Model neck appears to continue extending rearward in excess of physical ATD response.	
	151 ms Increased model neck extension	
	171 ms Model neck returning to upright position	

Table 49: Side by side comparison of Model NoHR and Series NoHR

Model NoHR	Time	Series NoHR
	<p>51 ms</p> <p>Model and sled test compare well.</p>	
	<p>71 ms</p>	
	<p>91 ms</p> <p>Model neck extending in advance of ATD neck.</p>	
	<p>111 ms</p> <p>Neck extends further. Model extension appears to exceed ATD extension.</p>	
	<p>131 ms</p> <p>Model neck extension exceeds ATD neck extension in sled test</p>	
	<p>151 ms</p> <p>Increased neck extension</p>	
	<p>171 ms</p> <p>Physical ATD neck returning to upright position, model neck still extended</p>	

It is important to note the difference between head position (Figure 60) and head accelerations, which are difficult to discern from video images. In the case of Model HR, a stiffer neck would have enabled the head to remain in a more upright position during the test and the impact against the headrest would cause higher x-accelerations (fore-aft direction). The peak measured z-accelerations are less than half that for the x-acceleration. With the presence of the headrest, there is little motion in the z-direction, so the less stiff model neck does not affect the z-axis (vertical axis) model response as much and Model HR z-acceleration correlates well with the sled test data.

In the case of Model NoHR, the absence of the headrest permits far greater motion of the head and neck extension. Limitations due to the lack of MADYMO model ATD neck response validation in rear impact become all the more apparent. In Model NoHR, the less stiff neck also contributes to excessive neck extension, while peak head accelerations remain low. Model NoHR upper neck forces are dominated by the axial response (F_z), here too the ATD model neck allows a great deal of extension with lower forces than the physical ATD neck experiences. With the amount of observed neck extension in the model, it supports the model data that peak axial (z) forces are seven times the peak transverse forces (x) forces. The upper neck force in the x-direction drives the upper neck moment, and is sufficient to produce good validation.

A key limitation to the model development in general, and these models in particular are the methods used to represent the physical systems. It is not a one-to-one correspondence between the physical set-ups and the models. Clearly, each piece on the wheelchair does not have a matching piece on the model – nor does the model ATD represent the physical ATD in a piece by piece fashion. The goal of the model is to

simulate the behavior of the physical system. In our case, there were several decisions that were made, simplifying the model. Although the sled tests indicated that there was vertical excursion of the seatback along the seatback canes, this was not modeled. Instead, the model seatback was positioned to represent the position of the physical wheelchair seatback at time of peak loading. This was an acceptable approximation as the chest accelerations were well validated in both Model HR and Model NoHR. Also, MADYMO uses a simplified rigid body model, and as such does not accommodate parameters such as flexing of the frame or hardware. In these models, this means that the wheelchair frame is described as a point mass with inertial properties, however the relative stiffness of the frame cannot be assessed.

Despite all this, the models validate well with the exception of the head and neck, which is due to the MADYMO neck characteristics. The model tiedown loads, wheelchair accelerations, lap belt loads and chest accelerations will all be effective predictors of actual wheelchair response in rear impact. They will be useful for development of wheelchair design guidelines. The head and neck response must be examined more closely. In all cases the head and neck responses follow the trends from the sled test data, although their peak responses are lower. Parametric sensitivity analysis will focus on Model HR with its better validation. Critical for neck injury outcome measures is the axial neck loading and the neck bending moments, which both validate well in this model. Head x-accelerations are low, but in combination with the z-acceleration, it will be useful to examine ratios of head accelerations. In general, head accelerations tend to be low unless the head hits a hard surface, which will not happen in these simulations. Additional research into the behavior of the MADYMO Hybrid III 6-

year old ATD and the effects of its response are needed to better understand its limitations. Future work will examine the MADYMO neck response to increased stiffness, and also assess the effect of increased neck stiffness on injury risk outcome measures.

7.0 CERVICAL SPINE STIFFNESS CHARACTERIZATION OF THE ENCRYPTED MADYMO HYBRID III 6-YEAR OLD ATD MODEL

The MADYMO neck characteristics are encrypted making it difficult to describe neck response based on joint characteristics. The Hybrid III 6-year old child ATD is specified under Title 49 CFR, part 572, Subpart N, and requires neck calibration testing for the ATD neck in flexion and extension using a test pendulum. Results are typically described by plotting neck bending moment about the occipital condyle in response to neck rotation about the pendulum axis. A MADYMO model simulation of Part 572, Subpart N, calibration neck testing for flexion and extension tests was developed and neck rotation and neck moment data were compared against data from a physical ATD (pATD) calibrated neck. The MADYMO neck response is described and compared using the same moment to angle comparison as is the calibration tests for the pATD neck.

7.1 INTRODUCTION

The Hybrid III 6-year old ATD and its neck response have provoked controversy regarding its biofidelity (Malott et al., 2004; Bilston, 2007) since actual incidence rates of severe pediatric neck injury in rear impact motor vehicle crashes remain lower than would be anticipated from ATD testing and ATD measurements fail to reliably predict

actual injury. Yet, other members of the Hybrid III ATD family have been successfully used in rear impact testing (Viano, D. C. and Davidsson, 2002) with results using the 50th percentile male consistent with field data. The Hybrid III 6-year old neck was modified in response to airbag deployment testing and is not a scaled version of the other members of the Hybrid III ATD family. The Hybrid III 6-year old ATD has not yet been validated for rear impact.

In addition to neck modifications that reflect ATD to airbag interaction response, the Hybrid III allows for more instrumentation than the Hybrid II. The Hybrid II accommodates triaxial head accelerometers, but lacks neck instrumentation capabilities. Available instrumentation makes the Hybrid III more suitable for creating response corridors needed for simulation model development and validation. The Hybrid III 6-year ATD has been used extensively in sled testing (Oster and Trommler, 1996; Sherwood et al., 2003; Malott et al., 2004; Ha, D. et al., 2007) and is specified in FMVSS 208 (National Highway Traffic Safety Administration, 1993). Despite speculation surrounding ATD neck biofidelity, the Hybrid III 6-year old ATD remains the best human surrogate available today for prediction of 6-year old dynamic response and potential injury.

TNO MADYMO¹² supports modeling using the Hybrid III 6-year old ATD with an ellipsoid multi-body model. However, the MADYMO ATD model is validated for frontal impact, but not for rear impact (TNO, 2005). In addition, MADYMO neck joint responses are proprietary, prohibiting direct assessment of neck response characteristics from individual joint parameters.

¹² TNO Automotive Safety Solutions, <http://www.tass-safe.com>

The Hybrid III 6-year old child dummy user's manual (Society of Automotive Engineers: Dummy Testing Equipment Subcommittee, 2003) provides calibration test procedures for the ATD neck for flexion and for extension. These are mechanical pendulum tests that require mounting the ATD head and neck to the end of a pendulum, then impacting the pendulum into an aluminum honeycomb block to produce a velocity profile specific for flexion or extension. Neck flexion/extension is characterized by comparing the resulting neck rotation to the calculated neck moments about the occipital condyle.

In this study, MADYMO simulation software is used to construct models to mirror the neck flexion and extension calibration tests specified by ATD neck component testing per NHTSA 572.73 and described in the *Hybrid III Six-year-old Child Dummy User's Manual* (Society of Automotive Engineers: Dummy Testing Equipment Subcommittee, 2003). Although all MADYMO neck characteristics are encrypted, overall neck response can be characterized per NHTSA 572.73 and the Hybrid III 6-year old child dummy user's manual. Results from modeling efforts presented in Chapter 6, suggest that the MADYMO model ATD (mATD) neck motion exceeds actual pATD kinematics in rear impact. This study directly compares mATD neck flexion and extension response to pATD neck responses.

7.2 METHODS

The pATD neck shown in Figure 61 (right), is constructed with a single molded rubber segmented neck that permits dynamic flexion and extension articulations, and is designed

to produce human-like angle versus moment response (Society of Automotive Engineers: Dummy Testing Equipment Subcommittee, 2003). A cable extends through the longitudinal axis of the neck to support high axial loading, and front and rear nodding blocks limit fore and aft motion of the head. The diagram also displays the location of the D-plane; this reference plane is a horizontal plane parallel to the base of the skull and is used to describe pATD neck rotation relative to the pendulum arm longitudinal center line.

In contrast, the mATD has four joints in the MADYMO neck. The lowest joint is a fixed bracket joint attaching the neck to the spine (not shown). In addition, the mATD has 3 moveable joints in the neck (Figure 61, left). The upper and lower neck joints are ball joints that permit rotational motion in three planes. The mid neck joint is a translational-rotational joint that permits neck flexion-extension motion, as well as translational motion (stretching) in the axial direction.

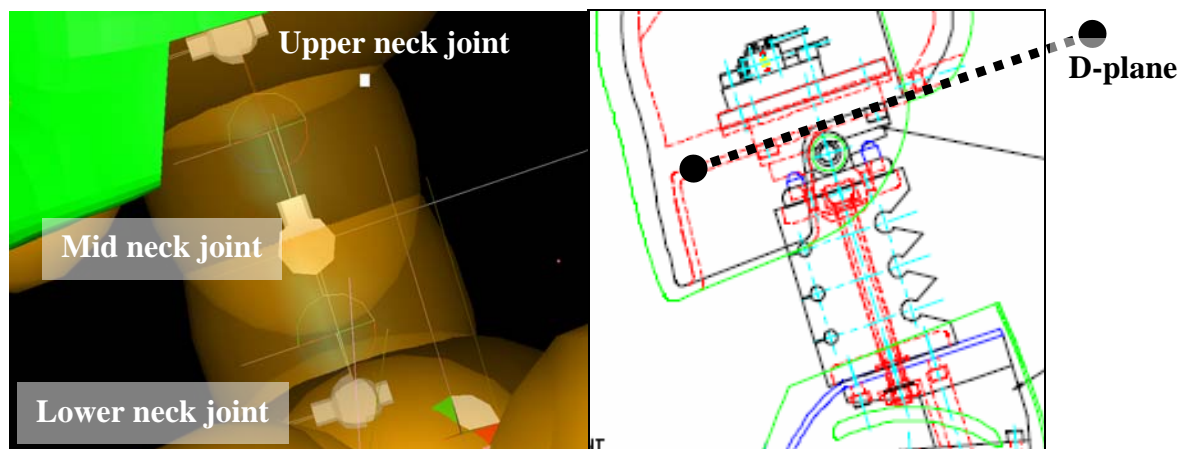


Figure 61: MADYMO mATD neck displayed (left) with upper, mid and lower neck joints. Physical ATD neck schematic displayed (right) with D-plane location. The D-plane position relative to the pendulum arm longitudinal center line describes the flexion-extension neck angles during calibration testing.

Table 50 summarizes all elements of the mATD neck. Four separate bodies compose the neck. Two ellipsoid neck elements define the neck surface; NeckLow_ell is associated with NeckLow_bod, NeckUp_ell with NeckUp_bod. Four joints control the relationships between the bodies. NeckLCL_jnt firmly fixes the neck to the thorax with a non-moving bracket joint. Two spherical joints can rotate with three degrees of freedom and are located in the upper and lower neck. The mid-neck joint has two degrees of freedom; it permits flexion and extension about the y-axis, and permits stretching in the axial direction (z-axis). Table 50 also identifies the names of all neck joint restraints, characteristics (encrypted), and functions (encrypted).

Table 50: Summary of MADYMO neck elements

Bodies (4) and Surfaces (2)		
Body name		Surface name
NeckLCLow-Bod		NeckLow_ell
NeckLow_bod		NeckUp_ell
NeckMid_bod		
NeckUp_bod		
Joints (4)		
Joint name	Joint type	Joint connections
NeckLCL_jnt	Joint.brac	Thoracic spine body to neckLCLow_bod
NeckPivotLow_jnt	Joint.sphe	neckLCLow_bod to NeckLow_bod
NeckPivotMid_jnt	Joint.revo tran	neckLow_bod to NeckMid_bod
NeckPivotUp_jnt	Joint.sphe	NeckLow_bod to NeckMid_bod
Joint restraints (3): all are RESTRAINT.SIX DOF elements		
Restraint name	Number of degrees of freedom with restraint characteristics	Names of associated restraint characteristics – (*encrypted)
NeckLow_six	3 DOF restraints	*Sixdof_char_34 *Sixdof_char_35 *Sixdof_char_36
NeckMid_six	2 DOF restraints	*Sixdof_char_37 *Sixdof_char_38
NeckUp_six	3 DOF restraints	*Sixdof_char_39 *Sixdof_char_40 *Sixdof_char_41
Characteristics (8) and functions (16): The characteristics are all encrypted and information on the associated functions are also encrypted. All loading, unloading and damping is encrypted, as are limits, etc.		
Encrypted characteristics (8)		Encrypted functions (16)
Sixdof_char_34		Fid_54 Fid_63
Sixdof_char_35		Fid_57 Fid_66
Sixdof_char_36		Fid_58 Fid_69
Sixdof_char_37		Fid_55 Fid_67
Sixdof_char_38		Fid_59 Fid_68
Sixdof_char_39		Fid_56 Fid_64
Sixdof_char_40		Fid_60 Fid_61
Sixdof_char_41		Fid_62 Fid_65

The *Hybrid III six-year-old Child Dummy User's Manual* (Society of Automotive Engineers: Dummy Testing Equipment Subcommittee, 2003) provides comprehensive information, procedure and performance specifications for pATD neck flexion and extension calibration testing. During testing, the ATD head and neck assembly is mounted to the end of a 72.25 inch pendulum (Figure 62). The pendulum is fitted with a striker plate and accelerometer 65.25 inches from the pivot point. The pendulum is allowed to drop freely to produce specified impact velocities (Table 51). At impact, the pendulum striker plate contacts an aluminum honeycomb hexcell block, which is modified at the test site to produce the specified velocity-time profile (Table 51). Transducers measure the resulting upper neck forces and moments, and D-plane rotation with respect to the pendulum's longitudinal center line. The moment about the occipital condyles is measured in Nm's and is calculated using Equation 13. My and Fx are measured at the upper neck load cell.

Equation 13: Moment about the occipital condyles

$$\text{Moment} = [M_y] - [(0.01778) * (F_x)]$$

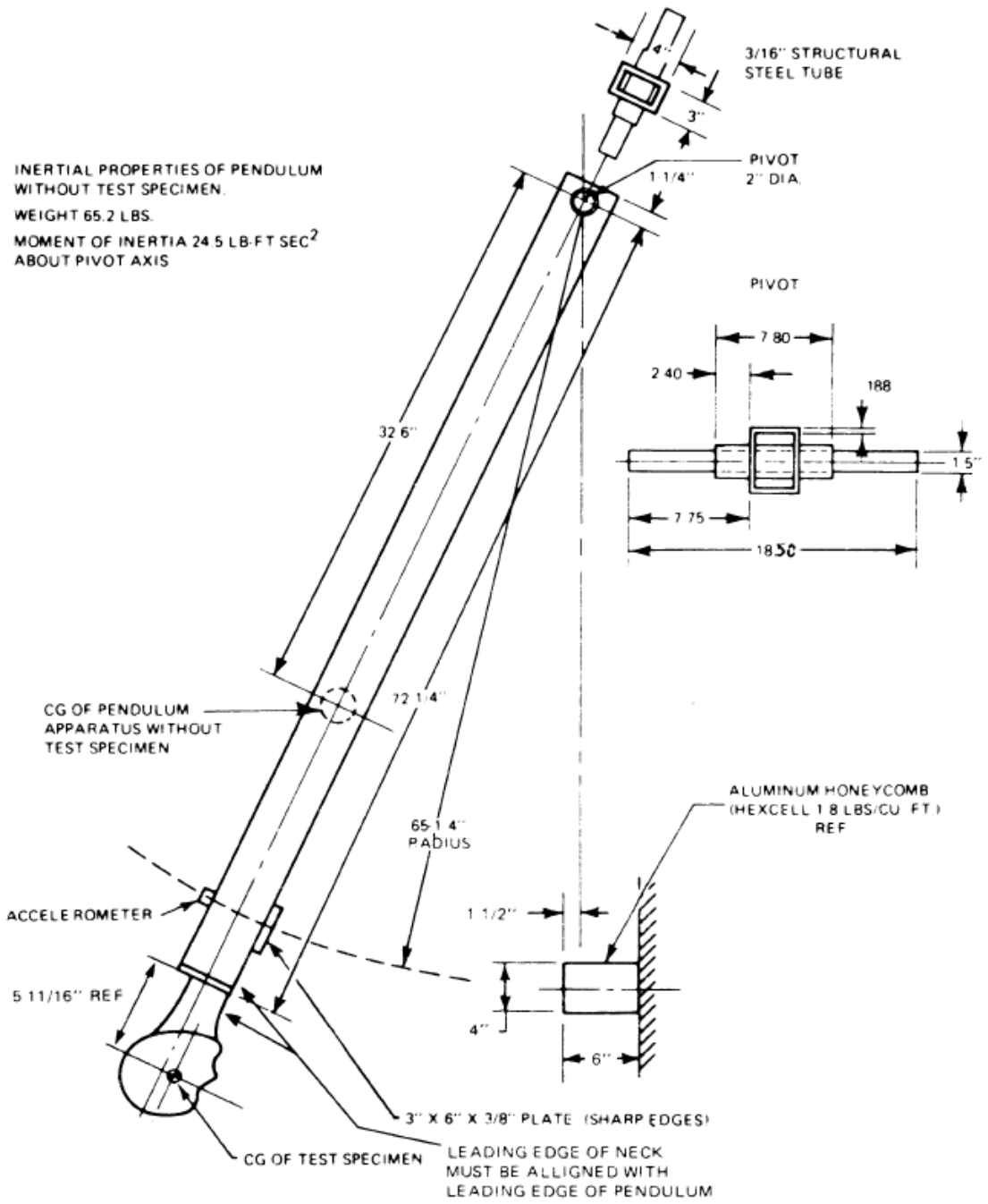


Figure 62: Neck component test schematic for neck flexion test

Table 51: Neck testing velocity profile specifications

	Neck Flexion		Neck Extension	
Initial Impact Velocity at Time = 0 ms	4.95 +/- 0.12 m/s		4.30 +/- 0.12 m/s	
	Total velocity change (m/s)	Velocity range (m/s)	Total velocity change (m/s)	Velocity range (m/s)
10 ms	1.2 – 1.6	3.23 – 3.87	1.0 – 1.4	2.78 – 3.42
20 ms	2.4 – 3.4	1.43 – 2.67	2.2 – 3.0	1.18 – 2.22
30 ms	3.8 – 5.0	0.00 – 1.27	3.2 – 4.2	0.00 – 1.22

This MADYMO simulation models the test method described in the Hybrid III 6-year old users manual, and incorporates the geometries specified for the pendulum and aluminum block. The mATD head and neck portion of the MADYMO 6-year old Hybrid III ATD are attached to the model pendulum with a fixed bracket joint mirroring the test set-up used to calibrate the pATD neck. The contact characteristics between the model pendulum striker plate and the aluminum hexcell block are modified to produce the velocity-time profile described in the pATD neck test specifications. Moments about the occipital condyles were calculated using Equation 13 and mATD upper neck joint My and Fx data. The mATD angle data corresponding to pATD rotation of the “D” plane of the head is calculated using the sum of MADYMO joint position outputs from the upper, mid and lower neck joints.

7.3 RESULTS

Two MADYMO models were built to individually simulate the neck flexion and extension neck calibration tests. In the neck flexion testing, the mATD head and neck

face the aluminum hexcell block; in extension testing, they face away from the block (Figure 63).

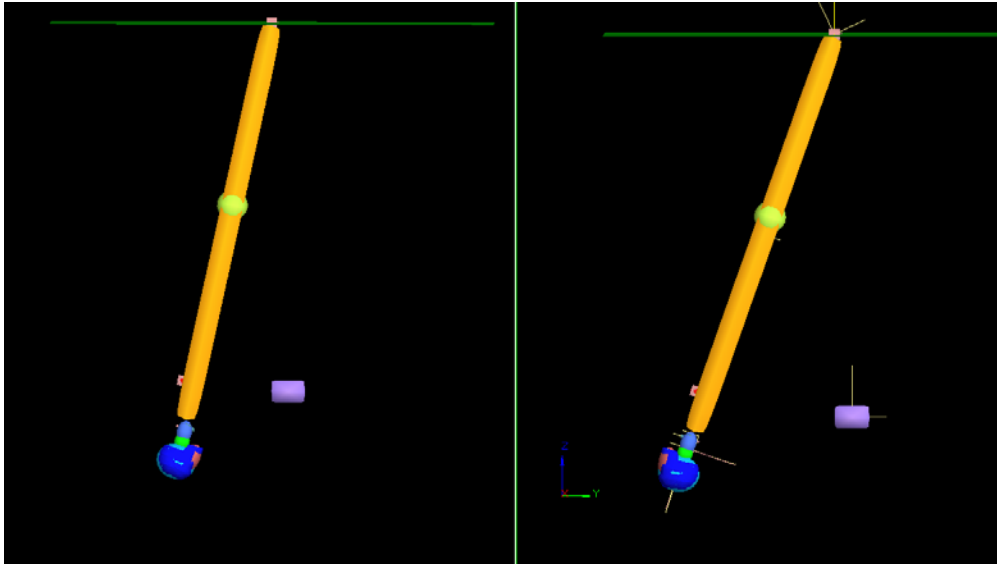


Figure 63: MADYMO neck flexion and extension simulation models

Neck calibration flexion and extension models both produced the pendulum velocity-time profiles specified in the Hybrid III 6-year old users manual neck calibration procedures. Figure 64 and Figure 65 display velocity-time target profiles in grey with model velocities shown in red. Both model pendulum velocities are within the pATD test target corridors.

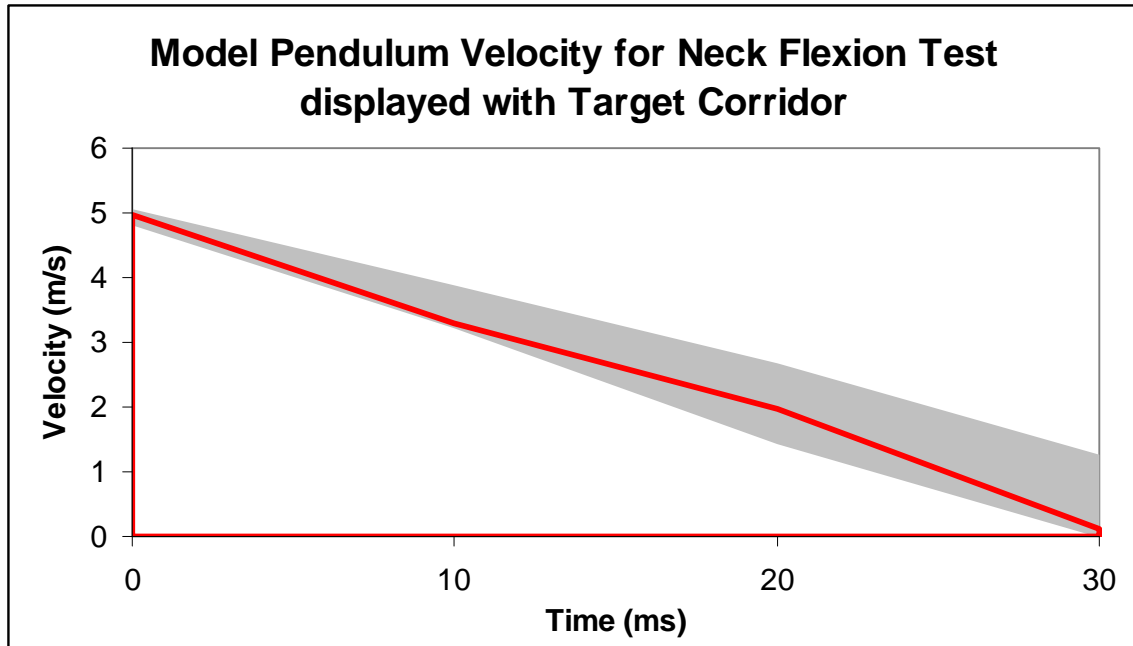


Figure 64: Model pendulum velocity for neck flexion displayed with target velocity corridor. Target corridor is displayed in grey shaded area with model velocity displayed in red.

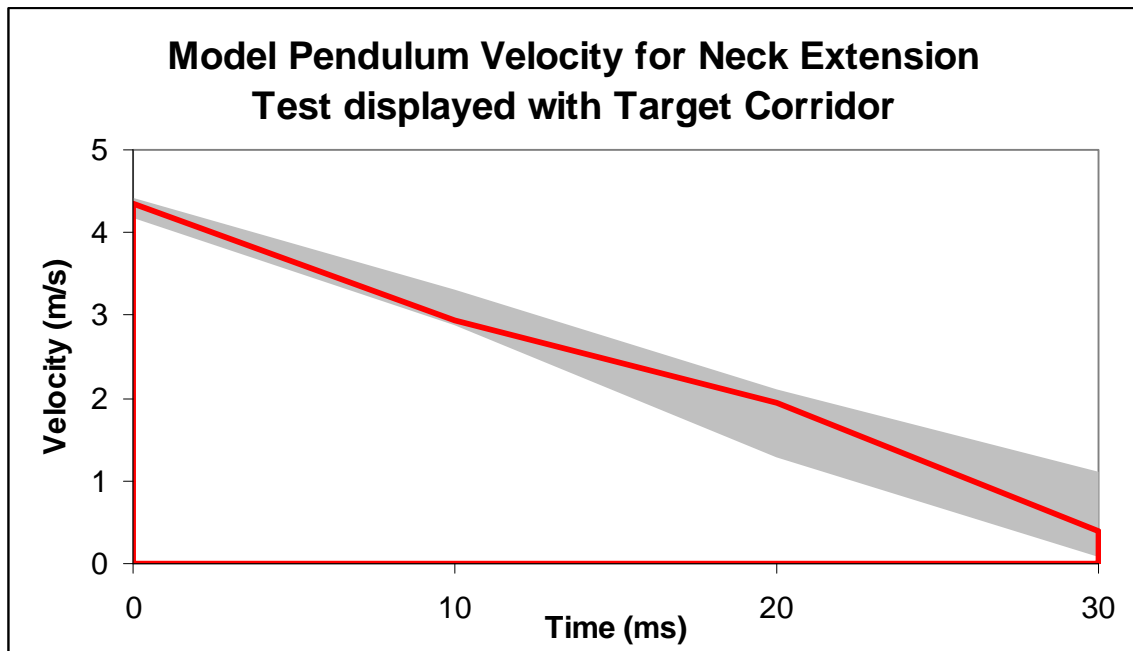


Figure 65: Model pendulum velocity for neck extension displayed with target velocity corridor. Target corridor is displayed in grey shaded area with model velocity displayed in red.

Neck moment about the occipital condyle is presented with respect to the neck rotation relative to the pendulum for both neck flexion (Figure 66) and extension (Figure 67). Peak moments are greater in flexion than in extension. Model neck extension response is more pertinent to the rear impact model since flexion occurs only during rebound. The mATD neck rotation relative to the pendulum is greater during extension testing than flexion testing although the target impact velocity is lower for neck extension testing than neck flexion testing.

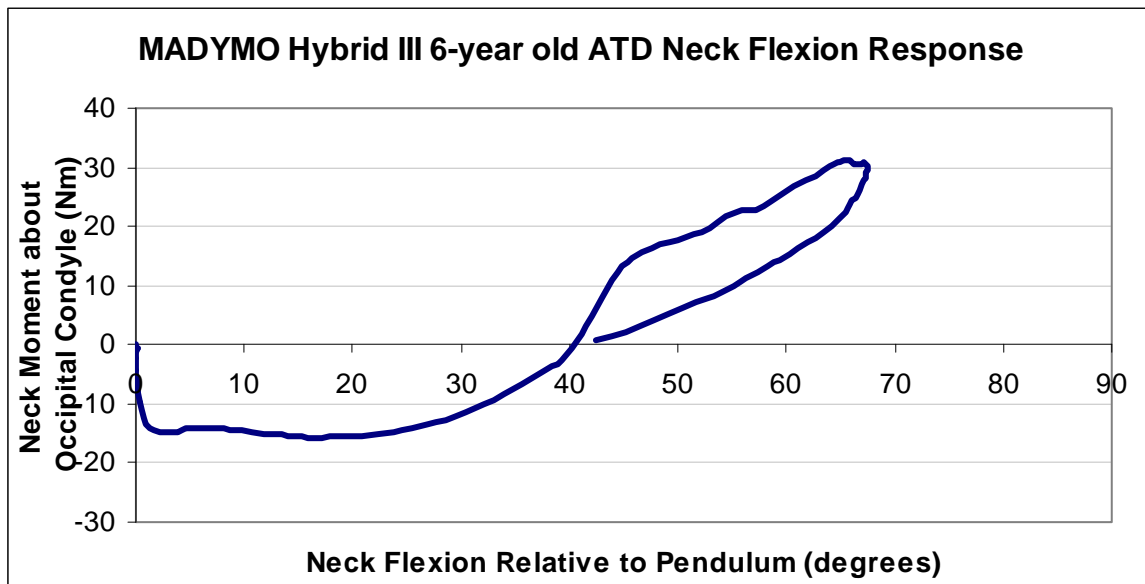


Figure 66: MADYMO Hybrid III 6-year old ATD Neck Flexion Response.

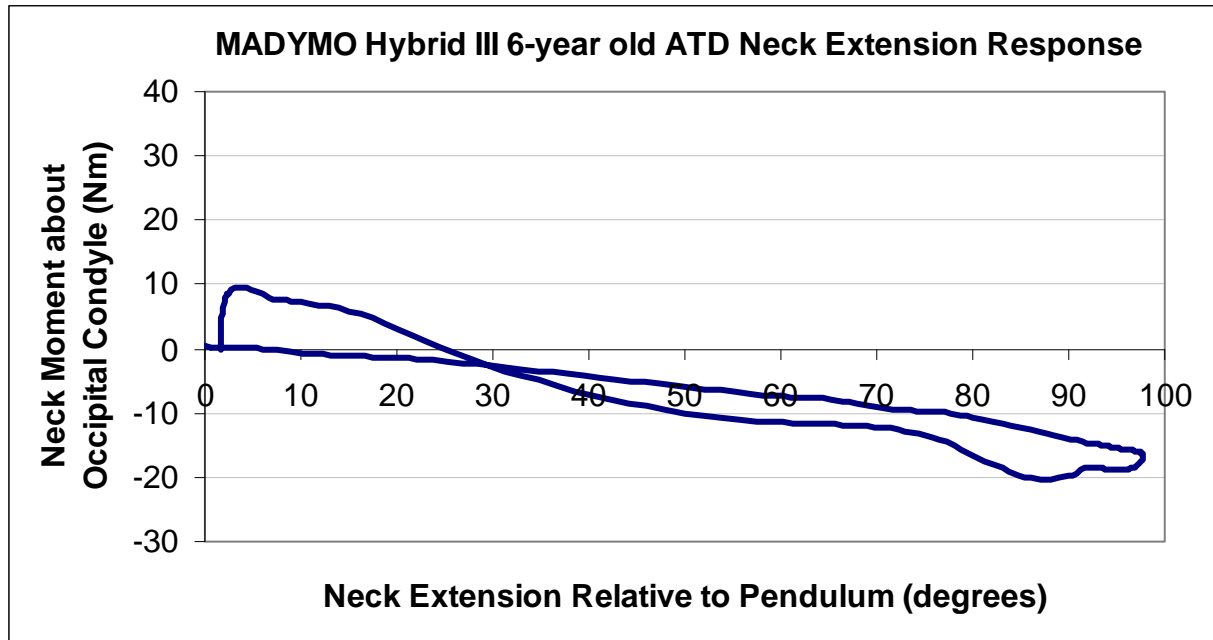


Figure 67: MADYMO Hybrid III 6-year old ATD Neck Extension Response

7.4 DISCUSSION

Flexion and extension neck calibration test data from the National Highway Traffic Safety Administration Vehicle Research and Test Center, Applied Biomechanics Division (East Liberty, Ohio) from a calibrated Hybrid III 6-year old ATD neck provide the basis for comparisons between mATD simulated tests results and pATD neck test outcomes. Comparisons of mATD and pATD neck bending moments about the occipital condyle in flexion (Figure 68) indicate identical peak values of 31 Nm, however mATD peaks at 65 degrees of neck flexion while the ATD moment peaks later at 74 degrees of neck flexion relative to the pendulum. Part 572 neck flexion calibration specifications require peak rotation between 74-92 degrees; within that rotation range, the peak moment must be between 27-33 Nm. The mATD neck does not meet this specification, as peak

bending moment at less neck flexion. Greater differences in neck moments occur at lower neck rotations with the two curves diverging from 5 to 15 degrees. Physical ATD neck moments are positive (flexion) from 18 to 41 degrees, while the model experiences negative (extension) neck moments about the occipital condyle. Note that for both mATD and ATD neck moments increase with increasing neck angle, then after peaking, decrease along a separate curve with decreasing neck rotation angle.

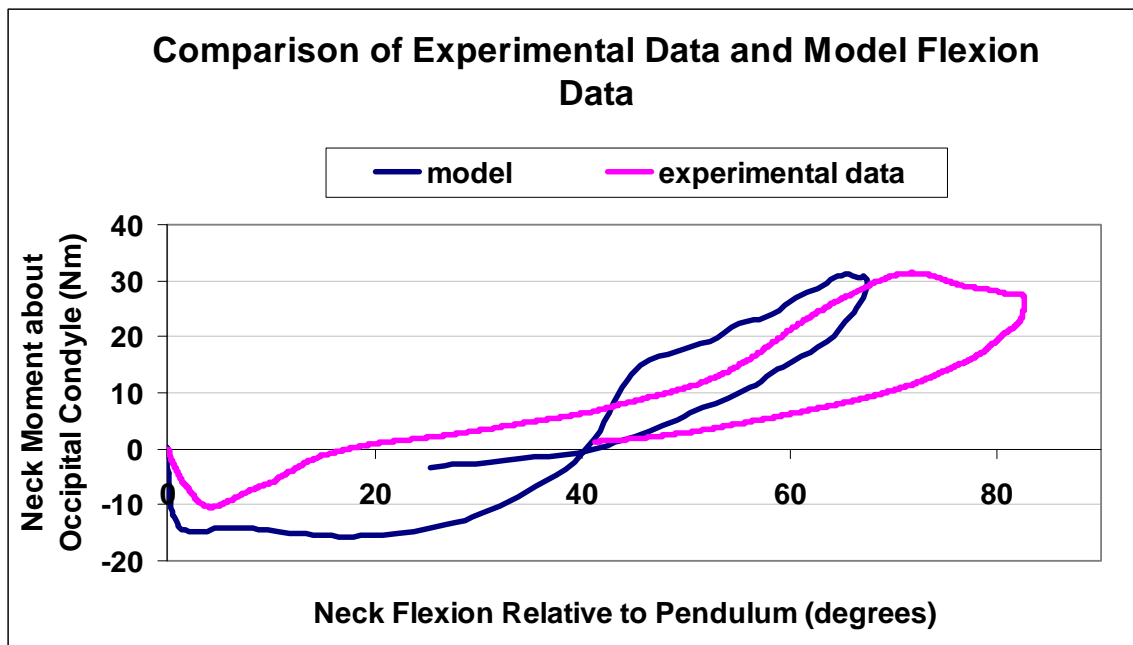


Figure 68: Comparison of experimental (pATD) and model (mATD) data for neck flexion testing

In neck extension testing (Figure 69) the neck extension angle is measured relative to the pendulum, thus extension angles are positive. Extension bending moments are negative. Similar to flexion peaks, in extension the peak neck moments about the occipital condyle are similar (20 Nm) but occur at a smaller angle in the model than during pATD neck extension testing. Part 572 neck extension calibration specifications

require peak rotation between 85-103 degrees; within that rotation range, the peak moment must be between (-19) to (-24) Nm. Both the mATD and ATD necks meet this specification for neck extension. The two curves match closely at 60 degrees, but differ at smaller angles. Model neck moments are positive (flexion) from 15 to 25 degrees while pATD neck moments are negative (extension) for the same neck extension angles. Also similar to the flexion response, as the model neck angle increases the moments decrease along a similar curve, then as the neck returns to the neutral position the neck moments increase along a second curve. In summary, the overall peak mATD and pATD neck extension responses are similar, the model differs from the experimental data smaller extension angles.

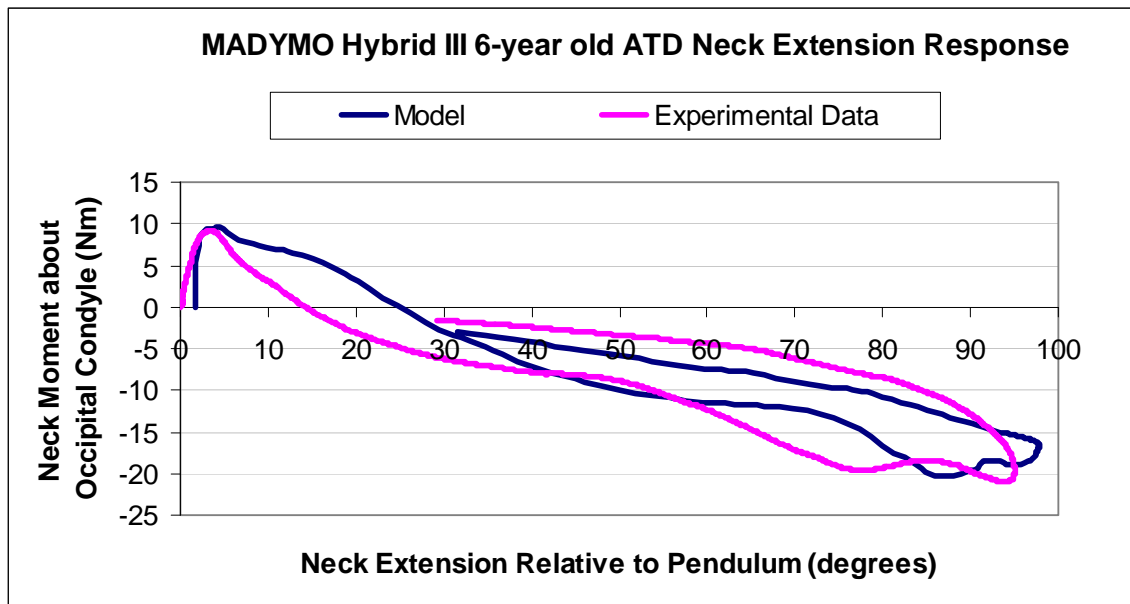


Figure 69: Comparison of experimental and model data for neck extension testing

There are two separate issues to consider when evaluating the impact of the differences between the mATD and the ATD responses. The first is to consider the ATD

neck range of motion with respect to the mATD neck. The second is to consider the impact that these differences may have on the injury parameters.

My research focused on comparing mATD neck responses during a 16 mph, 11 g, 60 ms rear impact sled tests (Figure 70). Model HR indicates that a peak neck extension of 57 degrees occurs late in the impact event at 130 ms; Model NoHR peak neck extension of 94 degrees occurs later at 166 ms. Figure 70 displays the mATD neck extension angle from Model HR and Model NoHR simulation results from Chapter 6. The -6 degree initial neck angle indicates that the mATD neck position is in a slightly flexed position at the start of the rear impact crash pulse. This neck position is a result of the original sled acceleration when the mATD head initially is accelerated forward relative to the wheelchair as the test sled is accelerated rearward on the test track. The mATD neck does not return to the neutral position before the rear impact (deceleration) pulse. The maximum 15 degree flexion rotation occurs at 60 ms as the ATD torso first moves rearward into the wheelchair seatback followed by the head. This is actually neck flexion, thus results from the flexion test comparison should be considered.

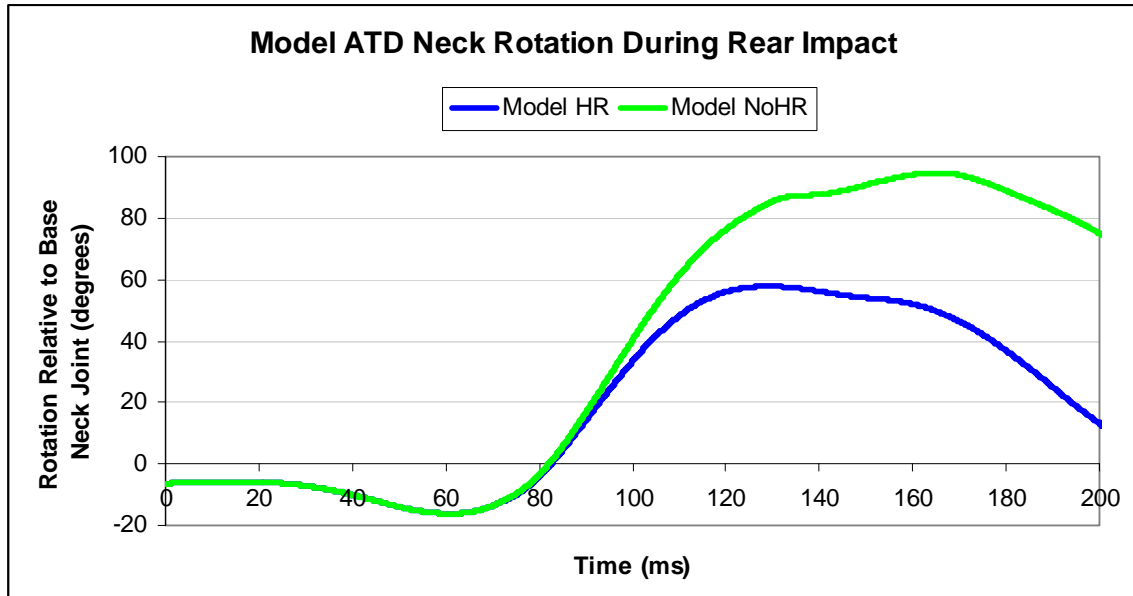


Figure 70: Model ATD neck rotation during rear impact. Negative angles indicate neck flexion, positive angles indicate neck extension.

Figure 71 displays a comparison of the neck flexion test from pATD and mATD from 0 to 45 degrees. At 15 degrees, mATD differs markedly from the ATD response. During the neck extension portion of the response, the moments at 60 degrees and 90 degrees have much closer comparison, however it is worthwhile to note the differing responses before reaching those peaks (Figure 72). The sled test models have an initial peak flexion of 15 degrees. Comparisons between the mATD and pATD neck flexion data indicate that pATD neck has a very small neck flexion moment at 15 degrees, while there is a much larger (-16 Nm) flexion moment in the mATD neck at the same angle.

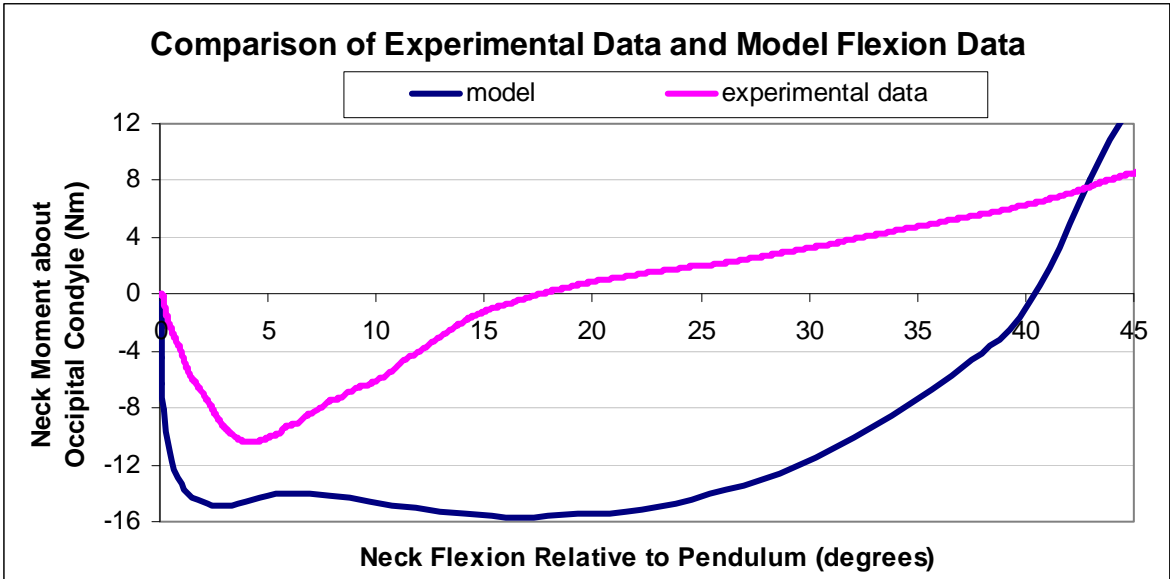


Figure 71: Comparison of experimental (pATD) and model (mATD) neck flexion test data from 0 to 45 degrees of neck rotation. Negative neck moments indicate extension, positive values indicate flexion moments.

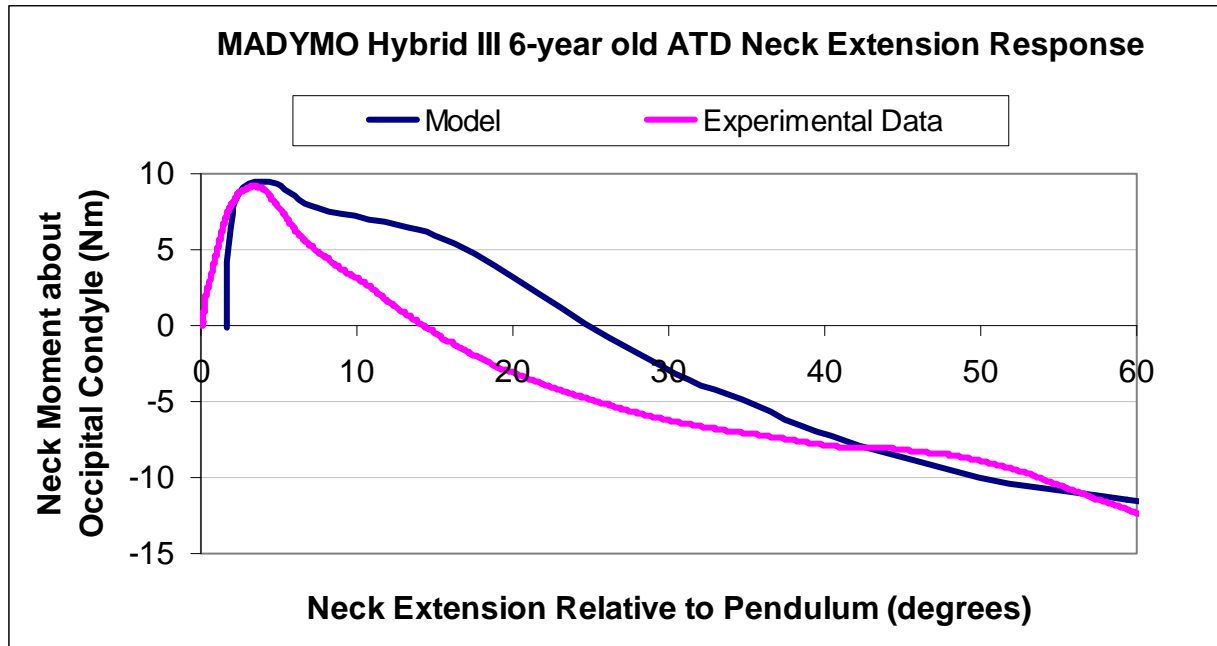


Figure 72: Comparison of neck extension test response from 0 to 60 degrees of neck rotation

Validation results presented in Chapter 6 indicate that the models are producing low peak head accelerations. Results from this study suggest that the mATD neck flexion bending moment response characteristics at small angles may serve to reduce the overall head accelerations. Likewise, the neck validation results from the sled test models are supported by the differences between the mATD and pATD neck responses.

Two injury risk criteria are the head injury criteria (HIC) and the neck injury criteria (N_{ij}). HIC is a combined measure of head acceleration and duration of those accelerations. Neck injuries are of particular concern in rear impact as up to 70% of injury producing vehicle accidents involve whiplash injuries (Volvo, 2003). The mATD neck response validity plays a critical role in the injury risk criteria outcome measures. The HIC is dependent on linear head acceleration, which in turn is dependent on neck response. Our sled test data suggested that likelihood of head injury was low since all

measured values were far lower than the PRV=700 for HIC15, yet it is worthwhile to note that while mATD responses were lower, they were of comparable order of magnitude (Table 52). Nij depends on peak upper neck bending moments and upper neck forces. Results from the neck calibration extension simulation indicate that peak mATD extension angles and moments compare well to the pATD measured during calibration testing. The mATD and pATD peak moment responses compare well in extension calibration testing; likewise, results calculated from sled test simulation models indicate that Nij values also compare well.

Table 52: Comparison of injury risk criteria with protection reference values (PRV)

Headrest				
	Model HR	Series HR (3 sled tests)		
HIC15, PRV=700	29.9	50.8	51.6	67.1
Nij, PRV=1	0.458	0.382	0.373	0.332
No Headrest				
	Model NoHR	Series NoHR (2 sled tests)		
HIC15, PRV=700	25.7	97.3	75	
Nij, PRV=1	0.878	1.51	0.874	

Given the controversy surrounding the biofidelity of the pATD neck, it is critical to be aware that mATD's predictability of the pATD's injury criteria values is not indicative of the absolute likelihood of injury. Rather, it can be used as a tool to compare outcomes across different scenarios. In this case, it would suggest that neck injury is more likely in rear impact in wheelchairs not equipped with headrests.

It is also noteworthy, that mATD neck response can be effectively characterized by subjecting a model to a simulated neck calibration test in both flexion and extension. MADYMO's encryption all of the neck response characteristics limit the ability to define

the neck response based on characteristics of the individual neck joints. MADYMO does permit the addition of resistive forces and moments to the three model neck joints.

Changes to the MADYMO neck response based on the addition of these resistive loads can be described using the methods outlined in this study. Future work will examine the effect of modifying MADYMO neck stiffness on ATD injury risk outcome measures assessed rear impact sled testing.

8.0 PARAMETRIC SENSITIVITY ANALYSIS

Parametric sensitivity analysis was used to develop wheelchair and headrest design guidelines for pediatric manual wheelchairs in rear impact, assess the sensitivity of pediatric injury outcome measures to wheelchair, headrest and crash pulse parameters, and evaluate the effect of a stiffer 6-year old ATD neck on injury risk outcome measures.

8.1 INTRODUCTION

Sled testing can provide excellent kinematic data allowing for direct assessment of wheelchair and ATD response (Fuhrman, S. I. et al., 2006; Fuhrman, S. I. et al., 2008), but may also have data collection limitations. Anthropomorphic test devices (ATD) can be instrumented to measure accelerations, forces and bending moments without compromise to the ATD response characteristics. Instrumentation of the wheelchair is more limited; wheelchair accelerations and wheelchair tiedown and occupant restraint (WTORS) loads can be measured without affecting wheelchair kinematics, while other component outcome measures of interest cannot be assessed without disturbing wheelchair response. For example, load cells can be used to measure wheelchair seatback loading, but may affect seatback response.

Computer modeling, validated against sled tests, can be used to assess difficult to quantify sled test outcomes such as seatback, headrest and wheel loads. A parametric sensitivity analysis is a tool that can be used to assess the sensitivity of a system's behavior to changes in individual parameters (Varma et al., 1999). It's used to determine the influence of various individual parameters on design objectives (Thieffry, 2008). This technique has been successfully used with wheelchair computer simulation applications to determine the range of wheelchair responses for development of design guidelines in frontal impact (Bertocci, G. E. et al., 1996a; Ha, DongRan, 2004).

In this study, a parametric sensitivity analysis was used to develop design guidelines for rear impact and to predict ATD injury outcome measure ranges for consideration in occupant protection. Also, in response to on-going concerns related to the biofidelity of the six-year old Hybrid III ATD neck (Malott et al., 2004; Bilston, 2007), parametric sensitivity analysis was used to address the potential effects from biofidelity-related issues on outcome results.

Objectives of the parametric sensitivity analysis conducted as part of this study were three-fold:

- (1) to develop design guidelines for manual pediatric wheelchairs and headrests in rear impact
- (2) to evaluate the sensitivity of pediatric injury outcome measures under rear impact conditions to wheelchair and headrest parameters
- (3) to assess the effect of stiffer mATD neck on injury risk measure outcomes in rear impact

This study used a previously validated MADYMO computer simulation model (Chapter 6) to develop wheelchair and headrest design guidelines and to examine the effect of wheelchair parameters on injury risk outcome measures. The headrest included model formed the basis of these studies since sled testing results indicate that under identical test conditions, testing with a headrest places additional/greater loads on the wheelchair and front tiedowns (Fuhrman, S. I. et al., 2006). Additionally, our research found that greater than 80% of all pediatric wheelchairs are equipped with wheelchair mounted headrests (Fuhrman, S. I. et al., 2005). This points to the value of conducting the parametric sensitivity analyses using the headrest included model (Model HR), reflecting the most frequently prescribed headrest-included wheelchair configuration, and the more severe test conditions for development of wheelchair and headrest design guidelines. Evaluation of the effect of neck stiffness on injury risk outcomes was evaluated using both Model HR and Model NoHR (no headrest) baseline models since neck response is more pronounced without a headrest (Fuhrman, S. I. et al., 2008). Model NoHR allows for greater evaluation of neck modification effects in rear impact, and the use of both models allows for direct comparisons between scenarios.

8.2 METHODS

The parametric sensitivity analysis is divided into three sub-analyses. The first analysis uses Model HR to examine the effect of crash pulse, seatback joint parameters (stiffness and angle), seatback parameters (contact stiffness and height) and headrest parameters (proximity, height and stiffness) on wheelchair loads (seatback, headrest, rear wheels,

front securement points). The second analysis considers these same parameters and their effect on injury risk measures (head and chest accelerations, HIC and Nij). The third analysis examines the effect of the Hybrid III 6-year old ATD neck response on injury outcome measures in both Model HR and Model NoHR.

Table 53 details the parametric sensitivity analysis. Two test pulses, seven seatback contact stiffnesses, five seat to seat pan joint stiffnesses, six seatback joint damping coefficients, five seatback heights, four seatback angles, five headrest heights, five headrest proximities and five headrest stiffnesses were evaluated using Model HR. In the third sub-analysis, four neck stiffnesses were used to compare injury risk outcome measures for both baseline Model HR and baseline Model NoHR.

Table 53: Parametric sensitivity test matrix

Parameter	Baseline	<u>Additional configurations</u>	<u>Injury Outcome Measures</u>	<u>Wheelchair and Headrest Outcome Measures</u>	<u>Additional comments</u>
Crash Pulse Parameter (Model HR)					
Test pulse	25 km/h, 11g, 60ms	25 km/h, 14g, 40 ms*	HIC, Nij, max linear head acceleration, chest acceleration	headrest loads, seatback loads, front securement point loads, rear wheel loads, seatback deflection	*Current proposed ISO/TC 173 rear impact standard. ISO. 2006. ISO/TC 173: Proposed Standard on Wheelchairs – Forward facing wheeled mobility aids in rear impact. International Standard Organization. Oct 2006.
Wheelchair Parameters (Model HR)					
Seatback joint stiffness	baseline joint function	See Figure 74 and Figure 75	HIC, Nij, max linear head acceleration, chest acceleration	headrest loads, seatback loads, front securement point loads, and rear wheel loads, seatback deflection	Increased stiffness has been shown to reduce likelihood of occupant ejection in rear impact, but may be associated with increase likelihood of neck injury.
Seatback joint damping coefficient	17.4 Nm-s/deg	1.7, 3.5, 8.7, 26.2, 34.9 Nm-s/deg	HIC, Nij, max linear head acceleration, chest acceleration	headrest loads, seatback loads, front securement point loads, and rear wheel loads, seatback deflection	Increased stiffness has been shown to reduce likelihood of occupant ejection in rear impact, but may be associated with increase likelihood of neck injury.
Seatback height	top edge of seatback 2.5 cm below top of ATD shoulder	+/- 2.5 cm, +/- 5 cm	HIC, Nij, max linear head acceleration, chest acceleration	headrest loads, seatback loads, front securement point loads, and rear wheel loads, seatback deflection	Seatback height is measured at the top edge of the seatback. Typical seat heights for this type of wheelchair range from 2.5 cm above the shoulder to ~T2.
Seatback to seat angle	90 degrees, at 5 degrees of posterior tilt	Seatback to seat pan angles: 100, 110, 120 degrees	HIC, Nij, max linear head acceleration, chest acceleration	headrest loads, seatback loads, front securement point loads, and rear wheel loads, seatback deflection	Maximum recommended seatback angle is 30 degrees or less for transportation purposes.
Seatback contact stiffness	Current stiffness - see Figure 76	Baseline incremented by: -25%, +25%, +50%, 2x, 3x and maximum experimental stiffness (Ha, D et al., 2000a)	HIC, Nij, max linear head acceleration, chest acceleration	headrest loads, seatback loads, front securement point loads, and rear wheel loads, seatback deflection	Initial seatback stiffness and test range based on Ha's component testing results (Ha, D et al., 2000a).

Headrest Parameters (Model HR)					
Headrest height	ATD head centered in front of headrest pad	+/- 2.5 cm, +/- 5cm	HIC, Nij, max linear head acceleration, chest acceleration	headrest loads, seatback loads, front securement point loads, and rear wheel loads, seatback deflection	Headrest positioning for function may be lower than for optimal occupant protection. The top edge of the headrest may be as high as the top of head.
Headrest proximity	Current position located 5cm behind ATD head	+/- 2.5 cm, +/- 5 cm	HIC, Nij, max linear head acceleration, chest acceleration	headrest loads, seatback loads, front securement point loads, and rear wheel loads, seatback deflection	Children who do not need a headrest for function may prefer to place the headrest further from the head to reduce interference with field of view. Close proximity of the headrest to the head improves head support and has been shown to improve head restraint for automotive protection in rear impact.
Headrest stiffness	Current stiffness	+/-10%, +/-20%	HIC, Nij, max linear head acceleration, chest acceleration	headrest loads, seatback loads, front securement point loads, and rear wheel loads, seatback deflection	Baseline stiffness was based on experimental results from dynamic pendulum testing (see Chapter 3)
ATD Parameters (Model HR and Model NoHR)					
Cervical spine stiffness	MADYMO encrypted	Resistive forces and moments added to the MADYMO mid-neck joint: 5N/5Nm, 10N/10Nm, 15N/15Nm	HIC, Nij, max linear head acceleration, chest acceleration	None	Neck stiffness is increased in response to concerns about ATD neck lacking biofidelity due to limited incidence of neck injury in children as seen in field data (Winston et al., 2004).

8.2.1 Crash pulse parameter

Baseline crash pulse of 16 mph, 11g, 60 was based on the proposed rear impact crash pulse at the time of testing, and represents an impact more severe than 95% of National Automotive Sampling System (NASS) rear impact field data (Flannagan and Manary, 2005). Since then the proposed standard has changed (ISO, 2006) and the new proposed crash pulse is 16 mph, 14g (Figure 73). Sled test data from Salipur et al (Salipur et al., 2007) were used to evaluate Model HR against the current proposed rear impact test pulse.

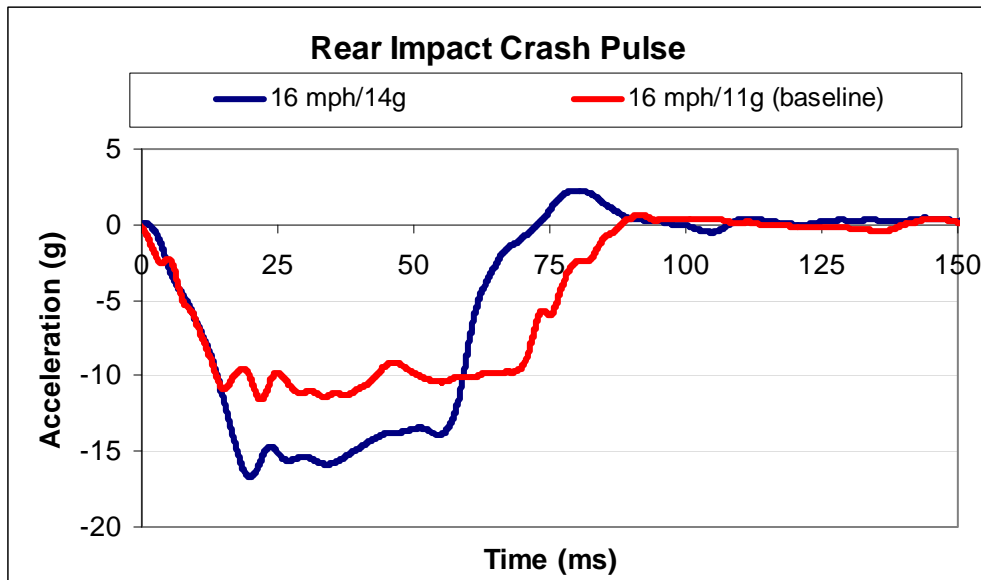


Figure 73: Rear impact crash pulse. Baseline (16 mph/10g) displayed in red, 16 mph/14g crash pulse displayed in blue.

8.2.2 Wheelchair parameters

Model HR baseline uses seatback joint stiffness, seatback joint damping and seatback contact functions to simulate the seatback behavior during crash testing. The physical wheelchair and seating system response to crash loads is not only defined by the seatback joint and seatback cushion characteristics, but also wheelchair seatback cane deformation, wheelchair frame deformation, seating attachment point behavior and dynamic interaction effects between the ATD and the wheelchair. The MADYMO model does not represent a one-to-one correspondence of each component in the wheelchair to a component in the model; rather, the model is a simplification of the physical wheelchair and seating system and their interaction with the pATD. The MADYMO model seat characteristics combine to represent the physical wheelchair and seat responses. MADYMO model characteristics were effective in creating well-validated chest accelerations within the model.

Model seatback joint characteristics are described with both loading and unloading functions as well as damping coefficients; both affect the seatback joint behavior. The baseline model peak angle deflection is 2.5 degrees – far lower than the experimental peak, 10-14 degree, joint deflections measured during our crash testing. Modeling the effect of larger joint deflections is of obvious interest. With the development of a rear impact standard, wheelchair manufacturers may choose to replace their current seatback joints with more robust and likely stiffer models, making evaluation of stiff seatback joints also of interest.

Mechanical joints have mechanical joint tightness, angular displacement and mechanical friction. The model seatback joint is represented by a revolute joint with a single axis, controlled by joint stiffness (loading and unloading functions) and a joint damping coefficient. Van Roosmalen (Van Roosmalen, L et al., 2000a) measured three adult wheelchair seating system

joints responses to loading using FMVSS 207 (Department of Transportation (DOT), 1993) test protocols. Their observed joint stiffnesses ranged from 42.4 – 186 Nm/deg. Figure 74 displays van Roosmalen’s experimentally determined joint stiffnesses (dashed lines), with Model HR baseline function displayed in red. The model outputs were evaluated for the maximum and minimum experimental stiffness, a mid-range stiffness (three times model baseline), baseline, and a less stiff function (20% of baseline), bracketing a large range of potential seatback joint stiffnesses. In all cases, unload functions are 50% of load functions (Figure 75).

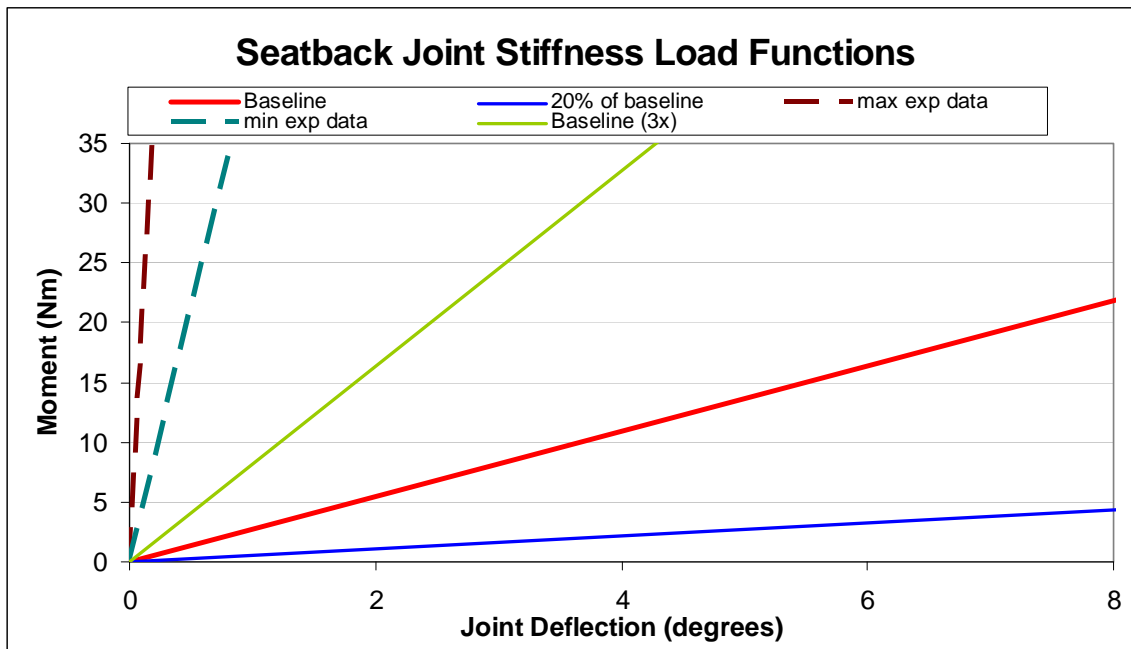


Figure 74: Seatback joint stiffness vs angular displacement load functions. Dashed lines represent minimum and maximum experimental functions (van Roosmalen, L. et al., 2000b). The red line is the model baseline function.

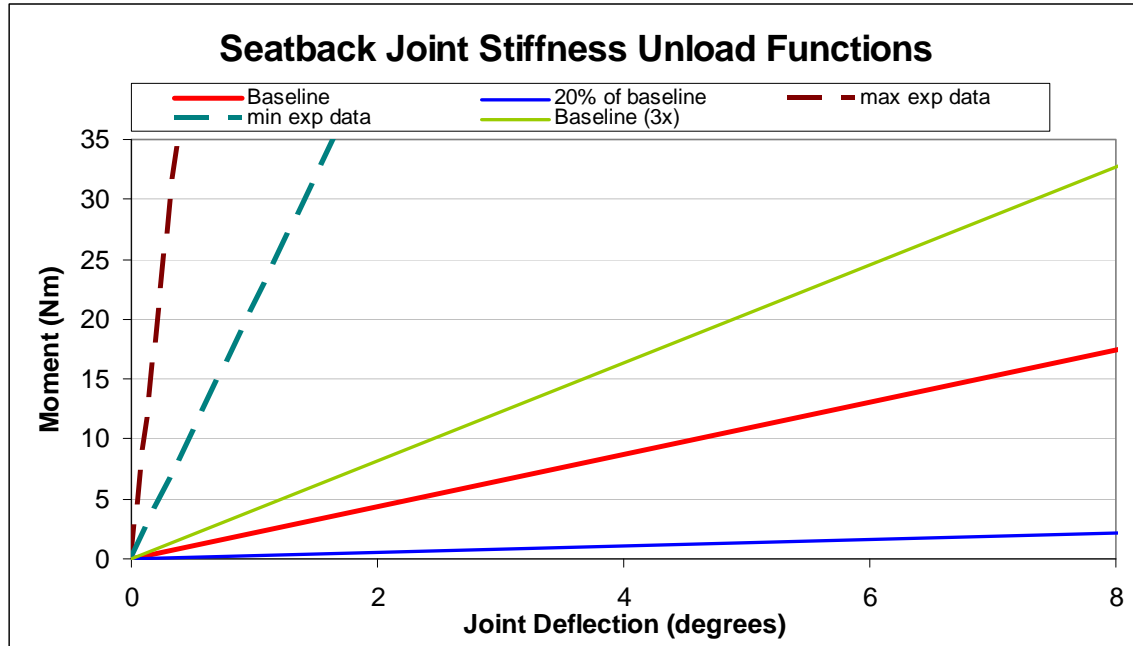


Figure 75: Seatback joint stiffness unload functions. Dashed lines are minimum and maximum experimental load functions (van Roosmalen, L. et al., 2000b). The red represents the model unload function.

The effect the seatback joint damping coefficient on wheelchair and headrest parameters and ATD injury was evaluated using six seatback joint damping coefficients. Baseline seatback joint damping coefficient was 17.5 Nm-s/deg. Based on our experimental results, it was desirable to evaluate joint parameters that would permit the seatback to deflect at least 10-14 degrees. Lower seatback joint damping coefficients (1.75, 3.5, 8.75 Nm-s/deg) as well as higher seatback joint damping coefficients (27.2, 34.9 Nm-s/deg), combine to produce a range of seatback joint angle deflections of 0-17 degrees.

Behavior of the model seatback joint must be considered together with the ATD to seatback contact characteristics. The seatback force-deflection properties used in the model reflect a combined response. Quasi-static testing of five commercial seatbacks with attachment hardware (Ha, D. et al., 2000b) yielded a range of force-deflection data. Figure 76 displays the

minimum and maximum force-deformation curves from the tested seatbacks (dashed lines). My model baseline curve (red) falls near the minimum experimental data. Additional stiffness profiles were evaluated in the parametric analysis ranging from -25% of the baseline model, up to three times (300%) the baseline model, as well as the maximum stiffness measured by Ha.

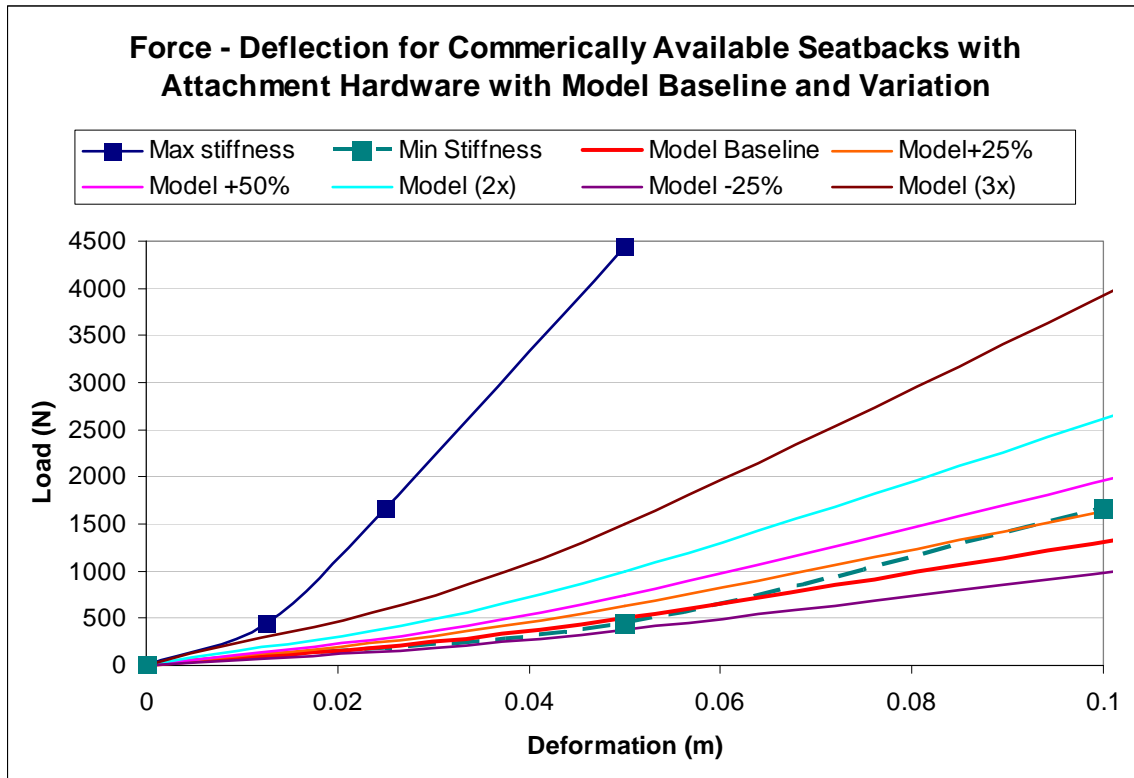


Figure 76: Force-deflection for commercially available seatbacks with attachment hardware (Ha, D et al., 2000a) with model baseline and variation. Experimental data is displayed with boxes, baseline is shown by red line.

Wheelchair configurations can vary, and there are no specifications for optimal placement of seating components since the clients' functional needs can be so variable. Discussions with Bette Cotzin and Terri Wonsettler, therapists who have combined 50 years of pediatric seating experience, (Cotzin, 2008; Wonsettler, 2008) indicated that there are, however, typical ranges that are commonly seen for children using manual pediatric wheelchairs. Seatback

heights typically range from 1” above the child’s shoulder down to approximately the T2 vertebra. According to the therapists, seatbacks that are lower than this are typically seen only on ultra-light wheelchairs and would not be equipped with headrests. Also, children who need minimal back support from their wheelchairs are far more likely to transfer to a vehicle seat during transportation in motor vehicles. The effects of varying the wheelchair seatback height parameter was evaluated for seatback heights within this range, at 1” intervals.

All sled testing was conducted with a 90 degree seatback to seat pan angle with a five degree posterior tilt. Many wheelchair users sit with seatback angles greater than 90 degrees to improve comfort, function and position. Wheelchair transportation safety guidelines recommend that seatback angles not exceed 30 degrees from the vertical (University of Michigan, 2007). The effects of varying the seatback angle parameter was assessed for seatback angles from the baseline (5 degrees from the vertical) to a maximum 35 degrees at 10 degree intervals.

At all seatback angles, shoulder belt positioning was considered to ensure that the shoulder belt passed across the midline position of the ATD shoulder. For 5 degree (baseline) and 15 degree seatback from vertical positions, the wall-mounted shoulder belt anchor (D-ring) position remained in the baseline position. For 25 and 35 degrees of seatback angle relative to vertical, it was necessary to reposition the D-ring to ensure that the shoulder belt passed across the mid-point of the ATD clavicle and directly over the mid-point of the ATD shoulder. Shoulder belt D-ring placement conformed to test specifications as indicated in ISO 10542: Wheelchair tiedown and occupant restraint systems for forward facing wheelchair-seated passengers – Part 1: Requirements and test methods – Frontal impact (ISO, 1999a). As specified, the D-ring was located such that the horizontal distance between the top of the ATD shoulder and the D-ring was 400-600mm; the angle that the shoulder belt (from shoulder mid-point to D-ring) made with

the horizontal was between 0-45 degrees as specified. This modification was necessary to ensure proper initial model acceleration, but does not affect the output results as the shoulder belt is not loaded in rear impact.

8.2.3 Headrest parameters

Headrest pad position is also dependent on pediatric client needs. Bette Cotzin (Cotzin, 2008) reported that like many therapists, she often orders headrests for her clients who need additional head support during transportation in a motor vehicle. For clients who need continual head support, headrests are typically placed in contact with the head. For those who need head support only while resting, the headrest may be placed in a more posterior position. The effects of varying the headrest proximity parameter were therefore evaluated for head-to-headrest proximity of 0 - 4”.

Ideally, headrests are adjusted so that the middle of the headrest pad is centered behind the middle of the client’s head. The top of the headrest is always above the mid-line of the head – and may extend to the top of the head. To achieve this range, the effects of varying the headrest parameter were evaluated for five heights: baseline (headrest centered behind head), up 1” and 2”, and down 1” and 2”.

The baseline headrest stiffness was determined experimentally using pendulum impact testing as described in Chapter 3. During pendulum testing, the headrest type that was later used in sled testing was mounted using standard attachment hardware to a wheelchair seatback. The seatback was affixed to the test jig and the pendulum, equipped with a Hybrid III 6-year old head-cap, was used to capture the overall dynamic force-displacement loading and unloading responses of the headrest and headrest mounting hardware. For this parametric

analysis, baseline force-displacement results were varied by -20%, -10%, +10% and +20% to model both stiffer and less stiff scenarios (Figure 77 and Figure 78).

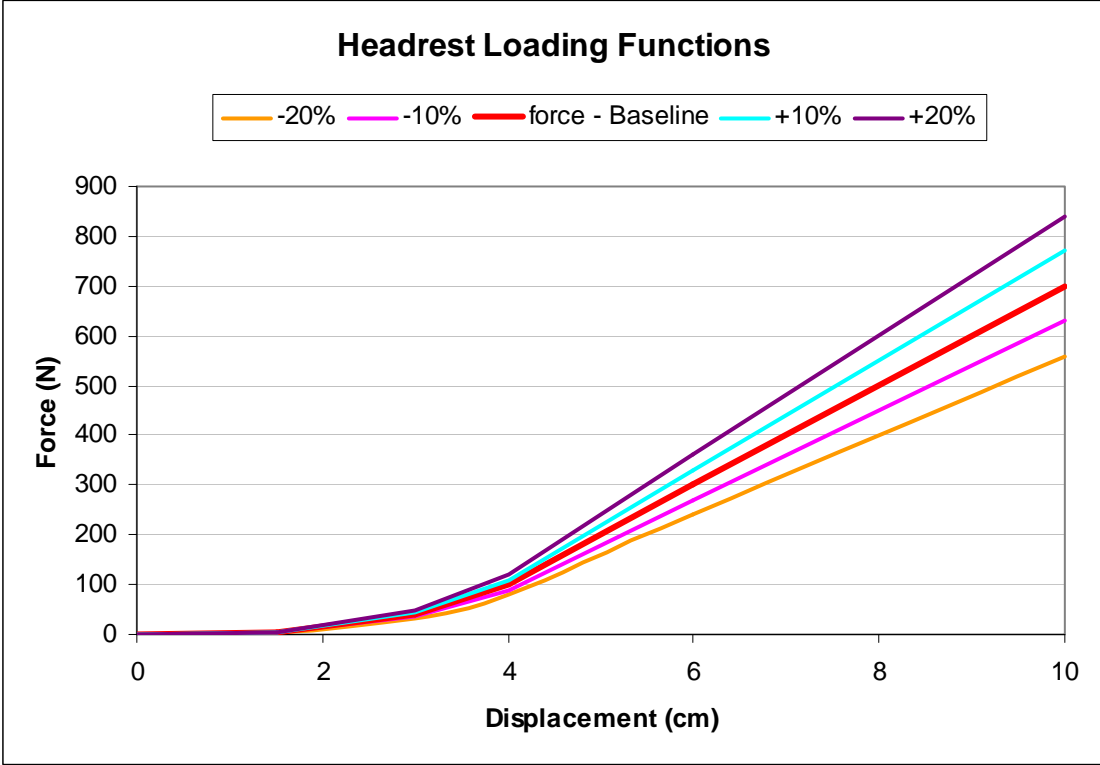


Figure 77: Headrest loading functions. Baseline force-displacement displayed with red line.

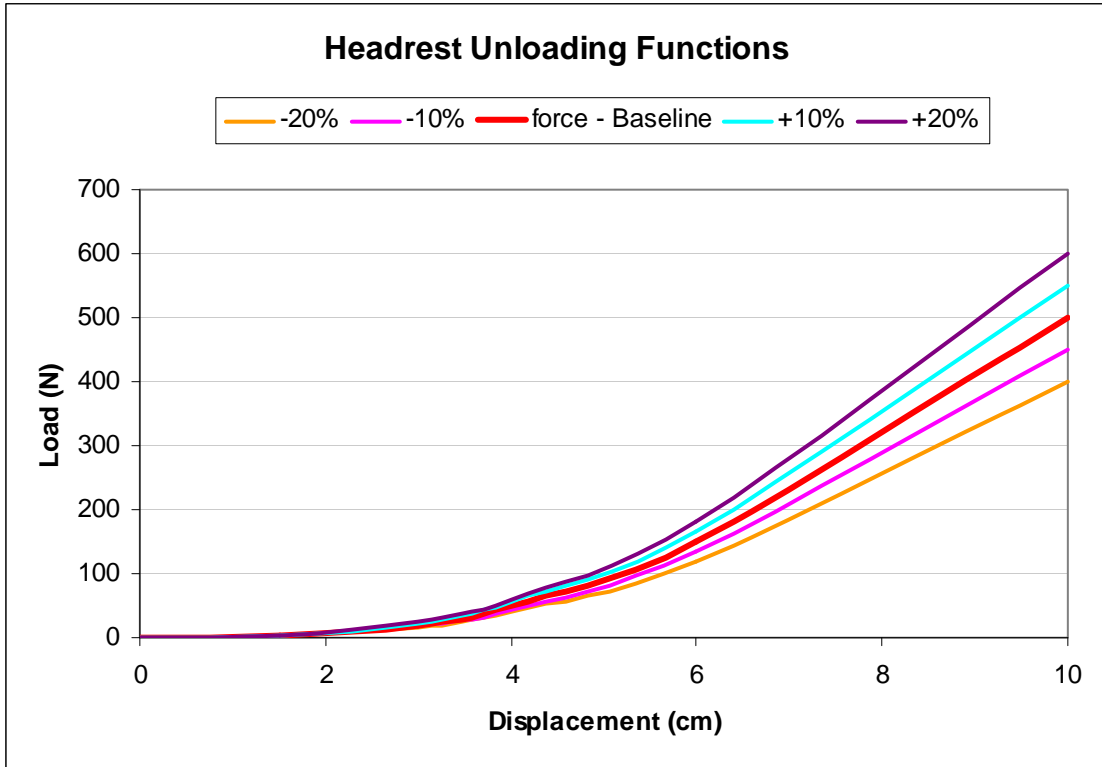


Figure 78: Headrest unloading functions. Baseline force-displacement displayed with red line.

8.2.4 ATD parameters

The Hybrid III ATD neck response has been scrutinized for its biofidelity (Winston et al., 2004; Bilston, 2007) since field data suggests that the incidence of severe pediatric neck injury in rear impact motor vehicle crashes remains lower than anticipated based on Hybrid III 6-year old ATD responses. Sherwood and Shaw (Sherwood et al., 2003) examined the Hybrid III 6-year old ATD neck frontal impact response and compared it to 12-year old cadaver kinematics. They found the ATD neck to be more flexible than cadaver testing suggested.

MADYMO encrypts all neck joint characteristics, yet it is still possible to add resistive forces and moments to joints. Since upper neck joint force (F_x) and moment (M_y) data are used

to calculate resulting moments about occipital condyles, it was preferable to not modify that joint directly. Instead the neck mid-joint resistive forces and moments were increased in three increments over the baseline model. Resulting neck characteristics are described for both flexion (Figure 79) and extension (Figure 80). The sensitivity of Model HR and Model NoHR head and chest accelerations, head injury criteria (HIC15) and neck injury criteria (Nij) to changes in neck stiffness were evaluated and compared.

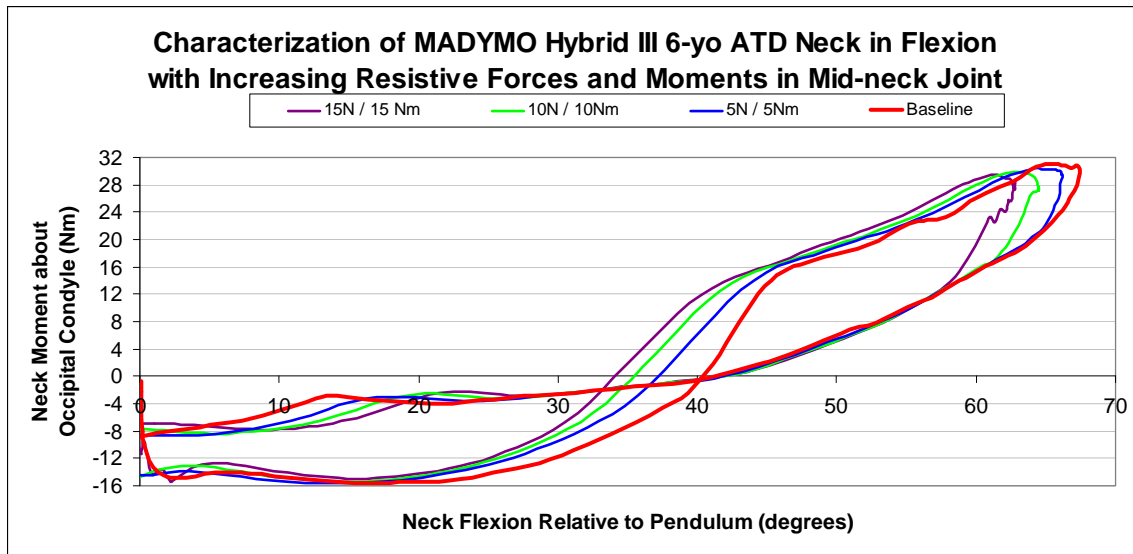


Figure 79: Characterization of MADYMO Hybrid III 6-year old ATD in flexion. Additional resistive forces and moments are added to the mid-neck joint. Red line indicates the baseline neck flexion response.

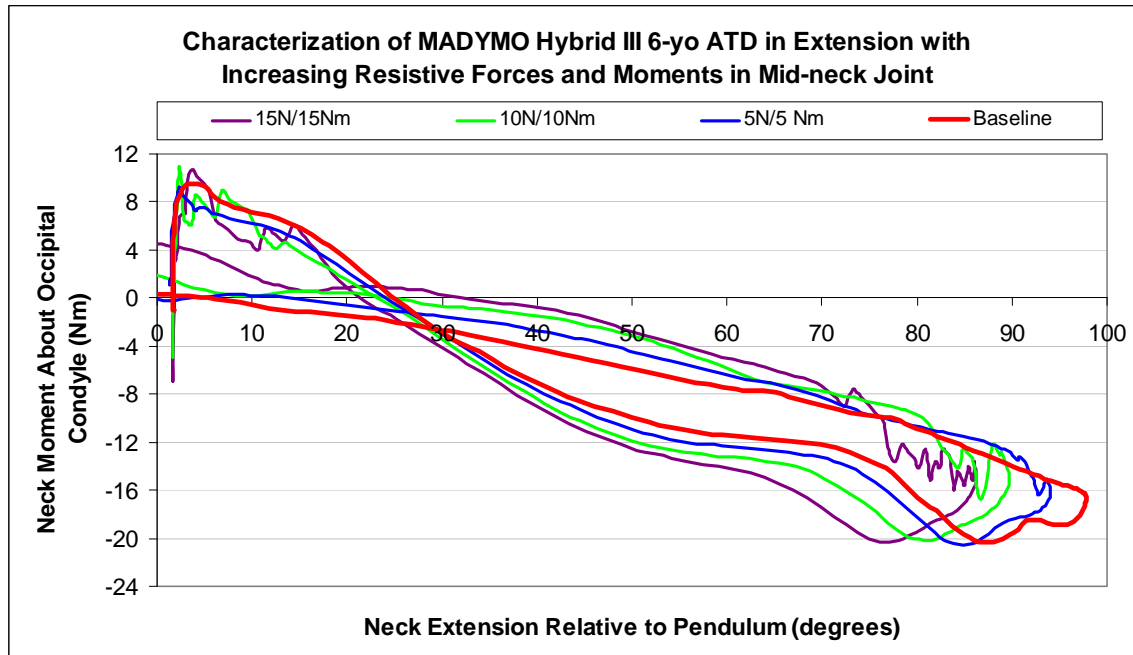


Figure 80: Characterization of MADYMO Hybrid III 6-year old ATD neck in extension with increasing resistive forces and moments in the mid-neck joint. Baseline neck extension response is displayed in red.

8.3 RESULTS

Results from the parametric sensitivity analysis are divided into three sections to individually address the study objectives. The first section describes the wheelchair and headrest design guidelines. The second section describes the effects of varying crash pulse severity, wheelchair parameters and headrest parameters on injury risk outcome measures. The third section presents results from increasing ATD neck stiffness on injury risk outcome measures.

8.3.1 Results: wheelchair and headrest design guidelines

Results for peak front wheelchair securement point loads, wheel loads, seatback loads, seatback joint deflection and headrest loads are presented below. Each is evaluated across five wheelchair, three headrest parameters and two crash pulse severities.

8.3.1.1 Wheelchair front securement point loads

In rear impact, the front securement points carry the full load during impact (Fuhrman, S. I. et al., 2006). Wheelchair front securement point loading is typically not symmetric between the two front securement points, an effect of the 3-point occupant restraint crossing only one shoulder. During actual transportation in a motor vehicle, wheelchair users may be positioned on either side of the vehicle and will wear the shoulder belt on the corresponding shoulder. For this reason, peak baseline securement point loads (3394N) were averaged together to produce a mean baseline. The minimum and maximum values were calculated from all peak data values from both front securement points. Results (Figure 81) indicate that the greatest securement point loads occurred with the closest headrest proximity (3821N). Seatback joint damping also played a role in front securement point loading, with peak loads (3628N) occurring with greatest seatback joint damping. Increased initial seatback angle was associated with decreased front securement points loads. No trends were noted with increased seatback stiffness. Total range of peak securement point loading was 2617 – 3821 N.

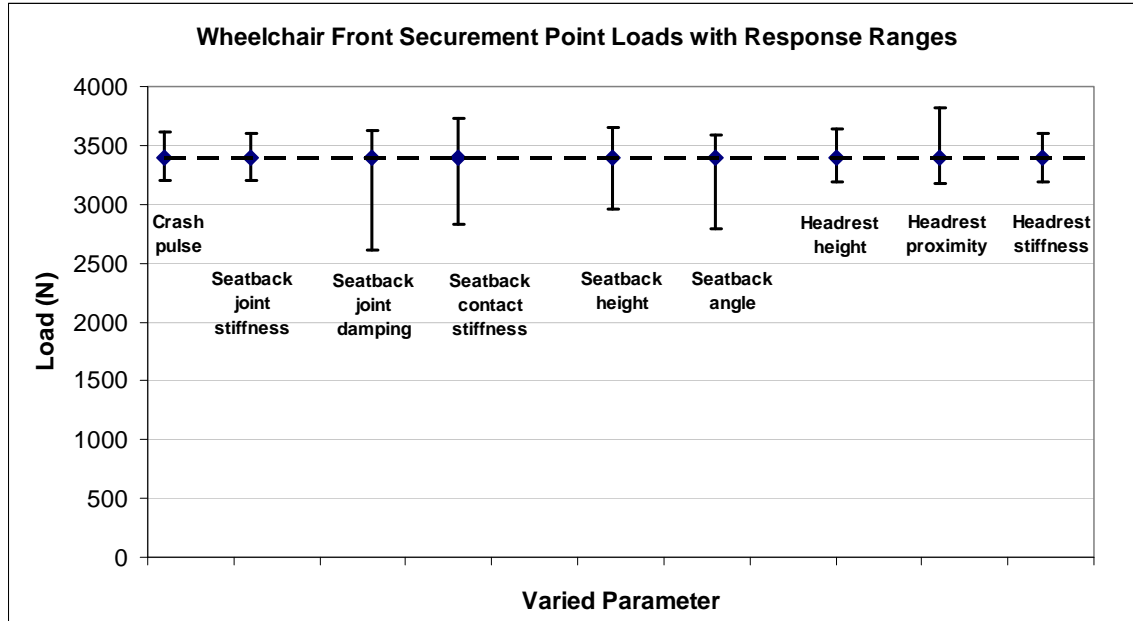


Figure 81: Wheelchair front securement point loads with response ranges. The effect of wheelchair, headrest and crash pulse parametric variation on peak front securement points. Baseline securement point load was 3394 N. Total range was 2617 – 3821 N.

8.3.1.2 Rear wheel loads

Rear wheel loads were most influenced by seatback to seat pan angle, and by crash severity (Figure 82). Like the front securement point loads, rear wheel loads also were affected by asymmetric loading caused by three-point occupant restraint geometry effects. Reported baseline wheel load (1300 N) was an average of peak right and left wheel loads. Maximums and minimums were calculated from the combined right and left wheel load data. Maximum peak rear wheel loads (1549 N) occurred with 35 degree seatback angle. At increased seatback angles, the ATD torso also had an increased angle resulting in the ATD center of gravity being located further back with respect to the rear wheels contributing to additional rear wheel loading. Rear wheel loading was also very sensitive to increased crash pulse severity, with a 17% increase in

rear wheel loads (1520 N) associated with the more severe crash pulse. Seatback contact stiffness affected rear wheel loads, with increased seatback stiffness associated with increased wheel loads. Peak rear wheel loads were 1224 – 1549 N overall.

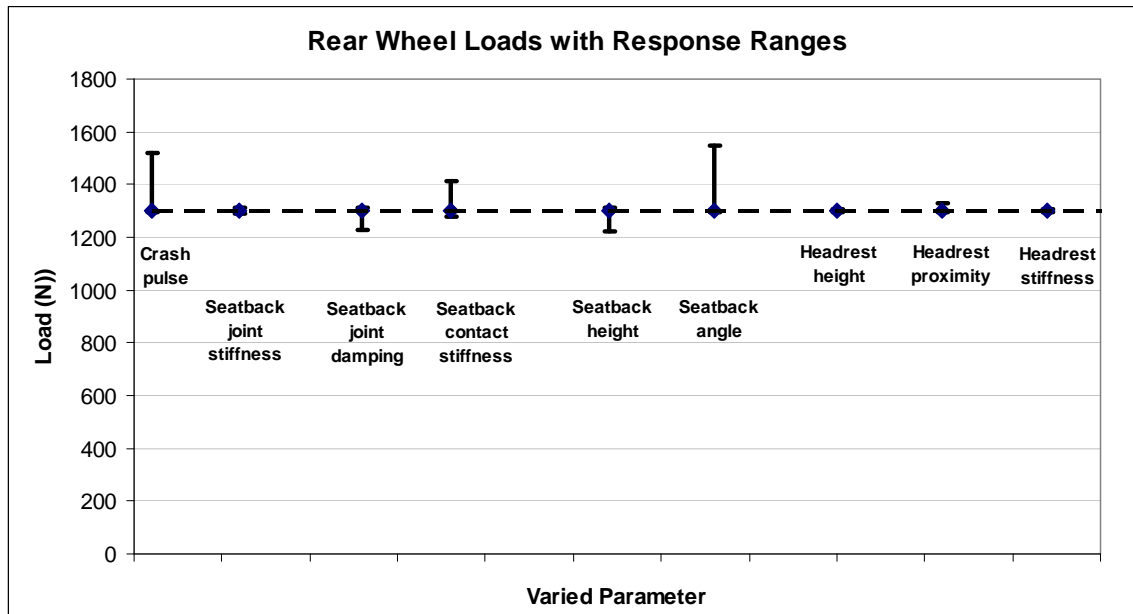


Figure 82: Rear wheel loads with response ranges. The effect of wheelchair, headrest and crash pulse parametric variation on peak rear wheel loads. Baseline wheel load was 1300 N. Total range was 1224 – 1549N.

8.3.1.3 Wheelchair seatback joint deflection

Seatback joint deflection was extremely sensitive to changes in seatback joint damping (Figure 83). Baseline seatback joint deflection was 2.5 degrees. A 90% reduction to the baseline seatback joint damping coefficient was associated with a seven-fold increase in seatback joint deflection (17.4 degrees). With the model’s high baseline seatback joint damping coefficient, other parameters appeared to have little influence on seatback joint deflection. As would be anticipated, increased joint stiffness resulted in decreased seatback joint deflection; at maximum

stiffness, the seatback joint deflection was reduced to 1.3 degrees. The range of observed seatback joint deflections was 1.3 – 17.4 degrees.

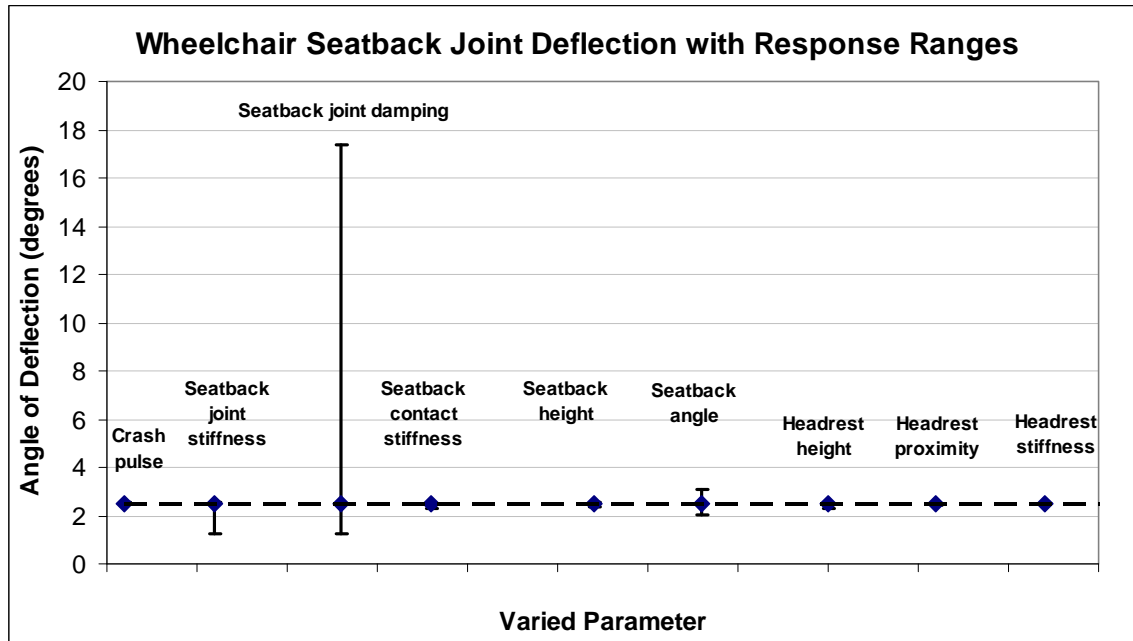


Figure 83: Wheelchair seatback joint deflection. The effect of wheelchair, headrest and crash pulse parametric variation on peak wheelchair seatback deflection. Baseline seatback deflection was 2.5 degrees. Total range as 1.3-17.4 degrees.

8.3.1.4 Wheelchair seatback loads

Baseline peak wheelchair seatback load was 2572 N (Figure 84). Similar to the rear wheel loads, the seatback loads were most sensitive to the seatback to seat pan angle, with maximum peak wheelchair seatback load (3845 N) associated with maximum seatback angle (35 degrees from vertical). This was to be somewhat expected since at increased seatback angles, the weight of the ATD torso contributes to wheelchair seatback loading. The more severe crash pulse also caused increased loading (3017 N) on the wheelchair seatback. Minimum peak

seatback loads (2322 N) occurred at decreased seatback joint damping coefficient. The range of seatback loads was 2322 – 3834 N.

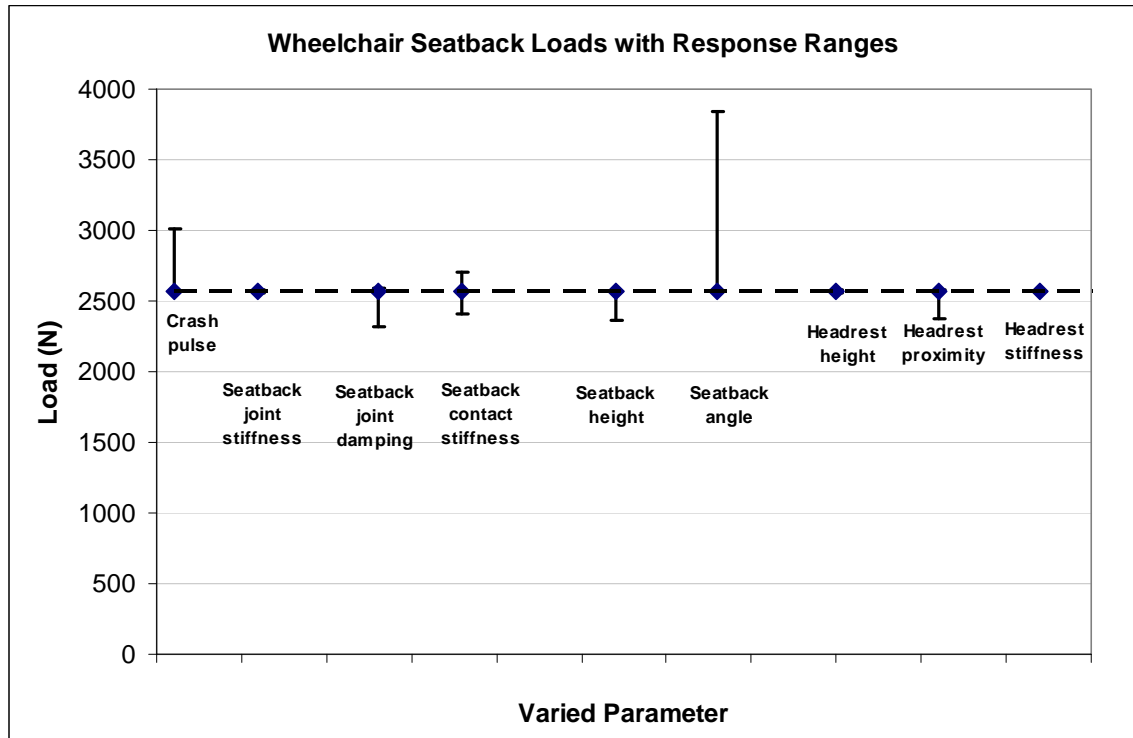


Figure 84: Wheelchair seatback loads with response ranges. The effect of wheelchair, headrest and crash pulse parametric variation on peak wheelchair seatback loads. Baseline seatback load was 2572N. Total range was 2322 – 3845 N.

8.3.1.5 Wheelchair headrest loads

Baseline peak wheelchair headrest load (664 N) proved to be most sensitive to increased seatback angle (Figure 85), with 35 degrees of seatback angle associated with a 40% decrease in wheelchair headrest loads (382 N). The headrest load was sensitive to headrest parameters. Minimum headrest load occurred when the headrest was lowered 2". Decreased headrest

horizontal proximity increased headrest loads; increased headrest stiffness also increased headrest loads. As the seatback height was reduced, the headrest loading increased. When the seatback height was decreased, the headrest height relative to the ATD head was maintained. When seatback height was decreased, the headrest then carries a larger portion (762 N) of the ATD loading forces. Although seatback contact stiffness affected headrest loads, no associated trends were observed. Headrest loads were 382 – 762 N.

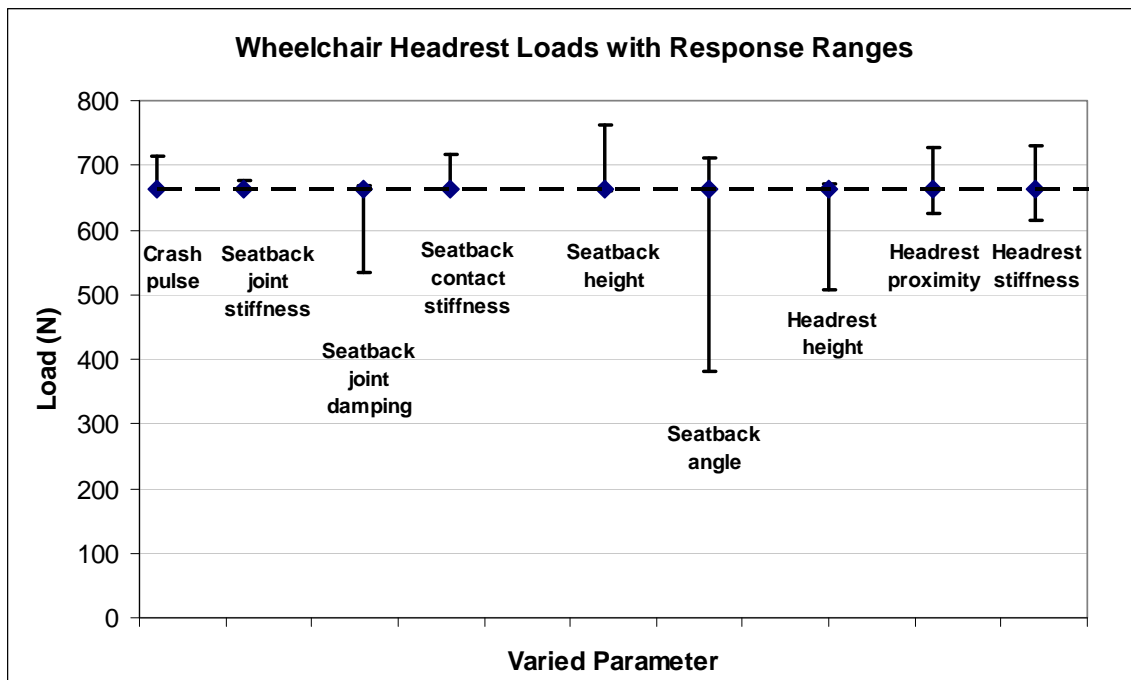


Figure 85: Wheelchair headrest loads with response ranges. The effect of wheelchair, headrest and crash pulse parametric variation on peak wheelchair headrest loads. Baseline headrest load was 664N. Total range was 382 – 762 N.

8.3.2 Results: Pediatric injury outcome measures

Parametric sensitivity analysis can provide information on the sensitivity of the pediatric injury outcome measures to wheelchair, headrest and crash pulse parameters. Head and chest accelerations, head injury criteria for 15 ms (HIC15), and neck injury criteria (Nij) in tension-extension are all examined.

8.3.2.1 Head acceleration

Linear head acceleration protection reference value (PRV) for the 6-year old ATD is 764 m/s^2 (Klinich et al., 1996). All linear head accelerations were below PRVs. Baseline head acceleration (225 m/s^2) did not appear to be very sensitive to parameter variation (Figure 86), with maximum peak head accelerations 8% greater than baseline (243 m/s^2). Increased headrest height, increased headrest distance from the ATD head, and increased headrest stiffness all marginally increased peak head accelerations by less than 6%. Seatback height had the largest effect with greatest head accelerations occurring with highest seatback height. Peak head acceleration decreases occurred with increased joint deflection caused by decreased seatback joint damping coefficient and by decreased joint stiffness. Peak head accelerations were 119 - 243 m/s^2 .

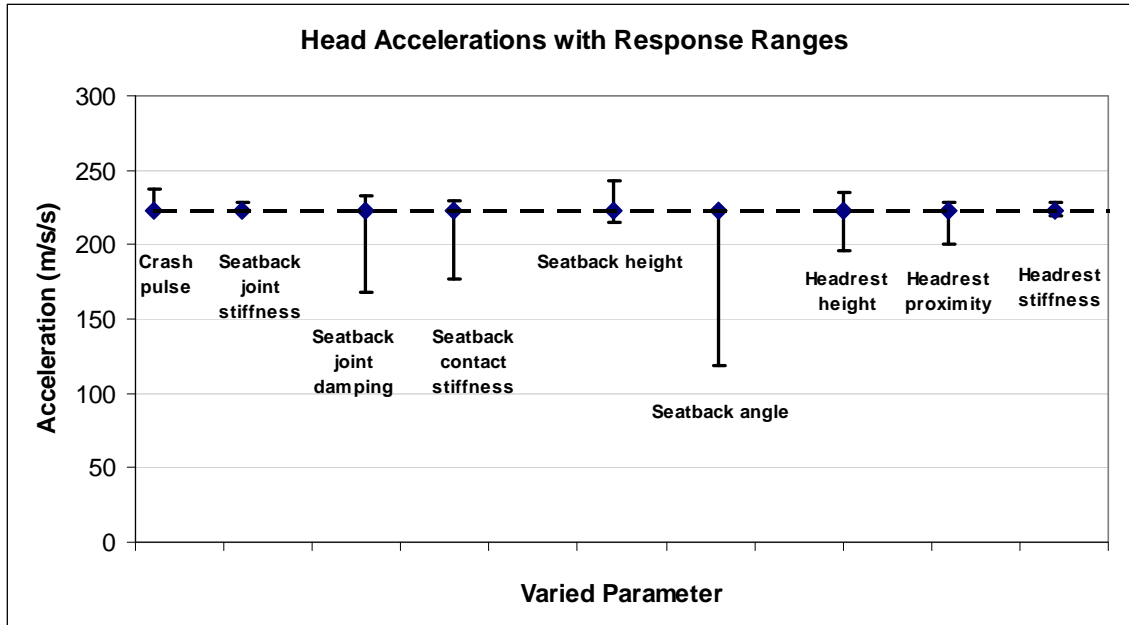


Figure 86: Head accelerations. The effect of wheelchair, headrest and crash pulse parametric variation on peak head accelerations. Baseline head acceleration was 223 m/s². Total range was 119 – 243 m/s².

8.3.2.2 Chest acceleration

Maximum chest acceleration is specified in FMVSS 208 (National Highway Traffic Safety Administration, 1993) and FMVSS 213 (National Highway Traffic Safety Administration, 1999), and limited to 588 m/s². All chest acceleration values are less than half this threshold. Chest acceleration was strongly affected by seatback parameters and crash pulse severity (Figure 87). Headrest parameters did not affect chest acceleration. Baseline peak chest acceleration (233 m/s²) was increased by increased seatback contact stiffness (246 m/s²) and by increased crash pulse severity (262 m/s²). Chest accelerations were greatly reduced by increased seatback angle (132 m/s²) and decreased seatback joint damping. Chest accelerations were 132 – 262 m/s².

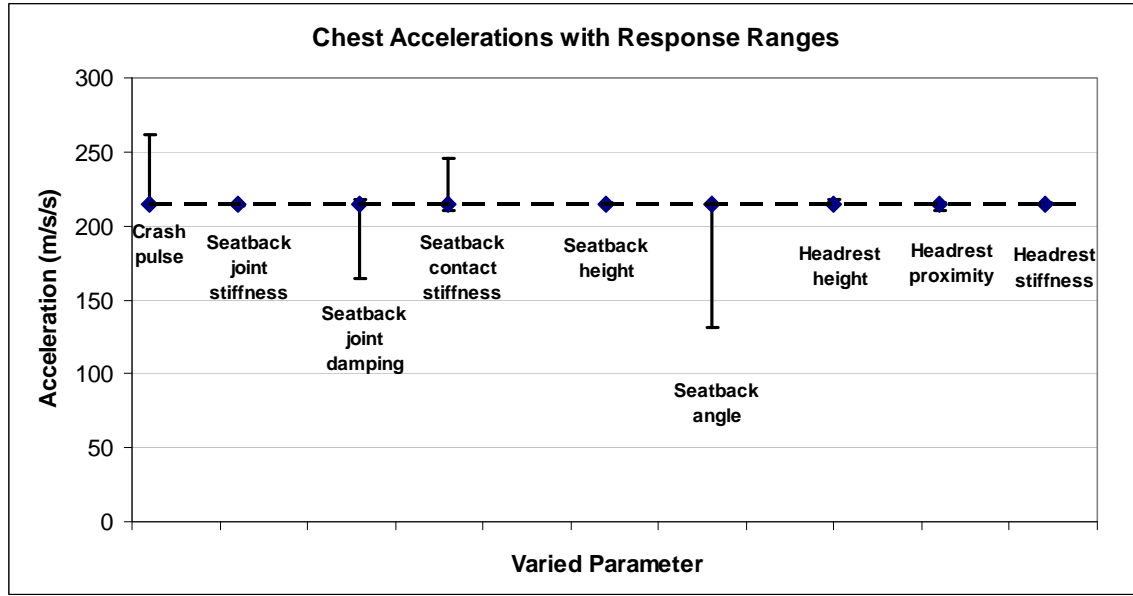


Figure 87: Chest accelerations. The effect of wheelchair, headrest and crash pulse parametric variation on peak chest accelerations. Baseline chest acceleration was 233 m/s². Total range was 132 – 262 m/s².

8.3.2.3 HIC – Head injury criteria

Head injury criteria (HIC) is a measure of both the peak head accelerations and the duration of the accelerations. HIC15 is measured across a 15 ms time interval and is specified in FMVSS 208 – *Occupant crash protection* (National Highway Traffic Safety Administration, 1993). All HIC15 results (Figure 88) were well below injury thresholds (Eppinger et al., 1999). Yet, reductions in seatback stiffness reduced the 29.9 baseline value by more than 50%, and increased seatback angle was even more effective in reducing HIC15 to 6.9. Large HIC15 decreases were observed with seatback contact variation, yet no associated trends were observed. Increased headrest height, increased headrest stiffness and increased head to headrest distance all increased HIC15 by less than 10%. HIC15 values ranged from 6.9 to 33.0.

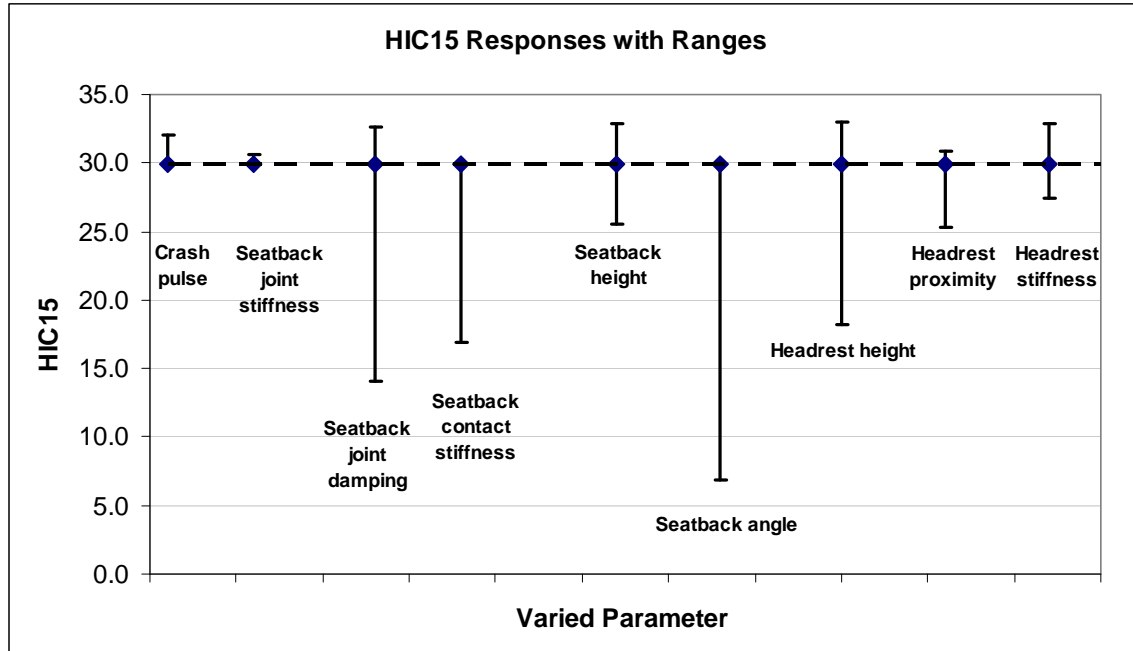


Figure 88: HIC15 - Head injury criteria. The effect of wheelchair, headrest and crash pulse parametric variation on peak HIC15 values. Baseline HIC15 was 29.9. Total range was 6.9 – 33.0.

8.3.2.4 Nij – Neck injury criteria

As previously discussed in Chapter 5, neck injury criteria (Nij) is a normalized measure of the upper neck axial forces and the upper neck bending moment. In rear impact, the Nij of interest is the tension-extension measure. Baseline model Nij is 0.457 (Figure 89). Nij is very sensitive to parameters that affect the head and chest relative accelerations, which create the neck axial forces and neck bending moments. When the headrest height was lowered by 2”, the Nij increased by 50% to 0.677. When the headrest was placed in very close proximity to the head, Nij was reduced 30% to 0.318. These results support recommendations to keep the headrest close to the center of the head. Decreased seatback stiffness was associated with decreased Nij, as the

seatback absorbed impact energy. Increase headrest stiffness, served to limit neck extension and reduced Nij. Nij results were 0.197 – 0.677.

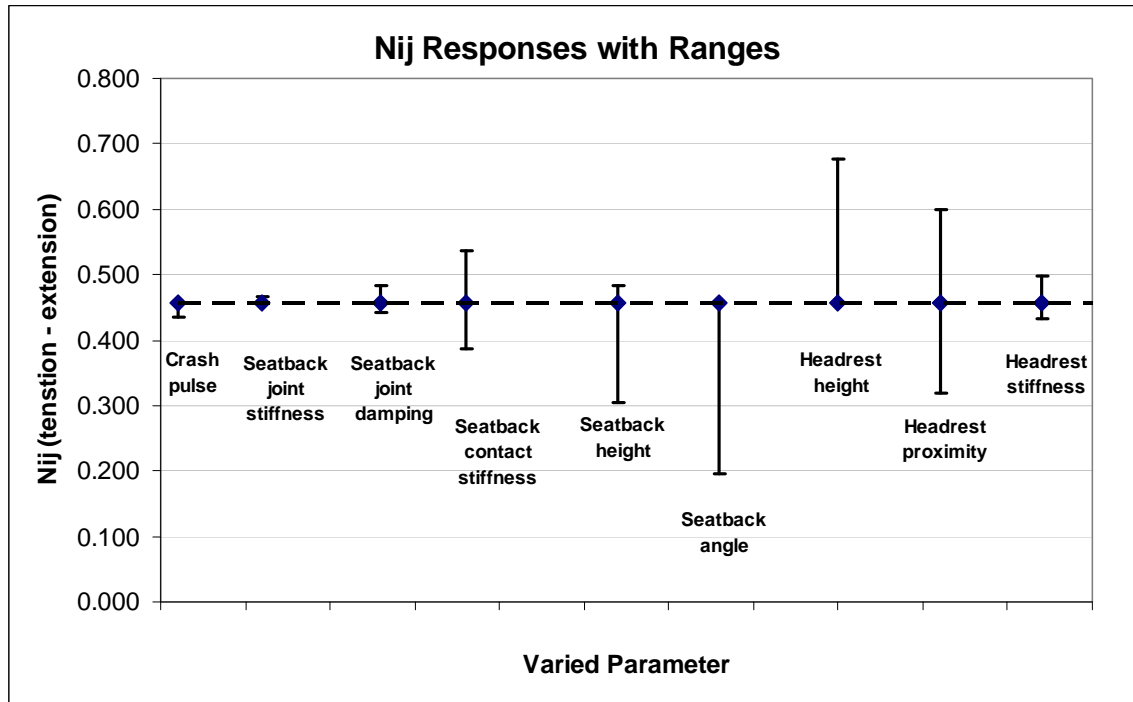


Figure 89: Nij - Neck injury criteria (tension-extension). The effect of wheelchair, headrest and crash pulse parametric variation on peak Nij values. Baseline Nij was 0.457. Total range was 0.197 – 0.677.

8.3.3 Results: Effect of neck stiffness modification on injury outcome measures in read impact

Modification to the MADYMO Hybrid III 6-year old neck characteristics is limited to adding resistive forces and moments to the neck joints, effectively increasing neck stiffness. This does not affect the stiffness of the neck joint loading and unloading functions, joint damping coefficients or joint damping functions, which are all encrypted in the MADYMO software.

However, it is effective in neck flexion and extension (Figure 79 and Figure 80). Controversy regarding the Hybrid III 6-year old neck is focused on its ability to predict the likelihood of injury in pediatric populations. The effect of additional neck resistance on injury risk outcome measures was evaluated using both Model HR and Model NoHR; Model HR since it is the most frequently prescribed wheelchair configuration, and Model NoHR as it allows for the evaluation to encompass a greater range of neck motion. Comparisons are made between the two scenarios.

8.3.3.1 Head and chest accelerations

Figure 90 displays Model HR and Model NoHR baseline head and chest accelerations. Both head and chest accelerations are below protection reference values; head - 764 m/s^2 (Klinich et al., 1996), chest - 588 m/s^2 (National Highway Traffic Safety Administration, 1999). Baseline head accelerations are slightly higher for Model HR (223 m/s^2) than for Model NoHR (211 m/s^2) reflecting the impact of the mATD head against the headrest pad. Additional neck resistance limits the neck motion thereby increasing the Model HR head acceleration (223 – 228 m/s^2) as the head impacts the headrest pad. In Model NoHR, the converse is true; in model NoHR peak head accelerations occur later when the back of the mATD head impacts the top of the wheelchair seatback. Increased neck restraint reduces neck extension and the back of mATD head is accelerated less (191 – 211 m/s^2) when it impacts the top of the wheelchair seatback.

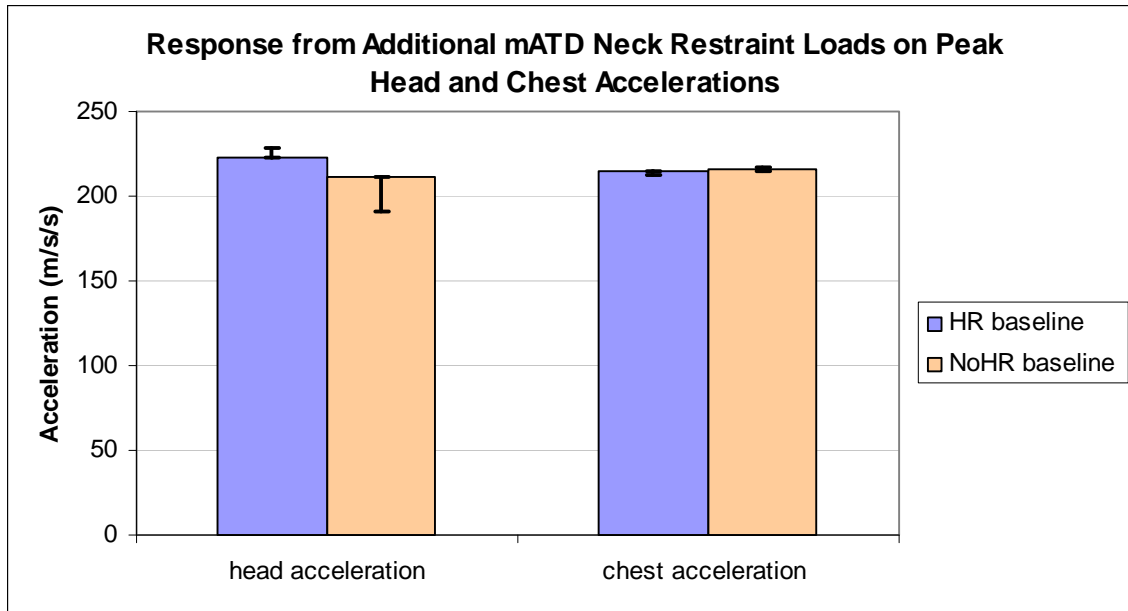


Figure 90: Response from additional mATD neck restraint loads on peak head and chest accelerations. Colored bars depict Model HR and Model NoHR baseline head and chest accelerations. Maximum and minimum ranges are displayed for Model HR and Model NoHR.

Baseline chest accelerations are comparable for Model HR (215 m/s²) and Model NoHR (216 m/s²). Model HR has a range of 212 – 215 m/s²; Model NoHR had a comparable range of 215-217 m/s². The close proximity of the ATD torso to the seatback limited the effect of increased neck stiffness on chest accelerations.

8.3.3.2 Head injury criteria (HIC15)

Baseline HIC15 (Figure 91) is far below protection reference values, PRV = 700, (Eppinger et al., 1999) for Model HR (29.9) and Model NoHR (25.7). As may be predicted from reviewing the simple head acceleration results, the impact of the ATD head against the headrest pad is less severe than the impact of the ATD head against the top of the seatback – although neither is likely to produce head injury. The HIC15 measure is sensitive to both the magnitude of

the head acceleration and to acceleration duration. Unlike head accelerations, HIC15 is reduced for both Model HR and Model NoHR with increased neck restraint loads and moments. Model HR HIC reduction contrasts with the increase in Model HR peak head accelerations and highlights the duration component of the HIC measure. Increased neck restraints reduced Model NoHR HIC15 measure by 21% to 20.3.

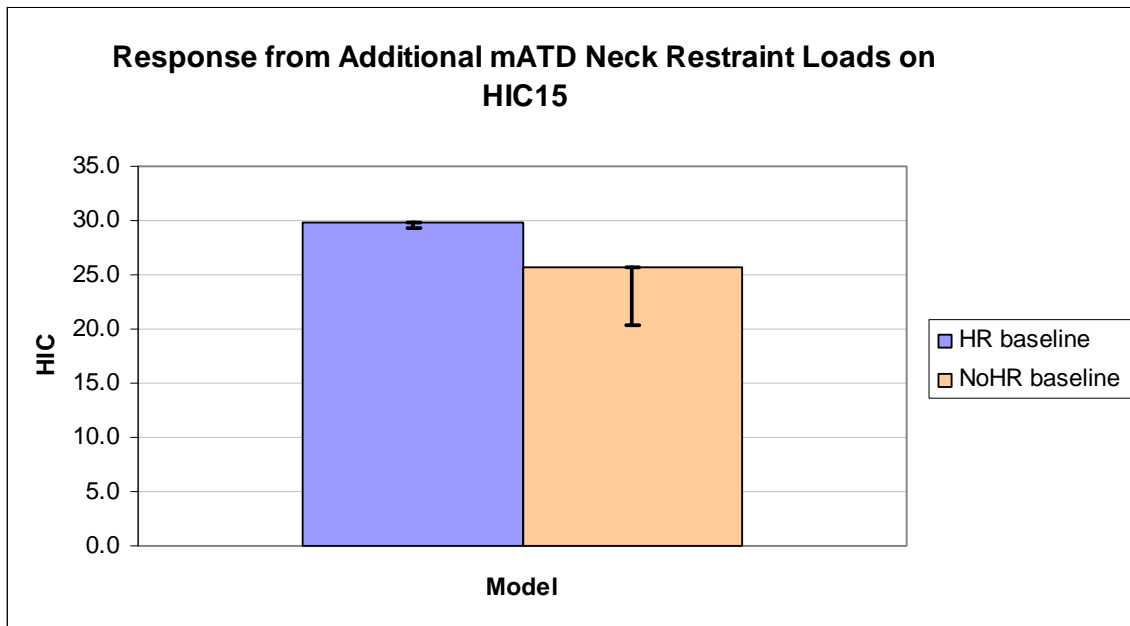


Figure 91: Response from additional mATD neck restraint loads on HIC15 across two models. Colored bars depict Model HR and Model NoHR baseline HIC15. Maximum and minimum ranges are displayed for Model HR and Model NoHR.

8.3.3.3 Neck injury criteria (Nij)

Neck injury criteria baseline Model HR (0.457) and Model NoHR (0.879) are both below injury protection reference value = 1 (Kleinberger, Michael et al., 1998). However, Model NoHR

Nij is 1.9 times greater than Model HR. The response of Nij to increased neck restraint mirrors the head acceleration response. Reduced neck motion increases the Nij response (0.457 – 0.508) of Model HR neck, while identical changes to mATD in Model NoHR produce reductions in Nij (0.732 – 0.879). Thus, a more restrained neck would be associated with less likelihood of neck injury in the no headrest scenario.

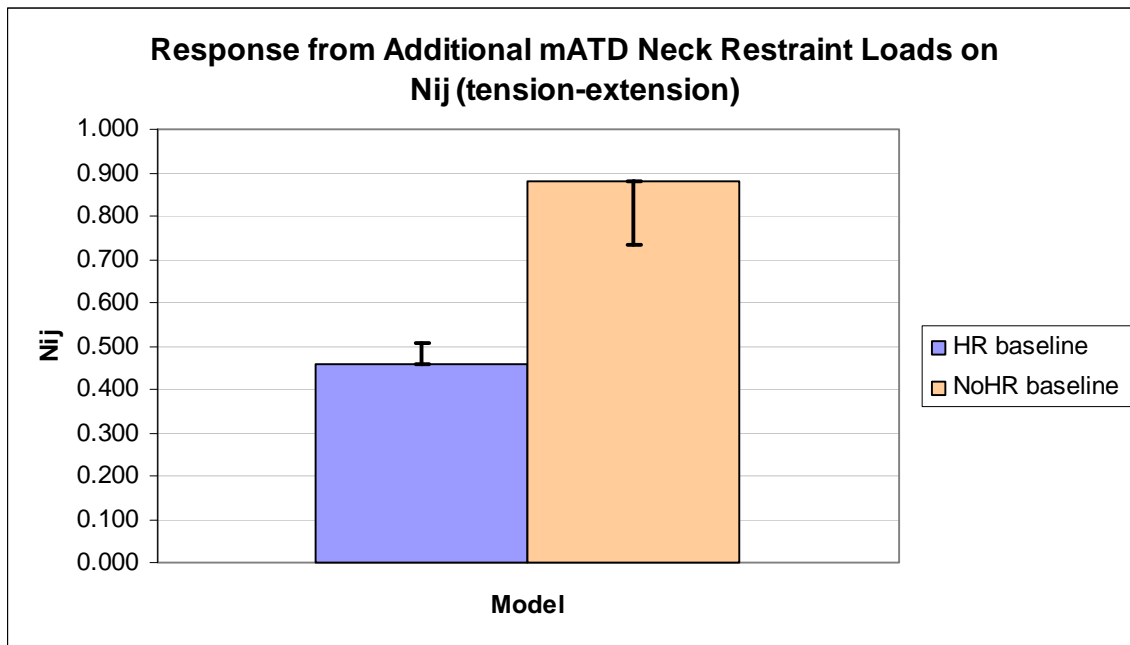


Figure 92: Response from additional mATD neck restraint loads and moments on Nij (tension-extension) across two models.

8.4 DISCUSSION

The purpose of this study was three-fold: to establish design criteria for manual pediatric wheelchairs in rear impact, to determine the effect of wheelchair parametric variation on injury

risk outcome measures, and to evaluate the sensitivity of injury risk outcomes to changes in mATD neck response. Parametric sensitivity analysis was used to assess the sensitivity of the model to the individual model parameters.

Components in the MADYMO rigid body models do not necessarily translate directly from wheelchair components present in physical testing. For example, MADYMO mATD does not mirror pATD element by element, rather mATD is a model that ideally produces results comparable to and validated against pATD results (TNO, 2005). Likewise, experimentally determined headrest contact functions collectively describe not only the compression of the headrest pad, but also include the dynamic response of the headrest stem and mounting hardware. Model seating parameters (seatback contact stiffness, seatback joint stiffness, seatback joint damping coefficient) combine to provide a simplified description of the complex behavior of the physical wheelchair component characteristics and their response to pATD loading during rear impact sled testing. Two computer simulation models (Model HR and Model NoHR) were built and validated to reproduce wheelchair, headrest and pATD dynamic responses in rear impact.

Parametric sensitivity analysis is a powerful tool that allowed us to extrapolate beyond the unique model configuration. The sensitivity of the model to variations in each parameter was evaluated independently. By including a full range of potential parametric values, the model response was evaluated, design criteria developed and potential injury response predicted. A limitation of the single-parameter sensitivity analysis is that interactions and magnifying effects between multiple parameters cannot be evaluated.

Care should be taken in extending the results of this study to adult wheelchairs in rear impact. Pediatric wheelchairs tend to have stiffer frames than adult wheelchairs, since typically

the hardware is identical and the frame tubing diameters are the same but shorter in length. These characteristics combine to create a stiffer frame in pediatric sizes. Coupled with the stiffer frame, the pediatric ATD applies smaller loads to the pediatric wheelchair and headrest than the 50th percentile male ATD to the adult wheelchair and headrest under identical crash conditions.

8.4.1 Wheelchair and headrest design criteria

Table 54 provides a data summary for wheelchair and headrest design criteria. Baseline values, range of response from parametric sensitivity analysis and percent change from baseline values are all presented. Additional information on the parameter with the greatest effect is listed under “notes” in the final column. Often specific wheelchair responses did not vary in a predictable increasing/decreasing relationship with increasing parametric values, reflecting the complexity of the wheelchair and headrest response and interactions. It appears that seatback joint angle and response play critical roles in wheelchair loading patterns. This is an important design consideration for manufacturers since sled testing typically is conducted with the wheelchair in a more upright position.

Table 54: Pediatric wheelchair and headrest design criteria in rear impact

Design Criteria				
	Baseline	Range	<u>Percent change from baseline</u>	<u>Notes</u>
Front Securement Point Load (N)	3394	2617 – 3821	-23% / +13%	Greatest securement point loads with closest headrest proximity
Wheel Load (N)	1300	1224 – 1549	-6% / +19%	Greatest wheel loads with greatest seatback angle, also with more severe crash pulse
Seatback Deflection (degrees)	2.5	1.3 - 17.4	-49% / 7x baseline	Greater seatback deflection with reduced seatback joint damping
Seatback Load (N)	2572	2322 – 3845	-10% / +49%	Higher loads with increased seatback angle
Headrest Load (N)	664	382 – 762	-42% / +14%	Higher loads with decreased seatback height

A limitation of data used from Ha on combined seatback and attachment hardware stiffness (Ha, D. et al., 2000b) and from van Roosmalen on seatback joint stiffness (Van Roosmalen, L et al., 2000a) is that both data sets were based on quasi-static testing and neglect dynamic damping effects. Additional dynamic testing of seating systems may provide more realistic seating system parameters for model inputs.

From the Model HR validation, it is worthwhile to note that model head x-accelerations were 60% lower than would be predicted from sled testing. Based on this, anticipated headrest loading would be higher than suggested from model outputs – an additional consideration for manufacturers.

8.4.2 Injury risk outcomes

Table 55 summarizes the sensitivity of injury risk outcome measures to variation in wheelchair and headrest parameters and to crash pulse severity. Of all the injury response measures, N_{ij} is most sensitive to modifications in the headrest parameters in rear impact. This supports current recommendations for wheelchair headrest use and placement for travel in a motor vehicle. The Rehabilitation Engineering Research Center on Wheelchair Transportation Safety recommends that the wheelchair mounted headrest be placed close to the head and the center of the headrest pad should align superior to the ears. (RERC on Wheelchair Transportation Safety, 2007) Not surprisingly, increased seatback angle is associated with decreased N_{ij} and therefore likelihood of neck injury, since at increased seatback angles the head naturally positions itself closer to the headrest. Neck injury is a key concern in rear impact events (Department of Transportation, 2002).

Table 55: Sensitivity of injury risk response measures to wheelchair, headrest and crash pulse parameters.

Injury Risk Response				
	Baseline	Range	Percent change from baseline	Notes
Head acceleration (m/s²)	223	119 – 243	-46% / +9%	Greatest head accelerations with highest seatback height
Chest acceleration (m/s²)	233	132 – 262	-43% / +12%	Greatest chest accelerations with more severe crash pulse and greater seatback contact stiffness
HIC15	29.9	6.9 - 33.0	-77% / +10%	Largest HIC values with increased seatback joint damping, higher seatback height, higher headrest height and greater headrest stiffness
N_{ij} (tension-extension)	.0457	0.197 - 0.677	-57% / +48%	Largest N_{ij} values with decreased headrest height, increased head to headrest distance

An additional note is that large increases in head acceleration were not produced within this parametric analysis. This supports conclusions from the model validation that the mATD neck is contributing to low head accelerations as compared to sled testing.

Chest accelerations were sensitive to seatback contact stiffness, but since the chest is well supported in rear impact by the seatback, chest accelerations did not exhibit large increases from baseline. HIC15 was sensitive to headrest stiffness, and also to increased seatback joint damping and seatback height.

Nij is strongly dependent on headrest position. Figure 93 displays the Nij with headrest proximity. The vertical lines indicate the leading surface of the headrest. The baseline position was located 5 cm behind the head, which is the maximum recommended distance from the head. Headrest proximity was incremented at 2.5 cm intervals. A 32% reduction in Nij can be achieved by placing the headrest very close to the posterior head surface. Headrest positions 7.5 cm and 10 cm behind the head increase Nij by 18% and 31% above baseline ($N_{ij} = 0.457$). Nij references do not indicate a Nij value that would best predict an AIS = 1 whiplash-type neck injury (Kleinberger, M. et al., 1999). However, it is anticipated that smaller Nij values would be associated with less likelihood of neck injury. Headrest position located 10 cm behind the head resulted in Nij values 1.8 times the Nij value when the headrest is placed in the optimal position directly behind the head. These results support current recommendations to place the wheelchair mounted headrest in close proximity to the head during transportation in a motor vehicle (RERC on Wheelchair Transportation Safety, 2007).

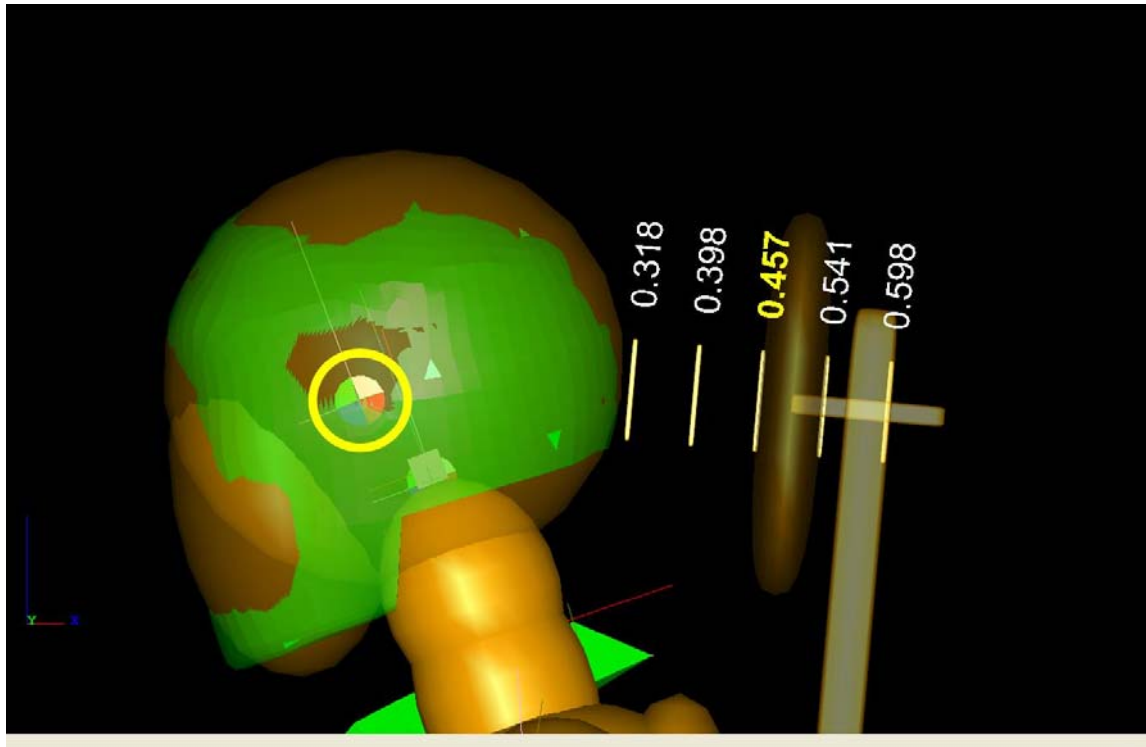


Figure 93: Nij response displayed with headrest proximity leading surface position. Head center of gravity highlighted with yellow circle.

Figure 94 displays Nij in response to headrest height. The yellow circle highlights the ATD head center of gravity. The ATD head is positioned such that the head center of gravity is in line with the center of the headrest pad. The headrest pad measures 15 cm (6 inches) in the vertical direction. The positions at the top of the headrest pad are indicated with horizontal lines, with baseline ($N_{ij} = 0.457$) indicated in yellow font. Headrest height was varied in 2.5 cm increments. Results indicate that setting a minimum headrest height will suffice to afford neck protection, with little difference once the minimum height is met. The top surface of the headrest pad must be a minimum of 5 cm above the head center of gravity. This result mirrors the current wheelchair headrest recommendation to position the headrest such that the top surface of the

headrest pad is at least 2.5 cm (1") above the top of the ear(RERC on Wheelchair Transportation Safety, 2007).

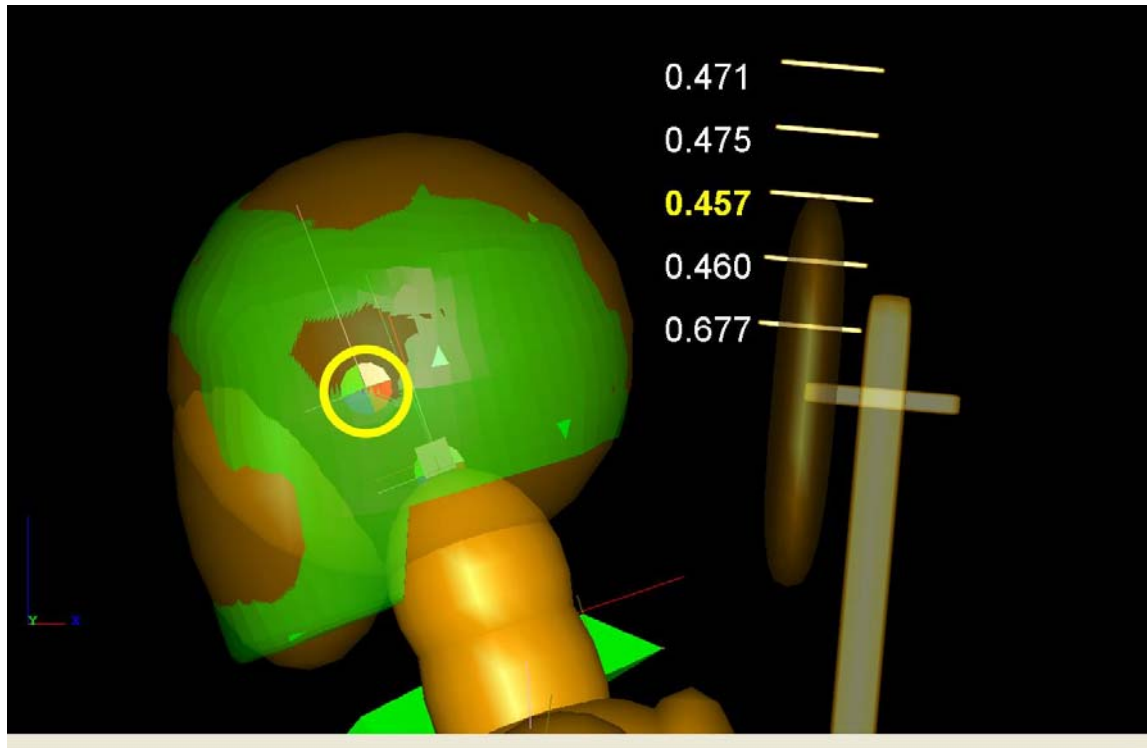


Figure 94: Nij displayed with headrest height. Baseline Nij value (0.457) shown in yellow. Head center of gravity highlighted with yellow circle.

8.4.3 Effects of mATD neck restraint loads and moments on injury risk outcome measures

Table 56 summarizes the sensitivity of the injury risk outcome measures to changes in the MADYMO Hybrid III 6-year old ATD mid-neck joint restraint loads and moments. Application of restraint loads is a limited approach to modifying the mATD neck flexion-extension response. However, it does allow for evaluation of the effects of a stiffer neck. It does not limit peak rotations, but requires more force to attain those positions. The effects of the additional restraint loads are most pronounced at peak extension and peak flexion.

Table 56: Effects of increased neck restraint loads and moments on injury risk measures.

Effects of increased neck joint restraint loads and moments				
	Model HR		Model NoHR	
	Baseline	Range	Baseline	Range
Peak head acceleration (m/s²)	223	223 - 228	211	191 – 211
Peak chest acceleration (m/s²)	215	215 - 242	216	215 – 217
HIC15	29.9	29.4 - 29.9	25.7	20.3 - 25.7
Nij (tension-extension)	0.457	0.457 - 0.508	0.879	0.732 - 0.879

Neck injury frequently occurs in rear impact (Department of Transportation, 2002). Additional neck restraint loads suggest that for Model NoHR, the occupant may be less likely to sustain a serious neck injury than the baseline NoHR model would suggest. This would support field data observations (Winston et al., 2004; Bilston, 2007) that suggest that actual likelihood of neck injury is less than predicted by the Hybrid III 6-year old ATD response.

Pediatric neck response has historically not been studied using human participants. Neck response data has been scaled and based on animal studies or studies with adults. A single study was conducted with a 12 year old cadaver (Sherwood et al., 2003) and compared to pediatric

ATDs. Currently Arbogast (Arbogast, 2008) is conducting a first ever study of male children (n = 30) aged 6-17 years in low speed frontal impact collisions and comparing the results to adult response under identical conditions. Her results hold promise in providing data on pediatric human subjects, and will contribute to better validated pediatric ATDs.

8.4.4 Study limitations

Study results study are limited by on-going concerns with respect to the 6-year old Hybrid III neck biofidelity. The 6-year old pATD has not been validated in rear impact. This issue is compounded by limitations in the MADYMO software. MADYMO's validation techniques and criteria are confidential. Based on correspondence with TNO MADYMO, it appears that the mATD is validated only in frontal impact and based on "engineering judgment". Further, the mATD 6-year old neck is not validated against the pATD neck in rear impact. Yet, these are the best pediatric surrogates currently available for study of pediatric injury response. Additional research is needed to develop the next generation of biofidelic pediatric ATDs.

Conclusions based on the parametric sensitivity analyses are predicated on baseline model validity. Model HR validated well for wheelchair tiedowns loads, wheelchair accelerations, lap belt loadings and chest accelerations (Chapter 6). It is therefore anticipated that design criteria such as securement point loads, wheel loads and wheelchair seatback loads would be well predicted by these analyses.

Model HR neck response and head acceleration was not as strongly validated and parametric sensitivity analyses results must be interpreted with caution. Model HR head acceleration results (Chapter 6) correlated well ($r = 0.88$) with mean Series HR sled test data, but had lower peak values than Series HR sled test results. Parametric sensitivity analyses indicate

that model head accelerations increased by 9% across all parameters and model headrest loading increased by 14% across all parameters. This suggests that for physical wheelchairs equipped with headrests, pATD head acceleration may also have low sensitivity to parametric variation. Physical ATD head accelerations recorded during sled testing (chapter 5) may be representative of a range of parameter variation and sled test data could contribute to crashworthy headrest design.

Model HR and Model NoHR neck forces and moments were partially validated (Chapter 6). Results from Chapter 7 suggest that it is the mATD characteristics that contributed to these results. An investigation into the sensitivity of neck injury outcome measures to added neck stiffness suggests that despite the limitations to the ATD neck, wheelchair headrests still confer benefit for pediatric occupant protection.

Parametric sensitivity analysis was used to evaluate the sensitivity of the model outcome variables to selected single input parameters. The use of parametric sensitivity analysis is appropriate because it is an accurate representation of model component responses; model outcomes are based on the mechanical properties and dynamic responses of the model components. The analysis is a first step in development of wheelchair design guidelines and relative injury risk assessment in rear impact. This work can be extended to examine the combined effects of multiple parameter variations using a multi parameter sensitivity analysis. The dual parameter sensitivity analysis is limited to evaluating interactions between single parameter pairs, and requires reconfiguration of the base simulation model to evaluate each parametric combination.

A statistical multivariate regression analysis could be developed based on results from exercising the MADYMO simulation model. Data from both the single parameter sensitivity analysis and additional configurations would be used to create the statistical model. A statistical model would assess each parameter's contribution to the outcome measure and evaluate the impact of parametric interactions on outcome measures. The development of multivariate regression models could provide additional information by simplifying the model to only those parameters and interactions shown to have a significant effect on the one or more outcome variables of interest. The predictive value of this approach is constrained by the type of regression model used. This secondary analysis would be a useful tool in extending the current simulation model results and would allow for design optimization.

This study represents a first step to establishing pediatric wheelchair and headrest design guidelines in rear impact. This data has the potential to contribute to improving transportation safety for pediatric wheelchair users.

9.0 CONCLUSIONS

A combination of sled testing and a computer simulation was used to investigate the role that wheelchairs and wheelchair mounted headrests can play in rear impact occupant protection for children who remain seated in their wheelchair while traveling in motor vehicles. The goals of this study were to establish pediatric wheelchair and headrest design guidelines and to determine the effect of headrests on relative injury risk outcome measures under rear impact conditions.

9.1 PROJECT REVIEW

Initial research reviewed the literature (Chapter 2) and surveyed clinicians, establishing wheelchair mounted headrests as an area of concern (Chapter 3). Two series of three sled tests (16 mph, 11g) were conducted using a Hybrid III 6-year old anthropomorphic test device (ATD) seated in identically configured manual pediatric wheelchairs. Series HR sled tests were conducted with identical single pad headrests; Series NoHR sled tests were conducted with no headrests. Each wheelchair was properly secured with 4-point strap type tiedowns, and the ATD was properly restrained using a 3-point occupant restraint system. In Chapter 4, sled test results were used to investigate pediatric wheelchair kinematics and WTORS loading was characterized for rear impact. In Chapter 5, comparisons between ATD responses to rear impact sled testing were analyzed to determine the effect of headrest use on injury risk outcome measures.

In Chapter 6, sled test data was then used to establish response corridors for MADYMO computer simulation model development, and to define statistical test target thresholds for subsequent model validation. Two separate simulation models were developed: Model HR included a headrest, Model NoHR did not include a headrest. A method was developed for characterizing the model ATD (mATD) neck response (Chapter 7). Model ATD neck response was compared against physical ATD (pATD) neck response. Last a parametric sensitivity analysis (Chapter 8) was used to develop wheelchair and headrest design guidelines for pediatric manual wheelchairs in rear impact, assess the sensitivity of pediatric injury outcome measures to wheelchair, headrest and crash pulse parameters, and evaluate the effect of a stiffer 6-year old ATD neck on injury risk outcome measures.

9.2 RESULTS

Wheelchair kinematic data, WTORS load data, and ATD head acceleration and neck load and moment data from rear impact all provided much new information. Sled test results indicated that headrest presence affected wheelchair kinematics and WTORS loading. Headrest-equipped wheelchairs had greater mean peak seatback deflections, mean peak front and rear tiedown loads and decreased mean lap belt loads, suggesting that in rear impact headrest presence increases the loads on the wheelchair. Rear impact tiedown loads differed from previously measured loads in frontal impact, with comparable tiedown load levels reversed in frontal and rear impacts. The front tiedowns carried larger loads in rear impact despite lower impact severity. Headrest presence increased mean peak front tiedown loads. These outcomes have implications for

wheelchair and tiedown design, highlighting the need for all four tiedowns to have an equally robust design, and have implications in the development of rear impact wheelchair transportation safety standards.

Physical ATD head and neck responses to rear impact conditions were compared across two scenarios. Head and neck injury outcomes measures included: linear head acceleration, head injury criteria (HIC) values, neck injury criteria (Nij) values, and combined rotational head velocity and acceleration. Neck and head injury outcome measures improved by 34-70% in sled tests conducted with headrests compared to tests without headrests. Headrest use reduced Nij values and the likelihood of concussion from values above established injury thresholds to values below injury thresholds. Injury measure outcome reductions suggested lower head and neck injury risks for wheelchair-seated children using wheelchair-mounted headrests as compared to non-headrest users in rear impact. Use of relative comparisons across two test scenarios served to minimize effects of pATD biofidelity limitations.

Computer simulation model validation criteria were developed based on statistical test comparisons between sled test data from the same test series (Series HR, Series NoHR). Development of the criteria highlighted the variability between sled tests. Comparisons between the sled tests within Series HR indicate that Pipkorn (Pipkorn and Eriksson, 2003) recommended target thresholds were not met for 35% of the statistical tests. Comparisons between the sled tests within Series NoHR indicate that Pipkorn recommended target thresholds were not met for 43% of the statistical tests. When the sled test variability was within the Pipkorn thresholds, Pipkorn thresholds were used for computer simulation model validation. When the variability of the sled test data exceeded Pipkorn thresholds, the target thresholds were modified (expanded) to reflect this variability. Using the revised target thresholds, the two models were validated. Model HR

was fully validated for right and left tiedown loads, wheelchair center of gravity acceleration, lap belt loads, and chest acceleration. Overall Model HR validated for 86.6% of all comparisons. Model NoHR was also well validated for tiedowns, wheelchair accelerations, lap belt loads and chest accelerations, with 86.3% of all tests meeting target thresholds. Overall, Model NoHR 77% of all comparisons to sled test data met target thresholds. Model HR and Model NoHR are well validated overall, however the neck forces in the fore-aft directions (Fx) did not validate well and more research was needed on mATD neck response.

Model ATD neck response cannot be characterized by investigating the MADYMO neck characteristics since these are all encrypted. A pendulum test method exists for calibrating the pATD neck and is described in the Hybrid III Six-year Old Child Dummy User's Manual (Society of Automotive Engineers: Dummy Testing Equipment Subcommittee, 2003). A MADYMO computer simulation model of the calibration test was created using the standard MADYMO 6-year old ATD head and neck for both the flexion and extension tests. Calibration model pendulum response was within the velocity-time profile specifications. Results were compared to physical test data from a calibrated Hybrid III 6-year old ATD. Results suggest that model peak extension results compare well to physical tests results. However at smaller angles the comparison is weaker. Model peak calibration flexion results do not meet the calibration specifications exhibiting greater neck flexion moments at smaller neck flexion angles than both the specification and the physical neck flexion calibration data. However, sled test neck injury criteria (N_{ij}) compare well with sled test model N_{ij} results. This suggests that the peak extension behavior of the mATD neck, may be adequate to compare N_{ij} results.

The purpose of the parametric sensitivity analysis was three-fold: to establish design criteria for manual pediatric wheelchairs in rear impact, to determine the effect of wheelchair

parametric variation on injury risk outcome measures, and to evaluate the sensitivity of injury risk outcomes to changes in mATD neck response. Parametric sensitivity analysis was used to assess the sensitivity of the model to the individual model parameters. Model HR sensitivity was evaluated for crash pulse severity, wheelchair parameters and headrest parameters. Injury risk outcome measure sensitivity was evaluated for the effect of increased neck stiffness, and then evaluated across both Model HR and Model NoHR. Conclusions based on the parametric sensitivity analyses are predicated on baseline model validity. Model HR validated well for wheelchair tiedowns loads, wheelchair accelerations, lap belt loadings and chest accelerations (Chapter 6). It is therefore anticipated that design criteria such as securement point loads, wheel loads and wheelchair seatback loads would be well predicted by these analyses. Since model head and neck outcomes have weaker validation, care must be taken in interpreting these results.

9.3 LIMITATIONS

Biofidelity is a potential limitation in all testing using human surrogates. This study used the Hybrid III 6-year old ATD whose biomechanical response was based on the Hybrid III 50th percentile male, and scaled using pediatric anthropometric and mass data and the elastic modulus of pediatric bone (Irwin and Mertz, 1997). This ATD was upgraded in 1997 to reflect more recent evaluations of airbag deployment effects on children (First Technology Safety Systems, 2005). The ATD represents the current state of the science for human biofidelity of a 6 year old child, yet is potentially representative of only the narrow portion of the able-bodied population described by the 50th percentile 6-year old.

The Hybrid III 6-year old ATD and its neck response have provoked controversy regarding its biofidelity (Malott et al., 2004; Bilston, 2007) since actual incidence rates of severe pediatric neck injury in rear impact motor vehicle crashes remain lower than would be anticipated from ATD testing and ATD measurements fail to reliably predict actual injury. The 6-year old pATD has not been validated in rear impact. This issue is compounded by limitations in the MADYMO software. MADYMO's validation techniques and criteria are confidential. Based on correspondence with TNO MADYMO, it appears that the mATD is validated only in frontal impact and based on "engineering judgment". Further, the mATD 6-year old neck is not validated against the pATD neck in rear impact.

A pediatric ATD was used in these studies. At 51 lbs, it creates lower peak loads than an adult ATD would produce. This is a design consideration since wheelchair manufacturers often use identical hardware on adult and pediatric wheelchairs.

Variability between sled test study response data was quantified by development of model validation thresholds. Sled test variability may have been caused by a variety of test specific conditions, including differences between identical model wheelchairs, tiedown pre-tensioning, and pATD positioning. In addition, more subtle differences such as air pressure in the tires and tightness of the wheelchair hardware may have all contributed to the observed variability between sled tests. The expanded validation thresholds reflected this variability.

Just as the pATD neck uses a rubber block with a steel axial cable to model the human neck response, the mATD neck does not mirror the pATD neck by modeling each component, instead it models the pATD neck response. So, too Model HR and Model NoHR were developed to simulate the physical responses observed during Series HR and Series NoHR sled testing. In the development of Model HR and Model NoHR, several approximations and simplifications

were made. For example, during sled testing the wheelchair seatback was forced by the pATD upward along the seatback canes. Although this motion could be replicated in the model, the model results could not be validated against the sled test data. The decision was made to create the model with a no-excursion seatback; the model seatback was located at height of peak loading. This approximation was demonstrated to be acceptable based on model validation results.

9.4 FUTURE WORK

Future work centers on addressing questions and limitations from this study. Salipur (Salipur et al., 2007) has address WTORS loading for adult manual wheelchairs in rear impact and his master's thesis (not yet published) reports design guidelines for an adult manual wheelchair. However, evidence from our studies suggests that in rear impact wheelchair loading is more severe with a wheelchair mounted headrest. Development of wheelchair design guidelines is needed for adult wheelchairs equipped with wheelchair mounted headrests.

During the evaluation of seatback angle on model outcomes, the shoulder belt wall anchor was relocated in compliance with ISO 10542: Wheelchair tiedown and occupant restraint systems for forward facing wheelchair-seated passengers – Part 1: Requirements and test methods – Frontal impact (ISO, 1999a). This modification was necessary to ensure proper initial model acceleration, but did not affect the output results as the shoulder belt is not loaded in rear impact. However, there is a large acceptable region for mounting the wall anchor that would also comply with ISO 10542:1. It would be worthwhile to investigate the role that the wall anchor point plays in frontal impact.

A limitation of the single-parameter sensitivity analysis is that interactions between multiple parameters cannot be evaluated. Further parametric studies can be conducted on this model to evaluate the interactive effects between multiple parameters. Multivariate regression models can also be developed using additional model simulations. Regression models could be used to assess the significance of each parameter in the outcome measure, and to evaluate parametric interaction effects. The effect of clinically relevant multivariate modifications to the base model could be rapidly predicted yielding key information for both manufacturers and clinicians.

Rear impacts account for most injury producing accidents (Volvo, 2003). Continued work is needed in the development of a rear impact wheelchair standard for individuals who remain seated in their wheelchairs while traveling in a motor vehicle.

Of key concern is the biofidelity of the pATD. More work is needed to develop the next generation of pediatric ATDs. Further, the MADYMO software mATD needs to be subjected to a more rigorous validation in frontal impact for neck flexion response, as well as validated against the pATD in extension.

APPENDIX A

MODEL HR

```
<?xml version="1.0" encoding="UTF-8"
standalone="no"?>
<!DOCTYPE MADYMO SYSTEM "mtd_3d.dtd">
<MADYMO
  RELEASE="R6.3.2"
  >
  <TYPEDEFS>
  <INCLUDE
    FILE="typedefs.xml"
  />
  </TYPEDEFS>
  <RUNID>
  <![CDATA[
Hybrid III 6 year old child dummy model
ellipsoid model in default position
]]>
  <PRODUCT_INFORMATION
    DESCRIPTION="MADYMO Hybrid III 6 year
old child dummy model"
    FILE="d_hyb36yel_usr.xml (user-file)"
    VERSION="2.6"
    DATE="$Date: 2005/11/14 12:43:23 $"
    STATE="$State: R63 $"
  >

  </RUNID>
  <CONTROL_ALLOCATION
    NR_PROC="1"
    I_SIZE="1000000"
    R_SIZE="2000000"
    C_SIZE="100000"
  />
  <CONTROL_ANALYSIS.TIME
    TIME_START="-0.45"
    TIME_END="0.25"
    TIME_STEP="2.500000E-05"
    INT_MTH="EULER"
    ANALYSIS_TYPE="DYNAMIC"
    CONSTRAINT_TOL="1.000000E-09"
    RAMP="0.0 0.1"
    RACO="0.01 0.1"
  />
  <CONTROL_OUTPUT
    TIME_START_OUTPUT="-0.025"
    FILTER_IGNORE="OFF"
    PADDING_TIME="0.01"

    TIME_STEP="0.001"
    TIME_STEP_ANI="0.002"
    WRITE_DEBUG="NONE"
  >
  <TIME_HISTORY_MB
    DESCRIPTION="Output signals Hybrid III 6
year old ellipsoid dummy model"
    SYSTEM="Hybrid_III_6_year_old"
    BODY_OUTPUT_LIST="ALL"

    BODY_REL_OUTPUT_LIST="ChestDeflection_dis
ChestDeflection_vel_CFC180
ChestDeflection_vel_CFC600"

    JOINT_CONSTRAINT_OUTPUT_LIST="LumbarSpineLow_ice
_F
LumbarSpineLow_ice_T
NeckLow_ice_F
NeckLow_ice_T
NeckUp_ice_F_CFC600
NeckUp_ice_F_CFC1000
NeckUp_ice_T
FemurL_ice_F FemurL_ice_T
FemurR_ice_F
FemurR_ice_T"
  >
  <COMMENT>
  <![CDATA[
Available output signals

  BODY_OUTPUT_LIST
  Pelvis_acc
  ThoraxT4_acc
  HeadCG_acc
  SternumUp_acc
  SternumLow_acc
  ThoraxT1_acc
  ThoraxUp_acc
  ThoraxLow_acc
  BODY_REL_OUTPUT_LIST
  ChestDeflection_dis
  ChestDeflection_vel_CFC180
  ChestDeflection_vel_CFC600

  JOINT_CONSTRAINT_OUTPUT_LIST
  LumbarSpineLow_ice_F
```

```

LumbarSpineLow_ice_T
NeckLow_ice_F
NeckLow_ice_T
NeckUp_ice_F_CFC600
NeckUp_ice_F_CFC1000
NeckUp_ice_T
FemurL_ice_F
FemurL_ice_T
FemurR_ice_F
FemurR_ice_T
]]>
  </COMMENT>
  </TIME_HISTORY_MB>
  <TIME_HISTORY_MB
    DESCRIPTION="output signals from tiedowns"
    BELT_OUTPUT_LIST="/LRear_tiedown_out
/Left_front_tiedown_out          /RRear_tiedown_output
/Right_Front_tiedown_out"
  />
  <TIME_HISTORY_MB
    BELT_OUTPUT_LIST="/lap_belt/lap_belt_1
/lap_belt/lap_belt_2"
    DESCRIPTION="output signals from lapbelt"
  />
  <TIME_HISTORY_MB

JOINT_DOF_OUTPUT_LIST="/wheelchair_system/sb_joint_out
put"
  DESCRIPTION="output signals seatback joint"
  />
  <TIME_HISTORY_MB

BODY_OUTPUT_LIST="/wheelchair_system/WC_CG_LinearAc
c_output"
  DESCRIPTION="output signal WC CG
acceleration"
  />
  <TIME_HISTORY_MB

BODY_OUTPUT_LIST="/wheelchair_system/front_caster_output
"
  DESCRIPTION="output signal front caster"
  />
  <TIME_HISTORY_MB
    JOINT_DOF_OUTPUT_LIST="ALL"
    DESCRIPTION="Joint_position_output"
  />
  <ANIMATION
    EXTENDED="ON"
  />
  <TIME_HISTORY_CONTACT
    CONTACT_OUTPUT_LIST="ALL"
    DESCRIPTION="contacts_outputs"
  />
  <TIME_HISTORY_INJURY
    INJURY_LIST="ALL"
  />
  <TIME_DURATION_INJURY
    INJURY_LIST="ALL"
  />
  </CONTROL_OUTPUT>
  <SYSTEM.REF_SPACE
    ID="1"
    NAME="sled_track"
  >
  <SURFACE.PLANE
    ID="1"
    NAME="track_surface"
    POINT_1="0.0 0.0 -0.01"
    POINT_2="4.5 0.0 -0.01"
    POINT_3="4.5 1.88 -0.01"
  />
  </SYSTEM.REF_SPACE>
  <SYSTEM.MODEL
    ID="2"
    NAME="sled_system"
  >
  <POINT_OBJECT.MB
    NAME="LFront_sled_secure_pnt"
    BODY="sled_body"
    POS="- .571 -.3268 0"
    ID="1"
  />
  <POINT_OBJECT.MB
    NAME="RFront_sled_secure_pnt"
    BODY="sled_body"
    POS="- .571 .3268 0"
    ID="2"
  />
  <POINT_OBJECT.MB
    NAME="LRear_sled_secure_pnt"
    BODY="sled_body"
    POS=".7244 -.1524 0"
    ID="3"
  />
  <POINT_OBJECT.MB
    NAME="RRear_sled_secure_pnt"
    BODY="sled_body"
    POS=".7244 .1524 0"
    ID="4"
  />
  <POINT_OBJECT.MB
    NAME="D_ring_pnt"
    BODY="sled_body"
    POS=".5074 .3048 1.0033"
    ID="5"
  />
  <POINT_OBJECT.MB
    NAME="LFloor_anchor_pnt"
    BODY="sled_body"
    POS=".5605 -.17145 0.0"
    ID="6"
  />
  <POINT_OBJECT.MB
    NAME="RFloor_anchor_pnt"
    BODY="sled_body"
    POS=".5605 .17145 0.0"
    ID="7"
  />
  <POINT_OBJECT.MB
    NAME="L_SB_Floor_anchor_pnt"
    BODY="sled_body"
    POS=".5605 -.17145 0.0"
    ID="8"
  />
  <OUTPUT_BODY
    NAME="sled_velocity_output"
    ID="1"
    SIGNAL_TYPE="LIN_VEL"
  >
  <CRDSYS_OBJECT_1.MB
    BODY="sled_body"
  />
  </OUTPUT_BODY>
  <OUTPUT_BODY
    NAME="sled_acc_output"
    ID="3"
    SIGNAL_TYPE="LIN_ACC"
  >
  <CRDSYS_OBJECT_1.MB

```



```

/>
<BODY.RIGID
  ID="6"
  INERTIA="0.01922 0.02888 0.0481 0.0 0.0 0.0"
  MASS="2.4"
  NAME="wseat_body"
/>
<BODY.RIGID
  ID="7"
  INERTIA="0.044092 0.026473 0.017618 0.0 0.0
0.0"
  MASS="2.2"
  NAME="wback_body"
/>
<BODY.RIGID
  ID="8"
  INERTIA="1.000000E-003 1.000000E-003
1.000000E-003 0.0 0.0 0.0"
  MASS="0.001"
  NAME="accelerometer"
/>
<SURFACE.ELLIPSOID
  CHAR="rwh_contact"
  DEGREE="2"
  ID="1"
  NAME="RRear_wheel_surface"
  SEMI_AXIS="0.289 0.032 0.289"
  >
  <CRDSYS_OBJECT_1.MB
    BODY="RRear_wheel_body"
    POS="0.0 0.0 0.0"
  />
</SURFACE.ELLIPSOID>
<SURFACE.ELLIPSOID
  CHAR="rwh_contact"
  DEGREE="2"
  ID="2"
  NAME="LRear_wheel_surface"
  SEMI_AXIS="0.289 0.032 0.289"
  >
  <CRDSYS_OBJECT_1.MB
    BODY="LRear_wheel_body"
    POS="0.0 0.0 0.0"
  />
</SURFACE.ELLIPSOID>
<SURFACE.ELLIPSOID
  CHAR="fwh_contact"
  DEGREE="2"
  ID="3"
  NAME="RFront_wheel_surface"
  SEMI_AXIS="0.062 0.024 0.062"
  >
  <CRDSYS_OBJECT_1.MB
    BODY="RFront_wheel_body"
    POS="0.0 0.0 0.0"
  />
</SURFACE.ELLIPSOID>
<SURFACE.ELLIPSOID
  CHAR="fwh_contact"
  DEGREE="2"
  ID="4"
  NAME="LFront_wheel_surface"
  SEMI_AXIS="0.062 0.024 0.062"
  >
  <CRDSYS_OBJECT_1.MB
    BODY="LFront_Wheel_body"
    POS="0.0 0.0 0.0"
  />
</SURFACE.ELLIPSOID>
<SURFACE.ELLIPSOID
  CHAR="wseat_contact"
  DEGREE="8"
  ID="5"
  NAME="wseat_surface"
  SEMI_AXIS="0.19 0.155 0.015"
  >
  <CRDSYS_OBJECT_1.MB
    BODY="wseat_body"
    POS="0.0 0.0 0.0"
  />
</SURFACE.ELLIPSOID>
<SURFACE.ELLIPSOID
  CHAR="wback_contact"
  DEGREE="8"
  ID="6"
  NAME="wback_surface"
  SEMI_AXIS="0.155 0.01 0.19"
  >
  <CRDSYS_OBJECT_1.MB
    BODY="wback_body"
    POS="0.0 0.0 0.0"
  />
</SURFACE.ELLIPSOID>
<SURFACE.ELLIPSOID
  CHAR="footrest_contact"
  DEGREE="8"
  ID="7"
  NAME="footrest_surface"
  SEMI_AXIS="0.076 0.1225 0.0025"
  >
  <CRDSYS_OBJECT_1.MB
    BODY="frame_cg_body"
    ORIENT="foot_ori"
    POS="0.35 0.0 -0.75"
  />
</SURFACE.ELLIPSOID>
<SURFACE.ELLIPSOID
  DEGREE="2"
  ID="8"
  NAME="frame_cg_surface"
  SEMI_AXIS="0.01 0.01 0.01"
  >
  <CRDSYS_OBJECT_1.MB
    BODY="frame_cg_body"
    POS="0.0 0.0 0.0"
  />
</SURFACE.ELLIPSOID>
<SURFACE.ELLIPSOID
  DEGREE="9"
  ID="9"
  NAME="total_cg_surface"
  SEMI_AXIS="0.015 0.005 0.01"
  >
  <CRDSYS_OBJECT_1.MB
    BODY="accelerometer"
    POS="0.0 0.0 0.0"
  />
</SURFACE.ELLIPSOID>
<SURFACE.ELLIPSOID
  DEGREE="8"
  ID="50"
  NAME="r_hor1"
  SEMI_AXIS="0.245 0.0127 0.0127"
  >
  <CRDSYS_OBJECT_1.MB
    BODY="frame_cg_body"
    POS="-0.043 -0.1402 -0.146"
  />
</SURFACE.ELLIPSOID>
<SURFACE.ELLIPSOID

```

```

DEGREE="8"
ID="51"
NAME="l_hor1"
SEMI_AXIS="0.245 0.0127 0.0127"
>
<CRDSYS_OBJECT_1.MB
  BODY="frame_cg_body"
  POS="-0.043 0.1402 -0.146"
/>
</SURFACE.ELLIPSOID>
<SURFACE.ELLIPSOID
  DEGREE="8"
  ID="52"
  NAME="r_hor2"
  SEMI_AXIS="0.286 0.0127 0.0127"
  >
  <CRDSYS_OBJECT_1.MB
    BODY="frame_cg_body"
    POS="-0.084 -0.1402 0.0574"
  />
</SURFACE.ELLIPSOID>
<SURFACE.ELLIPSOID
  DEGREE="8"
  ID="53"
  NAME="l_hor2"
  SEMI_AXIS="0.286 0.0127 0.0127"
  >
  <CRDSYS_OBJECT_1.MB
    BODY="frame_cg_body"
    POS="-0.084 0.1402 0.0574"
  />
</SURFACE.ELLIPSOID>
<SURFACE.ELLIPSOID
  DEGREE="8"
  ID="54"
  NAME="r_ver1"
  SEMI_AXIS="0.0127 0.0127 0.089"
  >
  <CRDSYS_OBJECT_1.MB
    BODY="frame_cg_body"
    POS="-0.243 -0.1402 -0.0443"
  />
</SURFACE.ELLIPSOID>
<SURFACE.ELLIPSOID
  DEGREE="8"
  ID="55"
  NAME="l_ver1"
  SEMI_AXIS="0.0127 0.0127 0.089"
  >
  <CRDSYS_OBJECT_1.MB
    BODY="frame_cg_body"
    POS="-0.243 0.1402 -0.0443"
  />
</SURFACE.ELLIPSOID>
<SURFACE.ELLIPSOID
  DEGREE="8"
  ID="56"
  NAME="r_ver2"
  SEMI_AXIS="0.0127 0.0127 0.089"
  >
  <CRDSYS_OBJECT_1.MB
    BODY="frame_cg_body"
    POS="-0.118 -0.1402 -0.0443"
  />
</SURFACE.ELLIPSOID>
<SURFACE.ELLIPSOID
  DEGREE="8"
  ID="57"
  NAME="l_ver2"
  SEMI_AXIS="0.0127 0.0127 0.089"
  >
  <CRDSYS_OBJECT_1.MB
    BODY="frame_cg_body"
    POS="-0.118 0.1402 -0.0443"
  />
</SURFACE.ELLIPSOID>
<SURFACE.ELLIPSOID
  DEGREE="8"
  ID="58"
  NAME="r_ver3"
  SEMI_AXIS="0.0127 0.0127 0.089"
  >
  <CRDSYS_OBJECT_1.MB
    BODY="frame_cg_body"
    POS="0.1893 -0.1402 -0.0443"
  />
</SURFACE.ELLIPSOID>
<SURFACE.ELLIPSOID
  DEGREE="8"
  ID="59"
  NAME="l_ver3"
  SEMI_AXIS="0.0127 0.0127 0.089"
  >
  <CRDSYS_OBJECT_1.MB
    BODY="frame_cg_body"
    POS="0.1893 0.1402 -0.0443"
  />
</SURFACE.ELLIPSOID>
<SURFACE.ELLIPSOID
  DEGREE="8"
  ID="60"
  NAME="r_ver4"
  SEMI_AXIS="0.0127 0.0127 0.305"
  >
  <CRDSYS_OBJECT_1.MB
    BODY="wback_body"
    POS="-0.16 0 0.065"
  />
</SURFACE.ELLIPSOID>
<SURFACE.ELLIPSOID
  DEGREE="8"
  ID="61"
  NAME="l_ver4"
  SEMI_AXIS="0.0127 0.0127 0.305"
  >
  <CRDSYS_OBJECT_1.MB
    BODY="wback_body"
    POS="0.16 0 0.065"
  />
</SURFACE.ELLIPSOID>
<SURFACE.ELLIPSOID
  DEGREE="8"
  ID="62"
  NAME="r_leg"
  SEMI_AXIS="0.0127 0.0127 0.1639"
  >
  <CRDSYS_OBJECT_1.MB
    BODY="frame_cg_body"
    ORIENT="leg_ori"
    POS="0.3035 -0.1402 -0.0713"
  />
</SURFACE.ELLIPSOID>
<SURFACE.ELLIPSOID
  DEGREE="8"
  ID="63"
  NAME="l_leg"
  SEMI_AXIS="0.0127 0.0127 0.1639"
  >
  <CRDSYS_OBJECT_1.MB
    BODY="frame_cg_body"

```

```

    ORIENT="leg_ori"
    POS="0.3035 0.1402 -0.0713"
  />
</SURFACE.ELLIPSOID>
<SURFACE.ELLIPSOID
  DEGREE="8"
  ID="64"
  NAME="mid1"
  SEMI_AXIS="0.0127 0.128 0.0127"
  >
  <CRDSYS_OBJECT_1.MB
    BODY="frame_cg_body"
    POS="-0.163 0.0 -0.146"
  />
</SURFACE.ELLIPSOID>
<SURFACE.ELLIPSOID
  DEGREE="8"
  ID="65"
  NAME="mid2"
  SEMI_AXIS="0.0127 0.128 0.0127"
  >
  <CRDSYS_OBJECT_1.MB
    BODY="frame_cg_body"
    POS="0.067 0.0 -0.146"
  />
</SURFACE.ELLIPSOID>
<SURFACE.ELLIPSOID
  DEGREE="8"
  ID="66"
  NAME="mid3"
  SEMI_AXIS="0.0127 0.128 0.0127"
  >
  <CRDSYS_OBJECT_1.MB
    BODY="frame_cg_body"
    POS="-0.243 0.0 0.0227"
  />
</SURFACE.ELLIPSOID>
<SURFACE.ELLIPSOID
  CHAR="armrest_contact"
  DEGREE="8"
  ID="67"
  NAME="r_arm"
  SEMI_AXIS="0.17 0.0095 0.0095"
  >
  <CRDSYS_OBJECT_1.MB
    BODY="frame_cg_body"
    POS="-0.0603 -0.1702 0.3101"
  />
</SURFACE.ELLIPSOID>
<SURFACE.ELLIPSOID
  NAME="l_anti_tipper_top"
  DEGREE="8"
  SEMI_AXIS="0.0762 .009525 .009525"
  ID="69"
  >
  <CRDSYS_OBJECT_1.MB
    POS="-0.33 .12 -.05715"
    BODY="frame_cg_body"
  />
</SURFACE.ELLIPSOID>
<SURFACE.ELLIPSOID
  DEGREE="8"
  SEMI_AXIS="0.0889 .009525 .009525"
  NAME="l_anti_tipper_bottom"
  ID="70"
  >
  <CRDSYS_OBJECT_1.MB
    BODY="frame_cg_body"
    ORIENT="anti_tipper_ori"
    POS="-0.4162 .12 -.13335"
  />
</SURFACE.ELLIPSOID>
<SURFACE.ELLIPSOID
  DEGREE="2"
  SEMI_AXIS="0.0174625 .0047625 .0174625"
  NAME="l_anit_tipper_wheel"
  ID="71"
  >
  <CRDSYS_OBJECT_1.MB
    POS="-0.438 .12 -.22225"
    BODY="frame_cg_body"
  />
</SURFACE.ELLIPSOID>
<SURFACE.ELLIPSOID
  ID="72"
  NAME="r_anti_tipper_top"
  DEGREE="8"
  SEMI_AXIS="0.0762 .009525 .009525"
  >
  <CRDSYS_OBJECT_1.MB
    POS="-0.33 -.12 -.05715"
    BODY="frame_cg_body"
  />
</SURFACE.ELLIPSOID>
<SURFACE.ELLIPSOID
  ID="73"
  DEGREE="8"
  SEMI_AXIS="0.0889 .009525 .009525"
  NAME="r_anti_tipper_bottom"
  >
  <CRDSYS_OBJECT_1.MB
    BODY="frame_cg_body"
    ORIENT="anti_tipper_ori"
    POS="-0.4162 -.12 -.13335"
  />
</SURFACE.ELLIPSOID>
<SURFACE.ELLIPSOID
  ID="74"
  DEGREE="2"
  SEMI_AXIS="0.0174625 .0047625 .0174625"
  NAME="r_anit_tipper_wheel"
  >
  <CRDSYS_OBJECT_1.MB
    POS="-0.438 -.12 -.22225"
    BODY="frame_cg_body"
  />
</SURFACE.ELLIPSOID>
<SURFACE.ELLIPSOID
  DEGREE="10"
  SEMI_AXIS="0.009 .009 .110"
  NAME="vert_hr_stem"
  ID="75"
  >
  <CRDSYS_OBJECT_1.MB
    POS="0.0 0.02 0.260"
    BODY="wback_body"
  />
</SURFACE.ELLIPSOID>
<SURFACE.ELLIPSOID
  DEGREE="10"
  SEMI_AXIS="0.004 .04 .004"
  NAME="hor_hr_stem"
  ID="76"
  >
  <CRDSYS_OBJECT_1.MB
    POS="0.0 0.02 0.33"
    BODY="wback_body"
  />
</SURFACE.ELLIPSOID>
<SURFACE.ELLIPSOID
  DEGREE="2"
  SEMI_AXIS="0.0174625 .0047625 .0174625"
  NAME="r_anit_tipper_wheel"
  ID="77"
  >
  <CRDSYS_OBJECT_1.MB
    POS="-0.438 -.12 -.22225"
    BODY="frame_cg_body"
  />
</SURFACE.ELLIPSOID>

```

```

DEGREE="3"
SEMI_AXIS=".145 .0125 .075 "
NAME="Headrest_pad"
ID="77"
>
<CRDSYS_OBJECT_1.MB
  POS="0 -0.01 0.33"
  BODY="wcbback_body"
/>
</SURFACE.ELLIPSOID>
<SURFACE.ELLIPSOID
  CHAR="armrest_contact"
  DEGREE="8"
  ID="68"
  NAME="l_arm"
  SEMI_AXIS="0.17 0.0095 0.0095"
  >
  <CRDSYS_OBJECT_1.MB
    BODY="frame_cg_body"
    POS="-0.0603 0.1702 0.3101"
  />
</SURFACE.ELLIPSOID>
<JOINT.FREE
  ID="1"
  NAME="CG_ref_joint"
  >
  <CRDSYS_OBJECT_1.MB
    BODY="/sled_system/sled_body"
    POS="0.0 0.0 .31"
  />
  <CRDSYS_OBJECT_2.MB
    BODY="frame_cg_body"
    POS="0.0 0.0 0.0"
  />
</JOINT.FREE>
<JOINT.BRAC
  ID="2"
  NAME="wcseat_joint"
  >
  <CRDSYS_OBJECT_1.MB
    BODY="frame_cg_body"
    ORIENT="seat_ori"
    POS="-0.045 0.0 0.11"
  />
  <CRDSYS_OBJECT_2.MB
    BODY="wcseat_body"
    POS="0.0 0.0 0.0"
  />
</JOINT.BRAC>
<JOINT.REVO
  R1="0"
  NAME="seatback_rev_jnt"
  ID="10"
  >
  <CRDSYS_OBJECT_1.MB
    ORIENT="back_ori"
    POS="-0.205 0.0 0.175"
    BODY="frame_cg_body"
  />
  <CRDSYS_OBJECT_2.MB
    ORIENT="seatback_ori"
    BODY="wcbback_body"
    POS="0.0 -0.01 -0.15"
  />
</JOINT.REVO>
<JOINT.BRAC
  NAME="accelerometer_joint"
  ID="11"
  >
  <CRDSYS_OBJECT_1.MB
    BODY="frame_cg_body"
    POS="-0.08 -0.16 0.035"
  />
  <CRDSYS_OBJECT_2.MB
    BODY="accelerometer"
    POS="0.0 0.0 0.0"
  />
</JOINT.BRAC>
<JOINT.REVO
  ID="6"
  NAME="RRear_wh_joint"
  >
  <CRDSYS_OBJECT_1.MB
    BODY="frame_cg_body"
    ORIENT="wheel_ori"
    POS="-0.215 -0.2102 -0.021"
  />
  <CRDSYS_OBJECT_2.MB
    BODY="RRear_wheel_body"
    ORIENT="wheel_ori"
    POS="0 0 0"
  />
</JOINT.REVO>
<JOINT.REVO
  ID="7"
  NAME="LRear_wh_joint"
  >
  <CRDSYS_OBJECT_1.MB
    BODY="frame_cg_body"
    ORIENT="wheel_ori"
    POS="-0.215 0.2102 -0.021"
  />
  <CRDSYS_OBJECT_2.MB
    BODY="LRear_wheel_body"
    ORIENT="wheel_ori"
    POS="0.0 0.0 0.0"
  />
</JOINT.REVO>
<JOINT.REVO
  ID="8"
  NAME="RFront_wh_joint"
  >
  <CRDSYS_OBJECT_1.MB
    BODY="frame_cg_body"
    ORIENT="wheel_ori"
    POS="0.185 -0.1802 -0.248"
  />
  <CRDSYS_OBJECT_2.MB
    BODY="RFront_wheel_body"
    ORIENT="wheel_ori"
    POS="0.0 0.0 0.0"
  />
</JOINT.REVO>
<JOINT.REVO
  ID="9"
  NAME="LFront_wh_joint"
  >
  <CRDSYS_OBJECT_1.MB
    BODY="frame_cg_body"
    ORIENT="wheel_ori"
    POS="0.185 0.1802 -0.248"
  />
  <CRDSYS_OBJECT_2.MB
    BODY="LFront_Wheel_body"
    ORIENT="wheel_ori"
    POS="0.0 0.0 0.0"
  />
</JOINT.REVO>
<RESTRAINT.JOINT
  Q1_CHAR="sb_joint_load"

```



```

ID="9"
JOINT="seatback_rev_jnt"
/>
<INITIAL_JOINT_POS
R3="3.1416"
D1="0"
D2="0"
D3="0"
JOINT="CG_ref_joint"
/>
<ORIENTATION.SUCCESIVE_ROT
AXIS_1="Z"
ID="1"
NAME="wheel_ori"
R1="-1.5708"
/>
<ORIENTATION.SUCCESIVE_ROT
AXIS_1="Y"
ID="2"
NAME="leg_ori"
R1="-0.6632"
/>
<ORIENTATION.SUCCESIVE_ROT
AXIS_1="Y"
ID="3"
NAME="foot_ori"
R1="-0.61087"
/>
<ORIENTATION.SUCCESIVE_ROT
AXIS_1="Y"
ID="4"
NAME="seat_ori"
R1="-0.087266"
/>
<ORIENTATION.SUCCESIVE_ROT
AXIS_1="Z"
ID="5"
NAME="back_ori"
R1="1.5708"
/>
<ORIENTATION.SUCCESIVE_ROT
NAME="anti_tipper_ori"
ID="6"
AXIS_1="Y"
R1="-1.309"
/>
<ORIENTATION.SUCCESIVE_ROT
NAME="seatback_ori"
ID="7"
AXIS_1="X"
R1="0.087266"
/>
<ORIENTATION.SUCCESIVE_ROT
NAME="wheelchair_ori"
ID="8"
AXIS_1="Z"
R1="0.5236"
/>
<ORIENTATION.SUCCESIVE_ROT
NAME="SB_trans_jnt_ori"
ID="9"
AXIS_1="Y"
R1="0"
AXIS_2="Z"
R3="0"
/>
<CHARACTERISTIC.LOAD
ID="50"
LOAD_FUNC="back_attachment_load"
NAME="back_attachment_char"
/>
/>
<CHARACTERISTIC.LOAD
ID="51"
LOAD_FUNC="seat_attachment_load"
NAME="seat_attachment_char"
/>
<CHARACTERISTIC.LOAD
ELAS_LIMIT=".6"
HYS_MODEL="1"
HYS_SLOPE="1E6"
NAME="sb_joint_load"
DAMP_COEF="1000"
UNLOAD_FUNC="seatback_stiffness_unload"
LOAD_FUNC="Seatback_stiffness_load"
ID="52"
/>
<CHARACTERISTIC.LOAD
HYS_SLOPE="5E4"
HYS_MODEL="1"
UNLOAD_FUNC="Headrest_joint_unload2"
LOAD_FUNC="Headrest_joint_load2"
NAME="Headrest_joint_rstrnt_char"
ID="53"
/>
<CHARACTERISTIC.CONTACT
CONTACT_MODEL="FORCE"
ID="1"
LOAD_FUNC="rear_wheel_load"
NAME="rwh_contact"
/>
<CHARACTERISTIC.CONTACT
CONTACT_MODEL="FORCE"
ID="2"
LOAD_FUNC="front_wheel_load"
NAME="fwh_contact"
/>
<CHARACTERISTIC.CONTACT
CONTACT_MODEL="FORCE"
ID="3"
LOAD_FUNC="wcseat_load"
NAME="wcseat_contact"
/>
<CHARACTERISTIC.CONTACT
DAMP_COEF="800"
CONTACT_MODEL="FORCE"
ID="4"
LOAD_FUNC="wcbk_load2"
NAME="wcbk_contact"
/>
<CHARACTERISTIC.CONTACT
CONTACT_MODEL="FORCE"
ID="5"
LOAD_FUNC="footrest_load"
NAME="footrest_contact"
/>
<CHARACTERISTIC.CONTACT
CONTACT_MODEL="FORCE"
ID="6"
LOAD_FUNC="armrest_load"
NAME="armrest_contact"
/>
<FUNCTION.XY
ID="1"
NAME="rear_wheel_load"
>
<TABLE
TYPE="XY_PAIR"
>
<![CDATA[
| XI      YI      |

```

```

0.00000000E+000 0.00000000E+000
6.00000000E-002 2.00000000E+004
]]>
</TABLE>
</FUNCTION.XY>
<FUNCTION.XY
ID="2"
NAME="front_wheel_load"
>
<TABLE
TYPE="XY_PAIR"
>
<![CDATA[
| XI      YI |
0.00000000E+000 0.00000000E+000
1E-3 2000
2.00000000E-002 1.00000000E+006
]]>
</TABLE>
</FUNCTION.XY>
<FUNCTION.XY
ID="3"
NAME="wcseat_load"
>
<TABLE
TYPE="XY_PAIR"
>
<![CDATA[ | XI      YI |
0.00000000E+000 0.00000000E+000
1.00000000E-001 3.0E3
]]>
</TABLE>
</FUNCTION.XY>
<FUNCTION.XY
ID="4"
NAME="wback_load"
>
<TABLE
TYPE="XY_PAIR"
>
<![CDATA[
| XI      YI |
0.00000000E+000 0.00000000E+000
1.00000000E-001 3.0E3
]]>
</TABLE>
</FUNCTION.XY>
<FUNCTION.XY
ID="53"
NAME="wback_load2"
>
<TABLE
TYPE="XY_PAIR"
>
<![CDATA[
| XI      YI |
0.00000000E+000 0.00000000E+000
.05 500
2.00000000E-001 3.0E3
]]>
</TABLE>
</FUNCTION.XY>
<FUNCTION.XY
ID="5"
NAME="footrest_load"
>
<TABLE
TYPE="XY_PAIR"
>
<![CDATA[

```

```

| XI      YI |
0.00000000E+000 0.00000000E+000
1.00000000E-001 2.00000000E+004
]]>
</TABLE>
</FUNCTION.XY>
<FUNCTION.XY
ID="6"
NAME="armrest_load"
>
<TABLE
TYPE="XY_PAIR"
>
<![CDATA[
| XI      YI |
0.00000000E+000 0.00000000E+000
1.50000000E-001 1.00000000E+004
]]>
</TABLE>
</FUNCTION.XY>
<FUNCTION.XY
ID="50"
NAME="back_attachment_load"
>
<TABLE
TYPE="XY_PAIR"
>
<![CDATA[
| XI      YI |
-1.00000000E-003 -1.00000000E+005
1.00000000E-003 1.00000000E+005
]]>
</TABLE>
</FUNCTION.XY>
<FUNCTION.XY
ID="51"
NAME="seat_attachment_load"
>
<TABLE
TYPE="XY_PAIR"
>
<![CDATA[
| XI      YI |
-1.00000000E-003 -1.00000000E+005
1.00000000E-003 1.00000000E+005
]]>
</TABLE>
</FUNCTION.XY>
<FUNCTION.XY
ID="40"
NAME="Seatback_stiffness_load"
>
<TABLE
TYPE="XY_PAIR"
>
<![CDATA[
| XI      YI |
0.00000000E+000 0.00000000E+000
1.60000000E-001 2.50000000E+001
1.00000000E-000 12.0000E+004
]]>
</TABLE>
</FUNCTION.XY>
<FUNCTION.XY
NAME="seatback_stiffness_unload"
ID="52"
>
<TABLE
TYPE="XY_PAIR"

```

```

>
<![CDATA[
  | XI      YI |
  0.00000000E+000 0.00000000E+000
  1.60000000E-001 2.00000000E+001

  1.00000000E-000 10.0000E+004
]]>
</TABLE>
</FUNCTION.XY>
<FUNCTION.XY
  NAME="Headrest_joint_load2"
  ID="56"
>
<TABLE
  TYPE="XY_PAIR"
>
<![CDATA[
  | XI      YI |
  0 0
  .017453 30
  .034907 100
  .05236 300
  .087266 1000
]]>
</TABLE>
</FUNCTION.XY>
<FUNCTION.XY
  NAME="Headrest_joint_unload2"
  ID="57"
>
<TABLE
  TYPE="XY_PAIR"
>
<![CDATA[
  | XI      YI |
  0 0
  .017453 15
  .034907 50
  .05236 150
  .087266 500
]]>
</TABLE>
</FUNCTION.XY>
<FUNCTION.XY
  NAME="Headrest_joint_load"
  ID="54"
>
<TABLE
  TYPE="XY_PAIR"
>
<![CDATA[
  | XI      YI |
  0 0
  .017453 15
  .034907 50
  .05236 150
  .087266 500
]]>
</TABLE>
</FUNCTION.XY>
<FUNCTION.XY
  NAME="Headrest_joint_unload"
  ID="55"
>
<TABLE
  TYPE="XY_PAIR"
>
<![CDATA[
  | XI      YI |
  0 0
  .017453 7.5
  .034907 25
  .05236 75
  .087266 250
]]>
</TABLE>
</FUNCTION.XY>
<GROUP_MB
  ID="1"
  NAME="R_rear_wh_surface"
  SURFACE_LIST="RRear_wheel_surface"
/>
<GROUP_MB
  ID="10"
  NAME="L_rear_wh_surface"
  SURFACE_LIST="LRear_wheel_surface"
/>
<GROUP_MB
  ID="2"
  NAME="front_wh_surfaces"
  SURFACE_LIST="LFront_wheel_surface
RFront_wheel_surface"
/>
<GROUP_MB
  ID="3"
  NAME="wcseat_contact_surface"
  SURFACE_LIST="wcseat_surface"
/>
<GROUP_MB
  ID="4"
  NAME="wback_contact_surface"
  SURFACE_LIST="wback_surface"
/>
<GROUP_MB
  ID="5"
  NAME="footrest_contact_surface"
  SURFACE_LIST="footrest_surface"
/>
<GROUP_MB
  ID="6"
  NAME="armrest_surfaces"
  SURFACE_LIST="l_arm_r_arm"
/>
<GROUP_MB
  ID="7"
  NAME="tiepoint_contact_surface"
  SURFACE_LIST="ALL"
/>
<GROUP_MB
  SURFACE_LIST="l_anit_tipper_wheel
l_anit_tipper_bottom l_anit_tipper_top r_anit_tipper_wheel
r_anit_tipper_bottom r_anit_tipper_top"
  NAME="anti_tipper_surface"
  ID="8"
/>
<GROUP_MB
  SURFACE_LIST="Headrest_pad"
  NAME="headrest_group"
  ID="9"
/>
</SYSTEM.MODEL>
<SYSTEM.MODEL
  ID="4"
  NAME="Hybrid_III_6_year_old"
/>
<SYSTEM.MODEL
  ID="5"
  NAME="lap_belt"
>

```

```

<GROUP_FE
  NAME="lapbelt_fe_group"
  ID="1"
  PART_LIST="ALL"
  FE_MODEL="Belt_1_fem"
  CONTACT_CHAR="BeltContact_chr"
/>
<CHARACTERISTIC.CONTACT
  ID="3"
  NAME="BeltContact_chr"
  CONTACT_MODEL="FORCE"
  LOAD_FUNC="BeltContact_fun"
/>
<FUNCTION.XY
  ID="1"
  NAME="BeltContact_fun"
  >
  <TABLE
    TYPE="XY_PAIR"
  >
<![CDATA[
  | XI  YI |
    0.0  0.0
    0.001 1000.0
]]>
  </TABLE>
</FUNCTION.XY>
<FE_MODEL
  ID="2"
  NAME="Belt_1_fem"
  >
  <CONTROL_FE_MODEL
ALPHA_REL_BODY="/sled_system/sled_body"
  ALPHA_COEF="800"
/>
  <CONTROL_FE_TIME_STEP
    REDUCTION_FACTOR="0.9"
    CRITICAL_ELEMENTS="20"
    TIME_INT_MTH="NORMAL"
  >
  <TABLE
    TYPE="COORDINATE.CARTESIAN"
  >
  <TABLE
    TYPE="ELEMENT.TRIAD3"
  >
  <PROPERTY.MEM3
    ID="1"
    NAME="Belt_prp"
    THICK="0.002000"
    STRAIN_FORM="GREEN"
  >
  <MATERIAL.HYSIS0
    ID="1"
    NAME="Belt_mat"
    CHAR="fe_belt_load_unload"
    DENSITY="800"
    TENSION_ONLY="ON"
    REDUCTION_FACTOR="0.010000"
  >
  <CHARACTERISTIC.MATERIAL
    ID="1"
    NAME="fe_belt_load_unload"
    LOAD_FUNC="fe_loading"
    UNLOAD_FUNC="fe_unloading"
    HYS_SLOPE="6.0e9"
    ELAS_LIMIT="0"
    HYS_MODEL="1"
  >
</FUNCTION.XY
  ID="1"
  NAME="fe_loading"
  >
  <TABLE
    TYPE="XY_PAIR"
  >
<![CDATA[
  | XI  YI |
    0.000 0.000
    0.021 2.0E7
    0.030 5.9E7
    0.040 8.0E7
    0.050 9.4E7
    0.060 1.1E8
    0.070 1.2E8
    0.080 1.3E8
    0.090 1.4E8
    0.100 1.6E8
    0.110 1.7E8
    0.120 1.9E8
    0.125 2.0E8
]]>
  </TABLE>
</FUNCTION.XY>
<FUNCTION.XY
  ID="2"
  NAME="fe_unloading"
  >
  <TABLE
    TYPE="XY_PAIR"
  >
<![CDATA[
  | XI  YI |
    0.000 0.000
    0.100 2.0E7
]]>
  </TABLE>
</FUNCTION.XY>
<PART
  ID="1"
  MATERIAL="Belt_mat"
  PROPERTY="Belt_prp"
/>
<RIGID_ELEMENT
  ID="1"
  NAME="Rigid_Belt_Ends_1"
  ELEMENT_LIST="1 2 "
/>
<RIGID_ELEMENT
  ID="2"
  NAME="Rigid_Belt_Ends_2"
  ELEMENT_LIST="3 4 "
/>
</FE_MODEL>
<INITIAL.FE_MODEL
  FE_MODEL="Belt_1_fem"
  POS="0.0 0.0 0.0"
/>
<BELT
  MASS_SPECIFIC=".04"
  ID="5"
  NAME="Belt_System_5"
  >
  <BELT_SEGMENT
    INITIAL_STRAIN=".04"
    ID="1"
    NAME="Belt_Segment_1"
  >
POINT_REF_1="/sled_system/L_SB_Floor_anchor_pnt"
  POINT_REF_2="FE_Connection_6004_pnt"

```

```

    CHAR="belt_loading"
  />
</BELT>
<BELT
  MASS_SPECIFIC=".04"
  ID="6"
  NAME="Belt_System_6"
  >
  <BELT_SEGMENT
    INITIAL_STRAIN=".04"
    ID="2"
    NAME="Belt_Segment_2"
  >
POINT_REF_1="/sled_system/RFloor_anchor_pnt"
  POINT_REF_2="FE_Connection_6005_pnt"
  CHAR="belt_loading"
  />
</BELT>
<POINT_OBJECT.MB
  ID="6004"
  NAME="FE_Connection_6004_pnt"
  FE_MODEL="Belt_1_fem"
  NODE="17"
  />
<POINT_OBJECT.MB
  ID="6005"
  NAME="FE_Connection_6005_pnt"
  FE_MODEL="Belt_1_fem"
  NODE="34"
  />
<CHARACTERISTIC.LOAD
  ID="8127"
  NAME="belt_loading"
  LOAD_FUNC="belt_load2"
  UNLOAD_FUNC="belt_unload4"
  HYS_MODEL="1"
  HYS_SLOPE="1E6"
  ELAS_LIMIT="0"
  />
<FUNCTION.XY
  ID="8056"
  NAME="belt_load"
  >
  <TABLE
    TYPE="XY_PAIR"
  >
<![CDATA[| XI YI |
0.0  0.0
0.021 1000.0
0.030 2950.0
0.040 4000.0
0.050 4700.0
0.060 5320.0
0.070 6000.0
0.080 6600.0
0.090 7250.0
0.100 8000.0
0.110 8680.0
0.120 9500.0
0.126 10000.0
]]>
  </TABLE>
</FUNCTION.XY>
<FUNCTION.XY
  ID="8058"
  NAME="belt_load2"
  >
  <TABLE
    TYPE="XY_PAIR"
  >
    <![CDATA[| XI YI |
0.0  0.0
0.02 2000.0
0.030 4000.0
0.040 8000.0
0.050 16000
]]>
    </TABLE>
  </FUNCTION.XY>
<FUNCTION.XY
  ID="8057"
  NAME="belt_unload"
  >
  <TABLE
    TYPE="XY_PAIR"
  >
    <![CDATA[| XI YI |
0.0  0.0
0.1 1000.0]]>
  </TABLE>
  </FUNCTION.XY>
<FUNCTION.XY
  ID="8059"
  NAME="belt_unload2"
  >
  <TABLE
    TYPE="XY_PAIR"
  >
    <![CDATA[| XI YI |
0.0  0.0
.1 8000]]>
  </TABLE>
  </FUNCTION.XY>
<FUNCTION.XY
  ID="8060"
  NAME="belt_unload3"
  >
  <TABLE
    TYPE="XY_PAIR"
  >
    <![CDATA[| XI YI |
0.0  0.0
.1 6000]]>
  </TABLE>
  </FUNCTION.XY>
<FUNCTION.XY
  ID="8061"
  NAME="belt_unload4"
  >
  <TABLE
    TYPE="XY_PAIR"
  >
    <![CDATA[| XI YI |
0.0  0.0
.1 4000]]>
  </TABLE>
  </FUNCTION.XY>
<OUTPUT_BELT
  FILTER="CFC60"
  NAME="lap_belt_1"
  ID="1"
  INPUT_CLASS="BELT_SEGMENT"
  INPUT_REF="Belt_System_5/Belt_Segment_1"
  />
<OUTPUT_BELT
  FILTER="CFC60"
  NAME="lap_belt_2"
  ID="2"
  INPUT_CLASS="BELT_SEGMENT"
  INPUT_REF="Belt_System_6/Belt_Segment_2"

```

```

/>
</SYSTEM.MODEL>
<SYSTEM.MODEL
  ID="6"
  NAME="shoulder_belt"
  >
  <FE_MODEL
    ID="3"
    NAME="Belt_1_fem"
    >
    <CONTROL_FE_MODEL
      ALPHA_REL_BODY="/sled_system/sled_body"
      ALPHA_COEF="400"
    >
    <CONTROL_FE_TIME_STEP
      REDUCTION_FACTOR="0.9"
      CRITICAL_ELEMENTS="20"
      TIME_INT_MTH="NORMAL"
    >
    <TABLE
      TYPE="COORDINATE.CARTESIAN"
    >
    <TABLE
      TYPE="ELEMENT.TRIAD3"
    >
    <PROPERTY.MEM3
      ID="1"
      NAME="Belt_prp"
      THICK="0.002000"
      STRAIN_FORM="GREEN"
    >
    <MATERIAL.HYSISO
      ID="1"
      NAME="Belt_mat"
      CHAR="fe_belt_load_unload"
      DENSITY="800"
      TENSION_ONLY="ON"
      REDUCTION_FACTOR="0.010000"
    >
    <CHARACTERISTIC.MATERIAL
      ID="1"
      NAME="fe_belt_load_unload"
      LOAD_FUNC="fe_loading"
      UNLOAD_FUNC="fe_unloading"
      HYS_SLOPE="6.0e9"
      ELAS_LIMIT="0"
      HYS_MODEL="1"
    >
    <FUNCTION.XY
      ID="1"
      NAME="fe_loading"
    >
    <TABLE
      TYPE="XY_PAIR"
    >
    <![CDATA[ | XI YI |
0.000 0.000
0.021 2.0E7
0.030 5.9E7
0.040 8.0E7
0.050 9.4E7
0.060 1.1E8
0.070 1.2E8
0.080 1.3E8
0.090 1.4E8
0.100 1.6E8
0.110 1.7E8
0.120 1.9E8
0.125 2.0E8

```

```

]]>
  </TABLE>
  </FUNCTION.XY>
  <FUNCTION.XY
    ID="2"
    NAME="fe_unloading"
    >
    <TABLE
      TYPE="XY_PAIR"
    >
    <![CDATA[ | XI YI |
0.000 0.000
0.100 2.0E7
]]>
  </TABLE>
  </FUNCTION.XY>
  <PART
    ID="1"
    MATERIAL="Belt_mat"
    PROPERTY="Belt_prp"
  >
  <RIGID_ELEMENT
    ID="1"
    NAME="Rigid_Belt_Ends_1"
    ELEMENT_LIST="1 2 "
  >
  <RIGID_ELEMENT
    ID="2"
    NAME="Rigid_Belt_Ends_2"
    ELEMENT_LIST="3 4 "
  >
  </FE_MODEL>
  <GROUP_FE
    PART_LIST="ALL"
    CONTACT_CHAR="BeltContact_chr"
    FE_MODEL="Belt_1_fem"
    NAME="shoulderbelt_fe_group"
    ID="1"
  >
  <CHARACTERISTIC.CONTACT
    ID="3"
    NAME="BeltContact_chr"
    CONTACT_MODEL="FORCE"
    LOAD_FUNC="BeltContact_fun"
  >
  <FUNCTION.XY
    ID="1"
    NAME="BeltContact_fun"
  >
  <TABLE
    TYPE="XY_PAIR"
  >
  <![CDATA[
| XI YI |
0.0 0.0
0.001 1000.0
0.1 1000
]]>
  </TABLE>
  </FUNCTION.XY>
  <INITIAL.FE_MODEL
    FE_MODEL="Belt_1_fem"
    POS="0.0 0.0 0.0"
  >
  <BELT
    MASS_SPECIFIC=".04"
    ID="6"
    NAME="Belt_System_6"

```

```

>
<BELT_SEGMENT
  ID="1"
  NAME="Belt_Segment_1"
  POINT_REF_1="/sled_system/D_ring_pnt"
  POINT_REF_2="FE_Connection_6006_pnt"
  CHAR="belt_loading"
/>
</BELT>
<BELT
  MASS_SPECIFIC=".04"
  ID="7"
  NAME="Belt_System_7"
  >
  <BELT_SEGMENT
    ID="2"
    NAME="Belt_Segment_2"
    POINT_REF_1="/sled_system/LFloor_anchor_pnt"
    POINT_REF_2="FE_Connection_6007_pnt"
    CHAR="belt_loading"
  />
</BELT>
<POINT_OBJECT.MB
  ID="6006"
  NAME="FE_Connection_6006_pnt"
  FE_MODEL="Belt_1_fem"
  NODE="22"
/>
<POINT_OBJECT.MB
  ID="6007"
  NAME="FE_Connection_6007_pnt"
  FE_MODEL="Belt_1_fem"
  NODE="44"
/>
<CHARACTERISTIC.LOAD
  ID="8127"
  NAME="belt_loading"
  LOAD_FUNC="belt_load"
  UNLOAD_FUNC="belt_unload"
  HYS_MODEL="1"
  HYS_SLOPE="3.0e5"
  ELAS_LIMIT="0"
/>
<FUNCTION.XY
  ID="8056"
  NAME="belt_load"
  >
  <TABLE
    TYPE="XY_PAIR"
    >
    <![CDATA[| XI YI |
0.0 0.0
0.021 1000.0
0.030 2950.0
0.040 4000.0
0.050 4700.0
0.060 5320.0
0.070 6000.0
0.080 6600.0
0.090 7250.0
0.100 8000.0
0.110 8680.0
0.120 9500.0
0.126 10000.0
]]>
  </TABLE>
</FUNCTION.XY>
<FUNCTION.XY
  ID="8057"
  NAME="belt_unload"
  >
  <TABLE
    TYPE="XY_PAIR"
    >
    <![CDATA[| XI YI |
0.0 0.0
0.1 1000.0]]>
  </TABLE>
</FUNCTION.XY>
</SYSTEM.MODEL>
<LOAD.SYSTEM_ACC
  DESCRIPTION="crash_pulse"
  AX_FUNC="/crashpulse_smoothed"
  SYSTEM_LIST="sled_system"
/>
<LOAD.SYSTEM_ACC
  DESCRIPTION="gravity"
  SYSTEM_LIST="/Hybrid_III_6_year_old
/wheelchair_system/lap_belt/shoulder_belt"
  AZ_FUNC="gravity"
/>
<INITIAL.JOINT_VEL
  DESCRIPTION="initial sled velocity"
  V1="3.9"
  JOINT="/sled_system/sled_joint"
/>
<INITIAL.JOINT_VEL
  V1="3.9"
  DESCRIPTION="initial wheelchair velocity"
  JOINT="/wheelchair_system/CG_ref_joint"
/>
<INITIAL.JOINT_VEL
  V1="3.9"
  DESCRIPTION="intial ATD velocity"
  JOINT="/Hybrid_III_6_year_old/Dummy_jnt"
/>
<BELT
  MASS_SPECIFIC=".04"
  NAME="RFront_tiedown_belt"
  ID="1"
  >
  <BELT_SEGMENT
    INITIAL_STRAIN=".005"
    NAME="Right_front_seg"
    ID="1"
    POINT_REF_1="/sled_system/RFront_sled_secure_pnt"
    POINT_REF_2="/wheelchair_system/RFront_WCsecurement_pnt"
    CHAR="/front_tiedown_exp_char"
  />
</BELT>
<BELT
  MASS_SPECIFIC=".04"
  NAME="LFront_tiedown_belt"
  ID="2"
  >
  <BELT_SEGMENT
    INITIAL_STRAIN=".005"
    NAME="LFront_tiedown"
    ID="1"
    POINT_REF_1="/sled_system/LFront_sled_secure_pnt"
    POINT_REF_2="/wheelchair_system/LFront_WCsecurement_pnt"
    CHAR="/front_tiedown_exp_char"
  />
</BELT>

```

```

</BELT>
<BELT
  MASS_SPECIFIC=".04"
  NAME="RRear_tiedown_belt"
  ID="3"
>
<BELT_SEGMENT
  INITIAL_STRAIN=".005"
  NAME="RRear_tiedown_seg"
  ID="1"
POINT_REF_1="/sled_system/RRear_sled_secure_pnt"
POINT_REF_2="/wheelchair_system/RRear_WCsecurement_pnt"
  CHAR="/rear_tiedown_exp_char"
/>
</BELT>
<BELT
  MASS_SPECIFIC=".04"
  NAME="LRear_tiedown_belt"
  ID="4"
>
<BELT_SEGMENT
  INITIAL_STRAIN=".005"
  NAME="LRear_tiedown_seg"
  ID="1"
POINT_REF_1="/sled_system/LRear_sled_secure_pnt"
POINT_REF_2="/wheelchair_system/LRear_WCsecurement_pnt"
  CHAR="/rear_tiedown_exp_char"
/>
</BELT>
<OUTPUT_BELT
  FILTER="CFC60"
  NAME="Right_Front_tiedown_out"
  ID="1"
  INPUT_CLASS="BELT_SEGMENT"
INPUT_REF="/RFront_tiedown_belt/Right_front_seg"
/>
<OUTPUT_BELT
  FILTER="CFC60"
  NAME="Left_front_tiedown_out"
  ID="3"
  INPUT_CLASS="BELT_SEGMENT"
INPUT_REF="LFront_tiedown_belt/LFront_tiedown"
/>
<OUTPUT_BELT
  FILTER="CFC60"
  NAME="RRear_tiedown_output"
  ID="5"
  INPUT_CLASS="BELT_SEGMENT"
INPUT_REF="RRear_tiedown_belt/RRear_tiedown_seg"
/>
<OUTPUT_BELT
  FILTER="CFC60"
  NAME="LRear_tiedown_out"
  ID="6"
  INPUT_CLASS="BELT_SEGMENT"
INPUT_REF="LRear_tiedown_belt/LRear_tiedown_seg"
/>
<OUTPUT_CONTACT
  FILTER="CFC60"
  SUM="ON"
  NAME="seatback_load_output"
  ID="1"
  CONTACT_LIST="/atd_wheelchairSB_cnt "
/>
<OUTPUT_CONTACT
  FILTER="CFC60"
  NAME="headrest_load_output"
  ID="2"
  SUM="ON"
  CONTACT_LIST="/FEhead_headrest
/mbHead_headrest"
/>
<OUTPUT_CONTACT
  NAME="RearWheel_load_output"
  ID="3"
  CONTACT_LIST="/L_Rear_wheel_contact
/R_Rear_wheel_contact"
/>
<OUTPUT_JOINT_DOF
  NAME="joint_position_outputs"
JOINT_LIST="/Hybrid_III_6_year_old/NeckPivotLow_jnt
/Hybrid_III_6_year_old/NeckPivotMid_jnt
/Hybrid_III_6_year_old/NeckPivotUp_jnt"
  ID="1"
  SIGNAL_TYPE="POS"
/>
<CHARACTERISTIC_LOAD
  ELAS_LIMIT="0.0"
  NAME="belt_char_load"
  LOAD_FUNC="belt_load_fund"
  UNLOAD_FUNC="belt_unload_func"
  HYS_MODEL="1"
  HYS_SLOPE="3.0E5"
  ID="1"
/>
<CHARACTERISTIC_LOAD
  DAMP_COEF="800"
  LOAD_FUNC="/tiedown_load"
  NAME="tiedown_char"
  ID="2"
/>
<CHARACTERISTIC_LOAD
  DAMP_COEF="800"
  LOAD_FUNC="/Front_tiedown_load"
  NAME="front_tiedown_char"
  ID="4"
/>
<CHARACTERISTIC_LOAD
  ELAS_LIMIT="0.0"
  NAME="belt_char_load2"
  LOAD_FUNC="/belt_load_func2"
  UNLOAD_FUNC="belt_unload_func"
  HYS_MODEL="1"
  HYS_SLOPE="2.3E5"
  ID="6"
/>
<CHARACTERISTIC_LOAD
  ELAS_LIMIT="0.0"
  NAME="belt_char_load3"
  LOAD_FUNC="/belt_load_func2"
  UNLOAD_FUNC="/belt_unload_func3"
  HYS_MODEL="1"
  HYS_SLOPE="2.3E5"
  ID="7"
/>
<CHARACTERISTIC_LOAD
  DAMP_COEF="200"
  HYS_MODEL="1"
  HYS_SLOPE="8E5"
  LOAD_FUNC="/front_tiedown_load_12"
  UNLOAD_FUNC="/front_tiedown_exp_unload"

```



```

NAME="front_tiedown_exp_char"
ID="9"
/>
<CHARACTERISTIC.LOAD
DAMP_COEF="200"
HYS_SLOPE="1.95E5"
HYS_MODEL="1"
UNLOAD_FUNC="/rear_tiedown_exp_unload"
LOAD_FUNC="/rear_tiedown_exp_load"
NAME="rear_tiedown_exp_char"
ID="10"
/>
<CHARACTERISTIC.CONTACT
DAMP_COEF="800"
NAME="wheel_cnt_def"
ID="3"
CONTACT_MODEL="FORCE"
LOAD_FUNC="/soft_wheel_cnt_func2"
/>
<CHARACTERISTIC.CONTACT
DAMP_COEF="100"
NAME="atd_wc_chr"
ID="5"
CONTACT_MODEL="FORCE"
LOAD_FUNC="/atd_wc_load"
/>
<CHARACTERISTIC.CONTACT
HYS_SLOPE="2E4"
HYS_MODEL="1"
DAMP_COEF="50"
NAME="headrest_contact"
ID="8"
UNLOAD_FUNC="/headrest_unloading5"
CONTACT_MODEL="FORCE"
LOAD_FUNC="/headrest_loading5"
/>
<CHARACTERISTIC.CONTACT
NAME="atd_wcSB_chr"
ID="11"
CONTACT_MODEL="FORCE"
LOAD_FUNC="/atd_wcSB_load"
/>
<CHARACTERISTIC.CONTACT
CONTACT_MODEL="FORCE"
HYS_MODEL="2"
HYS_SLOPE="1.000000E+010"
ID="12"
LOAD_FUNC="dummy_contact_func"
NAME="dummy_contact"
/>
<CHARACTERISTIC.CONTACT
NAME="knee_Tibia_Seat_cnt"
ID="13"
CONTACT_MODEL="FORCE"
LOAD_FUNC="/knee_loading"
/>
<CHARACTERISTIC.CONTACT
NAME="anti-tipper_cnt"
ID="14"
CONTACT_MODEL="FORCE"
LOAD_FUNC="/anti_tipper_fnc3"
/>
<CONTACT.MB_FE
NAME="pelvis_lapbelt_cnt"
ID="3"
MASTER_SURFACE="/Hybrid_III_6_year_old/Pelvis_gmb"
SLAVE_SURFACE="/lap_belt/lapbelt_fe_group"
>
<CONTACT_FORCE.CHAR
CONTACT_TYPE="SLAVE"
/>
</CONTACT.MB_FE>
<CONTACT.MB_FE
NAME="abdomen_lapbelt_cnt"
ID="4"
MASTER_SURFACE="/Hybrid_III_6_year_old/Abdomen_gmb"
SLAVE_SURFACE="/lap_belt/lapbelt_fe_group"
>
<CONTACT_FORCE.CHAR
CONTACT_TYPE="SLAVE"
/>
</CONTACT.MB_FE>
<CONTACT.MB_FE
NAME="femurs_lapbelt_cnt"
ID="5"
MASTER_SURFACE="/Hybrid_III_6_year_old/FemurL_gmb
/Hybrid_III_6_year_old/FemurR_gmb"
SLAVE_SURFACE="/lap_belt/lapbelt_fe_group"
>
<CONTACT_FORCE.CHAR
CONTACT_TYPE="SLAVE"
/>
</CONTACT.MB_FE>
<CONTACT.MB_FE
NAME="atd_shoulderbelt_cnt"
ID="6"
MASTER_SURFACE="/Hybrid_III_6_year_old/Dummy_gmb"
SLAVE_SURFACE="/shoulder_belt/shoulderbelt_fe_group"
>
<CONTACT_FORCE.CHAR
CONTACT_TYPE="SLAVE"
/>
</CONTACT.MB_FE>
<CONTACT.MB_FE
NAME="neck_shoulderbelt_cnt"
ID="7"
MASTER_SURFACE="/Hybrid_III_6_year_old/Neck_gmb"
SLAVE_SURFACE="/shoulder_belt/shoulderbelt_fe_group"
>
<CONTACT_FORCE.CHAR
CONTACT_TYPE="SLAVE"
/>
</CONTACT.MB_FE>
<CONTACT.MB_FE
NAME="feHead_seatback_cnt"
ID="14"
MASTER_SURFACE="/wheelchair_system/wcseat_contact_surface"
SLAVE_SURFACE="/Hybrid_III_6_year_old/Head_gfe"
>
<CONTACT_FORCE.CHAR
USER_CHAR="headrest_contact"
CONTACT_TYPE="USER_SLAVE"
/>
</CONTACT.MB_FE>
<CONTACT.MB_FE
NAME="shoulder_shoulderbelt_cnt"
ID="16"
MASTER_SURFACE="/Hybrid_III_6_year_old/Rshoulder_gmb
/Hybrid_III_6_year_old/ArmLowR_gmb"

```

```

SLAVE_SURFACE="/shoulder_belt/shoulderbelt_fe_group"
  >
  <CONTACT_FORCE.CHAR
    CONTACT_TYPE="SLAVE"
  />
</CONTACT.MB_FE>
<CONTACT.MB_FE
  NAME="hands_lapbelt_cnt"
  ID="17"

```

```

MASTER_SURFACE="/Hybrid_III_6_year_old/Lhand_gmb
/Hybrid_III_6_year_old/Rhand_gmb"
  SLAVE_SURFACE="/lap_belt/lapbelt_fe_group"
  >
  <CONTACT_FORCE.CHAR
    CONTACT_TYPE="SLAVE"
  />
</CONTACT.MB_FE>
<CONTACT.MB_FE
  NAME="FEhead_headrest"
  ID="21"

```

```

MASTER_SURFACE="/wheelchair_system/headrest_group"
SLAVE_SURFACE="/Hybrid_III_6_year_old/Head_gfe"
  >
  <CONTACT_FORCE.CHAR
    CONTACT_AREA=".01"
    USER_CHAR="/headrest_contact"
    CONTACT_TYPE="USER_MASTER"
  />
</CONTACT.MB_FE>
<CONTACT.MB_MB
  INITIAL_TYPE="CORRECT"
  DAMP_COEF="200"
  FRIC_COEF=".7"
  NAME="Front_wheel_contact"
  ID="1"
  MASTER_SURFACE="/sled_system/sled_mbg"

```

```

SLAVE_SURFACE="/wheelchair_system/front_wh_surfaces"
  >
  <CONTACT_FORCE.CHAR
    USER_CHAR="/wheel_cnt_def"
    CONTACT_TYPE="USER_SLAVE"
  />
</CONTACT.MB_MB>
<CONTACT.MB_MB
  INITIAL_TYPE="CORRECT"
  DAMP_COEF="800"
  FRIC_COEF=".7"
  NAME="R_Rear_wheel_contact"
  ID="2"
  MASTER_SURFACE="/sled_system/sled_mbg"

```

```

SLAVE_SURFACE="/wheelchair_system/R_rear_wh_surface"
  >
  <CONTACT_FORCE.CHAR
    CONTACT_TYPE="USER_SLAVE"
    USER_CHAR="/wheel_cnt_def"
  />
</CONTACT.MB_MB>
<CONTACT.MB_MB
  INITIAL_TYPE="CORRECT"
  DAMP_COEF="200"
  NAME="atd_wheelchairseat_cnt"
  FRIC_COEF=".4"
  ID="8"

```

```

MASTER_SURFACE="/Hybrid_III_6_year_old/Dummy_gmb"

```

```

SLAVE_SURFACE="/wheelchair_system/wcseat_contact_surface"
  >
  <CONTACT_FORCE.CHAR
    USER_CHAR="/dummy_contact"
    CONTACT_TYPE="USER_SLAVE"
  />
</CONTACT.MB_MB>
<CONTACT.MB_MB

```

```

SLAVE_SURFACE="/wheelchair_system/L_rear_wh_surface
/wheelchair_system/R_rear_wh_surface
/wheelchair_system/armrest_surfaces
/wheelchair_system/wcback_contact_surface
/wheelchair_system/wcseat_contact_surface"
  DAMP_COEF="800"
  NAME="arms_wheelchair_cnt"
  FRIC_COEF=".8"
  ID="9"

```

```

MASTER_SURFACE="/Hybrid_III_6_year_old/ArmLowL_gmb
/Hybrid_III_6_year_old/ArmLowR_gmb
/Hybrid_III_6_year_old/ArmUpL_gmb
/Hybrid_III_6_year_old/ArmUpR_gmb"
  >
  <CONTACT_FORCE.CHAR
    CONTACT_TYPE="SLAVE"
  />
</CONTACT.MB_MB>
<CONTACT.MB_MB
  DAMP_COEF="200"
  NAME="legs_wcSeat_cnt"
  FRIC_COEF=".4"
  ID="10"

```

```

MASTER_SURFACE="/Hybrid_III_6_year_old/FemurL_gmb
/Hybrid_III_6_year_old/FemurR_gmb"

```

```

SLAVE_SURFACE="/wheelchair_system/wcseat_contact_surface"
  >
  <CONTACT_FORCE.CHAR
    CONTACT_TYPE="SLAVE"
  />
</CONTACT.MB_MB>
<CONTACT.MB_MB
  DAMP_COEF="800"
  FRIC_COEF=".2"
  NAME="tibias_wcSeat_cnt"
  ID="11"

```

```

MASTER_SURFACE="/Hybrid_III_6_year_old/KneeL_gmb
/Hybrid_III_6_year_old/KneeR_gmb
/Hybrid_III_6_year_old/TibiaL_gmb
/Hybrid_III_6_year_old/TibiaR_gmb"

```

```

SLAVE_SURFACE="/wheelchair_system/wcseat_contact_surface"
  >
  <CONTACT_FORCE.CHAR
    USER_CHAR="/knee_Tibia_Seat_cnt"
    CONTACT_TYPE="USER_SLAVE"
  />
</CONTACT.MB_MB>
<CONTACT.MB_MB
  DAMP_COEF="800"
  FRIC_COEF=".8"

```

```

NAME="foot_contacts_cnt"
ID="12"

MASTER_SURFACE="/Hybrid_III_6_year_old/ShoeL_gmb
/Hybrid_III_6_year_old/ShoeR_gmb"

SLAVE_SURFACE="/wheelchair_system/footrest_contact_surfac
e/wheelchair_system/wcseat_contact_surface"
>
<CONTACT_FORCE.CHAR
CONTACT_TYPE="MASTER"
/>
</CONTACT.MB_MB>
<CONTACT.MB_MB
FRIC_COEF=".5"
NAME="hands_to_body_cnt"
ID="18"

MASTER_SURFACE="/Hybrid_III_6_year_old/Lhand_gmb
/Hybrid_III_6_year_old/Rhand_gmb"

SLAVE_SURFACE="/Hybrid_III_6_year_old/Dummy_gmb"
>
<CONTACT_FORCE.CHAR
CONTACT_TYPE="SLAVE"
/>
</CONTACT.MB_MB>
<CONTACT.MB_MB
NAME="hands_wheelchair_cnt"
ID="13"

MASTER_SURFACE="/Hybrid_III_6_year_old/Lhand_gmb
/Hybrid_III_6_year_old/Rhand_gmb"

SLAVE_SURFACE="/wheelchair_system/wcback_contact_surfac
e/wheelchair_system/wcseat_contact_surface"
>
<CONTACT_FORCE.CHAR
CONTACT_TYPE="MASTER"
/>
</CONTACT.MB_MB>
<CONTACT.MB_MB
DAMP_COEF="800"
NAME="mbHead_seatback_cnt"
ID="15"

MASTER_SURFACE="/Hybrid_III_6_year_old/Head_gmb"

SLAVE_SURFACE="/wheelchair_system/wcback_contact_surfac
e"
>
<CONTACT_FORCE.CHAR
CONTACT_TYPE="MASTER"
/>
</CONTACT.MB_MB>
<CONTACT.MB_MB
DAMP_COEF="1000"
NAME="sled_anti_tipper_cnt"
FRIC_COEF=".001"
ID="19"
MASTER_SURFACE="/sled_system/sled_mbg"

SLAVE_SURFACE="/wheelchair_system/anti_tipper_surface"
>
<CONTACT_FORCE.CHAR
USER_CHAR="anti-tipper_cnt"
CONTACT_TYPE="USER_SLAVE"
/>
</CONTACT.MB_MB>
<CONTACT.MB_MB

DAMP_AMP_FUNC="/HeadContactDamp_func"
FRIC_COEF=".2"
DAMP_COEF="1000"
NAME="mbHead_headrest"
ID="20"

MASTER_SURFACE="/Hybrid_III_6_year_old/Head_gmb"

SLAVE_SURFACE="/wheelchair_system/headrest_group"
>
<CONTACT_FORCE.CHAR
CONTACT_AREA=".01"
USER_CHAR="/headrest_contact"
CONTACT_TYPE="USER_MASTER"
/>
</CONTACT.MB_MB>
<CONTACT.MB_MB

DAMP_AMP_FUNC="/Hybrid_III_6_year_old/HeadContactDam
p_fun2"
NAME="atd_wheelchairSB_cnt"
DAMP_COEF="200"
FRIC_COEF=".4"
INITIAL_TYPE="CORRECT"
ID="22"

MASTER_SURFACE="/Hybrid_III_6_year_old/Dummy_gmb"

SLAVE_SURFACE="/wheelchair_system/wcback_contact_surfac
e"
>
<CONTACT_FORCE.CHAR
USER_CHAR="/wheelchair_system/wcback_contact"
CONTACT_TYPE="USER_SLAVE"
/>
</CONTACT.MB_MB>
<CONTACT.MB_MB
INITIAL_TYPE="CORRECT"
DAMP_COEF="800"
FRIC_COEF=".7"
NAME="L_Rear_wheel_contact"
ID="23"
MASTER_SURFACE="/sled_system/sled_mbg"

SLAVE_SURFACE="/wheelchair_system/L_rear_wh_surface"
>
<CONTACT_FORCE.CHAR
CONTACT_TYPE="USER_SLAVE"
USER_CHAR="/wheel_cnt_def"
/>
</CONTACT.MB_MB>
<FUNCTION.XY
NAME="sled_pulse_forward"
ID="1"
>
<TABLE
TYPE="XY_PAIR"
/>
</FUNCTION.XY>
<FUNCTION.XY
ID="2"
NAME="gravity"
>
<TABLE
TYPE="XY_PAIR"
>
<![CDATA[
|XI YI |
-1 -9.81

```

```

2-9.81
]]>
</TABLE>
</FUNCTION.XY>
</FUNCTION.XY>
NAME="belt_load_fund"
ID="3"
>
<TABLE
  TYPE="XY_PAIR"
/>
</FUNCTION.XY>
</FUNCTION.XY>
NAME="belt_unload_func"
ID="4"
>
<TABLE
  TYPE="XY_PAIR"
/>
</FUNCTION.XY>
</FUNCTION.XY>
ID="9"
NAME="dummy_contact_func"
>
<TABLE
  TYPE="XY_PAIR"
>
<![CDATA[
| XI      YI |
0.00000000E+000 0.00000000E+000
3.00000000E-001 5.00000000E+004
]]>
</TABLE>
</FUNCTION.XY>
</FUNCTION.XY>
DESCRIPTION="rear tiedowns"
ID="10"
NAME="tiedown_load"
>
<TABLE
  TYPE="XY_PAIR"
>
<![CDATA[
| XI      YI |
0.00000000E+000 1.00000000E+003
7.50000000E-2 1.80000000E+004
]]>
</TABLE>
</FUNCTION.XY>
ID="203"
NAME="wheel_cnt_func"
>
<TABLE
  TYPE="XY_PAIR"
>
<![CDATA[
| XI      YI |
0.00000000E+000 0.00000000E+000
1.00000000E-001 3500]]>
</TABLE>
</FUNCTION.XY>
</FUNCTION.XY>
NAME="Front_tiedown_load"
ID="204"
>
<TABLE
  TYPE="XY_PAIR"
>
<![CDATA[
| XI      YI |
0.00000000E+000 1.00000000E+003
7.50000000E-2 1.80000000E+004
]]>
</TABLE>
</FUNCTION.XY>
NAME="atd_wc_load"
ID="206"
>
<TABLE
  TYPE="XY_PAIR"
>
<![CDATA[
| XI      YI |
0 0
.150 100
]]>
</TABLE>
</FUNCTION.XY>
</FUNCTION.XY>
NAME="belt_load_func2"
ID="207"
>
<TABLE
  TYPE="XY_PAIR"
>
<![CDATA[
| XI      YI |
0.0 0.0
0.021 1000.0
0.030 2950.0
0.040 4000.0
0.050 4700.0
0.060 5020.0
0.070 5100.0
0.080 5600.0
0.090 5850.0
0.100 6000.0
0.110 6280.0
0.120 6500.0
0.126 7000.0
]]>
</TABLE>
</FUNCTION.XY>
</FUNCTION.XY>
NAME="belt_unload_func2"
ID="208"
>
<TABLE
  TYPE="XY_PAIR"
>
<![CDATA[
| XI      YI |
0.0 0.0
0.1 1500.0
]]>
</TABLE>
</FUNCTION.XY>

```

```

<FUNCTION.XY
  NAME="belt_unload_func3"
  ID="209"
  >
  <TABLE
    TYPE="XY_PAIR"
  >
<![CDATA[
  |XI  YI|
  0.0 0.0
  0.12 3500.0
]]>
  </TABLE>
</FUNCTION.XY>
<FUNCTION.XY
  NAME="Headrest_unloading"
  ID="211"
  >
  <TABLE
    TYPE="XY_PAIR"
  >
<![CDATA[
  | XI  YI |
  0      0
  0.0425  2.4
  0.0435  3
  0.0465  4
  0.0475  5
  0.05    7
  0.057   12
  0.062   17
  0.065   22
  0.068   27
  0.07    32
  0.073   42
  0.076   52
  0.078   62
  0.079   72
  0.0794  74
  0.0795  77
  0.07955 78
  0.0796  79
  0.0797  80
  0.0798  80.5
]]>
  </TABLE>
</FUNCTION.XY>
<FUNCTION.XY
  NAME="front_tiedown_exp_load"
  ID="212"
  >
  <TABLE
    TYPE="XY_PAIR"
  >
<![CDATA[
  | XI  YI |
  0.0000 0.0
  0.0006 114.0
  0.0042 451.9
  0.0076 1113.1
  0.0110 2327.7
  0.0145 3896.8
  0.0179 5538.9
  0.0212 7108.4
  0.0246 8538.3
  0.0281 9811.6
  0.0315 10985.7
  0.0348 12096.8
  0.0382 13182.9
  0.0416 14287.7
  0.0449 15397.9
  0.0482 16554.3
  0.0515 17778.0
  0.0549 19025.5
  0.0582 20262.7
  0.0614 21449.1
  0.0646 22695.2
  0.0680 23919.5
  0.0712 25145.2
  0.0745 26371.0
  0.0778 27596.8
  0.0811 28822.6
  0.0843 30048.4
  0.0876 31274.2
]]>
  </TABLE>
</FUNCTION.XY>
<FUNCTION.XY
  NAME="front_tiedown_exp_unload"
  ID="213"
  >
  <TABLE
    TYPE="XY_PAIR"
  >
<![CDATA[
  | XI  YI |
  0.0000 0.0
  0.0240 0.0
  0.0286 253.4
  0.0320 863.3
  0.0355 1682.1
  0.0389 2645.8
  0.0423 3742.2
  0.0455 4984.3
  0.0489 6424.8
  0.0523 8066.2
  0.0557 9949.7
  0.0591 11833.2
  0.0625 13716.7
  0.0659 15600.2
  0.0693 17483.7
  0.0727 19367.3
  0.0760 21250.8
  0.0794 23134.3
  0.0828 25017.8
  0.0862 26901.3]]>
  </TABLE>
</FUNCTION.XY>
<FUNCTION.XY
  NAME="rear_tiedown_exp_load"
  ID="214"
  >
  <TABLE
    TYPE="XY_PAIR"
  >
<![CDATA[
  | XI  YI |
  0.0000 0.0
  0.0001 23.4
  0.0022 280.8
  0.0046 373.2
  0.0069 468.4
  0.0091 585.1
  0.0114 713.2
  0.0137 874.7
  0.0162 1059.5
  0.0185 1259.9
  0.0207 1489.6
  0.0230 1745.5
  0.0253 2024.8
  0.0276 2327.9
  0.0298 2638.8
  0.0322 2951.5

```

```

0.0345 3296.7
0.0369 3644.9
0.0392 4002.9
0.0417 4368.9
0.0440 4600.0
0.0464 4900.0
0.0488 5200.0
0.0512 5500.0
0.0536 5800.0
0.0560 6100.0
0.0584 6400.0
0.0608 6700.0
0.0631 7000.0
0.0655 7300.0
0.0679 7600.0
0.0703 7900.0
0.0727 8200.0
0.0751 8500.0
0.0775 8800.0
0.0799 9100.0
0.0823 9400.0
0.0847 9700.0
0.0871 10000.0 ]]>
  </TABLE>
  </FUNCTION.XY>
  <FUNCTION.XY
    NAME="rear_tiedown_exp_unload"
    ID="215"
  >
    <TABLE
      TYPE="XY_PAIR"
    >
      <![CDATA[ | XI      YI |
0.0000 0.0
0.0240 0.0
0.0259 65.8
0.0282 143.5
0.0306 242.7
0.0329 400.0
0.0352 691.8
0.0375 1185.7
0.0398 1500.0
0.0422 1900.0
0.0446 2300.0
0.0470 2700.0
0.0494 3100.0
0.0518 3500.0
0.0542 3900.0
0.0566 4300.0
0.0589 4700.0
0.0613 5100.0
0.0637 5500.0
0.0661 5900.0
0.0685 6300.0
]]>
  </TABLE>
  </FUNCTION.XY>
  <FUNCTION.XY
    NAME="atd_wcSB_load"
    ID="216"
  >
    <TABLE
      TYPE="XY_PAIR"
    >
      <![CDATA[ | XI      YI |
0 0
.150 1000]]>
  </TABLE>
  </FUNCTION.XY>
  </FUNCTION.XY
    NAME="headrest_loading"
    ID="210"
  >
    <TABLE
      TYPE="XY_PAIR"
    >
      <![CDATA[ | XI      YI |
0 0
0.013 2.4
0.01321 3
0.0135 4
0.0144 5
0.018 7
0.024 12
0.03 17
0.034 22
0.037 27
0.04 32
0.046 42
0.051 52
0.055 62
0.061 72
0.063 74
0.066 77
0.067 78
0.07 79
0.072 80
0.074 80.5
0.079 82
]]>
  </TABLE>
  </FUNCTION.XY>
  <FUNCTION.XY
    NAME="knee_loading"
    ID="221"
  >
    <TABLE
      TYPE="XY_PAIR"
    >
      <![CDATA[[XI      YI |
0 0
.05 1
.06 1000]]>
  </TABLE>
  </FUNCTION.XY>
  <FUNCTION.XY
    NAME="anti_tipper_fnc"
    ID="222"
  >
    <TABLE
      TYPE="XY_PAIR"
    >
      <![CDATA[[XI      YI |
0 0
.005 1
.01 2
.011 500]]>
  </TABLE>
  </FUNCTION.XY>
  <FUNCTION.XY
    NAME="crashpulse_smoothed"
    ID="223"
  >
    <TABLE
      TYPE="XY_PAIR"
    >
      </FUNCTION.XY>
  </FUNCTION.XY
    NAME="soft_wheel_cnt_func"
    ID="224"
  >

```

```

>
<TABLE
  TYPE="XY_PAIR"
>
<![CDATA[
  | XI      YI      |
  0.0000000E+000 0.0000000E+000
  1.0000000E-001 2000]]>
</TABLE>
</FUNCTION.XY>
<FUNCTION.XY
  NAME="front_tiedown_load_11"
  ID="226"
>
<TABLE
  TYPE="XY_PAIR"
>
<![CDATA[ | XI      YI      |
0          0
0.0006     100
0.0042     500
0.0076     1500
0.009      5000
0.011      8000
0.0145     10000
0.0179     11000
0.0212     12000
0.0246     12500
0.0281     13000
0.0315     13500
0.0348     14000
0.0382     14500
0.0416     15000
0.0449     15397.9
0.0482     16554.3
0.0515     17778
0.0549     19025.5
0.0582     20262.7
0.0614     21449.1
0.0646     22695.2
0.068      23919.5
0.0712     25145.2
0.0745     26371
0.0778     27596.8
0.0811     28822.6
0.0843     30048.4
0.0876     31274.2
]]>
</TABLE>
</FUNCTION.XY>
<FUNCTION.XY
  NAME="front_tiedown_load_12"
  ID="227"
>
<TABLE
  TYPE="XY_PAIR"
>
<![CDATA[ | XI      YI      |
0          0
0.0006     100
0.0042     500
0.0076     1500
0.009      2000
0.011      10000
0.0145     11000
0.0179     11500
0.0212     12000
0.0246     12500
0.0281     13000
0.0315     13500
0.0348     14000
0.0382     14500
0.0416     15000
0.0449     15397.9
0.0482     16554.3
0.0515     17778
0.0549     19025.5
0.0582     20262.7
0.0614     21449.1
0.0646     22695.2
0.068      23919.5
0.0712     25145.2
0.0745     26371
0.0778     27596.8
0.0811     28822.6
0.0843     30048.4
0.0876     31274.2
]]>
</TABLE>
</FUNCTION.XY>
<FUNCTION.XY
  NAME="anti_tipper_fnc2"
  ID="228"
>
<TABLE
  TYPE="XY_PAIR"
>
<![CDATA[[XI      YI |
0          0
0.01       5
0.02       20
0.03       100
0.04       1000
]]>
</TABLE>
</FUNCTION.XY>
<FUNCTION.XY
  NAME="anti_tipper_fnc3"
  ID="229"
>
<TABLE
  TYPE="XY_PAIR"
>
<![CDATA[[XI      YI |
0          0
0.01       2
0.02       10
0.03       50
0.04       500
0.05       1000
]]>
</TABLE>
</FUNCTION.XY>
<FUNCTION.XY
  NAME="Headrest_unloading2"
  ID="230"
>
<TABLE
  TYPE="XY_PAIR"
>
<![CDATA[ | XI      YI      |
0          0
0.1025     2.4
0.1035     3
0.1065     4
0.1075     5
0.11       7
0.117      12
0.122      17
]]>
</TABLE>
</FUNCTION.XY>

```

```

0.125 22
0.128 27
0.13 32
0.133 42
0.136 52
0.138 62
0.139 72
0.1394 74
0.1395 77
0.13955 78
0.1396 79
0.1397 80
0.1398 90
]]>
</TABLE>
</FUNCTION.XY>
<FUNCTION.XY
  NAME="headrest_loading2"
  ID="231"
  >
  <TABLE
    TYPE="XY_PAIR"
  >
<![CDATA[ | XI YI |
0 0
0.013 2.4
0.01321 3
0.0135 4
0.0144 5
0.018 7
0.024 12
0.03 17
0.034 22
0.037 27
0.04 32
0.046 42
0.051 52
0.055 62
0.061 72
0.063 74
0.066 77
0.067 78
0.07 79
0.072 80
0.074 80.5
0.079 82
0.14 100
]]>
</TABLE>
</FUNCTION.XY>
<FUNCTION.XY
  NAME="headrest_loading3"
  ID="232"
  >
  <TABLE
    TYPE="XY_PAIR"
  >
<![CDATA[ | XI YI |
0 0
.015 10
.06 100
.10 300
]]>
</TABLE>
</FUNCTION.XY>
<FUNCTION.XY
  NAME="headrest_unloading3"
  ID="233"
  >
  <TABLE
    TYPE="XY_PAIR"
  >
<![CDATA[ | XI YI |
0 0
.015 5
.06 50
.10 150
]]>
</TABLE>
</FUNCTION.XY>
<FUNCTION.XY
  NAME="headrest_loading4"
  ID="234"
  >
  <TABLE
    TYPE="XY_PAIR"
  >
<![CDATA[ | XI YI |
0 0
.015 5
.03 50
.06 200
.10 500
]]>
</TABLE>
</FUNCTION.XY>
<FUNCTION.XY
  NAME="headrest_unloading4"
  ID="235"
  >
  <TABLE
    TYPE="XY_PAIR"
  >
<![CDATA[ | XI YI |
0 0
.015 2.5
.03 25
.06 100
.10 250
]]>
</TABLE>
</FUNCTION.XY>
<FUNCTION.XY
  NAME="headrest_loading5"
  ID="236"
  >
  <TABLE
    TYPE="XY_PAIR"
  >
<![CDATA[ | XI YI |
0 0
.015 5
.03 40
.04 100
.06 300
.10 700
]]>
</TABLE>
</FUNCTION.XY>
<FUNCTION.XY
  NAME="headrest_unloading5"
  ID="237"
  >
  <TABLE
    TYPE="XY_PAIR"
  >

```



```

>
<![CDATA[ | XI YI |
0 0
.015 2.5
.03 20
.04 50
.06 150
.10 500
]]>
</TABLE>
</FUNCTION.XY>
<FUNCTION.XY
NAME="soft_wheel_cnt_func2"
ID="238"
>
<TABLE
TYPE="XY_PAIR"
>
<![CDATA[
| XI YI |
0 0
.01 100
.03 500
.05 1000
.10 3000
]]>
</TABLE>
</FUNCTION.XY>
<FUNCTION.XY
ID="1004"
NAME="HeadContactDamp_funA"
>
<TABLE
TYPE="XY_PAIR"
>
<![CDATA[
| XI YI |
0.00000000E+00 0.00000000E+00
7.00000000E+06 3.14779000E-01
3.00000000E+07 1.02000000E+00]]>
</TABLE>
</FUNCTION.XY>
<FUNCTION.XY
ID="7008"
NAME="HeadContactDamp_funB"
>
<TABLE
TYPE="XY_PAIR"
>
<![CDATA[
| XI YI |
0.00000000E+00 0.00000000E+00
7.00000000E+06 1.2E-01
3.00000000E+07 1.02000000E+00
]]>
</TABLE>
</FUNCTION.XY>
<FUNCTION.XY
ID="7009"
NAME="HeadContactDamp_funC"
>
<TABLE
TYPE="XY_PAIR"
>
<![CDATA[
| XI YI |
0.00000000E+00 0.00000000E+00
3.50000000E+06 1
1.00000000E+07 6

```

```

]]>
</TABLE>
</FUNCTION.XY>
<FUNCTION.XY
ID="7010"
NAME="HeadContactDamp_fun3"
>
<TABLE
TYPE="XY_PAIR"
>
<![CDATA[
| XI YI |
0.00000000E+00 0.00000000E+00
7.00000000E+06 3.14779000E-01
3.00000000E+07 4.02000000E+00
]]>
</TABLE>
</FUNCTION.XY>
<FUNCTION.XY
NAME="headrest_loading6"
ID="7011"
>
<TABLE
TYPE="XY_PAIR"
>
<![CDATA[ | XI YI |
0 0
.0075 5
.015 40
.02 100
.03 300
.05 700
]]>
</TABLE>
</FUNCTION.XY>
<FUNCTION.XY
NAME="headrest_unloading6"
ID="7012"
>
<TABLE
TYPE="XY_PAIR"
>
<![CDATA[ | XI YI |
0 0
.0075 2.5
.015 20
.02 50
.03 150
.05 500
]]>
</TABLE>
</FUNCTION.XY>
<FUNCTION.XY
NAME="headrest_loading7"
ID="7013"
>
<TABLE
TYPE="XY_PAIR"
>
<![CDATA[ | XI YI |
0 0
.01 5
.02 40
.025 100
.03 250
.04 700
]]>

```

```

</TABLE>
</FUNCTION.XY>
<FUNCTION.XY
  NAME="headrest_unloading7"
  ID="7014"
>
<TABLE
  TYPE="XY_PAIR"
>
<![CDATA[
  | XI      YI |
0 0
.01 2.5
.02 20
.025 50
.03 125
.04 350
]]>
</TABLE>
</FUNCTION.XY>
<FUNCTION.XY
  NAME="headrest_loading8"
  ID="7015"
>
<TABLE
  TYPE="XY_PAIR"
>
<![CDATA[
  | XI      YI |
0 0
.03 200
.05 700
]]>

```

```

</TABLE>
</FUNCTION.XY>
<FUNCTION.XY
  NAME="headrest_unloading8"
  ID="7016"
>
<TABLE
  TYPE="XY_PAIR"
>
<![CDATA[
  | XI      YI |
0 0
.03 100
.05 350
]]>
</TABLE>
</FUNCTION.XY>
<FUNCTION.XY
  ID="7017"
  NAME="HeadContactDamp_funD"
>
<TABLE
  TYPE="XY_PAIR"
>
<![CDATA[
  | XI      YI |
0.00000000E+00 0.00000000E+00
3.50000000E+06 10
1.00000000E+07 60
]]>
</TABLE>
</FUNCTION.XY>
</MADYMO>

```

BIBLIOGRAPHY

- ANSI/RESNA (2000). ANSI/RESNA WC19: Wheelchairs Used as Seats in Motor Vehicles, American National Standards Institute (ANSI)/Rehabilitation Engineering and Assistive Technology Society of North America (RESNA).
- Arbogast, K. B. (2008). Studies of children in frontal impact. S. I. Fuhrman. Pittsburgh.
- Association for the Advancement of Automotive Medicine (2005). The abbreviated injury scale 2005. Barrington, IL, AAAM.
- Bertocci, G., Szobota, S. (2000). Effect of wheelchair seating stiffness on occupant crash kinematics and submarining risk using computer simulation. RESNA Annual Conference, Orlando, FL, Resna Press.
- Bertocci, G., Szobota, S., et al. (2000). "Development of Frontal Impact Crashworthy Wheelchair Seating Design Criteria Using Computer Simulation." Journal of Rehab Research and Development 37(5): 565-572.
- Bertocci, G. E., Digges, K., et al. (1996a). "Development of Transportable Wheelchair Design Criteria using Computer Crash Simulation." IEEE Transactions of Rehabilitation Engineering 4(3): 171-181.
- Bertocci, G. E., Digges, K., et al. (1996b). "Development of transportable wheelchair design criteria using computer crash simulation." IEEE Transactions of Rehabilitation Engineering 4(3): 171-181.
- Bertocci, G. E., Szobota, S., et al. (1999). "Computer simulation and sled test validation of a powerbase wheelchair and occupant subjected to frontal crash conditions." IEEE Transactions on Rehabilitation Engineering 7(2): 234-244.
- Bilston, L. E. (2007). "Reconstruction of Crashes Involving Injured Child Occupants: The Risk of Serious Injuries Associated with Sub-Optimal Restraint Use May Be Reduced by Better Controlling Occupant Kinematics." Traffic Injury Prevention 8(1): 47-61.
- Cavanaugh, J. "Skull fracture and translational brain injury." Last update. Retrieved: September 21, 2006, from <http://ttb.eng.wayne.edu/~cavanau/brain2.html>.

- Chawda, M. N., Hildebrand, F., et al. (2004). "Predicting outcome after multiple trauma: which scoring system?" *Injury* 35(4): 347-358.
- Cotzin, B. (2008). Discussion of issues and common practice for wheelchair seating configuration (personal communication). S. I. Fuhrman. Pittsburgh.
- Department of Transportation (2002). Rear Impact Protection: rulemaking public meeting. Detroit, Michigan, National Highway Traffic Safety Administration,.
- Department of Transportation (DOT) (1977). FMVSS 301 - Fuel Systems Integrity. Washington D.C.
- Department of Transportation (DOT) (1982a). Laboratory procedure for FMVSS 210: Seat belt assembly anchorages. Washington, D.C., Department of Transportation (DOT).
- Department of Transportation (DOT) (1982b). Seat belt assembly anchorages. Laboratory Procedure for FMVSS 210. Washington, D.C., Department of Transportation (DOT).
- Department of Transportation (DOT) (1993). FMVSS 207 Seating Systems.
- Department of Transportation (DOT) (1993a). FMVSS Seating Systems. Washington, D.C., Department of Transportation (DOT).
- Department of Transportation (DOT) (2000). FMVSS 202: Head Restraints for Passenger Vehicles. Washington D.C.
- Department of Transportation (DOT) (2002). FMVSS 201 Occupant protection in interior impact.
- Department of Transportation (DOT). "Quick reference guide to: Federal motor vehicle safety standards and regulations." Last update: January 2004. Retrieved: May 10, 2006, from <http://nhtsa.gov/cars/rules/standards/FMVSS-Regs/index.htm>.
- Depreitere, B., Van Lierde, C., et al. (2006). "Mechanics of acute subdural hematomas resulting from bridging vein rupture." *Journal of Neurosurgery* 104(6): 950-6.
- Economic Commission for Europe (2002b). Regulation no. 44 - Uniform provisions concerning the approval of restraining devices for child occupants of powered-driven vehicles ("child restraint system"). Geneva, United Nations.
- Edwards, J., Sullivan, K. (1997). "Where are all the children seated and when are they restrained?" *SAE transactions* 106(6): 2413-2420.
- Eppinger, R., Sun, E., et al. (1999). Development of Improved Injury Criteria for the Advanced Automotive Restraint Systems - II. Washington D.C., National Highway Traffic Safety Administration.

- Everly, J. S., Bull, M. J., et al. (1993). "A survey of transportation services for children with disabilities." American Journal of Occupational Therapy 47(9): 804-10.
- Farmer, C. M., Wells, J. K., et al. (2003). "Effects of Head Restraint and Seat Redesign on Neck Injury Risk in Rear-End Crashes." Traffic Injury Prevention 4(2): 83-90.
- First Technology Safety Systems. "First Technology Innovative Solutions." Last update. Retrieved: July 20, 2005, from <http://www.ftss.com/pcat/products.cfm?obr=NS&bm=3&pcat=vip-3yo>.
- Flannagan, C., Manary, M. (2005). ISO proposed rear impact standards and crash pulse severities. S. I. Fuhrman. Ann Arbor.
- Forziati, K. T. (1994). Development of a Methodology to Dynamically Evaluate the Efficacy and Safety of Wheelchair Occupant Support Devices. Mechanical and Aerospace Engineering, University of Virginia: 129.
- Fuhrman, M. G. (2005). trackTargetsManually.m. Pittsburgh.
- Fuhrman, S. I., Buning, M. E., et al. (2005). Prescription Patterns of Secondary Postural Support Devices and Concerns Related to Their Use During Vehicle Transportation. RESNA Annual Conference, Atlanta, Georgia, RESNA.
- Fuhrman, S. I., Karg, P., et al. (2006). Characterization of Pediatric Wheelchair Kinematics and WTORS Loading During Rear Impact. RESNA 29th International Conference on Technology and Disability, Atlanta, GA, RESNA Press.
- Fuhrman, S. I., Karg, P., et al. (2008). "Effect of Wheelchair Headrest Use on Pediatric Head and Neck Injury Risk Outcomes During Rear Impact." Accident Analysis and Prevention 40(4): 1595–1603.
- Gupta, V., Menon, R., et al. (1996). Improved occupant protection through advanced seat design. Washington, NHTSA: 181-191.
- Gurdjian, E. S., Webster, J. E., et al. (1955). "Observations on the mechanism of brain concussion, contusion, and laceration." Surgery, Gynecology, & Obstetrics 101: 680-690.
- Ha, D. (2004). Pediatric Wheelchair Transportation Safety: Transit Manual Wheelchair Design Guidelines and Injury risk of 6-year old Children in a Frontal Motor Vehicle Impact. Rehabilitation Science and Technology. Pittsburgh, University of Pittsburgh: 230.
- Ha, D., Bertocci, G., et al. (2000a). "Evaluation of Wheelchair Seating System Crashworthiness: Combination Wheelchair Seat Back Surfaces and Attachment Hardware." Journal of Rehabilitation Research and Development 37 (5)(Sept/Oct): 555-563.
- Ha, D., Bertocci, G., et al. (2007). "Development and Validation of a Frontal Impact 6 Yr Old Wheelchair Seated Occupant Computer Model." Assistive Technology 19(4): 223-238.

- Ha, D., Bertocci, G. E., et al. (2000b). "Evaluation of wheelchair back support crashworthiness: combination wheelchair back support surfaces and attachment hardware." Journal of Rehabilitation Research & Development 37(5).
- Hirose, H., Aikawa, T. (2005). Problem of impact test for head support, National Rehabilitation Center for Persons with Disabilities, Japan.
- Hobson, D., Schneider, L. "Wheelchair Transportation Safety Frequently Asked Questions." Last update: December 9, 2003. Retrieved: October 25, 2004, from http://www.ercwts.pitt.edu/RERC_WTS_FAQ/RERC_WTS_FAQ.html.
- Houston, D. J., Richardson Jr, L. E., et al. (2001). "The Effectiveness of Child Safety Seat Laws in the Fifty States." POLICY STUDIES REVIEW 18(1): 163-184.
- Iannelli, V. "State Car Seat Laws." About Last update: 2006. from http://pediatrics.about.com/od/weeklyquestion/a/seat_laws_ask.htm.
- Insurance Institute for Highway Safety. "Child restraint laws as of July 2005." Last update: 2006. Retrieved: February 27, 2005, from http://www.iihs.org/laws/state_laws/restrain2.html.
- Irwin, A., Mertz, H. J. (1997). Biomechanical basis for the CRABI and Hybrid III child dummies, Society of Automotive Engineers.
- ISO (1999a). ISO 10542-1: Wheelchair tiedowns and occupant restraint systems/Part 1 - Requirements and test methods, International Standards Organization.
- ISO (1999b). ISO 10542-2: Technical systems and aids for disabled or handicapped persons - Wheelchair tiedown and occupant-restraint systems - Part 2: Four point strap type tiedown systems. Geneva, Switzerland, International Organization for Standardization.
- ISO (1999c). ISO/DIS 10542-1: Wheelchair tiedowns and occupant restraint systems/Part 1 - Requirements and test methods, International Standards Organization.
- ISO (1999d). ISO/DIS 10542-2: Wheelchair tiedowns and occupant restraint systems/Part 2 - four point strap type tiedown systems, International Standards Organization.
- ISO (2005a). ISO 10542-3: Technical systems and aids for disabled or handicapped persons - Wheelchair tiedown and occupant-restraint systems - Part:3: Docking type tiedown systems. Geneva, Switzerland, International Organization for Standardization.
- ISO (2005b). ISO/FDIS 16840-3: Wheelchair seating - Part 3: Determination of static, impact and repetitive load strengths for postural support devices: 30.
- ISO (2006). ISO/TC 173: Proposed Standard on Wheelchairs – Forward facing wheeled mobility aids in rear impact, International Standards Organisation.

- ISO (2008). ISO 7176/19: Wheelchairs Used as Seats in Motor Vehicles. Geneva, Switzerland, International Organization for Standardization.
- James, M., Strother, C., et al. (1991). "Occupant protection in rear-end collisions: safety priorities and seat belt effectiveness." Society of Automotive Engineers 912913.
- Japan Traffic Safety Association (1997). Traffic Greenpaper: 115-118.
- Johansson, S. "Volvo for life: safety firsts." Last update. Retrieved: April 5, 2006, from <http://www.volvocars.us/Tier2/WhyVolvo/Safety/SafetyFirsts.htm>.
- Karg, P. (1993). Development of methodology to evaluate the transportation safety of adaptive seating devices. Biomedical Engineering, University of Virginia.
- Kaye, H. S., Kang, T., et al. (2000). Mobility Device Use in the United States. Disability Statistics Report. Washington D.C., Department of Education, National Institute on Disability and Rehabilitation Research. 14.
- Kaye, H. S., Kang, T., et al. (2002). "Wheelchair Use in the United States." Disability Statistics Abstract 23: 1-4.
- King, A. I. (2000). "Fundamentals of impact biomechanics: part I - biomechanics of the head, neck and thorax." Annual Review of Biomedical Engineering 2(1): 55-81.
- Kleinberger, M., Sun, E., et al. (1998). Development of improved injury criteria for the assessment of advanced automotive restraint systems. Washington D.C., National Highway Traffic Safety Administration: 114.
- Kleinberger, M., Sun, E., et al. (1999). Effects of Head Restraint Position on Neck Injury in Rear Impact.
- Kleiven, S. (2003). "Influence of Impact Direction on the Human Head in Prediction of Subdural Hematoma." Journal of Neurotrauma 20(4): 365-379.
- Klinich, K. D., Saul, R., et al. (1996). Techniques for developing child dummy protection reference values. Child Injury Protection Team, General Motors.
- LaPlante, M. P., Center, D. S. (2003). Demographics of Wheeled Mobility Device Users. Conference on Space Requirements for Wheeled Mobility.
- Lawrence, J. M., Siegmund, G. P. (2000). "Seat back and head restraint response during low-speed rear-end automobile collisions." Accident Analysis & Prevention 32: 219-232.
- Leary, A., Bertocci, G. (2001). Design criteria for manual wheelchairs used as motor vehicle seats using computer simulation. RESNA Annual Conference, Reno, NV.
- Lowenhielm, P. (1978). "Tolerance level for bridging vein disruption calculated with a mathematical model." Journal of Bioengineering 2(6): 501-7.

- Malott, A., Parenteau, C., et al. (2004). "Sled test results using the Hybrid III 6 year old: an evaluation of various restraints and crash configurations." SAE Technical Paper Series(2004-01-0316).
- Manary, M. A., Bezaire, B. A., et al. (2007). Crashworthiness of Forward-Facing Wheelchairs under Rear Impact Conditions. RESNA 30th International Conference on Technology and Disability, Phoenix, AZ.
- Manary, M. A., Schneider, L. W. (2004). Wheelchair seatback loads and deflections in rear impacts. RESNA 2004, Orlando, FL, Rehabilitation Engineering Society of North America.
- Margulies, S. S., Thibault, L. E. (1992). "A proposed tolerance criterion for diffuse axonal injury in man." Journal of Biomechanics 25(8): 917-23.
- McHenry, B. G. (2004). "Head Injury Criterion and the ATB." ATB Users' Group.
- McLean, A. J., Anderson, R. W. G. (1997). Head Injury. London, Chaoman & Hall.
- Molino, L. (1998). Determination of moment-deflection characteristics of automobile seat backs. Washington D.C., National Highway Traffic Safety Administration Office of Crashworthiness Standards Light Duty Vehicle Division.
- Nahum, A., Melvin, J. (1993). Accidental injury - biomechanics and prevention. NY, Springer-Verlag.
- Nance, M. L., Lutz, N., et al. (2004). "Optimal restraint reduces the risk of abdominal injury in children involved in motor vehicle crashes." Annals of Surgery 239(1): 127-31.
- National Highway Traffic Safety Administration (1993). FMVSS 208, Occupant Crash Protection.
- National Highway Traffic Safety Administration (1999). FMVSS 213: Child Restraint Systems, Child Restraint Anchorage Systems.
- National Highway Traffic Safety Administration. "Occupant Protection." Traffic Safety Facts: 2003 Data Last update. Retrieved: February 20, 2006.
- National Highway Traffic Safety Administration (2005). 49 CFR 572.73 - Neck assembly test procedure. Washington D.C., U. S. Government.
- National Organization on Disability. "Access to Transportation." 2000 N.O.D./ Harris Surey of Americans with Disabilities Last update. Retrieved: October 3, 2005.
- NHTSA (1993). FMVSS 208, Occupant Crash Protection.
- NHTSA (1997). Wheelchair Users Injuries and Deaths Associated with Motor Vehicle Related Incidents. Washington, DC, National Center for Statistics and Analysis.

- NHTSA (1999). FMVSS 213: Child Restraint Systems, Child Restraint Anchorage Systems.
- Ommaya, A. K. (1985). The biomechanics of head injury: experimental aspects. The biomechanics of trauma. A. M. Nahum and J. Melvin, Prentice-Hall.
- Ommaya, A. K., Goldsmith, W., et al. (2002). "Biomechanics and neuropathology of adult and paediatric head injury." British Journal of Neurosurgery 16(3): 220-242.
- Ommaya, A. K., Hirsch, A. E. (1971). "Tolerance for cerebral concussion from head impact and whiplash in primates." Journal of Biomechanics 4: 13-21.
- Oster, J., Trommler, B. (1996). "Comparison of the six-year-old hybrid III, part 572 and TNO P6 child dummies." Society of Automotive Engineers 962437: 371-381.
- Paskoff, G. (1995). Transportation of wheelchair users: an assessment of neck injury risk during rear collisions. Biomedical Engineering. Charlottesville, University of Virginia: 85.
- Pipkorn, B., Eriksson, M. (2003). A method to evaluate the validity of mathematical models. Autoliv Research. Stockholm, TNO Automotive.
- Pounder, D. J. (1997). "Shaken adult syndrome." American Journal of Forensic Medical Pathology 18(4): 321-4.
- Prasad, P., Kim, A., et al. (1997). Relationships between passenger-car seat back strength and occupant injury severity in rear-end collisions: field and laboratory studies, Society of Automotive Engineers.
- Rehabilitation Engineering Research Center for Wheelchair Transportation Safety. "RERC on Wheelchair Transportation Safety." Last update: December 9, 2005. Retrieved: July 1, 2007, from <http://www.rercwts.org>.
- Rehabilitation Engineering Research Center on Wheelchair Transportation Safety. "Wheelchairs Marketed with the ANSI/RESNA WC-19 Transit Option as of February 14, 2007." WC-19 your ticket to ride safety Last update. Retrieved: February 28, 2007, from http://www.rercwts.pitt.edu/RERC_WTS2_KT/RERC_WTS2_KT_Stand/RERC_WTS2_19_Chart.html.
- RERC on Wheelchair Transportation Safety (2007). Guidelines for use of secondary postural support devices by wheelchair users during travel in motor vehicles. Pittsburgh, PA.
- Rivara, F. P., Thompson, D. C., et al. (1999). "Effectiveness of primary and secondary enforced seat belt laws." American Journal of Preventive Medicine 16(1S1): 30-39.
- Saab. "Features and Specifications: Safety & Security." Last update. Retrieved: April 5, 2006, from <http://www2.saabusa.com/95s/features.asp?start=home>.

- Saczalski, K. J., Syson, S. R., et al. (1993). Field accident evaluations and experimental study of seat back performance relative to rear-impact occupant protection, Society of Automotive Engineers. SAE 930346: 151-176.
- Salipur, Z., Bertocci, G., et al. (2007). Wheelchair Tiedown and Occupant Restraint System Loading Associated with an Adult Manual ANSI WC19 Transit Wheelchair with a Seated 50th percentile ATD Exposed to Rear Impact. RESNA 30th International Conference on Technology and Disability, Phoenix, AZ, RESNA Press.
- Schneider, L. W., Hobson, D. A., et al. (1999). A rationale and guideline to recommended practice SAE J2249: wheelchair tiedowns and occupant restraint systems for use in motor vehicles. Technical Report No. 8. RERC on Wheeled Mobility. Pittsburgh, University of Pittsburgh: 67.
- Sherwood, C. P., Shaw, C. G., et al. (2003). "Prediction of cervical spine injury risk for the 6-year-old child in frontal crashes." Traffic Injury Prevention 4(3): 206-13.
- Snell, M. (1999). "Guidelines for safely transporting wheelchair users." OT Practice 4(5): 35-8.
- Snyder, R. G., Spencer, M. L., et al. (1975). Physical characteristics of children as related to death and injury for consumer product design, FDA.
- Society of Automotive Engineers (1995). J211 - 1 Instrumentation for impact test. Part 1- Electronic instrumentation. Warrendale, PA.
- Society of Automotive Engineers (1996). SAE J2249: Wheelchair tiedowns and occupant restraint systems for use in motor vehicles. Warrendale, PA, Society of Automotive Engineers.
- Society of Automotive Engineers: Dummy Testing Equipment Subcommittee (2003). Hybrid III six-year-old child dummy user's manual. Warrendale, PA, SAE International: 50.
- Souza, A. L., Bertocci, G. E. (2001). The effects of wheelchair seating system energy absorption on occupant submarining risk in a frontal impact using computer simulation. RESNA Annual Conference, Reno, RESNA Press.
- Standards Association of Australia (1987). Wheelchair occupant restraint assemblies for motor vehicles. SAA. Sydney.
- Sturtz, G. (1980). Biomechanical data of children. Twenty-fourth Stapp Car Crash Conference Proceedings. Warrendale, Society of Automotive Engineers.
- Thibault, L., Gennarelli, T. A., et al. (1987). The temporal and spatial deformation response of a brain model in inertial loading. The 31st Stapp Car Crash Conference, Warrendale, PA, Society of Automotice Engineers.
- Thieffry, P. (2008). "Parametric design analysis for evaluating a range of variables." ANSYS Advantage II(1): 44-45.

- Thomson, R., Romilly, D., et al. (1993). Dynamic requirements of automobile seatbacks, SAE.
- TNO (2005). MADYMO Model Manual: version 6.3. Livonia, TNO Automotive Safety Solutions.
- Transportation National Highway Traffic Safety Administration (1990). Current issues of occupant protection in car rear impacts. Washington D.C., U.S. Department of Transportation, NHTSA Office of Crashworthiness.
- U.S. Census Bureau Public Information Office. "U.S. Census Bureau News: nation's population one-third minority." Last update: May 10, 2006. Retrieved: Aug 17, 2006, from <http://www.census.gov/Press-Release/www/releases/archives/population/006808.html>.
- U.S. Food and Drug Administration (2007). 21CFR890 - Physical Medicine Devices. Washington D.C., U.S. Food and Drug Administration.
- University of Michigan. "Ride Safe." Last update: October 12, 2005. Retrieved: February 1, 2007, from <http://www.travelsafer.org/>.
- Van Rensburg, L. "Abbreviated injury scale - (AIS)." Last update: September 14, 2004. Retrieved: February 10, 2007, from http://www.rcsed.ac.uk/fellows/lvanrensborg/classification/trauma%20scores/abbreviated_injury_scale.htm.
- van Rooij, L., Sherwood, C., et al. (2003). "The effects of vehicle seat belt parameters on the injury risk for children in booster seats." Society of Automotive Engineers SP-1776(Journal of Passenger Car - Mechanical Systems).
- Van Roosmalen, L., Bertocci, G., et al. (2000a). "Proposed test method and evaluation of wheelchair seating system crashworthiness." Journal of Rehabilitation Research and Development 37 (5)(Sept/Oct): 543-553.
- van Roosmalen, L., Bertocci, G., et al. (2000b). "Proposed test method for and evaluation of wheelchair seating system (WCSS) crashworthiness." Journal of Rehabilitation Research & Development 37(5): 543-554.
- Van Roosmalen, L., Bertocci, G. E., et al. (2001). Computer simulation validation of a wheelchair mounted occupant restraint system under frontal impact. RESNA annual conference, Reno, RESNA Press.
- Varma, A., Morbidelli, M., et al. (1999). Parametric Sensitivity in Chemical Systems, Cambridge University Press.
- Viano, D., Olsen, S. (2001). "The Effectiveness of Active Head Restraint in Preventing Whiplash." Journal of Trauma - Injury, Infection & Critical Care 51(5): 959-969.
- Viano, D. C. (2002). Role of the seat in rear crash safety. Warrendale, Pa., Society of Automotive Engineers.

- Viano, D. C., Davidsson, J. (2002). "Neck Displacements of Volunteers, BioRID P3 and Hybrid III in Rear Impacts: Implications to Whiplash Assessment by a Neck Displacement Criterion (NDC)." Traffic Injury Prevention 3(2): 105-116.
- Volvo. "Head restraints and safety seats: the Volvo Whiplash Protection System (WHIPS)." Last update. Retrieved: April 5, 2006, from http://www.driveandstayalive.com/articles%20and%20topics/safety%20equipment/article_volvo-WHIPS-whiplash-protection-system.htm.
- Wagner, R. (1979). A 30 mph Front/Rear Crash with Human Test Persons, Society of Automotive Engineers.
- Watanabe, Y., Ichikawa, H., et al. (2000). "Influence of seat characteristics on occupant motion in low-speed rear impacts." Accident Analysis & Prevention 32(2): 243-250.
- Welcher, J. B., Szabo, T. J. (2001). "Relationships between seat properties and human subject kinematics in rear impact tests." Accident Analysis and Prevention 33(3): 289-304.
- Winston, F. K., Chen, I. G., et al. (2004). "Recent trends in child restraint practices in the United States." Pediatrics 113(5): e458-64.
- Wonsettler, T. (2008). Optimal headrest placement for function for pediatric clients (personal communication). S. I. Fuhrman. Pittsburgh.
- Yakupcin, J. (2005). "Child passenger safety in the school-age population." Pediatric Emergency Care 21(4): 286-290.
- Young, J., Reynolds, H., et al. (1976). Development and Evaluation of Masterbody Forms for 3- and 6-Year-Old-Child Dummies. Technical Report. Washington, D.C., Office of Aviation Medicine, Federal Aviation Administration.